



HAL
open science

New insights into physiopathogenetics of spinal muscular atrophy

Shaqraa Musawi

► **To cite this version:**

Shaqraa Musawi. New insights into physiopathogenetics of spinal muscular atrophy. Genetics. Université Claude Bernard - Lyon I, 2022. English. NNT : 2022LYO10008 . tel-03963669

HAL Id: tel-03963669

<https://theses.hal.science/tel-03963669>

Submitted on 30 Jan 2023

HAL is a multi-disciplinary open access archive for the deposit and dissemination of scientific research documents, whether they are published or not. The documents may come from teaching and research institutions in France or abroad, or from public or private research centers.

L'archive ouverte pluridisciplinaire **HAL**, est destinée au dépôt et à la diffusion de documents scientifiques de niveau recherche, publiés ou non, émanant des établissements d'enseignement et de recherche français ou étrangers, des laboratoires publics ou privés.



N°d'ordre NNT : 2022LYO10008

**THESE de DOCTORAT DE
L'UNIVERSITE CLAUDE BERNARD LYON 1**

**Ecole Doctorale N° 340
Biologie Moléculaire, Intégrative et Cellulaire**

Discipline : Génétique et biologie moléculaire

Soutenue publiquement le 07/09/2022, par :
Shaqraa MUSAWI

**New Insights into physiopathogenetics
of Spinal Muscular Atrophy**

Devant le jury composé de :

Coin, Frédéric, DR, IGBMC, Université de Strasbourg **Rapporteur**
PONTVIANNE, Frédéric, DR, LGDP, Université de Perpignan **Rapporteur**

CAMPALANS, Anna, DR, LCE, Institut de biologie François Jaco **Examinatrice**
Schaeffer, Laurent, PU, INMG, Université Lyon 1 **Examinateur**
VUILLEROT, Carole, DR, Cheffe de service Central de Rééducation pédiatrique, Hopital
Femme Mère Enfant **Présidente**

Giglia-Mari, Giuseppina, DR, INMG, Université Lyon 1 **Directrice de thèse**

Université Claude Bernard – LYON 1

Président de l'Université	M. Frédéric FLEURY
Président du Conseil Académique	M. Hamda BEN HADID
Vice-Président du Conseil d'Administration	M. Didier REVEL
Vice-Président du Conseil des Etudes et de la Vie Universitaire	M. Philippe CHEVALLIER
Vice-Président de la Commission de Recherche	M. Petru MIRONESCU
Directeur Général des Services	M. Pierre ROLLAND

COMPOSANTES SANTE

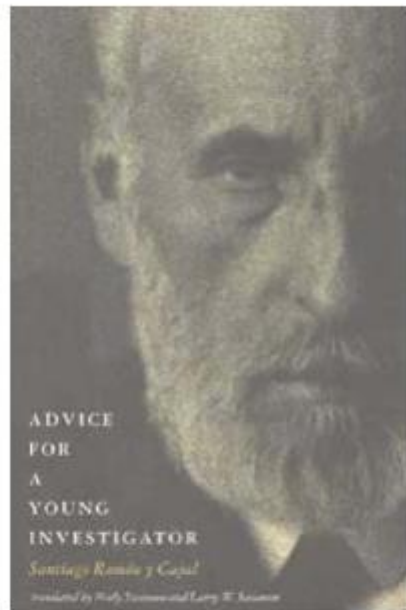
Département de Formation et Centre de Recherche en Biologie Humaine	Directrice : Mme Anne-Marie SCHOTT
Faculté d'Odontologie	Doyenne : Mme Dominique SEUX
Faculté de Médecine et Maïeutique Lyon Sud - Charles Mérieux	Doyenne : Mme Carole BURILLON
Faculté de Médecine Lyon-Est	Doyen : M. Gilles RODE
Institut des Sciences et Techniques de la Réadaptation (ISTR)	Directeur : M. Xavier PERROT
Institut des Sciences Pharmaceutiques et Biologiques (ISBP)	Directrice : Mme Christine VINCIGUERRA

COMPOSANTES & DEPARTEMENTS DE SCIENCES & TECHNOLOGIE

Département Génie Electrique et des Procédés (GEP)	Directrice : Mme Rosaria FERRIGNO
Département Informatique	Directeur : M. Behzad SHARIAT
Département Mécanique	Directeur M. Marc BUFFAT
Ecole Supérieure de Chimie, Physique, Electronique (CPE Lyon)	Directeur : Gérard PIGNAULT
Institut de Science Financière et d'Assurances (ISFA)	Directeur : M. Nicolas LEBOISNE
Institut National du Professorat et de l'Education	Administrateur Provisoire : M. Pierre CHAREYRON
Institut Universitaire de Technologie de Lyon 1	Directeur : M. Christophe VITON
Observatoire de Lyon	Directrice : Mme Isabelle DANIEL
Polytechnique Lyon	Directeur : Emmanuel PERRIN
UFR Biosciences	Administratrice provisoire : Mme Kathrin GIESELER
UFR des Sciences et Techniques des Activités Physiques et Sportives (STAPS)	Directeur : M. Yannick VANPOULLE
UFR Faculté des Sciences	Directeur : M. Bruno ANDRIOLETTI

Dedication

To my Family



“Each problem solved stimulates an infinite number of new questions, and that **today’s discovery contains the seed of tomorrow’s.**”

Advice for a Young Investigator

Santiago Ramón y Cajal

Acknowledgments

First of all, I would like to thank Mr. Frédéric COIN and Mr. Frédéric PONTVIANNE, who accepted to be the rapporteurs of my thesis and expressed their interest in my work. I hope you enjoy reading my manuscript. Thanks to Ms. Anna CAMPALANS, Ms. Carole VUILLEROT, and Mr. Laurent Schaeffer for being accepted to be part of my defense jury. Thank you for the kind remarks about my work.

Working under the restrictions of a global pandemic COVID-19 and being unable to see my family in Saudi Arabia for three years was not on my long list of expectations for my thesis 09/2019 to 09/2022. Therefore, many thanks to all who have helped me in countless ways during these times; thank you for your contributions to my journey throughout this Ph.D.

First and foremost, I will express my gratitude to my supervisor Dr. Giglia-Mari, Giuseppina, who offered guidance, advice, support, patience, and feedback throughout this thesis. Thank you for the kind remarks about my work and the comments that helped me improve my thesis. Throughout my thesis, you have always found time and energy to discuss my results enthusiastically and optimistically, and you have always been full of ideas, humor, and laughter. Thank you for giving me the opportunity to perform this work in your laboratory.

I am grateful to all the many past and present members of the Giglia-Mari lab who have created a congenial work environment and contributed many insights and discussions to this work.

A special thanks to Lise-Marie for helping me at the beginning of my project and for giving me support, advice, and motivation. Also, thank you for helping me during the writing of my thesis.

I am grateful to thank Leonardo BECCARI, who helped me enormously with the writing of my thesis. Thank you, very much, and good luck, with your projects.

I would like to thank Pierre-OLIVIER as well for his advice and for sharing his microscope expertise with me.

A special thank you as well goes to Charlene MAGNANI. I have always felt welcome to ask her for any possible help and support that I needed. Thanks for helping with many laboratory techniques.

Thanks to my office partners for creating a positive and inspirational work environment and for the discussions we have shared.

I am grateful to the members of my thesis monitoring committee Dr. Céline BALDEYRON and Dr. Patrick LOMONTE, for the productive meetings over the three years. Their advice has been instrumental in guiding the direction of my thesis project.

Science is often best a collective endeavor. Therefore, I would like to express my sincere gratitude to our collaborators outside the lab, including Dr. Olivier BINDA from Institut NeuroMyoGène and Ottawa University.

I also would like to acknowledge the Government of Saudi Arabia, the Ministry of Education, and Jazan University in Saudi Arabia. I am very grateful for the unlimited support at all levels and the careful follow-up of every detail during my scholarship in France (2015-2022). I have learned more than I thought, and I am ready to return the favor with all my energy, as you believed me initially.

Finally, I would like to thank my family, who I could not have done this without you. I want to thank my parents for their unconditional love. I appreciate all your words of wisdom and encouragement through the years.

Thanks to my small family, my husband Mousa, daughter Seba, and son Hassan who endured this long process with me, always offering support and love and giving me the strength to keep going. Without your constant love, thoughts, and inspiring words, I would not have made it this far.

Contents

Résumé en français.....	11
Summary	15
The title and address of the related unit or laboratory where the thesis was prepared	19
List of Figures.....	20
List of Tables.....	22
List of Abbreviations	23
Chapter one.....	27
General Introduction	27
1. DNA damage and repair (NER pathway).....	28
1.1. Damage and repair.....	28
1.2. Nucleotide Excision Repair pathway.....	31
1.3. Associated diseases.....	35
1.4. DNA repair mechanisms in dividing and non-dividing cells.....	38
1.5. Restoration of cell activity after damage.....	38
2. Crosstalk between nucleolus and Cajal Bodies under Stress Response	40
2.1. Nucleolus.....	41
2.2. Cajal Bodies and Gems.....	48
2.3. The Nucleolus and CBs under Stress.....	50
2.4. Fibrillarin (FBL), nucleolar and CB-associated protein.....	55
3. Overview of Spinal Muscular Atrophy (SMA)	56
3.1. Spinal Muscular Atrophy (SMA).....	56
3.2. Genetics of SMA.....	57
3.3. Symptoms and clinical Classification of SMA Subtypes	60
3.4. Mechanism.....	62
3.5. Diagnosis of SMA	65
3.6. Treatment of SMA.....	66
3.7. Genetics models of SMA	68
4. Survival Motor-neuron (SMN) functions	77

4.1.	SMN GENE.....	77
4.2.	Isoform of SMN.....	78
4.3.	Protein and Domain Organizations.....	80
4.4.	SMN protein expression and cellular localization.....	82
4.5.	SMN Functions.....	82
4.6.	SMN and Protein-Protein Interactions.....	93
4.7.	SMN and PRMTs.....	95
4.8.	Protein arginine methyltransferases (PRMTs).....	96
4.9.	SMN in DNA damage and repair.....	99
Chapter two.....		101
Background & Aim of the study.....		101
Reference.....		105
Chapter three.....		119
Materials & Methods.....		119
Chapter four.....		127
Results.....		127
I.	Nucleolar reorganization after cellular stress is orchestrated by SMN shuttling between nuclear compartments.....	128
II.	Coilin governs the displacement of RNAP1 in response to UV-C damage.....	169
III.	Design human siRNA libraries targeted the mechanistic of RNAP1 (displacement & repositioning) induced by UV-C for future screening project.....	184
IV.	Accumulation of damage in SMN deficiency cells & R loops resolving complex (SMN&SETX) in the nucleolus together with RNAP2.....	192
V.	SMN and Cockayne syndrome.....	203
VI.	SMN and motor neurons.....	210
Chapter five.....		219
Concluding remarks and future perspectives.....		219
Chapter six.....		224
Annex.....		224
Curriculum vitae.....		239

Résumé en français

Le noyau est l'organite cellulaire qui stocke l'information génétique des cellules eucaryotes. Toutes les fonctions cellulaires dépendent d'un contrôle efficace et étroitement régulé de l'expression des gènes. Pour cela, différents processus métaboliques de l'ADN et de l'ARN coexistent au sein du noyau, notamment la transcription des gènes codant pour les protéines et les gènes ribosomiques, la maturation de l'ARN, la régulation épigénétique de la chromatine, l'organisation, etc. Certains de ces processus se produisent dans des domaines spatialement séparés au sein du noyau via l'établissement d'organites nucléaires sans membrane. Parmi eux, le nucléole est le plus grand compartiment nucléaire : il héberge la transcription et la maturation des ARN ribosomiques nécessaires à la biogenèse des ribosomes.

Des agents physiques et chimiques menacent constamment l'intégrité de notre matériel génétique en provoquant différents types de lésions de l'ADN. Par exemple, l'exposition à la lumière UV et certains autres agents chimiques induisent des lésions de distorsion de l'hélice, qui constituent l'une des meilleures aubaines d'altération de notre matériel génétique. Ces lésions affectent les processus métaboliques de l'ADN, mettant ainsi en danger la viabilité cellulaire. De plus, s'ils ne sont pas correctement réparés, ils entraînent l'accumulation de mutations pouvant causer différents troubles humains (différentes pathologies), notamment des cancers et des altérations congénitales du développement. Pour éviter ces effets délétères, les cellules ont développé différents mécanismes de réparation de l'ADN, dont le système de réparation par excision de nucléotide (NER) l'un des plus polyvalents pour réparer une grande variété de lésions de l'ADN, y compris les dommages causés par les UV. Bien (qu'il existe une connaissance approfondie de) que la façon dont les cellules réparent la réponse aux dommages

à l'ADN médiée par le NER bénéficie de connaissances approfondies, on sait très peu de choses sur la façon dont les cellules restaurent leurs activités normales après avoir terminé les processus de réparation.

En raison de l'organisation particulière de l'ADNr en réseaux en tandem et de ses taux de transcription exceptionnellement élevés, il est sujet au développement d'hybrides ARN : ADN (boucles R) qui endommagent l'ADN. Si les dommages à l'ADNr ne sont pas réparés correctement, ils peuvent entraîner des maladies et un vieillissement prématuré. De plus, les dommages à l'ADN provoquent des changements spectaculaires dans l'architecture nucléolaire. Notre équipe a récemment découvert qu'après un stress génotoxique (irradiation UV), le RNAP1 et l'ADN nucléolaire sont exportés vers la périphérie du nucléole (déplacement). Étant donné que la plupart des protéines de réparation sont présentes à l'extérieur du nucléole, ce mouvement est considéré comme important pour permettre une réparation appropriée. Fait intéressant, la structure nucléolaire appropriée ne peut être restaurée (repositionnement) qu'après la réparation complète de toutes les lésions UV sur l'ADN nucléolaire. Le mécanisme exact de cette relocalisation est très mal connu. Prenant comme point de départ la réorganisation nucléolaire dépendante du stress, ma thèse lèvera la barrière scientifique concernant la compréhension des processus de maintenance cellulaire et d'homéostasie liés au nucléole après induction de stress.

Dans ma thèse, j'ai abordé cette question en m'intéressant aux mécanismes qui contrôlent la réparation et la restauration de l'organisation et de l'activité transcriptionnelle de l'ADN ribosomal. Plus précisément, j'ai étudié la dynamique de l'organisation nucléolaire lors du déplacement et du repositionnement des protéines nucléolaires causés par les dommages et la réparation de l'ADN en identifiant les facteurs impliqués dans ce processus. La fibrillarine (FBL), une protéine nucléolaire, s'est avérée fondamentale pour la restauration d'une structure

nucléolaire appropriée après l'achèvement de la réparation de l'ADN. Par conséquent, nous avons examiné si les partenaires d'interaction FBL tels que SMN a également joué un rôle dans ce processus.

Nous avons cherché à savoir si (SMN) pour Survival Motor Neuron qui permet la survie des neurones moteurs est impliquée dans la réorganisation nucléolaire induite par les dommages UV. Le rôle la protéine SMN a reçu une attention accrue dans plusieurs disciplines ces dernières années en raison de son association avec la première cause de maladie infantile mortelle, l'amyotrophie spinale (SMA), une maladie congénitale grave. La protéine SMN était particulièrement intéressant à analyser car son domaine Tudor interagit avec FBL. En outre, la SMN est une protéine impliquée dans différents processus métaboliques de l'ARN, en plus de plusieurs autres fonctions cellulaires critiques. En fait, le SMN peut être détecté dans le cytoplasme et le noyau. Dans le noyau, SMN se trouve dans les corps de Cajal (CB) avec Coilin et dans Gems sans Coilin. Les gemmes sont connues pour être enrichies en complexe SMN (SMN avec les protéines Gemins 2-8). La navette complexe SMN entre le cytoplasme et le noyau agit comme un chaperon pour favoriser l'assemblage des petites particules de ribonucléoprotéine nucléaire spliceosomale (snRNP) et joue donc un rôle crucial dans l'épissage du pré-ARNm.

Les nucléoles et CB sont des structures nucléaires dynamiques ; ce sont des cibles essentielles des voies de signalisation de la réponse au stress, entraînant des changements dans leur architecture, leur taille et leur teneur en protéines. La coiline est la protéine marqueur du CB. La présence de Coilin dans l'espace péri nucléolaire est principalement attribuée aux réponses au stress cellulaire qui entraînent la suppression de la transcription de l'ARNr. De plus, Coilin interagit avec FBL et SMN dans CB.

Résultats

Nous avons découvert une nouvelle fonction cellulaire inattendue pour le SMN dans la restauration de la structure nucléolaire appropriée après l'achèvement de la réparation de l'ADN. En effet, en l'absence de SMN, RNAP1 et FBL restent à la périphérie du nucléole, là où la transcription de RNAP1 va reprendre. Le redémarrage de la transcription de RNAP1 a été détecté à partir d'une localisation non canonique (la périphérie du nucléole). De plus, nous avons observé une navette dynamique du SMN à l'intérieur du nucléole 24 heures après l'induction des dommages et 24 heures avant la restauration de la structure nucléolaire. SMN fait la navette avec des protéines de son complexe, comme Gemin5. FBL et Coilin entreprennent différentes phases du processus de navette SMN. Sans Coilin, SMN ne peut pas atteindre la périphérie du nucléole, et sans FBL, SMN ne peut pas entrer dans le noyau. De plus, ni Coilin ni les cellules FBL ne sont capables de récupérer la localisation du nucléole de RNAP1. Ce va-et-vient est régi par des réactions de méthylation des protéines arginine méthyltransférases (PRMT).

De plus, des résultats préliminaires prometteurs mettent en évidence le rôle de Coilin dans l'étape de déplacement. Coilin interagit et agit comme un chaperon pour RNAP1 après des dommages UV-C en inhibant l'activité de RNAP1.

Nos découvertes identifient une nouvelle fonction de SMN et Coilin dans la réorganisation nucléolaire, établissant un nouveau lien entre CB et nucléole concernant la réponse aux dommages à l'ADN. Le positionnement aberrant de la transcription RNAP1 ainsi que le défaut de réorganisation nucléolaire peuvent contribuer au phénotype neurodégénératif des patients SMA.

Summary

Title in English: New Insights into physiopathogenetics of Spinal Muscular

Atrophy

The nucleus is the cell organelle that store the genetic information of eukaryotic cells. All cell functions depend on efficient and tightly regulated control of gene expression. For that, different DNA and RNA metabolic processes coexist within the nucleus, including transcription of protein-coding and ribosomal genes, RNA maturation, chromatin epigenetic regulation, organization, etc. Some of these processes occur in spatially segregated domains within the nucleus via the establishment of membrane-less nuclear organelles. Among them, the nucleolus is the largest nuclear compartment and hosts the transcription and maturation of the ribosomal RNAs required for ribosome biogenesis.

Physical and chemical agents constantly threaten our genetic material's integrity by causing different types of DNA lesions. For example, UV- light exposure and other certain chemical agents induce helix-distorting lesions, which constitute one the highest bargain for our genetic material. These lesions affect DNA metabolic processes, thus endangering cell viability. Besides, if not properly repaired, they lead to the accumulation of mutations that can cause different human disorders, including cancer and developmental congenital alterations. To avoid these deleterious effects, cells have developed different DNA repair mechanisms, with the Nucleotide Excision Repair system (NER) being one of the most versatile systems for repairing a wide variety of DNA injuries, including UV damage. While there is an extended knowledge of how cells repair NER-mediated DNA damage response, very little is known about how cells restore their normal activities after completing repair processes.

Because of the particular organization of rDNA in tandem arrays and its exceptionally high transcription rates, it is prone to RNA: DNA hybrids (R-loops) which cause DNA damage. If the rDNA damage is not repaired correctly that can lead to disease and premature aging. Moreover, DNA damage causes dramatic changes in nucleolar architecture. Our team recently found that after a genotoxic stress (UV irradiation) RNAP1 and nucleolar DNA are exported to the periphery of the nucleolus (displacement). Because most repair proteins are present outside the nucleolus, this movement is believed to be important for a proper repair reaction. Interestingly, the proper nucleolar structure can be restored (repositioning) only after the complete repair of all UV lesions on the nucleolar DNA. The exact mechanism of this relocation is very poorly understood. Taking stress-dependent nucleolar reorganization as a starting point, my thesis will lift the scientific barrier of understanding the cellular maintenance and homeostasis processes related to the nucleolus after stress induction.

In my thesis, I addressed this question by focusing on the mechanisms that control the repair and restoration of the organization and transcriptional activity of the ribosomal DNA. Specifically, I studied the dynamics of the nucleolar organization during displacement and repositioning of nucleolar proteins caused by DNA damage and repair by identifying the factors involved in this process. Fibrillarin (FBL), a nucleolar protein, has been found to be vital for the restoration of a proper nucleolar structure following the completion of DNA repair. Therefore, we examined whether FBL interacting partners such as SMN also played a role in this process.

We investigated whether the Survival Motor Neurons (SMN) is involved in the nucleolar reorganization induced by UV damage. The role of SMN has received increased attention across several disciplines in recent years due to its association with the first cause of fatal infant disease, Spinal Muscular Atrophy (SMA), a severe congenital disorder. SMN was particularly

interesting to analyse because its Tudor domain interacts with FBL. Moreover, SMN is a protein involved in different RNA metabolic processes, besides several other critical cellular functions. In fact, SMN can be detected in the cytoplasm and the nucleus. Within the nucleus, SMN is found in Cajal bodies (CB) together with Coilin and in Gems without Coilin. Gems are known to be enriched with SMN complex (SMN with Gemins proteins 2-8). SMN complex shuttle between cytoplasm and nucleus acts as a chaperone to promote the assembly of spliceosomal small nuclear ribonucleoprotein (snRNP) particles and hence plays a crucial role in pre-mRNA splicing.

Both nucleoli and CB are dynamic nuclear structures; they are essential targets of stress response signalling pathways, resulting in changes in their architecture, size, and protein content. Coilin is the marker protein for CB. The presence of Coilin in the peri-nucleolar space is primarily attributed to cellular stress responses that result in the suppression of rRNA transcription. In addition, Coilin interacts with FBL and SMN in CB.

Results

We discovered a new, unexpected cellular function for SMN in restoring the proper nucleolar structure after the completion of DNA Repair. Indeed, in the absence of SMN, RNAP1 and FBL remain at the periphery of the nucleolus, where RNAP1 transcription will resume. Restarting transcription of RNAP1 was detected from a non-canonical localization (the periphery of the nucleolus). Furthermore, we observed a dynamic shuttling of SMN inside the nucleolus 24 hours after damage induction and 24 hours before the nucleolar structure is restored. SMN shuttles with proteins from his complex, such as Gemin5. FBL and Coilin undertake different phases of the SMN shuttling process. Without Coilin, SMN cannot reach the nucleolus' periphery, and without FBL, SMN cannot enter the nucleus. Additionally, neither

Coilin nor FBL cells are able to recover RNAP1's nucleolus localization. And that methylation reactions from protein arginine methyltransferases (PRMTs) govern this shuttling.

Furthermore, promising preliminary results highlight the role of Coilin in the displacement step. Coilin interacts and acts as a chaperon for RNAP1 after UV-C damage by inhibiting RNAP1 activity.

Our findings identify a novel function of SMN and Coilin in the nucleolar reorganization, establishing a new link between CB and nucleolus regarding the DNA damage response. The aberrant positioning of RNAP1 transcription together with the defect in the nucleolar reorganization may contribute to the neurodegenerative phenotype of SMA patients.

Les mots clés en français :

AMS, SMN, ARNP1, Réparation de l'ADN, NER, ADNr, Lésions UV, Nucléole, Corps de Cajal, Coilin, Fibrillarine, PRMTs.

Keywords in English:

SMA, SMN, RNAP1, DNA repair, NER, rDNA, UV lesions, Nucleolus, Cajal bodies, Coilin, Fibrillarin, PRMTs.

The title and address of the related unit or laboratory where the thesis was prepared

The work for this thesis was performed at the NeuroMyoGène- Physiopathology and Genetics of Neurons and Muscles (INMG-PGNM) CNRS UMR 5261, Inserm U1315 at the Medical Faculty at Claude Bernard University Lyon 1. The thesis took place in the period from 9/2019 to 9/2022 supported by a grant from Jazan university from the Saudi government.



Université Claude Bernard



Lyon 1

List of Figures

Figure 1 : DNA damage and repair.	30
Figure 2 : NER mechanism steps.....	33
Figure 3 : Displacement and repositioning of RNAP1 induced by UV.	39
Figure 4 : Major subnuclear bodies.	41
Figure 5 : Organization of the nucleolus in human cells.	42
Figure 6 : Transcription unit of ribosomal DNA.....	44
Figure 7 : RNA Polymerase 1 transcription cycle.....	46
Figure 8 : Ribosome biogenesis.	47
Figure 9 : Association of the CB with the neuronal nucleolus.....	49
Figure 10 : Degeneration of motor neurons in SMA causes loss of muscle mass and strength (atrophy).	56
Figure 11 : Autosomal recessive inheritance of SMA and probability to have SMA child.	57
Figure 12 : Missense and nonsense mutations of SMN.	58
Figure 13 : Human SMN1 and SMN2.	59
Figure 14 : Signaling pathways implicated in neurodegeneration in SMA.....	64
Figure 15 : Diagnostic algorithm for SMA.....	66
Figure 16 : SMN protein sequence and function are conserved across species during evolution.	76
Figure 17 : Human SMN1 & 2 protein alignment.	77
Figure 18 : SMN transcripts.	79
Figure 19 : SMN domains and interactions.	81
Figure 20 : SMN in the cytoplasm and in the nucleus (Gems & CB).....	82
Figure 21 : SMN role in the transcription.	84
Figure 22 : SMN complex.....	86

Figure 23 : snRNP biogenesis and assembly..... 88

Figure 24 : The Sm core and U7 core structure..... 89

Figure 25 : The snoRNA structure..... 91

Figure 26 : SMN/FBL domains and interaction..... 93

Figure 27 : SMN/Coilin domains and interaction. 94

Figure 28 : The methylarginine forms. 96

List of Tables

Table 1 : The classically involved genes in NER pathway.	34
Table 2 : The seven complementation groups of Xeroderma Pigmentosum (XP).	36
Table 3 : Summary of the Effects of Different Stress Types on Nucleolar and CB Organization.	54
Table 4 : Clinical classification of SMA subtypes according to onset, milestones achieved, and clinical, typically associated <i>SMN2</i> copy numbers and life expectancy.	62
Table 5 : The approved SMA drug therapies.	68
Table 6 : The SMA mouse models..	73
Table 7 : Summary of PRMTs localization, type, and functions.	98

Annex

Table 8 : A list of 289 known interactors of SMN.....	233
Table 9 : PRMTs inhibited, (i) Type I preclinical compounds PRMTs inhibited; (ii) II and III preclinical compounds, and PRMTs inhibited; (iii) Inhibitors in Phase I clinical trials.	238

List of Abbreviations

5'ETS	5' External Transcribed Spacer
6-4PPs	6-4 Pyrimidine-pyrimidone Photoproducts
AAV	Adeno-Associated Virus
aDMA	Asymmetric dimethylarginine
BER	Base excision repair
C. elegans	Caenorhabditis elegans
CARM1	Coactivator Associated Arginine Methyltransferase 1
CB	Cajal body
CK	Creatine kinase levels
CNS	Central nervous system
CPDs	Cyclobutane Pyrimidine Dimers
CS	Cockayne syndrome proteins
CTD	Carboxy terminal domain
DFC	Dense fibrillar component
DJ	Downstream Distal Junction
DNA	Deoxyribonucleic acid
DNA-PKc	DNA-dependent protein kinase c
DRB	5,6-dichloro-1-b-D-ribobenzimidazole
DSBs	Double-strand breaks
EMA	European Medicines Agency
EMG	Electromyogram
ERCC1	Cross-complementing 1
ESCs	Embryonic stem cells
FBL	Fibrillarin
FC	Fibrillar center
FDA	Food and Drug Administration
FL	Full-length
FRAP	Fluorescent recovery after photobleaching
FUS	Fused in Sarcoma

Gap43	Growth-Associated Protein 43
GAR	Glycine-arginine-rich
GC	Granular component
Gems	Gemini of the Cajal bodies
GG-NER	Global genome NER
HEK293	Human embryonic kidney cells 293
HR	Homologous recombination
iCDR	Induced Centromeric Damage Response
IGF1	Insulin-Like Growth Factor
IMP1	mRNA-Binding Protein 1
iPSC	Induced pluripotent stem cells
IR	Ionizing radiation
ITS	Internal Transcribed Spacers
JNKs	c Jun NH2-Terminal Kinases
LIG1	DNA ligase I
LIG3	DNA ligase III
MAPKs	Mitogen-Activated Protein Kinases
MLPA	Multiplex Ligation-dependent Probe Amplification
MMA	Mono methylarginine
MMR	DNA mismatch repair
MOs	Morpholinos
mRNA	messenger RNA
NCBI	National Center for Biotechnology Information
NCV	Nerve conduction velocity
NER	Nucleotide excision repair
NHEJ	Non-homologous end-joining
NLS	Nuclear localization signals
NMD	Nonsense-mediated mRNA decay
NMDs	Neuromuscular diseases
NoLS	Nucleolar localization signal
NORs	Norganizing regions
NTIS	Nontranscribed Intergenic Spacer

MLOs	Membraneless Organelles
OMIM	Online Mendelian Inheritance in Man
PCNA	Proliferating cell nuclear antigen
PGD	Preimplantation genetic diagnosis
PIC	Pre-Initiation Complex
PJ	Proximal Junction
PMID	Pubmed ID
pre-mRNA	Precursor messenger RNA
PTRF	Pol 1 and Transcript Release Factor"
qPCR	Quantitative polymerase chain reaction
RFC	Replication factor C
RG	Arginine-glycine-rich
RNAi	RNA Interference
RNAP	RNA Polymerase
RNAP II	RNA Polymerase II
RNAP III	RNA Polymerase III
RNAP1	RNA Polymerase1
RNP	Ribonucleoprotein
RPA	Replication protein A
rpS2	40S ribosomal protein S2
rRNA	Ribosomal RNAs
sDMA	Symmetric dimethylarginine
SETX	Senataxin
SIN3A	SIN3 Transcription Regulator Family Member A
siRNA	Small interfering RNA
SL1	Selectivity Factor 1
SMN	Survival Motor Neurons
SMNΔ7	SMN without exon 7
snoRNA	Small Nucleolar Ribonucleo RNA
snoRNP	Small Nucleolar Ribonucleoprotein
snRNP	Small Nuclear Ribonucleoprotein

snRNP	Small nuclear ribonucleoprotein
ssDNA	Single-stranded DNA
TC-NER	Transcription-coupled NER
TFIIH	Transcription factor II H
tRNA	Transfer RNAs
TSS	Transcription start site
TTD	Trichothiodystrophy
TTF-1	Termination site, Transcription Termination Factor-1
Uba1	Ubiquitin-Like Modifying Activator 1
UBF	Upstream Binding Factor
UCE	Upstream Control Element
Unrip	Unr-interacting protein
USPL1	Ubiquitin-specific protease-like 1
UV	Ultraviolet
UV-DDB	UV-damaged DNA-binding protein
UVSS	UV-sensitive syndrome
WES	Whole Exome Sequencing
WGS	Whole Genome Sequencing
XP	Xeroderma Pigmentosum
α-SMN	axonal-SMN

Chapter one

General Introduction

1. DNA damage and repair (NER pathway).

1.1. Damage and repair

Deoxyribonucleic Acid (DNA) is the molecule that contains the biological instructions that make each individual unique. It carries the genetic information from one generation to another. However, DNA is constantly being modified by endogenous metabolic activities (e.g., reactive oxygen species and replication errors) or/and by environmental/exogenous (e.g., ultraviolet light, ion radiation, genotoxic chemicals) agents form different DNA lesions^{1 2 3 4}. DNA damage can occur at a rate of 10,000 to 1,000,000 molecular lesions per cell per day^{5 2}.

DNA damage has a wide range of consequences, including cell cycle arrest⁶, transcription inhibition^{7 8}, DNA replication stops, and apoptosis induction^{9 10}. Failure to repair DNA lesions can lead to the generation of mutations which, in turn, can cause various human diseases^{11 12}, including cancer, neurological abnormalities, immunodeficiency, and premature aging^{13 14}.

To avoid such harmful outcomes and maintain genome integrity, cells utilize a variety of repair pathways that have evolved to elicit lesion-specific responses according to the type of DNA damage, including a series of factors that participate in diverse and tightly regulated steps.

In Double-Strand Breaks (DSBs) both strands of a double helix are destroyed, are induced by ionizing radiation (IR). They are very dangerous to cells because they can produce genomic rearrangements¹⁵.

Non-homologous end-joining (NHEJ) and homologous recombination (HR) are the two ways of repairing DSBs. The NHEJ directly joins the two damage ends since it does not require a homologous template for repair; it is not confined to a specific cell cycle phase. In contrast, the HR needs the presence of an identical sequence to be used as a template for repairing the break, which occurs only during the S or G2 phases when a homologous template via the sister chromatid is available¹⁵.

Single-stranded DNA (ssDNA) damage is repaired by three excision repair mechanisms the: (i) base excision repair (BER), (ii) and DNA mismatch repair (MMR) and, (iii) nucleotide excision repair (NER).

The BER pathway can only repair base damage resulting from specific non-bulky DNA lesions that do not create major structural distortions in DNA¹⁶. Similarly, the MMR pathway corrects the small insertion/deletion loops or nucleotide mismatches¹⁷. Finally, NER can repair a wide range of helix-distorting DNA lesions, including ultraviolet (UV) induced Cyclobutane Pyrimidine Dimers (CPDs) and 6-4 Pyrimidine-pyrimidone Photoproducts (6-4PPs), as well as oxidative damage, bulky lesions, and intrastrand crosslinks caused by cancer chemotherapeutic drugs like cisplatin¹⁸. The NER mechanism is described in more detail below and a Schematic representation of DNA damaging agents with related DNA damage types and DNA repair mechanisms shown in (Figure 1).

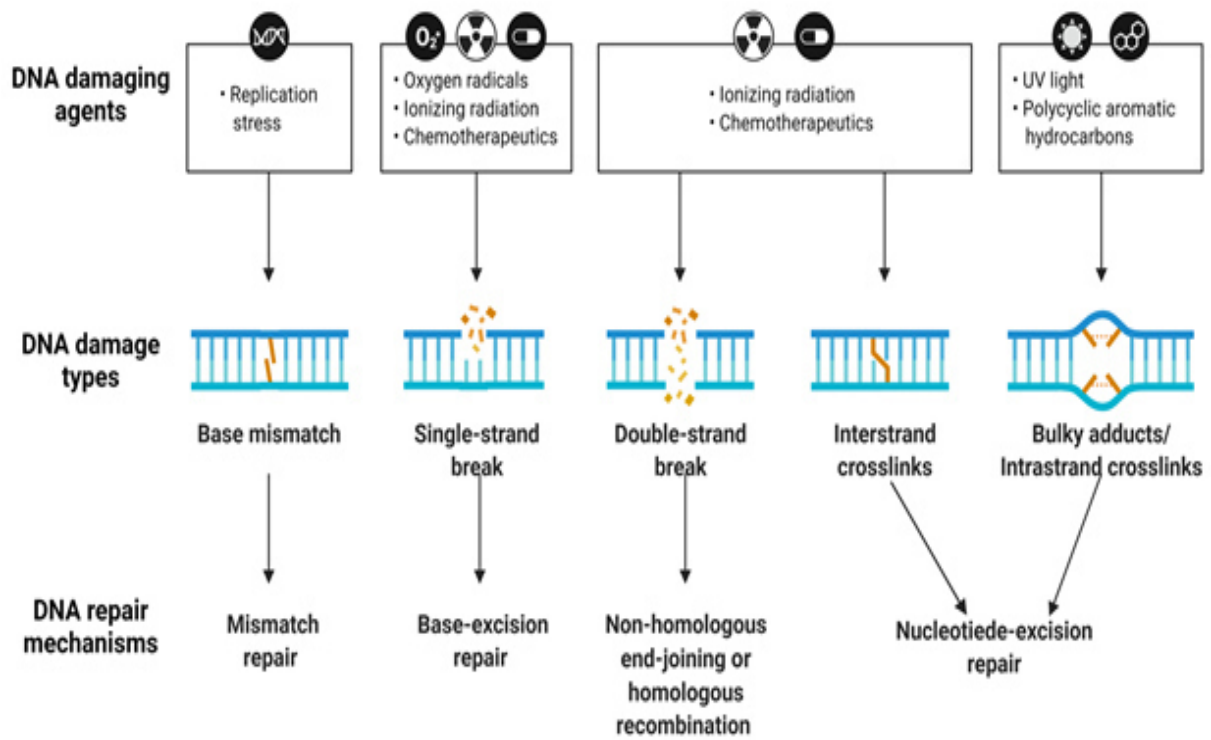


Figure 1 : DNA damage and repair.

Schematic representation of DNA damaging agents with related DNA damage types and DNA repair mechanisms.

1.2. Nucleotide Excision Repair pathway

NER is a highly conserved repair mechanism and is used in nearly all eukaryotic and prokaryotic cells¹⁹. There are four main steps in NER pathway that I will detailed below: (i) Damage recognition, (ii) Unwinding the DNA, (iii) Damage Excision and (iv) Synthesis of the new strand.

The NER mediated DNA damage repair is structured in different steps (Figure 2).

1.2.1.1. Damage Recognition (two sub pathway GG-NER & TC-NER)

Global genome NER (GG-NER) and transcription-coupled NER (TC-NER) are the two sub pathways that initiate NER^{20 21}. GG-NER can occur anywhere in the genome, whereas TC-NER is in charge of repairing the lesions in transcribed strand of active gene. The two sub pathways differ in how they recognize DNA damage, but ultimately converge in the same process.

(i)Global genome NER (GG-NER)

GG-NER is triggered by the GG-NER specific factor Xeroderma Pigmentosum proteins C (XPC), which is sometimes supported by UV-damaged DNA-binding protein (UV-DDB). The XPC protein binds to the strand opposite to the lesion rather than the chemical adduct itself²⁰.

(ii)Transcription-coupled nucleotide excision repair (TC-NER)

In TC-NER, a lesion on the transcribed strand within an active gene stopped elongating RNA Polymerase (RNAP). This arrested RNAP acts as a critical signal that engages the Cockayne syndrome proteins (CS) proteins CSA and CSB, to facilitate the eventual removal of the damage and resumption of transcription²¹.

1.2.1.2. Unwinding the DNA

The transcription factor II H (TFIIH) complex is recruited as soon as one of the two sub pathways recognizes the damage. It contains ten subunits, including two helicases, XPB (3'-5') and XPD (5'-3'). A mechanism in which TFIIH facilitates the opening of the DNA duplex around the lesion by activating its helicase subunits and creates a "bubble" platform for the recruitment of XPA and replication protein A (RPA); RPA protects the ssDNA. Consequently, XPA promotes the release of the TFIIH component ²².

1.2.1.3. Excision the damage

Two endonucleases are recruited: XPF–excision repair cross-complementing 1 (ERCC1) complex and XPG. The XPF–ERCC1 complex is recruited to the lesion by interacting directly with XPA, whereas XPG is particularly engaged via interacting with TFIIH and stabilizing the pre-excision complex. The two endonucleases, XPF–ERCC1 and XPG, are then responsible for DNA damage excision in 5' and 3', respectively ²³.

1.2.1.4. Synthesis of new DNA strand

DNA polymerases δ , ϵ or κ are involved in gap-filling repair synthesis after removing of the damaged fragment following the dual incision event. They cooperate with replication factor C (RFC) and proliferating cell nuclear antigen (PCNA). As a final step, nicks are sealed by DNA ligase III (LIG3) DNA ligase I (LIG1) complex.

All the steps are summarized from ¹⁸.

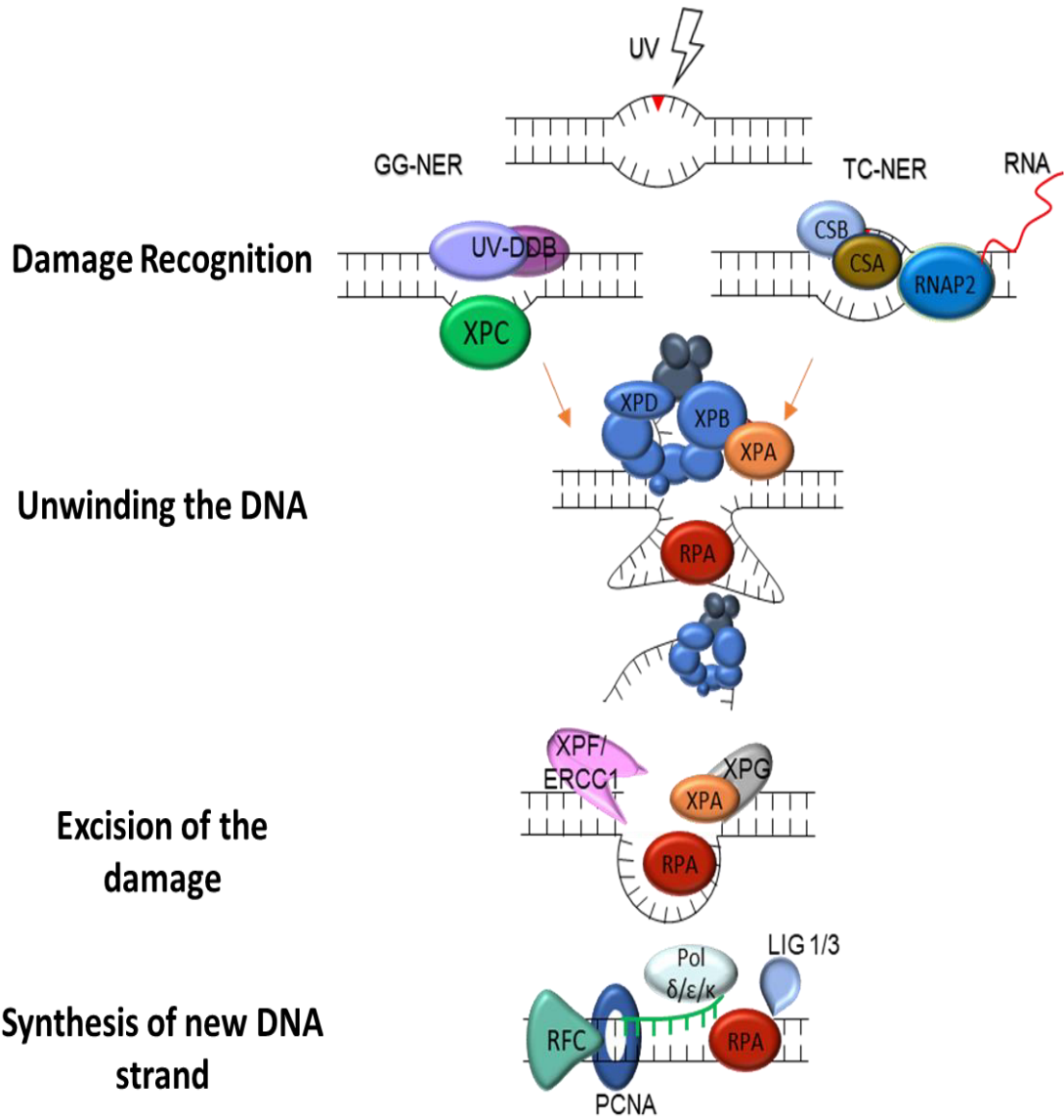


Figure 2 : NER mechanism steps.

Diagram of both the TC-NER and GG-NER pathways. The two pathways differ only in initial DNA damage recognition.

The classically involved genes in NER pathway are shown in (Table 1).

Human Gene (Protein) name	Subpathway	Function in NER
CCNH (<u>Cyclin H</u>)	Both	CDK Activator Kinase (CAK) subunit
CDK7 (<u>Cyclin-Dependent Kinase (CDK 7)</u>)	Both	CAK subunit
CETN2 (<u>Centrin-2</u>)	GGR	Damage recognition; forms complex with XPC
DDB1 (<u>DDB1</u>)	GGR	Damage recognition; forms complex with DDB2
DDB2 (<u>DDB2</u>)	GGR	Damage recognition ; recruits XPC
ERCC1 (<u>ERCC1</u>)	Both	Involved in incision on 3' side of damage: forms complex with XPF
ERCC2 (<u>XPD</u>)	Both	ATPase and helicase activity; transcription factor II H (TFIIH) subunit
ERCC3 (<u>XPB</u>)	Both	ATPase and helicase activity; transcription factor II H (TFIIH) subunit
ERCC4 (<u>XPF</u>)	Both	Involved in incision on 3' side of damage: structure specific endonuclease
ERCC5 (<u>XPG</u>)	Both	Involved in incision on 5' side of damage; stabilizes TFIIH; structure specific endonuclease
ERCC6 (<u>CSB</u>)	TC-NER	Transcription elongation factor; involved in transcription coupling and chromatin remodelling
ERCC8 (<u>CSA</u>)	TC-NER	Ubiquitin ligase complex; interacts with CSB and p44 of TFIIH
LIG1 (<u>DNA Ligase I</u>)	Both	Final ligation
MNAT1 (<u>MNAT1</u>)	Both	Stabilizes CAK complex
MMS19 (<u>MMS19</u>)	Both	Interacts with XPD and XPB subunits of TFIIH helicases
RAD23A (<u>RAD23A</u>)	GGR	Damage recognition; forms complex with XPC
RAD23B (<u>RAD23B</u>)	GGR	Damage recognition forms complex with XPC
RPA1 (<u>RPA1</u>)	Both	Subunit of RFA complex
RPA2 (<u>RPA2</u>)	Both	Subunit of RFA complex
TFIIH (<u>Transcription factor II H</u>)	Both	Involved in incision, forms complex around the lesion
XAB2 (<u>XAB2</u>)	TC-NER	Damage recognition; interacts with XPA, CSA, and CSB
XPA (<u>XPA</u>)	Both	Damage recognition
XPC (<u>XPC</u>)	GGR	Damage recognition

Table 1 : The classically involved genes in NER pathway.

(GGR); Global genome NER and (TC-NER); transcription-coupled NER.

1.3. Associated diseases

A number of severe autosomal recessive human diseases are caused by mutations in NER genes illustrating the importance of NER in genome maintenance. Mutations in XPA, XPB, XPC, XPD, XPE, XPF, and XPG cause all xeroderma pigmentosum. while CSA and CSB disruption are related to Cockayne syndrome disease ^{24 25}.

Furthermore, other syndromes such as UV-sensitive syndrome (UVSS), trichothiodystrophy (TTD), and the combinations between XP/CS and XP/TTD²⁵.

These pathologies share the feature of high sensitivity to UV radiation. However, while XP is a cancer-prone skin disease, CS syndrome and TTD are neurological diseases with segmental premature aging characteristics but no increased cancer frequency ^{26 27 28}. These diseases are discussed in greater detail below.

1.3.1.1. Xeroderma Pigmentosum (XP)

Xeroderma Pigmentosum (XP) is an autosomal recessive disease first described in the 1870 by Moritz Kaposi. The XP affects about 1 in 100,000 worldwide and 1 in 430,000 in Europe. There are seven complementation groups (XP-A through XP-G), plus one variant form the XP variant (XP-V) (Table 2). While XPA to XPG are involved in the NER pathway, the XPV (or POLH) encodes for DNA polymerase- η (eta), which is required to replicate DNA containing unrepaired DNA UV induced damage ²⁹.

XP symptoms include a severe sunburn after only a few minutes in the sun, freckling in sun-exposed areas, dry skin, changes in skin pigmentation, and a high risk of skin cancer. In addition to skin cancer predisposition, patients have an increased risk of developing several types of internal cancers at an early age. XP patients may display progressive neurologic degeneration as well. They are about 1,000 times more likely to develop skin cancer than individuals without the disorder.

There is no treatment for the disease; all therapies are symptomatic or preventative; by entirely avoiding exposure to sunlight ²⁹.

Type	OMIM N°	Gene	Description
Type A, XPA	<u>278700</u>	<u>XPA</u>	Xeroderma pigmentosum group A - the classical form of XP
Type B, XPB	<u>133510</u>	<u>XPB</u>	Xeroderma pigmentosum group B
Type C, XPC	<u>278720</u>	<u>XPC</u>	Xeroderma pigmentosum group C
Type D, XPD	<u>278730</u> <u>278800</u>	<u>XPD</u> <u>ERCC6</u>	Xeroderma pigmentosum group D or De Sanctis-Cacchione syndrome (can be considered as subtype of XPD)
Type E, XPE	<u>278740</u>	<u>DDB2</u>	Xeroderma pigmentosum group E
Type F, XPF	<u>278760</u>	<u>ERCC4</u>	Xeroderma pigmentosum group F
Type G, XPG	<u>278780</u> <u>133530</u>	<u>RAD2</u> <u>ERCC5</u>	Xeroderma pigmentosum group G and COFS syndrome type 3
Type V, XPV	<u>278750</u>	<u>POLH</u>	Xeroderma pigmentosum variant - these patients have a mutation in a gene that codes for a specialized DNA polymerase called <u>polymerase-η (eta)</u> . Polymerase-η can replicate over the damage and is needed when cells enter the <u>S-phase</u> in the presence of DNA replication.

Table 2 : The seven complementation groups of Xeroderma Pigmentosum (XP).

Types, Online Mendelian Inheritance in Man (OMIM) N°, Gene, and description are shown here.

1.3.1.2. Cockayne Syndrome (CS)

Cockayne Syndrome (CS), also called Neill-Dingwall syndrome, was first described in 1936 by Edward Cockayne, as an autosomal recessive neurodegenerative disorder. Mutations that cause CS are in the NER genes Cockayne syndrome A and B (CSA (OMIM N° 216400) and CSB (OMIM N° 133540). CS has an incidence of 1 in 250,000 live births and a prevalence of approximately 1 per 2.5 million. CS is divided into two complementation groups: 1) CSA, which is caused by a mutation on ERCC8 on chromosome 5q12–q31, and 2) CSB, which is

caused by a mutation on ERCC6 on chromosome 10q11. Around 70–75 % of CS cases are CSB. A combined form of XP and CS (XP/CS), accounts for almost 10% of reported CS cases are caused by mutations in the genes encoding XPD, XPB, or XPG.

CS patients are characterized by severe neurological manifestations such as microcephaly and cognitive abnormalities, pigmentary retinopathy, dental decay, segmental accelerated aging (progeria), and feeding difficulties. Interestingly, CS patients are not predisposed to develop skin cancer like XP patients.

CS patients can require symptomatic treatment because there is no permanent cure for this syndrome³⁰.

1.3.1.3. Trichothiodystrophy (TTD)

Trichothiodystrophy (TTD) (OMIM N° 601675) is an autosomal recessive disorder caused by mutations in the XPB, XPD, or TTDA gene.

Sulphur-deficient brittle hair is the hallmark of TTD. Other symptoms include ichthyosis, microcephaly, neurological abnormalities, early aging, and intellectual disability, depending on the severity of the condition. Like CS patients, approximately half of the reported TTD patients are sensitive to UV light and are not at risk for skin cancer²⁵.

1.3.1.4. UV-sensitive syndrome (UVSS)

UV-sensitive syndrome (UVSS) (OMIM N° 600630) is an autosomal recessive disease. UVSS can result from mutations in the CSA, CSB or UVSSA genes. UVSS patients develop normally, and they do not have skin cancer predisposition.

It is a condition marked by sensitivity to UV rays from the sun. A sunburn can develop on affected people even after a brief exposure to the sun. Additionally, these people may develop freckles, dryness, or color changes (pigmentation) on skin exposed to the sun over time³¹.

1.4. DNA repair mechanisms in dividing and non-dividing cells

The process through which cells become specialized during development, taking on specific structural, functional, biochemical traits and responsibilities, is known as differentiation. Cell replication is essential to produce the appropriate number of cells during development and to sustain organism growth and replace dead or damaged cells during both embryonic and postnatal life. Mammalian tissues are made up of a variety of cell types, including both dividing and non-dividing cells. The myocytes and neurons are terminally differentiated and thus non-dividing; they cannot enter the cell cycle again (post-mitotic cells).

Neurons are highly specialized due to their unique power and function within the body; they do not have the time or resources to replicate themselves as cardiac muscle cells, which devote all their energy to pumping blood. Therefore, failure to repair DNA damage in neuronal cells due to DNA damage results in neuronal death, eventually leading to neurodegenerative disorders^{32 33 34}. Given the neurological defects observed in XP and CS patients, most studies on neuronal DNA repair have focused on the NER pathway. Neuronal cell death in XP and CS patients is caused by a lack of ability to repair DNA damage. Multiple neurodegenerative disorders are characterized by defective DNA repair³⁵.

1.5. Restoration of cell activity after damage

In general, there is an extended knowledge on how cells repair DNA damage but very little is known on how cells restore their normal activities after completion of repair processes.

Recently, our team found that after a genotoxic stress induced by UV irradiation, RNAP1 and nucleolar DNA are exported to the periphery of the nucleolus³⁶. Interestingly, proper nucleolar structure can be restored only after the complete repair of all UV lesions on the nucleolar DNA (Figure 3).

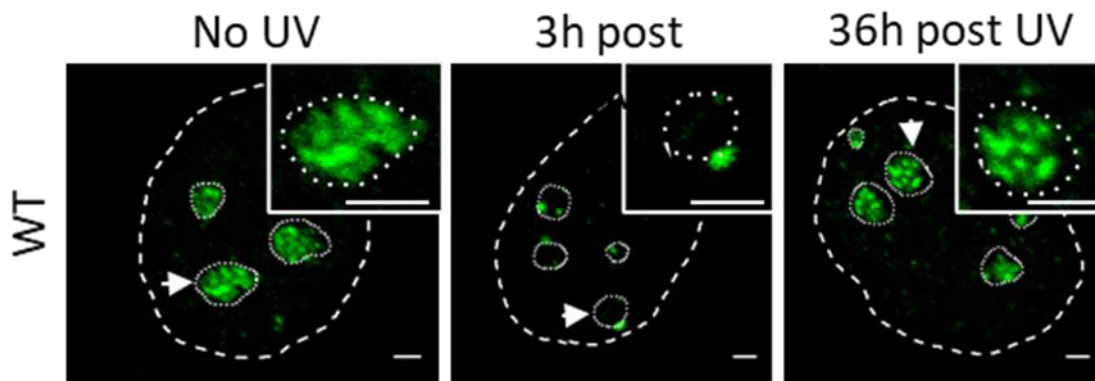


Figure 3 : Displacement and repositioning of RNAP1 induced by UV.

Confocal images of immunofluorescence staining against RNAP1 (green) performed on WT cells. Insets zoom into the nucleoli indicated with arrows. (Scale bars: 2 μ m.). Adapted from (Daniel et al; 2018).

Taking stress-dependent nucleolar reorganization as a starting point in my thesis to provide further advances in the fundamental knowledge of how nucleolar structure is modified by cellular stresses and how cells proceed to reestablish the proper nucleolar reorganization.

In the next section I discussed the nucleolus and Cajal bodies as two dynamic nuclear organelles. They represent important targets of cellular stress response, leading to complex changes in their structure, size, and protein content.

2. Crosstalk between nucleolus and Cajal Bodies under Stress Response

Nuclear bodies are membrane-less organelles (MLOs) found in the cell nuclei of eukaryotic cells. They are morphologically distinct regions within the nucleus; they can be distinguished from their surroundings using techniques like transmission electron microscopy, differential interference contrast microscopy, and immunofluorescent detection of proteins that localize to a particular nuclear body^{37 38}. The Nuclear Protein Database (<http://npd.hgu.mrc.ac.uk>) has immunofluorescent photos of these MLOs.

The nucleolus, nuclear speckle, nuclear stress body, Cajal body (CB), Gemini of Cajal body (Gems), histone locus body (HLBs), PML-Nuclear body (PML-NBs), and paraspeckle are all MLOs (Figure 4)^{37 38}.

MLOs ensure the temporal and spatial management of numerous biological processes. MLOs speed up biological reactions by concentrating specific proteins and RNAs. Recently, more and more relations between MLO malfunction and a number of disease processes^{39 40}.

Because of the focus of this thesis, I focused on the nucleolus, CB, and Gems and their relationship here in detail.

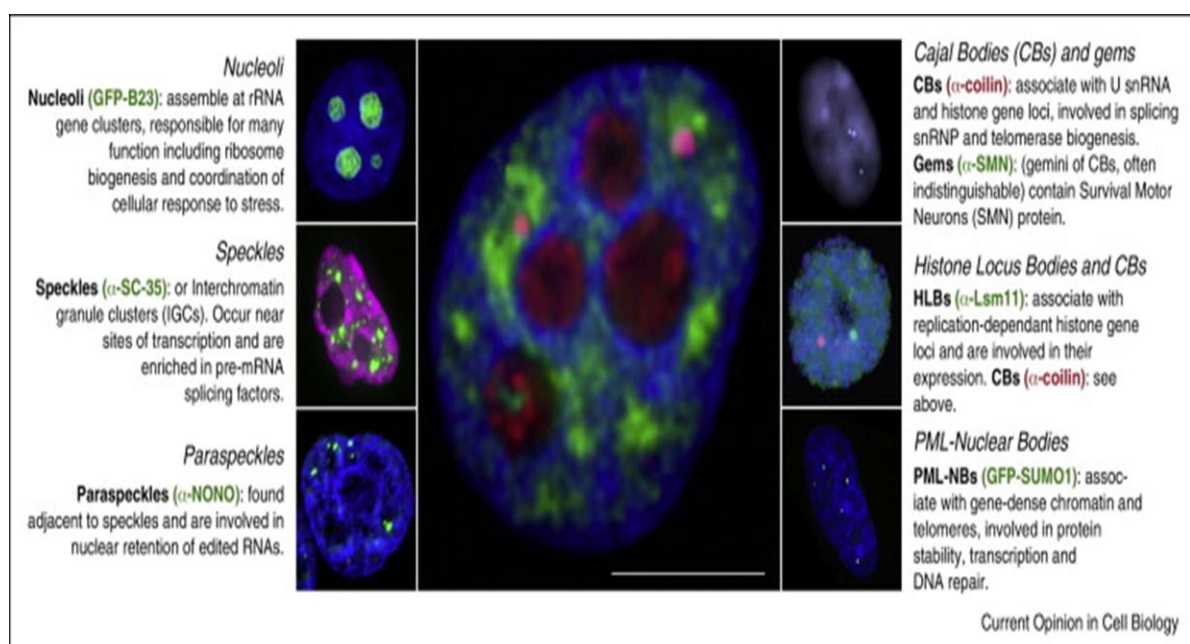


Figure 4 : Major subnuclear bodies. The central panel demonstrates the spatial relationships between different structures in a HeLa cell nucleus. DAPI (blue) and in green or red the protein marker for indicated nuclear bodies shown beside. Adapted from (Sleeman JE, Trinkle-Mulcahy L, 2014).

2.1. Nucleolus

The nucleolus is the biggest structure in eukaryotic cell nuclei. Early biologists noticed the nucleolus prominence over 200 years ago in light microscopy studies of Fontana, Valentin, and Wagner⁴¹. The nucleolus plays a primary role in ribosome biogenesis, including the transcription of ribosomal DNA (rDNA) inside nucleolus by RNAP1, rRNA processing, and modifications⁴². However, recent studies have shown that the nucleolus is a multifunctional nuclear structure that participates in cell cycle regulation, DNA replication, DNA repair, ribonucleoprotein biogenesis, and stress response^{43 42}.

Proteins, DNA, and RNA combine to form nucleoli. Three major components of the nucleolus are (i) The fibrillar center (FC), a clear area ranging from 0.1 to 1 μm ; (ii) the dense fibrillar component (DFC), a more dense area partially surrounding the FC; and (iii) the granular component (GC), mainly formed of granules with a diameter of 15-20 μm loosely distributed.

The rDNA transcription occurs at the boundary between the FC and the DFC. The protein FBL is found in the DFC and plays a role in rRNA processing and the pre-rRNA. The protein nucleophosmin (B23) is located in the GC and is involved in ribosome biosynthesis^{44 45}. An electron microscope can reveal the nucleolus' ultrastructure as shown in (Figure 5), whereas fluorescent protein tagging and fluorescent recovery after photobleaching (FRAP) can reveal its organization and dynamics.

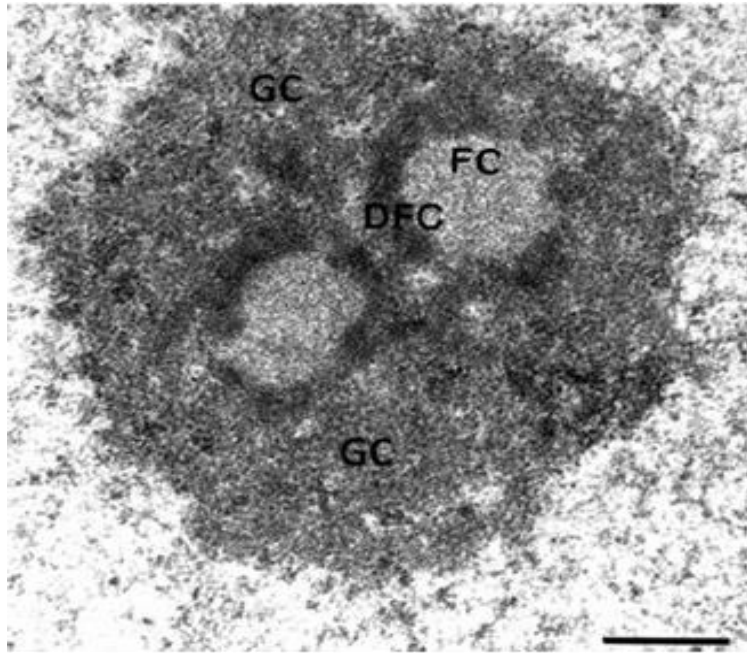


Figure 5 : Organization of the nucleolus in human cells.

Image of the nucleolus obtained by electron microscopy. Fibrillar Centers (FCs) are partially surrounded by the Dense Fibrillar Component (DFC) and embedded in the Granular Component (GC). Scale bar represents 0.5 μm . Adapted from (Sirri et al., 2002).

2.1.1.1. rDNA gene organization

The nucleoli of mammalian cells are disassembled as cells divide and reassembled at the end of mitosis around chromosomal areas of tandemly repeated clusters of rDNA genes called nucleolar organizing regions (NORs). These rDNA gene clusters are located in the short arms of the five acrocentric chromosomes 13, 14, 15, 21, and 22 (Figure 6)⁴⁶.

During mitosis, transcription of RNAP1 is repressed, and the transcription machinery, e.g., the Upstream Binding Factor (UBF) protein, remains attached to rDNA within NORs that were transcriptionally active during earlier interphase⁴⁷.

Nucleolar reassembly by active NORs is directly influenced by RNAP1 transcription at the end of mitosis. In contrast, inactive NORs do not participate in nucleolar reassembly and are not associated with RNAP1 transcription⁴⁸.

After mitosis, active NORs form PeriNucleolar Bodies (PNBs), which are subsequently fused with pre-rRNA processing complexes and nucleolar proteins, such as Fibrillarin (FBL) and Nucleolin, to build the interphasic nucleolus. When rRNA synthesis resumes after cell division, the number of nucleoli may differ between cells. A single nucleolus may form around a single NOR, or several active NORs can associate in a single nucleolus ⁴⁹.

The ribosomal DNA transcription unit is made up of three genes that encode the ribosomal RNAs 18S, 5.8S, and 28S. It exists a fourth rRNA named 5S, which is transcribed outside the nucleolus. Two of the three eukaryotic RNA polymerases (RNAP I and RNAP III) are required. Most rRNA transcripts (28S, 18S, and 5.8S) are transcribed by RNAP I; however, the 5S rRNA subunit (a component of the 60S ribosomal subunit) is transcribed by RNAP III.

The transcription unit includes a 5' External Transcribed Spacer (5'ETS), two Internal Transcribed Spacers (ITS), flanking the 5.8 rRNA, and a 3' ETS. There are 40 tandem replications of the transcription unit, separated by NTIS (Non transcribed Intergenic Spacer), which form the described NORs during mitosis. As a result, 400 copies of the rDNA can be found in every human somatic cell. An upstream Proximal Junction (PJ) and a downstream Distal Junction (DJ) flank the tandemly repeated array of rDNA forming the NOR ⁵⁰ (Figure 6).

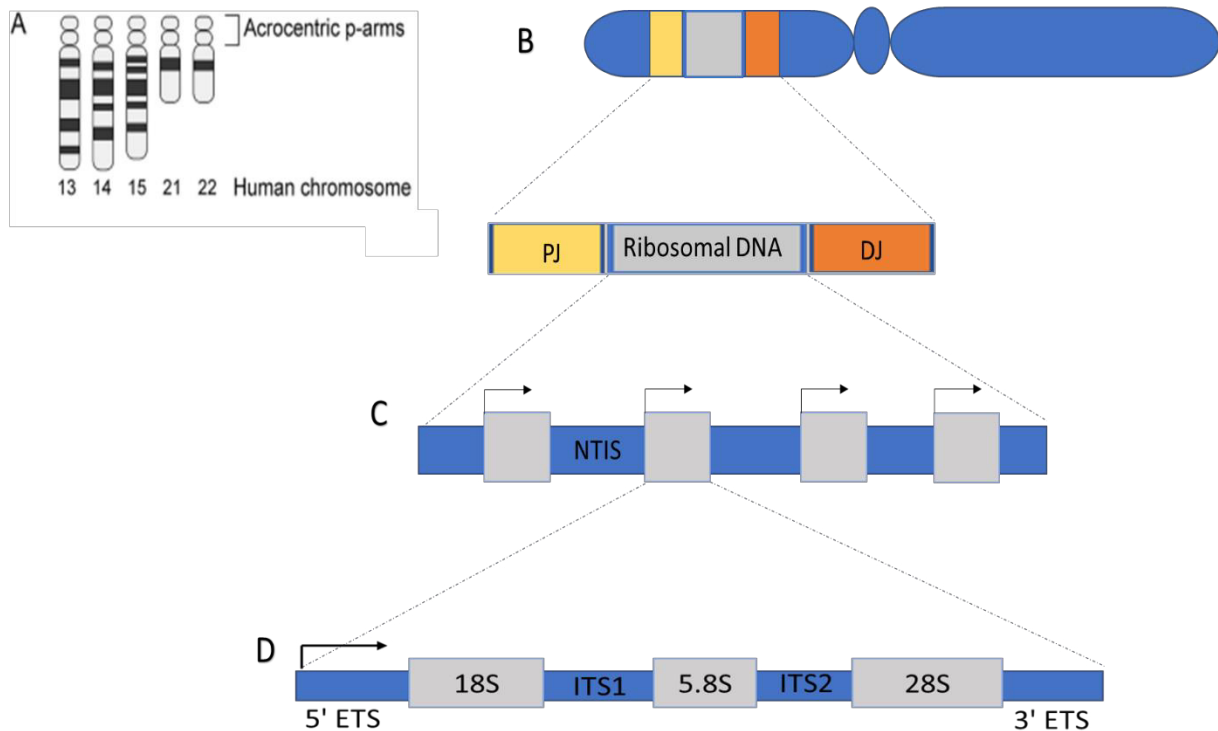


Figure 6 : **Transcription unit of ribosomal DNA**

(A) The five acrocentric chromosomes 13, 14, 15, 21, and 22 represent the NORs (B) The short arm of the acrocentric chromosome represents the rDNA transcription units; they are flanked by Proximal Junction and Distal Junction (PJ & DJ). (C) Each transcription unit is surrounded by Non-Transcribed Intergenic Spacers (NTIS). rDNA transcription unit is composed of three genes: 18S, 5.8S, and 28S, along with External/Internal Transcribed Spacers (ETS & ITS).

2.1.1.2. RNAP1 transcription

As much as 60% of eukaryotic transcription is carried out by RNAP1, even if only half of the rDNA genes are transcribed^{51 52}. In a coordinated manner, RNAP1 transcribes the rDNA genes in the nucleolus as a single unit. This result in the production of a 47S precursor rRNA transcript (pre-rRNA), which is processed and cleaved in different steps to obtain the three final rRNA 28S, 18S, and 5.8S rRNAs⁵³.

Gene promoters of rDNA in eukaryotic cells contain two elements significant for direct and efficient transcription: the Core promoter, essential for basal transcription, and the Upstream Control Element (UCE), located between -156 and -107 nucleotides upstream of the transcription start site (TSS) and responsible for stimulating transcription ⁵⁴.

RNAP1 transcription begins with the formation of a pre-Initiation Complex (PIC) at the promoter. As a component of the RNAP1 transcription machinery, Selectivity Factor 1 (SL1) consists of TBP and four TBP-Associated Factors (TAFs): TAFI110, TAFI63, TAFI48 and TAFI41 ⁵⁵. For RNAP1 to be recruited to the promoter, SL1 must be present, and it promotes a stable interaction between UBF and rDNA promoter ⁵⁶. RNAP1 PIC incorporation is also regulated by the transcription initiation factor RRN3. RRN3 also binds SL1 through its TAF subunits, thus facilitating polymerase recruitment to the PIC ⁵⁷.

The initiating form of RNAP1 is (RNAP1 β), initiates transcription by incorporating the first ribonucleotides into the rRNA sequence. However, for productive transcription, RNAP1 must dissociate from both the PIC complex and the promoter⁵⁸. During the promoter escape event, RRN3 is released from the polymerase. In response to promoter escape, RNAP1 β is converted into its elongation form RNAP1 α . However, effective elongation requires the presence of TFIIF on the rDNA ⁵⁹. SL1 and UBF remain promoter bound after RNAP1 clears the promoter to allow rapid re-assembly of the PIC and re-initiation of a new transcription cycle⁶⁰.

Several proteins are involved in transcription termination, as well as the specific sequence of rDNA that composes the terminator element, which is composed of several termination sites (T1-T10). They are located downstream of the rDNA gene. By binding the termination site, Transcription Termination Factor-1 (TTF-1) causes the polymerase to pause. Ultimately, transcription termination and RNAP1 dissociation from the rDNA is mediated by TTF-1 and the "Pol 1 and Transcript Release Factor" (PTRF), thus facilitating the re-initiation of transcription ⁶¹.

The different steps are shown in (Figure 7).

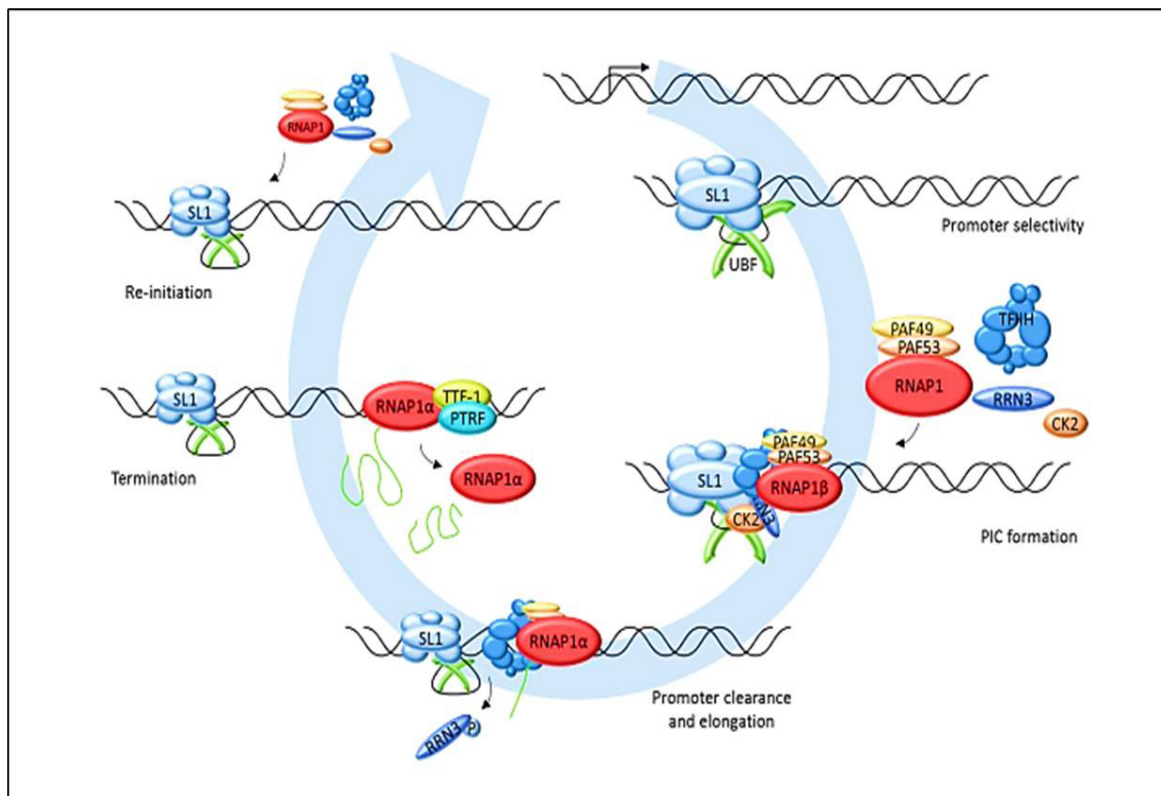


Figure 7 : RNA Polymerase 1 transcription cycle.

Adapted from Elena CERUTTI thesis.

2.1.1.3. rRNA maturation and Ribosome biogenesis

The huge pre-rRNA transcript undergoes several modifications, resulting in mature length rRNAs. The maturation process of pre-rRNA consists of cleavage steps, chemical modifications (pseudouridylation and 2'-O-methylation), and transport (from the nucleolus to the nucleoplasm and the cytoplasm). The maturation is carried out by a large number of snoRNPs (discussed in SMN function part of the introduction), which consists of snoRNAs and their associated proteins ⁶².

Then, the assembly steps generate pre-ribosomal particles. The small and large per ribosome subunits, are exported separately to the cytoplasm where they undergo the final processing stages to become the mature 40S and 60S ribosome subunits. These are formed by assembling the 28S, 18S, and 5.8S rRNAs with ribosomal proteins (RPs). The 40S (small ribosomal

subunit) only includes one rRNA species, 18S, whereas the 60S (large ribosomal subunit) has three rRNA species, 5S, 5.8S, and 28S. The assembly and maturation steps yield mature and functional ribosomes^{63 64 65}.

Ribosomes are macromolecular machinery that performs biological protein synthesis and are found in all cells. Ribosomes bind amino acids together in the order determined by the codons of mRNA molecules to produce polypeptide chains⁶⁶. The significant steps of ribosome biogenesis are shown in (Figure 8).

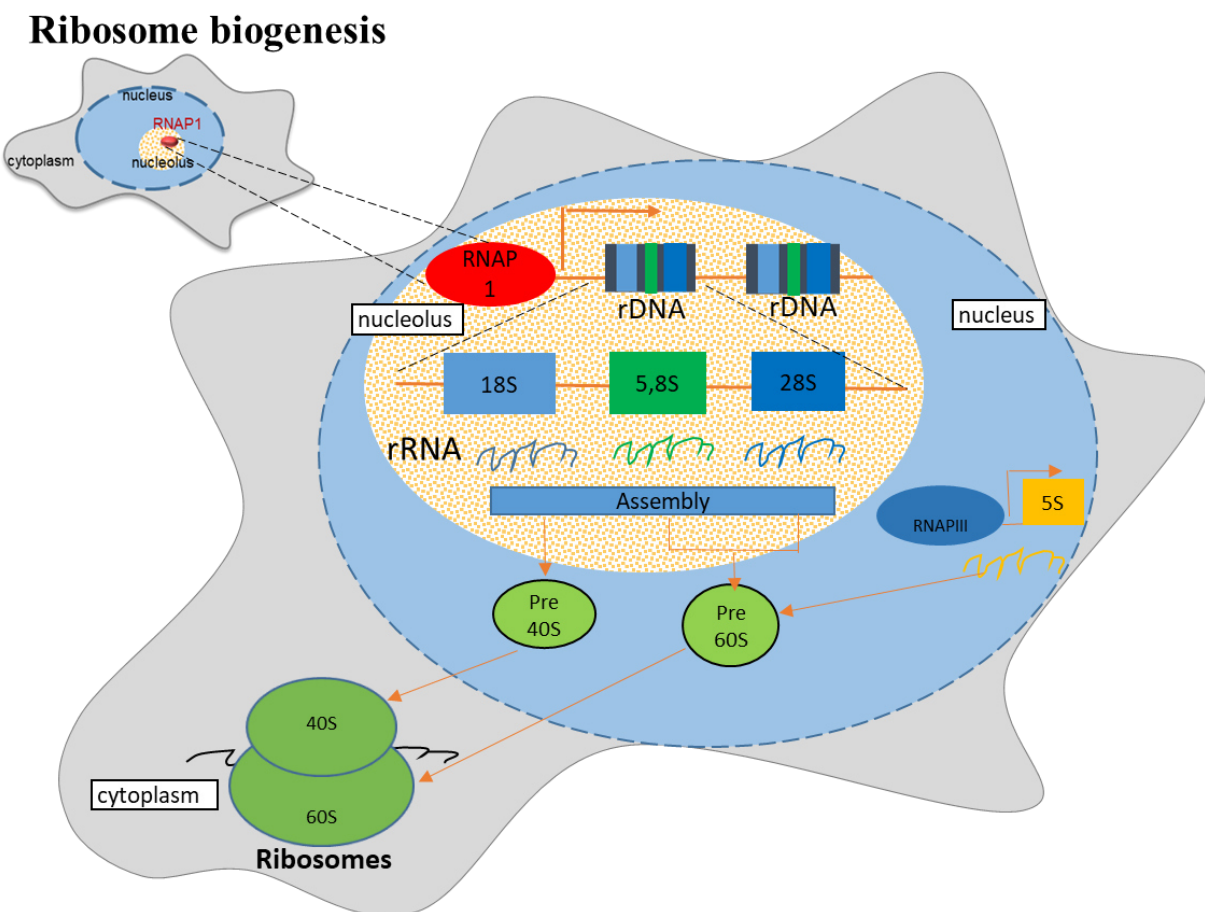


Figure 8 : Ribosome biogenesis.

The transcription of rDNA happens inside the nucleolus by RNAP1. The transcription is then spliced into 3 units the 28S, 5.8S, and 18S transcripts. The 5S rRNA is transcribed outside of the nucleolus by RNAP III. Combined these transcripts lead to the biogenesis of ribosomes: 28S, 5.8S, and 5S form the 60S and 18S forms the 40S ribosomal subunits. Finally, the assembly of the ribosomes in the cytoplasm are essential for protein synthesis.

2.2. Cajal Bodies and Gems

2.2.1.1. Cajal Bodies

Cajal bodies, previously called Coiled Bodies (based on their appearance as coiled threads on electron microscope images), are spherical nuclear bodies approximately 0.2 μm and 2.0 μm consisting of proteins and RNA. They are named after Santiago Ramón y Cajal the father of modern neuroscience, who first reported them in 1903^{67 68}. Generally, CBs are found at the periphery of chromosome territories at a multi-chromosome interface. According to a genome-wide chromosome conformation capture study (4C-seq) using CB-interacting loci, CB-associated regions are enriched in histone genes as well as U (sn/snoRNA) loci that form intra- and inter chromosomal clusters⁶⁹.

It is a dynamic nuclear body. Depending on the cell type and cell cycle stage, the CBs numbers vary (1-6 CBs/cell). Furthermore, not all cell types in adult tissues show CBs. They are generally found in the nucleus of proliferative cells (e.g., embryonic cells, tumor cells) as well as in metabolically active cells like neurons⁷⁰. Interestingly, CBs can be induced even in cells from adult tissues by increasing the relative abundance of small nuclear ribonucleoprotein (snRNP), which is essential for the pre-messenger RNA (pre-mRNA) splicing process⁷¹. snRNP discussed in detail in survival motor neuron (SMN) section.

The snRNP concentration itself depends on the metabolic state of the cell as it's implicated in the spliceosome process.⁷²

Regarding the cell cycle, the maximum CBs number is reached in the early G1 phase, and during G1 progression, they become larger, and their number decrease. In the M phase, CBs disassemble and reassemble in the G1 phase⁷³. Interestingly, the CB components analyzed so far have all been dynamic, with relatively fast turnover rates ranging from a few seconds to a few minutes⁷⁴. CBs are enriched in Coilin, SMN, FBL. As my thesis focused on these proteins more details about them are discussed in the following sections.

CBs are particularly abundant in neuronal nuclei, where they are frequently associated with the nucleolus ^{75 76 77} (Figure 9). In fact, it has been described a relationship between CBs number and neuronal size, so that CB content dynamically adapts to meet the high neural demand for splicing and ribosome biogenesis required to sustain metabolic activity.

For example, CB number varies across different types of sensory ganglion neurons in rats, with a mean number of 1.1 CBs per small neuron, 1.8 per medium neuron, and 2.9 per large neurons ⁷⁸.

As discussed before CBs disassemble during mitosis when transcription is off and reassemble in early G1 when transcription resumes. Accordingly, the behavior of neuronal CBs (post-mitotic cells) is strictly related to the global transcriptional and splicing activity required ⁷³.

Several neurological conditions, including motor neuron diseases, are associated with severe neuronal dysfunction caused by disruptions and loss of neuronal CBs. In particular, CB depletion in motor neurons of patients affected by Spinal Muscular Atrophy (SMA): a genetic neurodegenerative disorder result from a defect in SMN protein.

Interestingly, motor neurons from SMA patient exhibited a reduced number of CBs and a

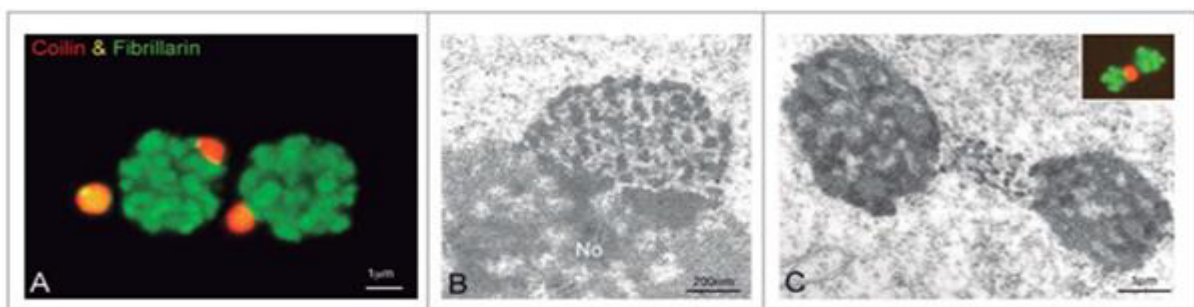


Figure 9 : Association of the CB with the neuronal nucleolus.

(A) Coilin and fibrillarins immunostaining illustrate the close association of CBs with nucleoli in a sensory ganglion neuron. (B) Electron micrograph of a nucleolus (No) attached CB. Note the association of the CB with the DFC of the nucleolus. (C) Electron micrograph of 2 nucleoli physically linked with a CB. (inset) Similar confocal picture co-stained for fibrillarins and coilins. Adapted from (Lafarga M, 2016).

defect in spliceosome maturation by SMN and snRNP ^{79 80}. Besides, SMN is necessary for maintaining the structure of the CBs and its loss severely impacts CB integrity ⁸¹.

2.2.1.2. Gemini of Cajal bodies (Gems)

Gemini of Cajal bodies, or gems and CBs are twins, nuclear organelles displaying identical size and shape and they are nearly indistinguishable under the microscope. However, they differ in some of their protein components:

While CBs are SMN positive and Coilin positive, gems are SMN positive and Coilin negative ⁷⁴. Besides, in fetal tissues and some cultured cell lines, SMN localizes to gems close to CBs ⁸². Instead, in adult tissues and fetal or adult motoneurons, gems do not exist separately from CBs ⁸³.

2.3. The Nucleolus and CBs under Stress

Nucleoli and CBs are key targets of cellular stress response signaling pathways, resulting in complicated alterations in their organization, size, and protein content ⁸⁴. (A summary of different stress types and their effect on nucleolar and CB organization is shown in (Table 3).

The nucleolar reorganization induced by DNA damage (e.g., following UV irradiation) and/or transcriptional suppression (e.g., by actinomycin D) is a well-known phenomenon ^{85 86}. The condensation and subsequent separation of the FC and GC and creation of "nucleolar caps" around the nucleolar remnant characterizes segregation ⁸⁶. Nucleolar proteins such as UBF, nucleoplasm proteins (mainly RNA-binding proteins), and Coilin help construct different types of caps. Moreover, following viral infections (e.g., coronavirus infection) can produce specific changes in nucleolar morphology, such as an increase in nucleolar FC size ⁸⁷.

Different types of stress, such as heat shock, transcriptional suppression, osmotic stress, starvation, and viral infection, also affect the CBs structure.

The majority of stress signals that cause CB disruption also cause transcription inhibition. In particular, UV-C irradiation inhibits snRNA transcription in a p53-dependent manner⁸⁸. This backs up the theory that UV-C-induced CB disruption causes CB activity to be shut down.

However, the redistribution of coilin and other CB components changes according to stress (as shown in (Table 3)). The number of CBs decreases as a result of nutrient stress, whereas UV-C irradiation, osmotic stress, and heat shock reversibly disrupt CBs, as shown by the redistribution of coilin to nucleoplasmic microfoci⁸⁹.

In addition, a subset of UV-C-irradiated cells forms nucleolar caps containing coilin similar to those observed upon inhibition of RNAP1 and II by actinomycin D^{90 86}.

Moreover, Coilin relocates to cap-like structures associated with the nucleolus in cells treated with DRB (5,6-dichloro-1-b-D-ribozimidazole), a kinase inhibitor that inhibits RNAP II transcription.

Stress Type	Trigger	Effects on Nucleolus	Effects on CBs	PubMed ID
DNA damage/ genotoxic stress	UV-C	Nucleolar segregation, delocalization of Ki-67	CB disruption and Coilin in nucleoplasm microfoci	PMID: 14609953 PMID: 15888320 PMID: 17088425
	IR (DSB)	Nucleolar disruption, ATM-dependent inhibition of RNA pol I activity	No major effect on coilin distribution	PMID: 14609953 PMID: 17554310
Temperature change	Heat shock	Nucleolar disruption	CBs smaller at 39 C; micro-CBs in Xenopus	PMID: 14609953 PMID: 7679389 PMID: 11973343
	Cold shock	N/A	CBs bigger at 32 C	PMID: 7679389
Hypoxia		Nucleolar disruption, VHL-dependent reduction of rRNA transcription	N/A	PMID: 14609953 PMID: 17102617
Osmotic stress		N/A	Disruption of CBs	PMID: 17088425
Viral infection	Adenovirus, Coronavirus, HCV, HIV, HPV, HSV-	Changes in nucleolar morphology and proteome	Coilin in nucleoplasmic microfoci and rosettes (adenovirus); ICP0- induced accumulation of	PMID: 19399920 PMID: 8862526

	1, Poliovirus, West Nile virus		coilin at damaged centromeres (HSV-1)	PMID: 20137801
Nutrient stress	Serum starvation	Reduction in ribosomal biogenesis	CB number decreases	PMID: 17041624 PMID: 19815529
Inhibition of RNA Polymerase I and/or II	Actinomycin D	Nucleolar disruption, release of RPs into the nucleoplasm	Coilin in nucleolar caps	PMID: 19114035 PMID: 19362532 PMID: 19878869 PMID: 7679389 PMID: 15758027
	DRB	Nucleolar disruption	Nucleolar association of coilin	PMID: 14609953
	a-Amanitin	Nucleolar disruption	Coilin in cap-like structures associated with the nucleolus	PMID: 14609953 PMID: 7679389
Inhibition of phosphatases	Okadaic acid	N/A	Accumulation of coilin in the nucleolus	PMID: 9013710
Inhibition of DNA and RNA synthesis	5-Fluorouracil	Nucleolar disruption, release of RPs into the nucleoplasm and p53 stabilisation. rRNA	N/A	PMID: 19114035 PMID: 19362532

		processing disrupted in the nucleolus		PMID: 19878869 PMID: 20159984
Alteration of proteasome activity	MG132	No disruption of nucleolar integrity, inhibition of late rRNA processing	No disruption of CBs	PMID: 14609953 PMID: 20159984
	Overexpression of PA28g	N/A	Disruption of CBs	PMID: 17088425
Alteration of snRNP biogenesis	Depletion of SMN, PHAX, TGS1	N/A	Disruption of CBs and nucleolar localization of coilin	PMID: 16687569
	SmB overexpression	N/A	Increase in CB number	PMID: 11792806
Oncogenic stress	c-myc or Ras activation	Upregulation of nucleolar proteins p14ARF and B23/NPM	N/A	PMID: 19543236 PMID: 20208519
Alteration of ribosome subunit biogenesis	Malfunction of nucleolar proteins (e.g., Bop1, B23/NPM, nucleostemin)	Release of RPs into the nucleoplasm following, in most cases, nucleolar disruption.	N/A	PMID: 19287375 PMID: 19114035 PMID: 19362532 PMID: 19878869

Table 3 : Summary of the Effects of Different Stress Types on Nucleolar and CB Organization.

IR, gamma irradiation; DSB, double-strand breaks; HCV, hepatitis C virus; HIV, human immunodeficiency virus; HSV-1, herpes simplex virus type 1; RP, ribosomal proteins; N/A, not available.

2.4. Fibrillarin (FBL), nucleolar and CB-associated protein

Fibrillarin is an essential and highly conserved nucleolar and CB-associated protein that is well known as a molecular marker of transcriptionally active RNAP1. It is a component of snRNP function in RNA splicing and one of the two classes (C/D box) of Small Nucleolar Ribonucleoproteins (snoRNP) operating in ribosomal RNA (rRNA) processing^{91 92}. In the nucleolus, FBL works as a ribose 2'-O-methylase targeting specific sites of rRNA modification by its association with a guide snoRNA that is complementary in sequence to the RNA around the modification site⁹³.

Interestingly, FBL is crucial to restore a proper nucleolar structure after DNA repair completion. Therefore, we studied whether FBL interacting partners were also involved in this process and how. Amongst these different FBL partners, SMN^{94 95}.

In the next two sections, I discussed the Spinal Muscular Atrophy (SMA) and its protein Survival Motor neuron (SMN).

3. Overview of Spinal Muscular Atrophy (SMA)

3.1. Spinal Muscular Atrophy (SMA)

SMA is a genetic autosomal recessive (AR) neurodegenerative disorder that affects nerves and muscles. It is characterized by the degeneration of lower motor neurons from the anterior horn of the spinal cord that controls muscle movement. Loss of motor neurons leads to muscles not receiving nerve signals that make muscles move, and atrophy is a medical term that means shrinkage^{96 97 98} (Figure 10).

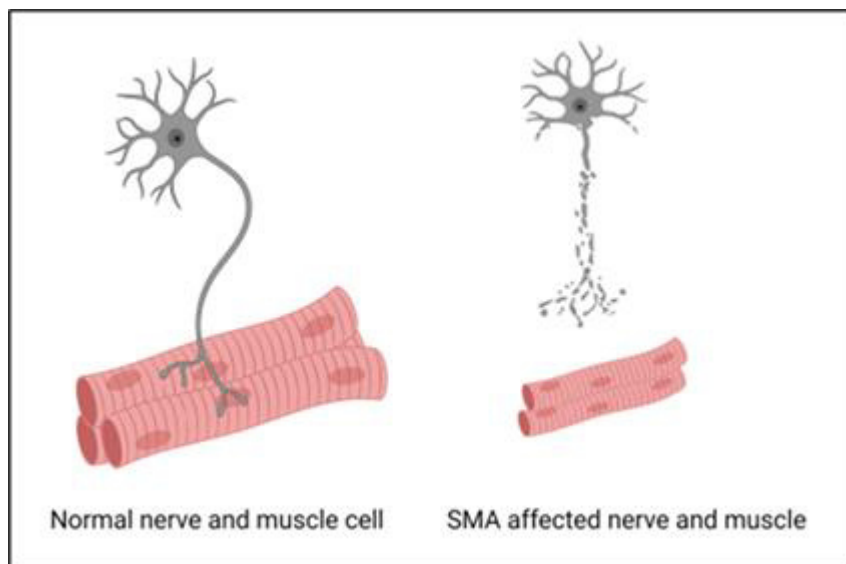


Figure 10 : Degeneration of motor neurons in SMA causes loss of muscle mass and strength (atrophy).

Guido Werdnig in Austria and Johann Hoffmann in Germany were the first to describe SMA in 1891 and 1893 respectively. It is the second most common AR condition in humans behind cystic fibrosis. It is the most common cause of childhood hereditary lethal disorder, usually leading to death within the first year of life⁹⁹. SMA is a disease that affects people worldwide, with an allele carrier frequency of about 1 in 35 and an incidence of 1:6,000–1:10,000 in the general population¹⁰⁰.

3.2. Genetics of SMA

In 1990, a new age of molecular understanding of SMA began. Two research groups found the location of the gene causing SMA on chromosome 5q^{101 102}. Then, in 1995, the gene *SMN1* (Survival Motor Neuron 1), located on chromosome 5q13.1 was identified as the main locus mutated in SMA¹⁰³, and mutations on this gene are carried by every 40 to 60 individuals.

If a child is born from two carrier parents (Figure 11):

1. Their child has a 1 in 4 (25%) chance of not having SMA and not being carriers.
2. Their child has a 1 in 2 (50%) chance of being carriers of the defective SMN gene but not having SMA.
3. Their child has a 1 in 4 (25%) chance of having SMA. (Two copies of a missing or faulty (mutated) survival motor neuron 1 (*SMN1*) gene). Illustrated in (Figure 13).

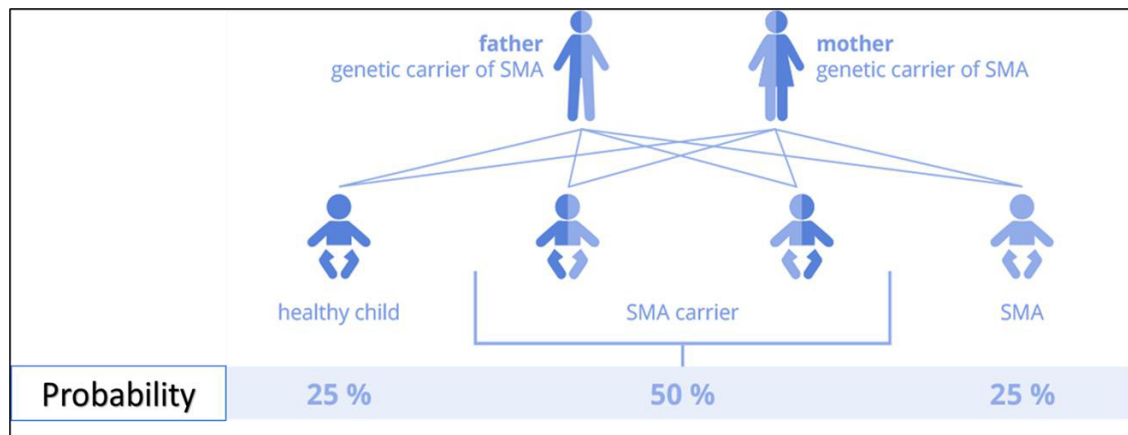


Figure 11 : Autosomal recessive inheritance of SMA and probability to have SMA child.

95% of cases of SMA are caused by homozygous disruption of the SMN1 locus^{103 104}. Moreover, mutations in all domains of SMN have been linked to SMA outlined in (Figure 12). Indeed, 2% de-novo mutations have been described in one of the 2 alleles¹⁰⁵. Nonetheless, the carrier frequency of *SMN1* deletions varies by ethnicity, with Asians having the greatest carrier frequency (2.4 %) ¹⁰⁶.

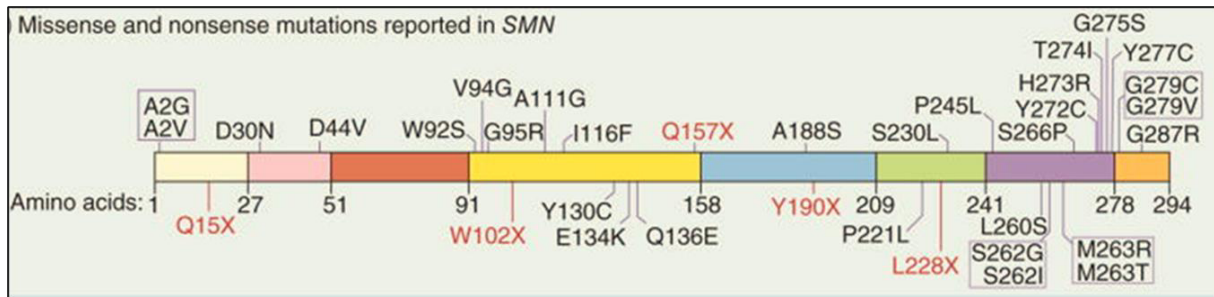


Figure 12 : Missense and nonsense mutations of SMN.

Diagrammatic presentation of SMN1 exons are presented as colored boxes with the number of amino acids noted within each box. Position and type of mutations are indicated, with missense mutations shown in black and nonsense mutations shown in red. Amino acids are represented by their one-letter codes. The presentation is adapted from (Howell MD, 2014).

Besides, in humans a duplication of the *SMN1* gene resulting two copies: (i) a telomeric copy (*SMN1*), the leading cause of SMA, and (ii) an inverted duplication in the same region of *SMN1*, for a second centromeric copy of the gene termed (*SMN2*). These *SMN1* and *SMN2* genes differ by a single nucleotide change mapping in exon 7. Thus, exon 7 of *SMN2* differs from *SMN1* counterpart by a C-to-T transition, causing the skipping of this exon during splicing in approximately 85.90% of the transcripts and resulting in the formation of a truncated protein that is unstable and rapidly destroyed^{107 108 109} (Figure 13).

However, the *SMN 2* locus still accounts for the production of roughly 10-15% of the total full-length (FL) SMN protein pool (Figure 13).

Thus, in SMA in patients, SMN2 produces only a small quantity of SMN protein. Loss of the SMN2 does not cause SMA however, the copy number of SMN2 is known to be inversely associated with the severity of SMA disease^{110 111} (Figure 13).

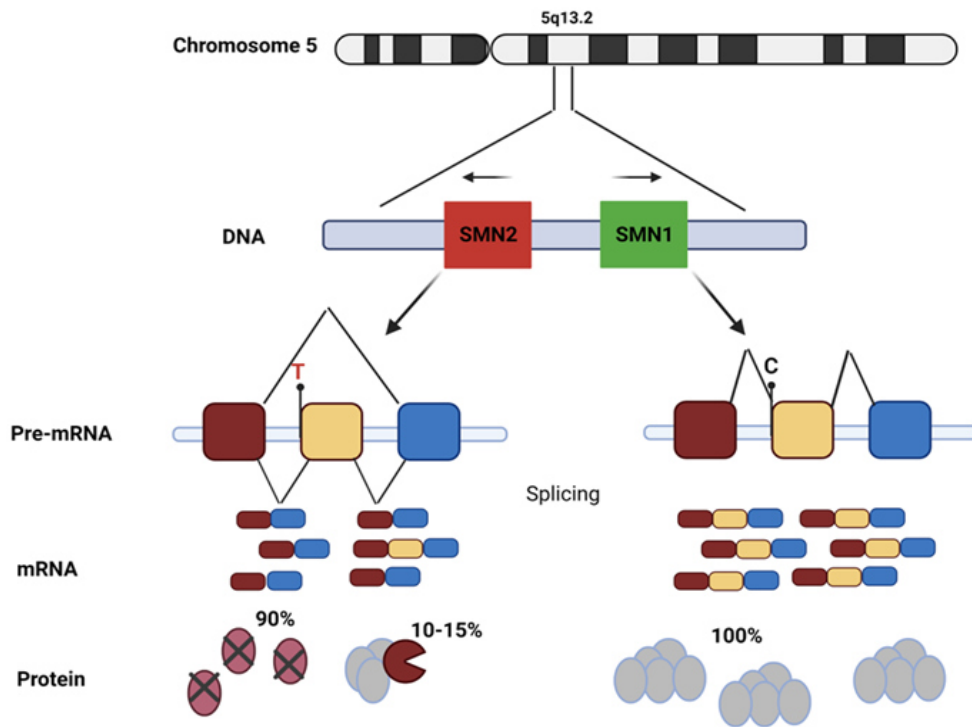


Figure 13 : Human SMN1 and SMN2.

The single nucleotide difference in exon 7 (C or T as indicated) of *SMN1* and *SMN2* genes affects their splicing. The single nucleotide change from C to T drastically reduces the efficiency of exon 7 inclusion and increases the production of the truncated mRNAs and proteins.

3.3. Symptoms and clinical Classification of SMA Subtypes

SMA is known as a multisystem disease that affects the skeletal muscle, heart, kidney, liver, pancreas, spleen, and immune system. Nevertheless, the classical presentation of muscle weakness and atrophy in SMA is caused by the degeneration of spinal cord motor neurons. The typical symptoms of SMA include floppy or weak arms and legs, movement problems (such as difficulty sitting up, crawling, or walking), bone and joint problems (such as an unusually curved spine), swallowing problems, and breathing difficulties. However, SMA does not affect intelligence or cause learning disabilities.^{112 113 114 115} . As summaries in (Table 4), the disease progression and severity rates differ between patients. Therefore, SMA has traditionally been classified into types 0–4 based on symptom severity, onset age, and the number of *SMN2* copies.

Some classifications define type 0 SMA with prenatal onset. Patients have, only one copy of *SMN2*. Decreased intrauterine movements may be felt prenatally during pregnancy. Patients have widespread weakness, hypotonia at birth, respiratory difficulties, and poor feeding. Life expectancy is reduced, the fetuses die in utero or soon after birth, some die within weeks of delivery, and most are unable to survive beyond 6 months of age without achieving any motor milestones^{116 117} .

Type 1 SMA (severe) (OMIM N° 253300), is the most prevalent form and the most severe phenotype, with about 45 % of cases. The onset of symptoms around 0–6 months of age. A 'floppy infant' displays symptoms such as flexion, proximal predominant limb weakness, respiratory insufficiency, and poor feeding. Patients could not gain the capacity to sit independently.

SMA type 1 is the main hereditary cause of death in early infancy, with a life expectancy of under 2 years without medication treatment.

Most SMA type 1 have one to two copies of SMN2 ^{116 118 97}.

Type 2 SMA (Intermediate) (OMIM N° 253550), which accounts for 30% of cases, manifests as weakness between the ages of 6 and 18 months. SMA type 2 has three *SMN2* copies. Patients frequently get the capacity to sit unassisted by 9 months, but they may lose this skill later and never be able to stand or walk on their own ^{116 119}.

Type 3 SMA (mild) (OMIM N° 253400), from 18 months to adulthood, accounts for 15% of all cases. They are distinguished by the ability to stand or walk without assistance ¹¹⁶. However, this capacity may deteriorate as the disease progresses. Patients have 3 and 4 copies of *SMN2*.

Type 4 SMA (very mild) (OMIM N° 271150), represent < 5% of SMA cases, with onset at 30 years or more. The milder type 4 patients usually present patients have more than 5 copies of *SMN2* ¹¹⁶.

SMA type	Type 0	Type 1	Type 2	Type 3	Type 4
Age of onset	Prenatal	Before 6 months	7–18 months	After 18 months	Second or third decade
Milestone achieved	Need respirator from birth	Unable to sit	Sit, never walk	Stand and walk independently	Walking during adulthood
SMN2 copy numbers	1	2	3-4	3-4	More than 5
Life expectancy	Less than 6 months	Less than 2 years	More than 2 years	Adult	Adult

Table 4 : Clinical classification of SMA subtypes according to onset, milestones achieved, and clinical, typically associated SMN2 copy numbers and life expectancy.

3.4. Mechanism

3.4.1.1. SMA and Motor Neuron

SMN is found in high concentrations in the spinal cord, brain, kidneys, and liver, moderate concentrations in skeletal and cardiac muscle, and low concentrations in fibroblasts and lymphocytes. A significant decrease of almost 100-fold in SMN level in type I SMA in the spinal cords is consistent with the features of this motor neuron disease ¹²⁰. Moreover, the SMA fetuses with severe muscle degeneration had smaller myotubes, indicating delayed muscle maturation and growth ¹²¹.

The SMN protein has an established function in small nuclear ribonucleoprotein (snRNP) assembly, which is essential for the pre-messenger RNA (pre-mRNA) splicing process ⁷¹. (The SMN functions are explained in detail in the next part of the introduction). Therefore, the standard hypothesis about the selectivity of SMA for motor neuron degradation is that the SMA disease progression may be influenced by pre-mRNA splicing. Alternatively, it has been proposed that in SMA, mRNA localization to these distal processes is disrupted because motor neurons have highly specialized, long-extending axons, which could be a source of motor neuron degeneration selectivity ¹²².

3.4.1.2. SMN and Signaling pathways implicated in neurodegeneration

As a result of insufficient SMN, neurons cannot survive and maintain essential cellular functions leading to the activation of intracellular stress signaling pathways that can contribute to neurodegeneration in SMA. Furthermore, SMN has been shown to interact with components of different signaling pathways and biological processes. Therefore, some studies investigated the reduction of SMN and its possible role in neurodegenerative pathways.

One study examined the activity of different Mitogen-Activated Protein Kinases (MAPKs) in spinal cord of human SMA. The activation of c Jun NH2-Terminal Kinases (JNKs) was discovered throughout this screening ¹²³.

JNK family has been shown to play essential roles in neuronal cell growth, differentiation, apoptosis, synaptic plasticity, and memory. This family of MAPK is encoded by three genes, Jnk1, Jnk2, and Jnk3. The Jnk1 and Jnk2 genes are ubiquitously expressed, but the Jnk3 gene is predominantly expressed in neurons and a minor amount in the heart and testis ^{124 125}. Reduced SMN levels in SMA mice cultured spinal cord motor neurons, as well as SMN knockdown by RNA Interference (RNAi) have been related with JNK3 activation, which contributes to motor neuron death. In line with that, Jnk3 deletion improves the phenotype in mice with a SMN depleted for exon 7 (SMN Δ 7), this improvement is not related to an increase of SMN protein. As a result, SMA phenotype amelioration in SMN Δ 7 mice by JNK3 deficiency is independent of the SMN, and SMN appears to function via JNK3 upstream regulators ¹²³.

RhoA/ROCK signaling is required for regulating cytoskeleton dynamics necessary for neuronal growth, differentiation, retraction, and degeneration. Activity changes in RhoA/ROCK downstream targets, including profilin IIa, are associated with many human conditions. Interestingly, it has been demonstrated that SMN interacts with profilin IIa which promotes actin polymerization ¹²⁶. Knockdown of SMN induces the activation of RhoA/ROCK and changes the phosphorylation status of its downstream targets, such as profilin IIa resulting in a free pool of hyperphosphorylated profilin IIa ¹²⁷. Interestingly, pharmacological inhibition of RhoA/ROCK using inhibitors (Y-27632 or Fasudil) increased the lifespan in a mouse model of intermediate SMA (Smn2B/-) ¹²⁸. However, this increase in the lifespan is without a significant change in SMN transcription and protein levels ¹²⁸; therefore, this inhibition may help only to stabilize the actin cytoskeleton and improve the functionality of SMN-deficient neuronal.

The ubiquitination pathway governs axonal and synaptic stability and SMN degradation^{129 130}
¹⁰⁹. Physical interaction between Ubiquitin-Like Modifying Activator 1 (Uba1) and SMN is observed in neuronal cytosol. SMN is also involved in ubiquitin homeostasis since Uba1 is significantly reduced in the spinal cord of severe SMA mice¹³¹. Consistently, restoration of Uba1 in zebrafish and mouse models of SMA has been demonstrated to ameliorate disease pathology¹³².

Interestingly, dysregulation of Uba1 is often accompanied by an accumulation of β -catenin, a substrate for ubiquitination. It appears that this effect is tissue-specific as an increase in β -Catenin is observed only in the spinal cord and not in the heart or liver. But it remains to be determined whether the increased levels of β -catenin alter the expression of specific genes that contribute to SMA pathogenesis¹³¹. A graphical model representing the signaling pathways implicated in neurodegeneration in SMA is shown in (Figure 14).

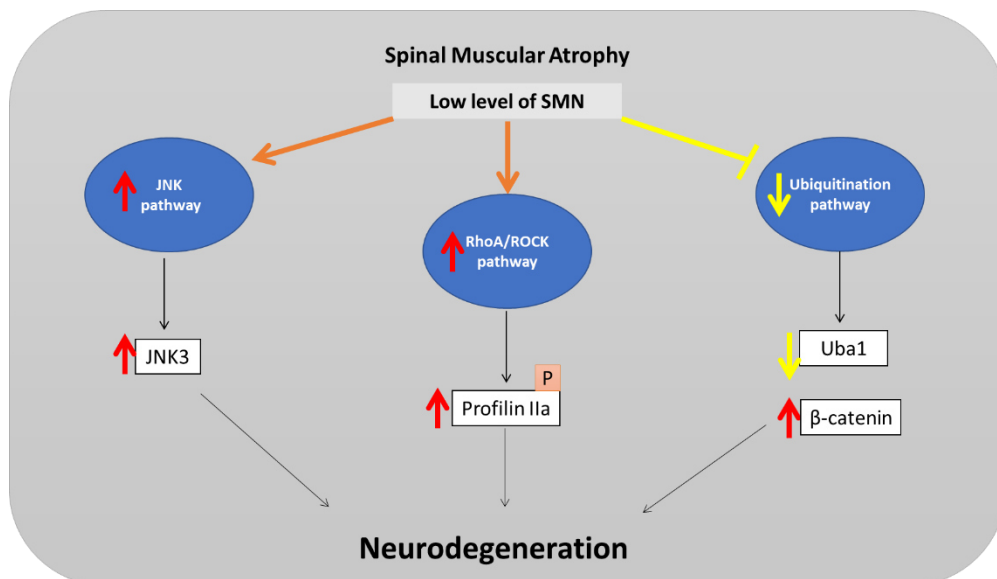


Figure 14 : Signaling pathways implicated in neurodegeneration in SMA.

3.4.1.3. SMA as a Multi-System Disorder

Although SMA is a motor neuron disease, the SMN protein is found in almost all tissues. SMA is known as a multisystem disease that affects the skeletal muscle, heart, kidney, liver, pancreas, spleen, and immune system. In SMA patients, especially in the more severe subtypes, congenital heart malformations, cardiac rhythm irregularities, sleep disturbances, reduced renal function, and pancreatic deficiencies have all been reported^{113 115 114}. Therefore, a range of healthcare professionals, such as specialist doctors, physiotherapists, occupational therapists, and speech and language therapists, are among the healthcare experts involved in SMA care.

3.5. Diagnosis of SMA

In general, a physical exam and a medical history are essential to diagnose SMA. More tests can be used to confirm the diagnosis; (i) Blood test: to check Creatine kinase levels, this enzyme is released into the bloodstream by degrading muscles. (ii) Genetic blood test (test): more specific that looks for the SMN1 gene. (iii) Nerve conduction test: by doing an electromyogram (EMG) to examines the electrical activity of nerves muscles, nerves, and muscle biopsy. However, according to the last recommendations for diagnosis, SMA in a typical case is diagnosed only through genetic testing for SMN1/SMN2 is the initial examination linen. A muscle biopsy is not required in the majority of cases (Figure 15)¹³³.

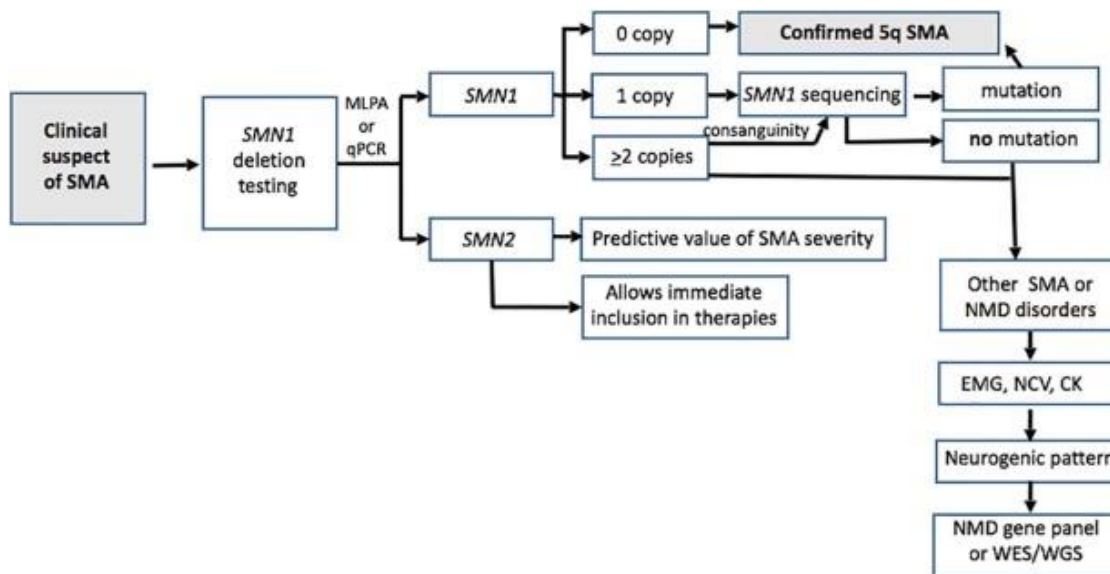


Figure 15 : Diagnostic algorithm for SMA. (SMA: spinal muscular atrophy; MLPA: Multiplex Ligation-dependent Probe Amplification; qPCR: quantitative polymerase chain reaction; SMN1: survival motor neuron 1; SMN2: survival motor neuron 2; NMD: neuromuscular disorders; EMG: electromyography; NCV: nerve conduction velocity; CK: creatine kinase levels; WES: whole exome sequencing; WGS: whole genome sequencing). The presentation adapted from (Mercuri E, 2018).

3.6. Treatment of SMA

The journey from gene discovery to therapy of SMA has been difficult, but it has also resulted in one of neurogenetics' most significant success stories. Although there is no cure, treatments can reduce some symptoms and prolong the patient's life. Researchers are working to find new ways to fight this disease. Therefore, in addition to these approved treatments mentioned below several other treatments are being explored in clinical trials ¹³⁴.

Three different treatments have been introduced and approved by the US Food and Drug Administration (FDA) in the last 4 years: nusinersen and risdiplam as disease-modifying therapy and onasemnogene abeparvovec, a gene replacement therapy. All three increase the production of SMN, by using different mechanisms of action. Each improves the patient's motor function and length of life. FDA-approved SMA drug therapies are summarized in (Table 5).

3.6.1.1. Spinraza® (nusinersen)

Spinraza® is the first drug approved for SMA treatment by the (FDA) in December 2016 and by the European Medicines Agency (EMA) in May 2017. Therefore, it was the first therapy in Europe to receive marketing authorization in 2017. Spinraza® was Developed by Novartis Gene Therapies and works for all SMA types of all ages ¹³⁵. Its active ingredient, nusinersen, is an antisense oligonucleotide that acts on *SMN2* gene splicing to increase the generation of functional SMN protein. It is delivered intrathecally (lumbar puncture); by injecting the drug into the space around the spinal canal.

3.6.1.2. Zolgensma® (onasemnogene abeparvovec)

Zolgensma® is a gene therapy medication that addresses the disease's underlying molecular defect. It was developed by Biogen and Ionis and approved for children below 2 years ¹³⁶. It works by intravenous infusing of a solution comprising an AAV (Adeno-Associated Virus) viral vector and a transgene with a functional copy of the *SMN1* gene.

3.6.1.3. Evrysdi® (ridsiplam)

Evrysdi® is a small molecule that influences the maturation of *SMN2* messenger RNA, allowing it to recombine the missing exon 7 and produce a fully functioning SMN protein. It was developed by Genentech, a member of the Roche Group, and approved for SMA treatment in adults and children aged 2 months or older. The treatment is given by mouth (orally) once a day at home. In March 2021, Evrysdi® received marketing authorization in Europe ¹³⁷.

Product	Spinraza® (nusinersen)	Zolgensma® (onasemnogene abeparvovec)	Evrysdi® (ridisiplam)
Mechanism	Repairs <i>SMN2</i> gene to produce a more functional protein	Replace missing/defective <i>SMN1</i> gene	Repairs <i>SMN2</i> gene to produce a more functional protein
Administration	Intrathecal injection	intravenous infusion	oral
Dossing	Every 4 months	once	daily
Age to take	All ages	< 2 years old	>2 months
Annual cost + duration	\$750.000 in first year, then \$375.000 lifetime	\$2.1m once	Up to \$340.000 lifetime

Table 5 : The approved SMA drug therapies.

3.7. Genetics models of SMA

Because of the complexity of SMN protein functions and the severity of SMA, there was an indispensable need for genetic models to improve our understanding of the pathophysiology of SMA. In vitro (ex vivo) models are particularly valuable for elucidating SMA's molecular mechanisms and testing possible early treatments. In vivo models are helpful for both understanding the phenotype of SMA and testing prospective therapies.

3.7.1.1. Ex vivo models of SMA

To create ex vivo models, SMN was silencing by different technique: (i) small interfering RNA (siRNA) against SMN to cells for a fast and efficient but short-term protein depletion ¹³⁸. (ii) CRISPR Plasmids have been used for SMN gene knockout. Moreover ¹³⁹, (iii) SMN shRNA

Plasmids or SMN shRNA Lentiviral Particles followed by puromycin selection are also used for stable SMN silencing, as I used in my experiments shown in the results chapter.

Moreover, SMA patient fibroblast cell lines for types I, II, and III commercially available on Coriell Institute for Medical Research (<https://catalog.coriell.org/Search?q=SMA>) are referred in a large number of publications. The SMA I fibroblast cell line was also used in my work in the results chapter. Furthermore, non-neuronal cell lines have also been used to study the SMN2 splicing, such as human embryonic kidney cells 293 (HEK293) cells and human HeLa cells^{140 141}.

Nevertheless, human neuronal cell lines were required as a cell therapy since the early death of motor neurons is a characteristic of SMA, but patient neuronal cells are inaccessible. Induced pluripotent stem cells (iPSC) technology has recently achieved motor neuron cellular models from SMA patient cells. By dedifferentiating any type of cell back into an embryonic-like cell that retains self-renewal capabilities multilineage differentiation, upon expressing of various reprogramming factors ectopically, the cells dedifferentiate acquiring embryonic stem cells (ESCs) features. In 2009, the first SMA iPSC line was created by reprogramming dermal fibroblasts from a Type 1 SMA patient and his healthy mother. As a result of the loss of SMN1, the SMA iPSCs had lower SMN protein levels than control iPSCs. Selective motor neuron death and reduced soma size phenotypes were observed in this cell line¹⁴².

3.7.1.2. In vivo models of SMA (Animal Models)

SMA develops only in humans because have two *SMN* copies (*SMN1* & *SMN2*)¹⁴³. In all animal and yeast models tested so far, they have only one copy of SMN, which is required for cell survival. For example, in the mouse model, the SMN deficiency causes early embryonic lethality¹⁴⁴. However, the human specific *SMN2* paralog is thought to rescue the embryonic lethality caused by *SMN1* homozygote disruption¹⁴³. In fact, all available animal models of

SMA have been generated by introducing the human *SMN2* copies, *SMN2* complementary DNA (cDNA), and mutations that encourage exon 7 skipping or decrease *SMN* functionality¹⁴⁵¹⁴⁶¹⁴⁷. This section discusses the most contributed and used animal models in the SMA field (Mouse, Zebrafish, *C. elegans*, and *Drosophila*) but not all.

3.7.1.2.1.1. Mouse Models

SMA has been studied using the mouse model to understand its basic pathogenesis and evaluate potential treatments. Over the years, many mouse models have been developed, displaying varying degrees of disease severity. Some of the most commonly used mouse models are summarize in (Table 6). The mouse *Smn1* protein is 82% identical to its human ortholog (Figure 16). As mentioned previously, *Smn1* is vital for survival in mice; therefore, embryonic lethality is associated with the complete knockout (*Smn*^{-/-})¹⁴⁴.

Instead, heterozygous mice (*Smn*^{+/-}) do not display a typical SMA phenotype¹⁴⁴. Likely because a reduction in *Smn1* levels > of 85 is required manifest the SMA phenotype¹⁴⁵.

The human *SMN2* produces ~10-15% FL *SMN2* transcript; it can overcome the lethality of *Smn1* knockout in mice and replicate the situation found in humans with SMA. A genetically modified mouse model has been created with the human *SMN2* transgene inserted into fertilized non-transgenic mouse oocyte. Adult mice homozygous for *Smn* gene deletion containing *SMN2* transgene were bred with heterozygous *Smn*^{+/-} mice to produce *Smn*^{+/-}; *SMN2*. Interbreeding of these mice then gave rise to severely afflicted mice *Smn*^{-/-}; *Tg*^{*SMN2/SMN2*} with (two copies of the transgene), known as the severe SMA mouse model. Interestingly, the *SMN2* copy number can determine the severity of this mouse model, as it does in humans. These mice have a 4–6day lifespan. Severe SMA mice have a substantial neuromuscular phenotype with decreased weight, limb tremors, and difficulty to right themselves.¹⁴⁶¹⁴⁷.

Moreover, second mouse model for SMA was generated by introducing a copy of the human SMN Δ 7 allele into a mouse *Smn*^{-/-} background carrying also the human *SMN2* transgene (*Smn*^{-/-}, Tg^{SMN2;SMN Δ 7/ Δ 7}) mice were generated ¹⁴⁸. By expressing an additional partially functional human SMN Δ 7 protein that increases the survival rate. These SMA mouse models less severe than the previous, although pups do not survive past the first two post-natal weeks (~14 days); the neuromuscular symptoms begin at P5 and progress slowly, compared to the other mouse models. The SMN Δ 7 SMA mice had trouble moving at P10, with abnormal gait and limb tremors. All of this is accompanied by a significant loss of motor neurons. Therefore, they are only suited for modeling severe infantile SMA and do not represent the chronic phase of the disease ¹⁴⁸.

Another way to overcome the lethality of SMN knockout in mice is the Cre-loxP system (used to drive tissue-specific DNA modification). It is a powerful tool for studying *Smn1* role in specific tissues. By crossing two transgenic mice lines, one with the *Smn1* gene flanked by two loxP sites and the other with a Cre recombinase transgene driven by a tissue specific promoter. A novel transgenic line with the *Smn1* gene deleted exclusively in tissues expressing the above-described promoter is obtained. This strategy has been used to knockdown *Smn1* in either muscle or neurons.

Neuron-specific knockout of *Smn1* leads to progressive degeneration of motor neurons ¹⁴⁹, while muscle-specific knockouts display progressive muscle necrosis resulting in dystrophy and death. This observation from muscle specific *Smn1* mutant mice points to the primary involvement of skeletal muscle in human SMA, which may contribute to motor defects in addition to motor neuron degeneration ¹⁵⁰.

Another approach to produce SMA mouse model has been to manipulate the mouse *Smn1* gene to mimic the human *SMN2* gene. In order to disrupt endogenous *Smn1* mouse splicing, a knock-in allele was used. *Smn1* mimic gene have been developed that include either wild-type *Smn1* exon 7 or altered exon 7 containing a C to T nucleotide transition. Unlike the wild-type mimic gene that produces only FL-SMN, the modified mimic gene produces *Smn1* with exon 7 alternatively spliced. A mouse model of SMA type II/III is thus derived, termed the 2B mouse, whose life expectancy is approximately 28 days. This model exhibits mild to moderate disease pathology¹⁴⁵.

Mouse line	Lifespan	Phenotype	Reference	Jackson Stock #
Smn1 knockout (Smn^{-/-})	Embryonic lethal	Mice with homozygous SMN disruption display massive cell death during early embryonic development	(Schrank et al., 1997).	006214
Severe (Smn^{-/-}; SMN2^{+/+})	4-6 days	Low birth weight, decreased movement, tremoring limbs, and labored breathing. Normal numbers of motor neurons at birth but motor neuron loss observed by P5	(Hsieh-Li et al., 2000; Monani et al., 2000)	005024
SMNΔ7 (Smn^{-/-}; SMN2^{+/+}; SMNΔ7^{+/+})	14 days	<u>The most widely used model in the field.</u> By P5, signs of muscle weakness appear and become progressively more pronounced with an abnormal gait, and shakiness in the hind limbs. Severe NMJ defects and loss of over 50% of spinal motor neurons by P10, but slightly less severe by then (Smn^{-/-}; SMN2^{+/+})	(Le et al., 2005)	005025
Neuron specific Smn1 exon 7 deletion	25 days	Tremors and muscle denervation	(Frugier et al., 2000)	006146
Muscle specific Smn1 exon 7 deletion	33 days	Severe muscle defects and paralysis	(Cifuentes-Diaz et al., 2001)	006149
Moderate Smn2B (Smn2B^{-/-})	18-30 days	Motor neuron pathology observed by P21	(Bowerman et al., 2012a)	034496

Table 6 : The SMA mouse models. P for the postnatal day.

3.7.1.2.1.2. Danio rerio (Zebrafish)

Zebrafish are used for neurogenetics research because of their conserved simple nervous system, and because the larva it is transparent, enabling in vivo imaging and motor studies. Zebrafish possess only one *smn1* gene as the other animal models, with 47% identical to the SMN1 human ortholog as shown in the alignment work done in (Figure 16). *smn1* gene homozygous mutant zebrafish display abnormal neuromuscular junctions and die during development¹⁵¹. Modified antisense oligonucleotide termed morpholinos (MOs) can be used to manipulate gene expression in zebrafish. MOs inhibit the translation of their target mRNA, thus inhibiting protein production. 61% decrease in *smn1* protein level was observed by this method. Besides, *smn1* knockdown by siRNA in zebrafish can recapitulate many aspects of motor neuron defects in SMA disease, including truncation and ectopic branching of motor axons. Indeed, the expression of wild-type *smn1* rescues these motor neuron defects¹⁵¹.

3.7.1.2.1.3. Caenorhabditis elegans

Caenorhabditis elegans (*C. elegans*) has been an effective model for studying gene functions associated with diseases and a good tool for rapidly investigating molecular pathways. In the *C. elegans* genome, the *SMN1* ortholog is *smn-1*, which encodes an SMN protein 22% identical to the SMN1 human ortholog as shown in (Figure 16). Gene knockdown can be quickly and easily achieved in the *C. elegans* only by feeding them with siRNA. Like the other model, *smn-1* in *C. elegans* is necessary for survival; a reduction in *smn-1* expression by siRNA leads to larval death¹⁵². Furthermore, mutations the *C. elegans smn-1* ortholog deleting most of its coding region result in developmental arrest, reduced lifespan, and progressive loss of motor functions. Interestingly, a transgene encoding *smn-1* expressed in neurons partially restores the

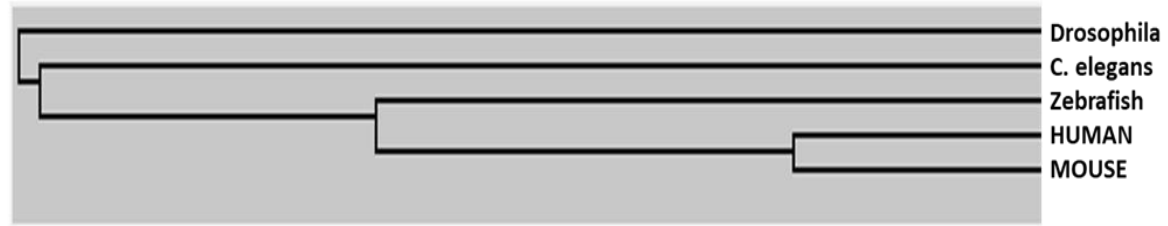
developmental arrest and motor defects, whereas muscle-specific transgenic expression does not, suggesting that *C. elegans* mn-1 predominantly functions in neurons ¹⁵³.

3.7.1.2.1.4. Drosophila melanogaster (fruit fly)

Similar to previous animal models discussed here and unlike humans, *Drosophila* contains only one survival motor neuron gene, *Smn*, with 22% protein identical to its human ortholog (Figure 16). Due to the maternal contribution of *Smn* protein, homozygous null *Smn* *Drosophila* survives beyond embryogenesis; then *Smn* is no longer being produced by the mother during the larval stage. Therefore, the animals exhibit progressively reduced motility, coordination, and growth, eventually leading to death before or at the pupal stage ^{152 154}.

Furthermore, point mutations in *Drosophila* *Smn* show motor neurons and muscle function defects. The flies exhibited axonal damage in the motor neurons innervating the flight muscles and actin disorganization ¹⁵⁴.

While, in humans, the most established role of SMN is the spliceosomal snRNPs assembly, which is essential for RNA splicing ⁷¹. (SMN roles are discussed in detail in the next section of the introduction). Interestingly, snRNP did not seem to be affected by SMN depletion in *Drosophila*. Thus, it appears that the effects of *Smn* on small nuclear RNAs might be species-specific ¹⁵⁵.

A**B**

HUMAN	1	MAMSSGGSGGGVPEQEDSVLFRRTGQSDDSDIWDITALIKAYDKAVASFKHALKNGDIC	60
MOUSE	1	MAM---GSGGAGSEQEDIVLFRRTGQSDDSDIWDITALIKAYDKAVASFKHALKNGDIC	57
Zebrafish	1	-----MANGAEDVVFRCRGTGQSDDSDIWDITALIKAYDKAVASFKNALKGEDGA	49
C. elegans	1	-----MAKIWSKSGDMEVDDVWDDTELIKMYDES LQEI SKNETSAK--	41
Drosophila	1	-----MSDETNAAVWDDSLVKTIVDES VGLAREALARLAD	36
		: : : * * * : * * * : : .	
HUMAN	61	ETSGK--PKTTPKRKPAKKNKSKQKNNTAASLQWKVGDKCSA I WSEDGCI--Y PATTIASI	116
MOUSE	58	ETPKK--PKG TARRKPAKKNKSKQKNATTPLKQWKVGDKCSA V NSEDGCI--Y PATITSI	113
Zebrafish	50	TPQEN--DNP GKRRKNNKNNKSRKRCNAAPDKEWVGDSCYAF WSEDGNI--Y TATITSV	105
C. elegans	42	-----I T SRKFKGEDGKMYT WKVGGKCMAPVEENGEVTDY PATITDI	83
Drosophila	37	STNKREEENAAAAEEEAGEI SATGGATSPEPVSFKVGDYARIT VVDG---VDYEGAVVSI	93
		. : : * * . * : : . * : : : .	
HUMAN	117	DFKRET--CVV V Y T G Y G N R E E Q N L S D L L S P I C E V A N N I E Q N A Q E N E N E S Q V S T D E S E N S R S	175
MOUSE	114	DFKRET--CVV V Y T G Y G N R E E Q N L S D L L S P T C E V A N S T E Q N T Q E N --E S Q V S T D D S E H S S R	170
Zebrafish	106	DQEKGT--CVV F Y T D Y G N E E E Q N L S D L L T E P P D M E D A L K T A N V K E --T E S S T E E S D R S F T	162
C. elegans	84	GGADNLEVGVTFIYGGQAVVQMKDLWLNEEA I A D A V K A -----E N D L Q K T K K T ----S T	134
Drosophila	94	NEEKGT--CVL R L Y G Y E N E Q E V L L V D L L P S W G K R V R R E Q F -----L I A K K D E D E Q L S R	144
		. : : * .. : * * ...	
HUMAN	176	PGNK-----SDNIKPKSAFWNSFLPPPPMPGPRGLGPKGLKFNGLFPFPPPPPHL	228
MOUSE	171	SLRS-----KAHSKSKAAPWTSFLPPPPMPGSGLGPKGLKFNGLFPFPPPPH	223
Zebrafish	163	PQKSGHAKHKSKSNFPMGPPSWFSPFPPGPPPPPHFKK-----MDGRRGEGPGPS	213
C. elegans	135	VNSVAHSNSKSTSSAPNTSMFFPS-----	158
Drosophila	145	PKASAGSHSKTPKSSRRSRI S G L L-----	168
HUMAN	229	LSCWLPFFESGPPPIIPPFPPICPDSDLDDADALGSM LISWYMSGYHTGYMGLFRONKKEGR	288
MOUSE	224	LPCWMPFFESGPPPIIPPFPPISPDCLDDT DALGSM LISWYMSGYHTGYMGLFRONKKEGK	283
Zebrafish	214	FPGWFPMLPLGPPMIPFPFMPDFGEDDEALGSM LISWYMSGYHTGYMGLRQGRKEAA	273
C. elegans	159	---FAFPVPE-----FNITAMAPVNQK E A M N S M L M S W Y M S G Y H T G Y Q A L A D Q K N V Q N	207
Drosophila	169	---VMFPMP-----PVFPMTIVGGGDGAE QDFVAMITAWYMSGYHTGLRQKKKEASTTSG	219
		* * : : : * * : * * * * * * * * * .	
HUMAN	289	CSHSLN--	294
MOUSE	284	CSHTN---	288
Zebrafish	274	ASKKSHRK	281
C. elegans	208	-----	207
Drosophila	220	KKKTPKK--	226

Figure 16 : SMN protein sequence and function are conserved across species during evolution.

A. Phylogenetic tree based on SMN protein sequence showing the genetic divergence among SMN from different species discussed here using the neighbor joining method. B. Amino acid sequence alignment of SMN proteins from different organisms. Identical and similar amino acids are outlined. The similarity % (Human: Mouse 81.293; Human: Zebrafish 46.205; Human: C. elegans 21.405; Human: Drosophila 21.549). This work made on the bioinformatic tool (Protein knowledgebase (UniProtKB)).

4. Survival Motor-neuron (SMN) functions

4.1. SMN GENE

The human SMN protein is encoded by two loci located on chromosome 5q13: *SMN1*¹⁰³ (Gene ID: 6606) and *SMN2* ((Gene ID: 6607)), the second having resulted from of a 500 kb inverted duplication. These genes display 99% nucleotide identity (Figure 17); with one nucleotide difference in exon 7, which is thought to be an exon splice enhancer.

Humans are the only species carrying two different *SMN 1* and *2*. The human *SMN* gene has 8 exons; the stop codon for the predicted protein occurs in exon 7; therefore, exon 8 is not translated (Figure 18).



Figure 17 : Human SMN1 & 2 protein alignment.

Similarity amino acids are outlined. The similarity is 98.58%. Works made on the bioinformatics tool (Protein knowledgebase (UniProtKB)).

4.2. Isoform of SMN

While the full length SMN protein is the predominant isoform expressed in most tissues/ cell types, different other isoforms have been described as well:

4.2.1.1. SMN Δ 7

The SMN Δ 7 protein is produced when exon 7 is skipped, the sixteen C-terminal amino acid residues of exon 7 are replaced by four amino acids (EMLA) that are coded by exon 8. This protein is highly unstable and rapidly degraded by the ubiquitin–proteasome pathway, EMLA serving as a degradation¹⁵⁶.

4.2.1.2. α -SMN

During splicing, intron 3 is retained, resulting in creating one of the axonal-SMN isoforms (α -SMN). α -SMN mRNA is significantly shorter and encodes a 19-kDa protein due to an in-frame stop codon in intron 3. The α -SMN plays an essential role in axonogenesis during mammalian brain development, as it stimulates axons growth, stimulates cell motility, and regulates insulin-like Growth Factor-1(IGF1). In general, α -SMN transcripts are not detected in adult tissues, as the nonsense-mediated mRNA decay (NMD) pathway degrades these transcripts¹⁵⁷.

4.2.1.3. SMN6B

SMN6B, is generated from both the SMN1 and SMN2 genes. In this isoform, an intronic Alu region is included as an alternative exon following exon 6. SMN6B is two times more stable than SMN Δ 7 but twofold less stable than FL SMN and is found in both the nucleus and the cytoplasm. However, the physiological role of SMN6B is unknown¹⁵⁸.

4.2.1.4. SMN Δ 5

SMN Δ 5 is an isoform excluding exon 5 and is found in muscles and the central nervous system (CNS). Its physiological function remains unclear¹⁵⁹.

Interestingly, other SMN isoforms are produced by skipping exons 5 and/or 3, and 7 but their functions are still unknown. The major transcript FL of SMN1 and the other isoforms discussed here are shown in (Figure 18).

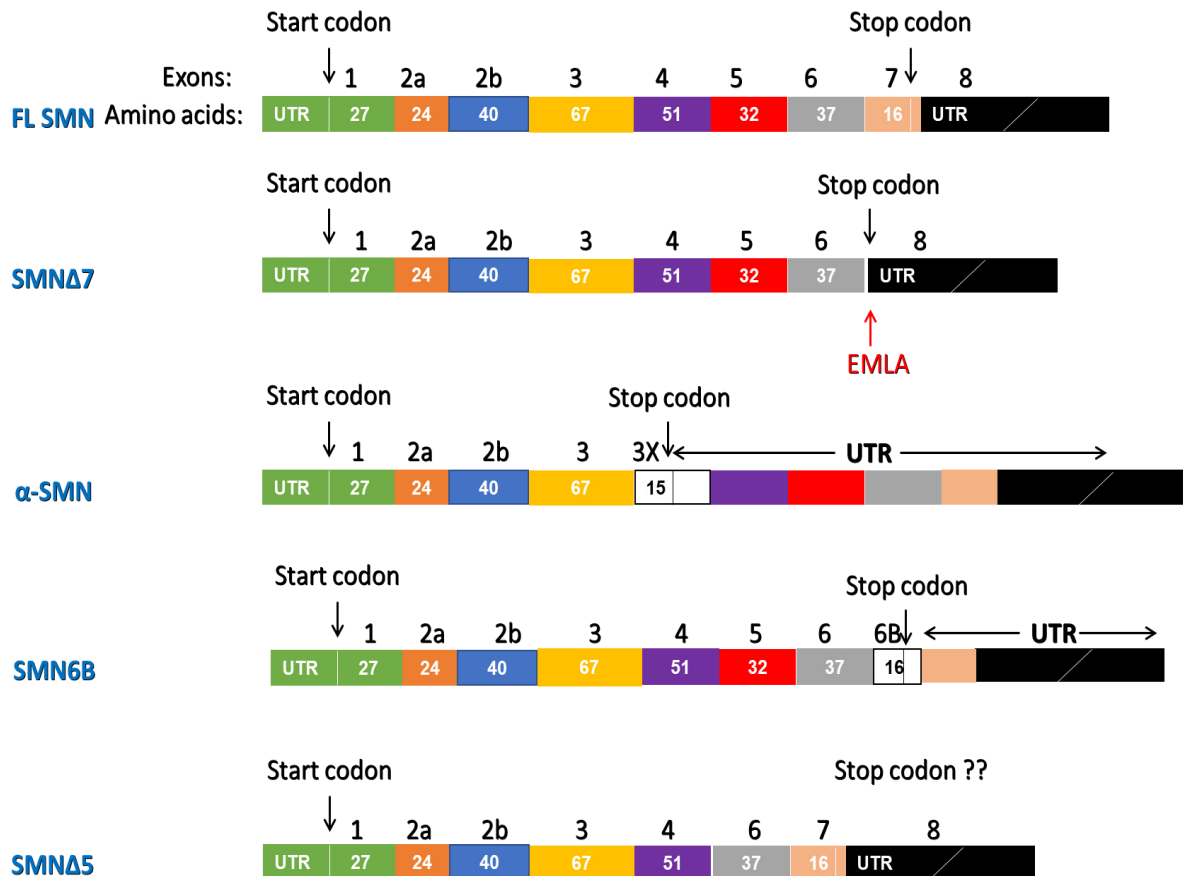


Figure 18 : SMN transcripts.

Diagrammatic representation of the major transcript and the full-length protein derived from SMN1, SMN Δ 7, α -SMN, SMN6B, SMN Δ 5. Exons are presented as colored boxes with the number of amino acids noted within each box. Arrows indicate locations of the start and stop codons.

4.3. Protein and Domain Organizations

SMN1 coded by eight exons: 1, 2a, 2b, 3, 4, 5, 6 and 7; exon 8 is not translated (Figure 18 & 19). Based on sequence conservation, it is supposed that SMN exons 2, 3, and 6 are extremely important for SMN function and might be sufficient for SMN rescue; these regions are responsible for mediating a number of SMN properties, including self-oligomerization, CB targeting and interaction with core components of the SMN complex and ribonucleoprotein (RNP) targets^{160 161}.

The FL *SMN1* and *SMN2* encode proteins of 38 kDa protein composed of 294-amino-acid protein with various domains, including an N-terminal (basic/lysine-rich domain), a central Tudor domain, a C-terminal proline-rich domain, and a YG box (Figure 19):

4.3.1.1. Basic/lysine-rich domain

The basic/lysine-rich region is encoded by exon 2 (2A and 2B), and this domain has been shown to interact with Gemin2 (one of the Gemini-SMN complex proteins discussed below) and RNA¹⁶². p53, a transcription regulator and tumor suppressor, also interacts with the domain encoded by exon 2¹⁶³.

4.3.1.2. Tudor domain

Tudor domain is a conserved structural domain involved in the protein-protein interaction. It has been shown to bind arginine-glycine-rich (RG) motifs in a methylarginine-dependent manner also, bind to methylated histone tails to facilitate protein-protein interactions, including RNA metabolism histone modification and DNA damage response proteins¹⁶⁴. Among the examples of these proteins, but not the only ones, are Coilin, FBL, GAR1, Fused in Sarcoma (FUS), Sm proteins, Histone 3 and the carboxy-terminal domain (CTD) of RNA Polymerase II (RNAP II).^{165 95 166 167 168 139}.

4.3.1.3. Proline-rich domain

Exons 4–6 encode three polyproline stretches; this sequence interacts with Profilins, which are a family of small proteins within the cell that regulate cellular actin dynamics ¹²⁶.

4.3.1.4. YG box

The SMN's last sixteen amino acids (coded by exon 7) (Figure 18, FL SMN) along with the YG box upstream (coded by exon 6) facilitate its self-oligomerization, which is vital for its stability and subcellular localization ^{162 169}. YG box is also involved in the interaction with Gemin3 (one of the Gemini-SMN complex proteins discussed below) ¹⁷⁰ and the interaction with SIN3 transcription regulator family member A (SIN3A) ¹⁷¹.

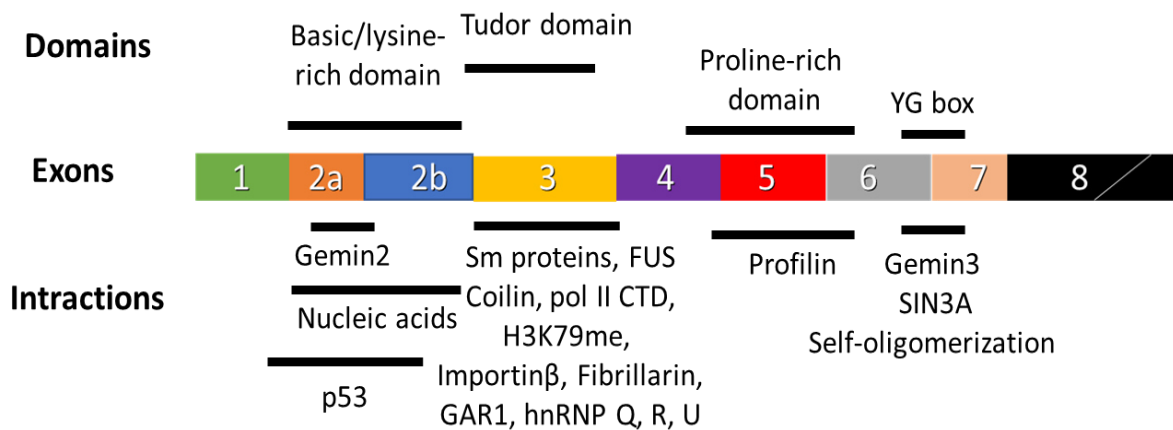


Figure 19 : SMN domains and interactions.

Diagrammatic representation of SMN domains, exons, and interactions. Exons are presented as colored boxes with the number of exons noted within each box the domains are indicated above and the interaction below.

4.4. SMN protein expression and cellular localization

The SMN protein is found throughout the body, with the highest levels in the lower motor neurons of the spinal cord. SMN localizes to both the nucleus and cytoplasm of all eukaryotic cells. In the nucleus, the SMN protein is predominantly concentrated in several prominent subnuclear bodies called Gems and CB (Figure 20) (Gems and CB were discussed before). They are nearly indistinguishable under the microscope ^{68 82}.

Moreover, SMN proteins are localized primarily in the nucleus in developing neurons, whereas in mature neurons, they are located mainly in cytoplasm and axons. SMN has also been found to be present in mature motor neuron growth cones ¹⁷².

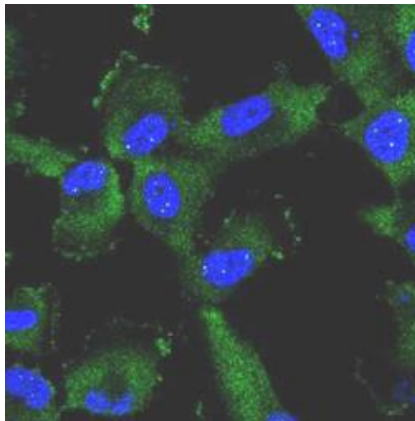


Figure 20 : SMN in the cytoplasm and in the nucleus (Gems & CB).

SMN in green and DAPI in bleu. Adapted from the Human Protein Atlas

4.5. SMN Functions

Ever since the identification of *SMN1* as the SMA determining gene, efforts have aimed to elucidate the function of the SMN protein and unravel the mechanism responsible for SMA. SMN protein has a multifunctional complicated physiological role. Mainly, SMN controls various aspects of the

RNA metabolism, including but not limited to the following: transcription ¹³⁹, pre-mRNA splicing ¹⁷³, snRNP assembly ^{174 175 176}, 3' end of histone mRNA processing ¹⁷⁷, snoRNPs assembly ^{95 94}, translation ¹⁷⁸, and mRNA trafficking ^{179 180 181 182}.

4.5.1.1. Transcription

SMN has been shown to play different roles in the initiation, elongation, and termination of gene transcription.

An interaction between SMN and the transcription factor E2 encoded by the papillomavirus facilitates E2-dependent transcriptional activation ¹⁸³. On the other hand, SMN interacts with the transcription co-repressor SIN3A, which participates in chromatin-associated transcription regulation, which serves as a scaffold for histone deacetylases (HDACs) and other proteins essential for maintaining the structure and function of chromatin ¹⁷¹. Finally, SMN also binds to the transcription factor p53, which has distinct nuclear localization, DNA binding, and transactivation domains. The SMN-p53 complex is localized to CBs ¹⁶³. The binding of SMN to E2, p53, and Sin3A suggests that SMN is involved in transcription initiation.

RNAP II creates R-loops, nucleic acid structures made up of an RNA–DNA hybrid and a single-stranded DNA that has been displaced. R-loops must be resolved for nascent transcripts to be released from the DNA template in transcription termination areas. By consequence, R-loops are a significant source of replication stress and genome instability that contributes to neurodegeneration ¹⁸⁴.

SMN interacts directly with the symmetrically dimethylated residues 1810 (R1810me2s) of RNAP II in the CTD. SMN binding to the R1810me2s stabilizes the interaction of Senataxin (SETX) with the CTD. SETX, a putative DNA/RNA helicase involved in the resolution of R-loops, forms a complex with SMN and RNAP II CTD ¹⁸⁵.

A consequence of this unwinding by SETX is the recruitment of the 5'-to-3' exonuclease XRN2, thus terminating transcription.

Knockdown of *SMN* or arginine mutation to alanine of the methylated residue results in the accumulation of RNAP II at termination regions of active genes across the genome¹³⁹. These data support the role of SMN in transcription termination (Figure 21).

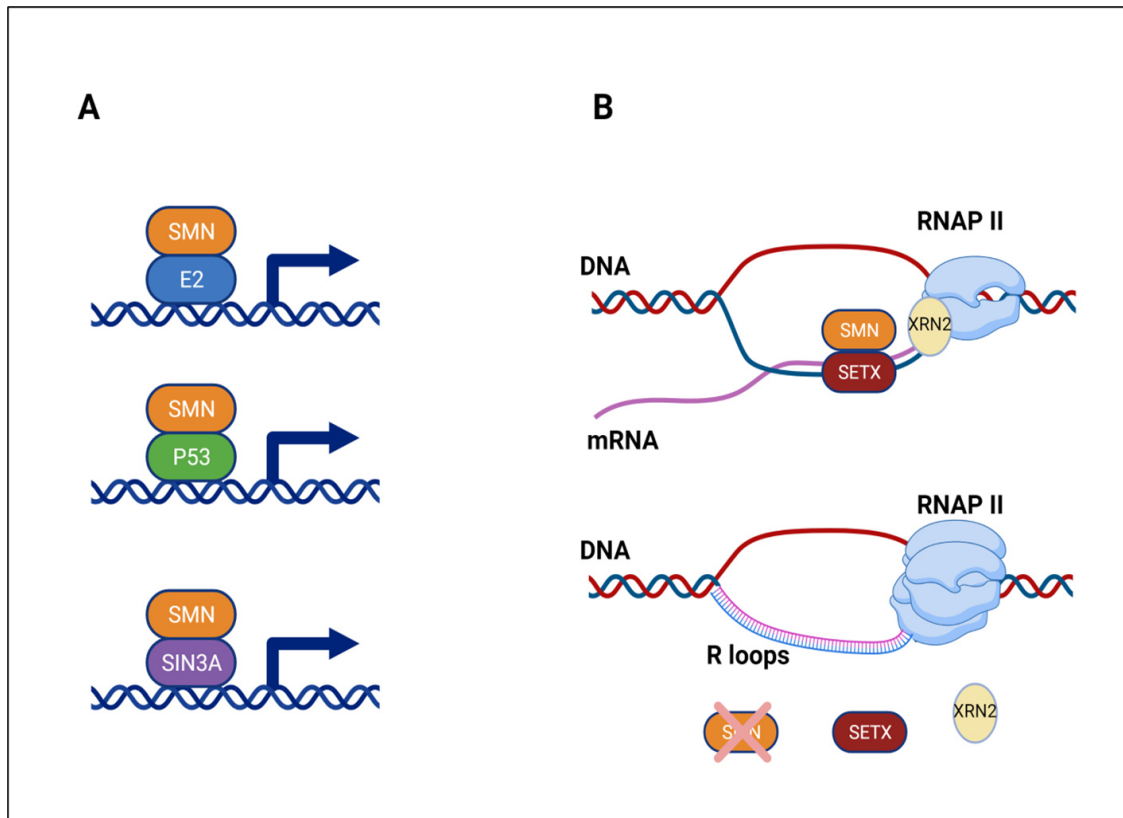


Figure 21 : SMN role in the transcription.

(A) SMN in the transcription initiation interact with E2, p53, and Sin3A transcription factors.

(B) SMN in transcription termination form a complex with SETX to remove the R-loops.

4.5.1.2. RNA maturation/ processing

4.5.1.2.1.1. Spliceosomal snRNP assembly

A spliceosome is a complex machine that catalyzes the removal of introns from pre-mRNA transcripts during splicing process. The contribution SMN snRNP during the splicing process was the first identified role of SMN. SMN's role in snRNP is carried out by a large complex that includes SMN, Gemin proteins (Gemins2–8)¹⁸⁶, and the UNR-interacting protein (Unrip), together with U-rich small nuclear RNA (snRNA) with a heptameric ring of Sm proteins (B, D1, D2, D3, E, F, and G) make up a spliceosomal snRNP¹⁸⁷ (Figure 24).

The process of snRNP biogenesis and assembly involves multiple distinct steps in the nucleus, and the cytoplasm is discussed below after the SMN complex.

4.5.1.2.1.2. The SMN complex

SMN complex is composed of nine members, SMN in combination with Gemin proteins (Gemins 2-8) and the Unrip. The Gemins were named based on the observation that they co-localize with SMN in nuclear Gems and Cajal bodies⁶⁸. SMN complex is a large macromolecular stable complex that can be detected in the cytoplasm and in the nucleus (Gems). It acts as a chaperone to promote the assembly of spliceosome snRNP particles and hence plays a crucial role in pre-mRNA splicing¹⁸⁶ (Figure 22).

SMN protein depletion reduces the stability of the other SMN complex components, impairing snRNP assembly. As a consequence, Gems disappear, and various of Gemins are depleted¹⁰⁶.

Gemin2 participates in the assembly of SmD1/D2/F/E/G proteins into a pentamer before they bind to snRNAs, which is the most conserved protein in the SMN complex¹⁷⁴.

Gemin3(DDX20) is a self-interacting phosphoprotein exhibiting RNA helicase activity as a result of its phosphorylation, which directs the binding of ATP to the protein¹⁷⁰.

Gemin4 carries a nuclear localization signal. Overexpression of Gemin4 results in the relocation of the SMN complex to the nucleoplasm. On the other hand, high levels of a Gemin4 variant lacking a nuclear localization signal tend to sequester Gemin3 and a portion of Gemin2 in the cytoplasm ¹⁸⁸.

Gemin5 contains tryptophane-aspartic acid domains that recognize the U-rich sequence known as the Sm site on snRNAs, which is then delivered to the SMN complex within the cytoplasm ¹⁸⁹. The Gemin6 and Gemin7 proteins can be considered as heterodimers; they interact through an interface similar to the one that mediates interactions between Sm proteins ¹⁹⁰. Gemin6, Gemin7, and Unrip form a stable cytoplasmic complex that requires Gemin8 to associate with SMN ¹⁹¹.

Unrip is required for spliceosomal snRNP assembly and binds to a subset of Sm proteins ¹⁹¹.

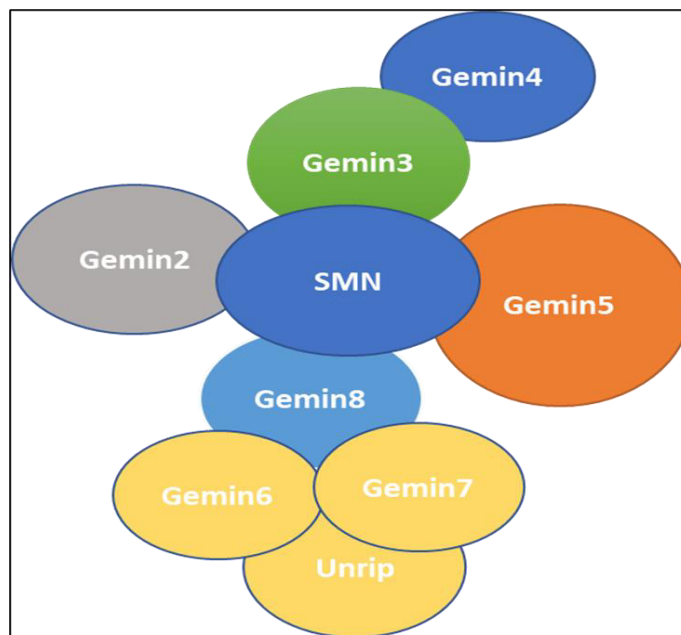


Figure 22 : SMN complex.

SMN, Gemins 2-8, and the Unrip.

4.5.1.2.1.3. The sequential steps of snRNP biogenesis and assembly

As the first step, snRNA is transcribed by RNAP II in the nucleus, and the newly synthesized snRNA undergoes co-transcriptional processing to include a 7-methylguanosine cap (m7G-cap) on the 5' end and cleavage of the 3' end to produce a pre-snRNA.

This pre-snRNA is then exported to the cytosol by a multiprotein export complex composed of Cap Binding Proteins (CBP20 and CBP80), Phosphorylated Adaptor for RNA Export (PHAX), Exportin 1 (Xpo1), and RanGTP.

Following the export complex's disassembly in the cytosol, the pre-snRNA undergoes further processing by the SMN complex, including loading the heptameric Sm ring to the pre-snRNA. Several steps ensure the specificity of the process. In particular, the Protein Arginine Methyltransferase 5 (PRMT5) complex is responsible for symmetrical dimethylation of a subset of Sm proteins, resulting in their tighter interaction with SMN. Moreover, Gemin5 is a component of the SMN complex that recognizes specific sites on the pre-snRNA for loading the heptameric Sm ring.

Pre-snRNA is hypermethylated by TGS1 on its m7G-cap following the loading of the Sm ring in order to form the TMG cap. A 3' end trimming is also performed on the pre-snRNA at this stage. For pre-snRNAs to form the TMG cap structure, SMN and TGS1 appear to interact directly.

Newly processed snRNA is transported back into the nucleus while still bound to the SMN complex. Nuclear localization signals are provided by the TMG cap and the Sm core. The nuclear import of snRNA is also facilitated by a direct interaction between SMN and Importin- β and WRAP53.

Upon entering the nucleus, snRNA undergoes final maturation in CBs. It is noteworthy that a number of nucleotides are pseudouridylated or 2'-O-methylated in snRNAs^{192 193}.

All these steps are summarized in (Figure 23).

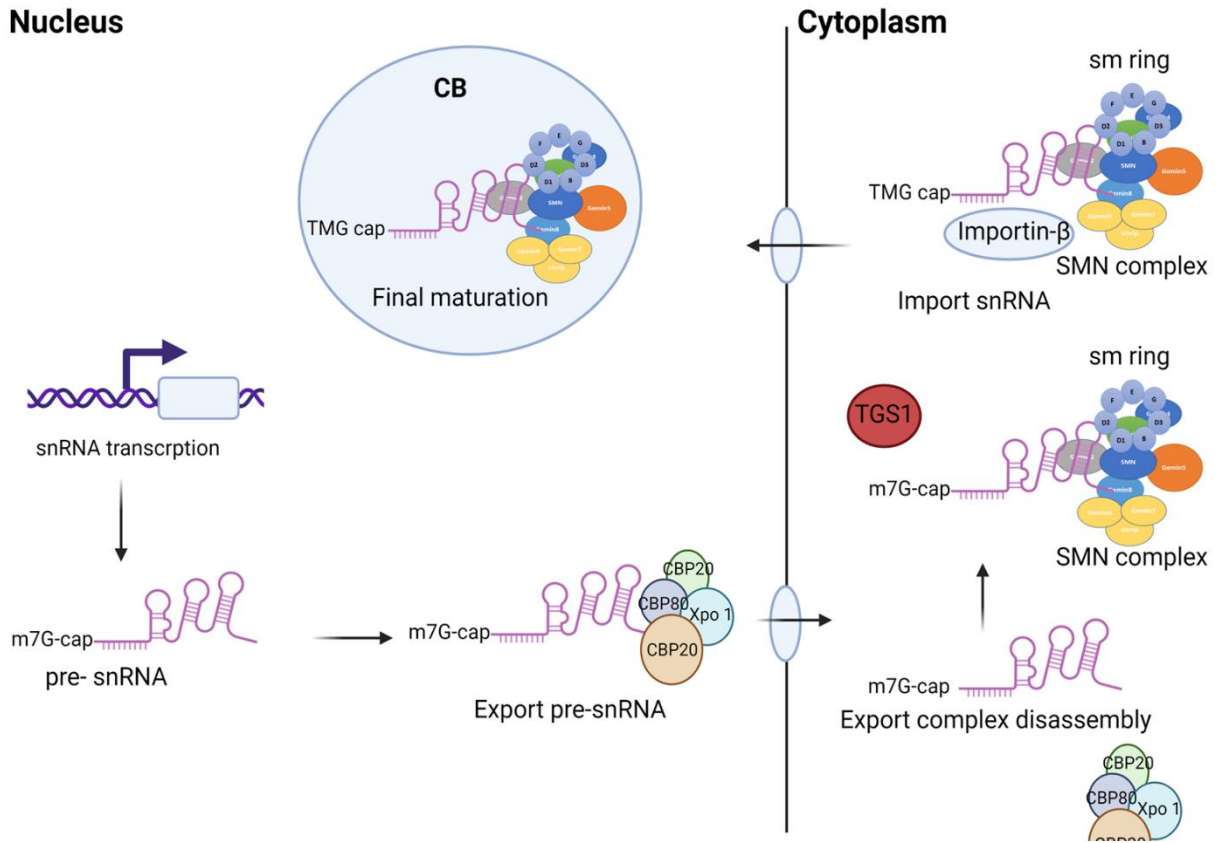


Figure 23 : snRNP biogenesis and assembly.

4.5.1.2.1.4. 3' end processing of histone mRNAs

Because histone mRNAs are not polyadenylated, they require special 3' end processing, where U7 snRNPs play a crucial role. A stem-loop structure is on the 3' end of histone mRNAs, followed by a cleavage site; in conjunction with a stem-loop-binding protein and other factors, U7 snRNP facilitates cleavage at the 3' end of histone mRNAs downstream of the cleavage site¹⁹⁴.

U7 snRNP architecture is similar to spliceosome snRNP, with a few exceptions. The heptameric ring of U7 snRNP harbors Sm-like proteins Lsm10 and Lsm11 instead of SmD1 and SmD2 seen in spliceosome snRNP¹⁹⁵ (Figure 24).

The SMN complex plays a similar role in U7 snRNP assembly as it does in spliceosome snRNP assembly¹⁹⁵. Interestingly, SMN loss induces accumulation of U7 snRNA and defective processing of the 3' end of histone mRNAs, thus impacting histone metabolism¹⁷⁷.

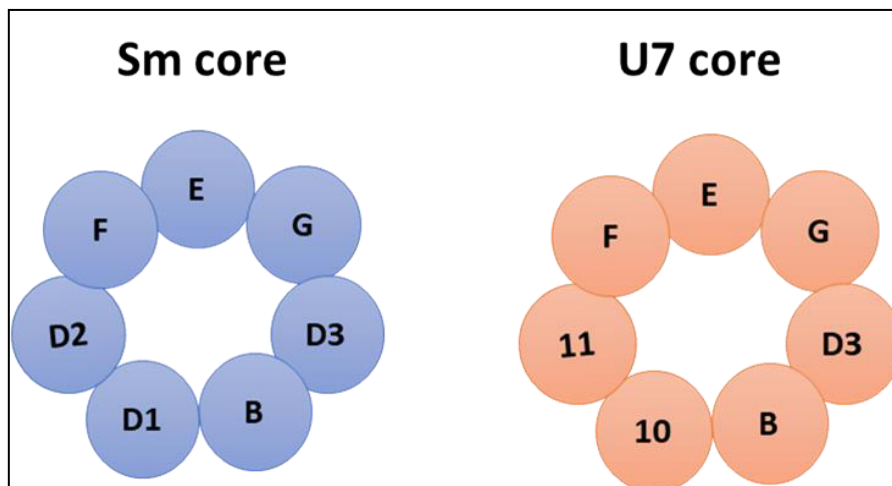


Figure 24 : The Sm core and U7 core structure.

U7 snRNP has Lsm10 and Lsm11 instead of SmD1 and SmD2 in sm snRNP.

4.5.1.2.1.5. Biogenesis of snoRNPs

Small Nucleolar Ribonucleoproteins snoRNPs are a class of ribonucleoproteins responsible for regulating post-transcriptional modifications of non-coding RNAs, such as ribosomal RNAs (rRNA), transfer RNAs (tRNA), and snRNAs. snoRNPs work by a short guide RNA Small Nucleolar Ribonucleo RNA (snoRNA) which identifies the position of post-transcriptional modifications and particular protein components. snoRNAs are classified into two groups based on their sequence and structural motifs: H/ACA box and C/D box. The H/ACA box snoRNAs promote pseudouridylation, whereas the C/D box snoRNAs promote 2'-O-methylation (Figure 25). The secondary structures of both types of snoRNAs are distinct. Defining the secondary structures of snoRNAs is essential for the interaction of the target RNAs with the proteins of snoRNP¹⁹⁶.

A single-stranded region carrying the H box (ANANNA, where N = G, U, C, A) and the 3'-end region having the ACA box (AYA, where Y = C or U) motifs link two hairpin structures in the H/ACA box snoRNAs (Figure 25A).

The C box motif (RUGAUGA, where R represents purine) is found towards the 5' end of the C/D box snoRNA, whereas the D box motif (CUGA) is located near the 3' end. The stem generated by the base pairing of the 5'-end sequences with the 3'-end sequences in the secondary structure of a snoRNA brings C and D box motifs close together (Figure 25B)¹⁹⁷.

SMN has been found to interact with GAR1 and FBL, two markers of snoRNP^{94 95}. In addition, decreased localization of the snoRNP chaperone Nopp140 in CBs was reported in SMA-patient-derived cells, linked to disease severity, indicating that SMN is involved in snoRNP synthesis and /or function¹⁹⁸.

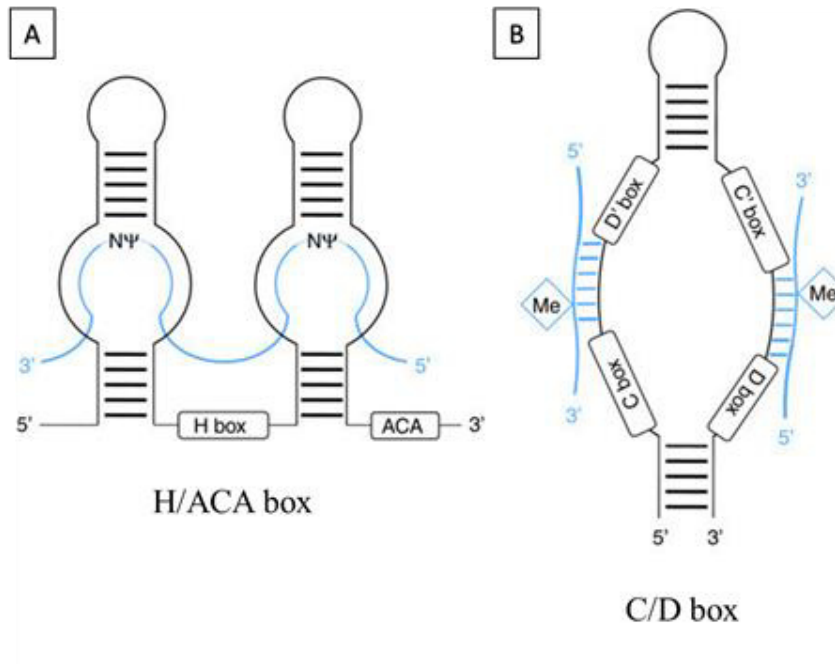


Figure 25 : The snoRNA structure.

(A) The structure of a H/ACA snoRNA and (B) a C/D box snoRNA. The targets for RNA modification are shown in blue. The image is adapted from (Gardner PP, 2019).

4.5.1.2.1.6. Pre-mRNA splicing

Precursor messenger RNA (pre-mRNA) transcript is spliced into a mature messenger RNA transcript (mRNA), contributing to protein diversity evolution. Splicing is typically required to form an mRNA molecule that can be translated into protein. Splicing of nuclear-encoded genes occurs in the nucleus during or shortly after transcription; it is a fundamental process that operates by splicing exons (coding regions) back together after eliminating all introns (RNA non-coding regions) by the spliceosome. The spliceosome, a collection of snRNPs, catalyzes a series of events that splice introns¹⁹⁹. Therefore, snRNP plays a crucial role in mRNA splicing; consequently, it is no surprise that SMN depletion causes widespread splicing defects²⁰⁰.

Furthermore, RNA helicases are required to splice pre-mRNA by unwinding the RNA structures of pre-mRNAs. In light of SMN association with RNA helicases, such as Gemin3, DDX1, DDX3, and DDX5, SMN likely modulates its own splicing as well as the splicing of other transcripts via helicase interactions ²⁰¹.

Moreover, SMN, through its interacting partners, including FUS a helicase that bind with RNAP II, SMN may indirectly alter transcription-coupled splicing control ¹⁶⁶. Also, because SMN regulates stopping at the transcription termination site, it could influence intron splicing by recruiting splicing factors during transcription termination ¹³⁹.

4.5.1.3. Translation

Coactivator Associated Arginine Methyltransferase 1 (CARM1) is a multifunctional protein implicated in transcription, splicing, and autophagy. SMN has been linked to the regulation of translation of CARM1 with an inverse relationship. Furthermore, SMA type I patient cells and SMA mouse models show upregulation of CARM1 ^{202 178}.

4.5.1.4. RNA trafficking

SMN is involved in the trafficking of β -Actin mRNAs in neuronal processes and growth cones. SMN assembled on β -Actin mRNA also interacted with hnRNP R, an RNA-binding protein ²⁰³. FMRP, HuD, Insulin-Like Growth Factor (IGF-1) mRNA-Binding Protein 1 (IMP1), and hnRNP Q, other RNA binding proteins (RBPs) implicated in mRNA trafficking in motor neurons, have all been demonstrated to interact with SMN ^{204 180 205}.

Furthermore, The SMN/HuD/IMP1 complex has recently been linked to the trafficking of growth-associated protein 43(Gap43) in motor neurons. Overexpression of HuD and IMP in

cultured primary motor neurons obtained from a severe animal model of SMA was consistently reported to restore axon outgrowth abnormalities ¹⁸¹.

4.6. SMN and Protein-Protein Interactions

SMN has been reported to interact with more than 289 proteins (Annex) (Table 8). Among these, FBL and Coilin and Protein arginine methyltransferases PRMTs, are the most relevant SMN partners related to the focus of this work and will be discussed in more details below.

4.6.1.1. SMN / FBL

(FBL discussed before in nucleolus and CB section).

FBL has 3 domains, (i) an N-terminal repeating region rich in glycine and arginine residues GAR domain responsible for the interaction with the Tudor domain of SMN (Jones et al. 2001, Pellizzoni et al. 2001), (ii) an RNA-binding domain in its core region with an RNP consensus sequence and (iii) a C-terminal alpha-helical domain (Figure 26).

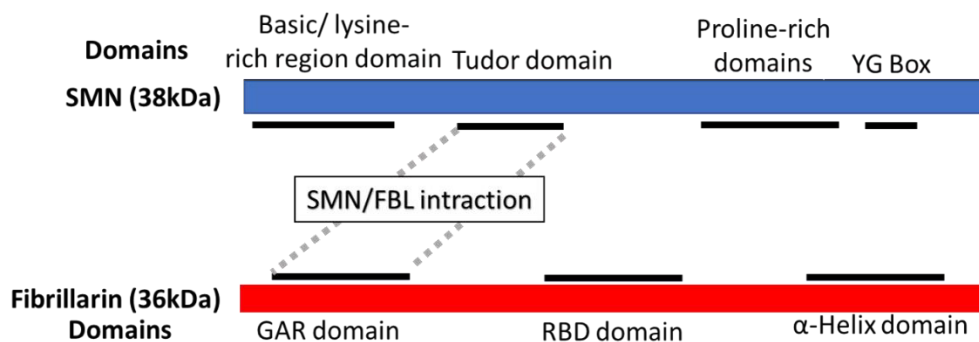


Figure 26 : SMN/FBL domains and interaction.

Schematic representation of SMN and FBL human protein.

4.6.1.2. SMN / Coilin

The modern era of CBs research started in the 1990s. By analyzing patient autoimmune sera, Tan and his colleagues discovered the human autoantigen p80 (Coilin), which has been widely utilized as a molecular marker for CBs ²⁰⁶. Coilin has a structural role in CBs. The coilin protein's N-terminus controls self-oligomerization, whereas the C-terminus controls the number of nuclear bodies formed per cell. Coilin also has nucleolar localization signals (NoLS), and nuclear localization signals (NLS). Coilin interacts with SMN through its RG box localized in the C terminus by ¹⁶⁵ (Figure 27). Asymmetrical dimethylarginine in RG box of coilin modulates its affinity for SMN and, consequently, the localization of SMN complexes within CBs ²⁰⁷.

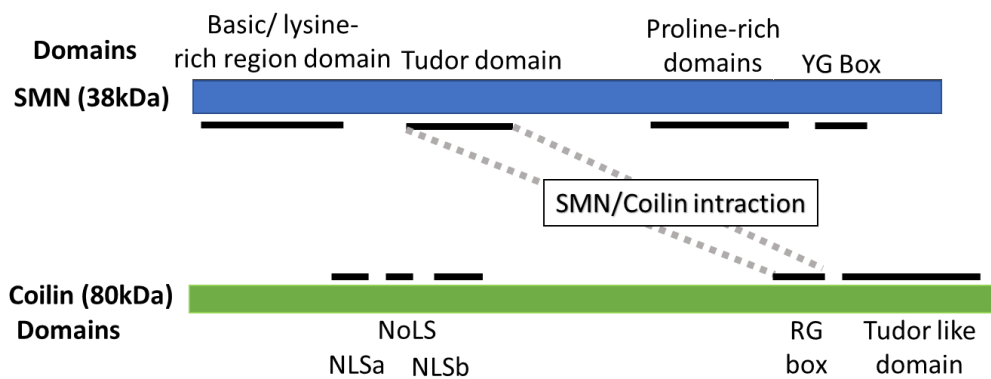


Figure 27 : SMN/Coilin domains and interaction.

Schematic representation of SMN and Coilin human protein. Nucleolar localization signal (NoLS), nuclear localization signals (NLS).

4.7. SMN and PRMTs

SMN participates in the metabolism of RNA by acting as a molecular chaperone for methylated arginine proteins needed for this function²⁰⁸. Furthermore, the Tudor domain in SMN protein is the well-characterized methylarginine-dependent binding module²⁰⁹. Tudor domains can bind both asymmetric dimethylarginine ADMA and symmetric dimethylarginine SDMA motifs and interact with several Protein arginine methyltransferases (PRMTs) such as PRMT1, PRMT5, and PRMT4 (CARM1) substrates^{165 95 166 167 139}. Therefore, PRMTs serve as a mediator of the interaction between SMN and its binding partners.

Moreover, there is a clear connection between methyl-binding requirements for SMN and SMA pathogenesis, as point mutations have been identified within the Tudor domain of SMN²¹⁰. Therefore, in the section below, I described the protein arginine methyltransferases, the ‘writers’ of arginine methylation in histone and non-histone proteins.

On the other hand, it has been demonstrated that PRMTs are strongly expressed in the nervous system and are critical for the maintenance of neuromuscular function. A conditional knockout of PRMT1 in neural stem cells leads to a severe defect in myelination of neurons as well as neonatal death²¹¹. Likewise, deletion of PRMT5 in neural stem cells results in neonatal death²¹².

4.8. Protein arginine methyltransferases (PRMTs)

Protein arginine methyltransferases post-translationally modify protein arginine residues; by catalyzing the transfer of a methyl group from S-adenosyl-L-methionine (AdoMet) to L-arginine on target proteins, changing their stability, localization, and/or function. They can methylate numerous nuclear and cytoplasmic substrates²¹³. The methylarginine was found in three forms: mono methylarginine MMA, asymmetric dimethylarginine aDMA, and symmetric dimethylarginine sDMA (Figure 28).

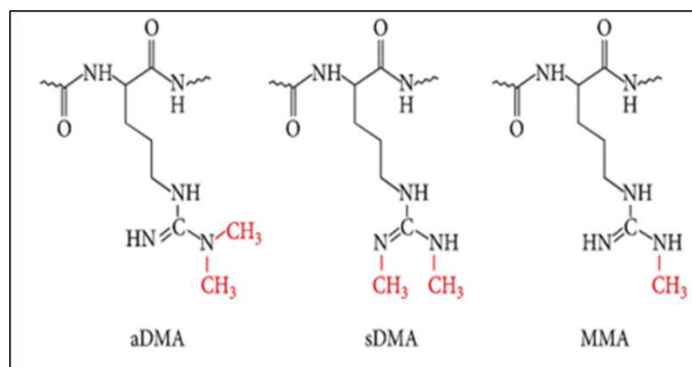


Figure 28 : The methylarginine forms.

aDMA; asymmetric dimethylarginine, sDMA; symmetric dimethylarginine, MMA; mono methylarginine

There are nine human PRMTs; classified into three types according to the final form of methylarginine products shown above: type I PRMTs (PRMT-1, 2, 3, 4, 6, and 8) catalyze the formation of MMA and aDMA; type II PRMTs (PRMT-5 and 9) catalyze the formation of MMA and sDMA and type III PRMT (PRMT7) can only generate MMA²¹⁴. A summary of PRMTs localization, type, and functions is found below in (Table 7).

Most cellular PRMTs activity is attributed to PRMT1, the most predominant type I PRMT in mammalian cells. PRMT1 is known to participate in numerous biological processes, including transcriptional activation, DNA repair, and signaling. PRMT2 enhances the transcriptional activity of hormone receptors in a ligand-dependent manner. The PRMT3 protein methylates the 40S ribosomal protein S2 (rpS2) and contributes to the maturation of the 80S ribosome. PRMT4, also known as CARM1 was previously discovered (in SMN functions) to enhance transcriptional activation by several nuclear hormone receptors. It is crucial for chromatin remodeling and gene activation as a transcriptional coactivator. The PRMT5 protein methylates the histones H2A and H4 and many other proteins. The PRMT6 nuclear protein, which prefers substrates with glycine-arginine-rich (GAR) motifs, controls transcription and is involved in the pathogenesis of the human immunodeficiency virus (HIV), DNA repair, and cell cycle progression. The PRMT7 gene is involved in the biogenesis of nuclear ribonucleoprotein particles and DNA repair. A full-length PRMT8 found in the brain is expressed and localized to the plasma membrane. The PRMT9 enzyme is a non-histone methyltransferase involved in U2 snRNP maturation ^{214 215}.

PRMTs	Cellular localization	Types	Biological Function
PRMT1	Cytoplasm / nucleus	Type I	Transcriptional activation (H4R3), nuclear localization, DNA repair, signaling
PRMT2	Cytoplasm / nucleus	Type I	Transcriptional coactivator, nuclear retention, apoptosis
PRMT3	Cytoplasm	Type I	Ribosome assembly
PRMT4 (CARM1)	Cytoplasm / nucleus	Type I	Transcriptional activation (H3R2, H3R17, H3R26), Muscle differentiation, T cell development, tumorigenesis

PRMT5	Cytoplasm / nucleus	Type II	Transcriptional repression (H3R8 and H4R3), Transcriptional elongation, RNA processing, signaling, mitosis, muscle and germ cell differentiation, tumorigenesis
PRMT6	nucleus	Type I	HIV replication, DNA repair
PRMT7	Cytoplasm / nucleus	Type III	Imprinting in male germ cell (H4R3)
PRMT8	Plasma membrane	Type I	Involved in the somatosensory and limbic systems
PRMT9	Cytoplasm	Type II	involved in U2 snRNP maturation

Table 7 : Summary of PRMTs localization, type, and functions.

The functions of PRMTs (1-7) are adapted from (Pal S, 2007), and (8-9) are adapted from (Tewary et al, 2019).

PRMTs abnormalities are linked to a variety of diseases, including cancer, cardiovascular disease, and recently neuromuscular diseases (NMDs)^{216 217 218}. As a result, PRMTs have attracted a lot of attention as potential therapeutic targets. PRMT inhibitors that are both selective and powerful are essential because they can be utilized as chemical tools to understand better PRMTs function in epigenetics in oncology and in the prospective therapies to target PRMTs up-regulation in diverse disorders.

A list of PRMT inhibitors provided in the Annex (Table 9).

4.9. SMN in DNA damage and repair

Multiple neurodegenerative disorders are characterized by defective DNA repair. Recently, in non-dividing SMA neurons, the low levels of SMN cause DNA-dependent protein kinase c (DNA-PKcs) deficiency, which impairs NHEJ and leads to an accumulation of R-loops DNA damage, and neurodegeneration. Conversely, SMN ectopic expression and increased gene expression of *SMN2* reduce R-loops, restore DNA-PKcs level and enhance NHEJ mediated DNA repair which reduced neuronal degeneration^{138 219}. This is one of the main pieces of evidence relating SMN protein with the DNA damage response and/or in DNA lesion protection.

Moreover, SMA patient cells, as well celled depleted of SMN by shRNA, display increased levels of the DNA damage marker γ H2AX^{139 138}. Accordingly, increased DNA damage and skeletal muscle cell death have been reported as some of the earliest phenotypes in SMA model mice²²⁰.

Different evidences indicate that SMN is necessary for resolving R-loops hybrids formed by RNAP II at transcription termination (as discussed above) sites, since, SMN deficiency causes a genome-wide RNAP II accumulation in termination regions of active genes, downregulation of SETX, and R-loops accumulation^{139 138}. SMN deficiency causes a genome-wide RNAP II accumulation in termination regions of active genes, downregulation of SETX, and R-loops accumulation^{139 138}.

Furthermore, severe SMN deficiency results in genome-wide splicing abnormalities caused by intron retention and DNA damage signature shown by RNAseq experiments performed in the spinal cords of inducible SMA mice and in human SMA cells culture models. Ultimately, R-loop accumulation and transcription fork stalling promote, DSBs thus threatening genome integrity ²²¹. In fact, SMN-deficient cells display high levels of DNA damage in the rDNA, likely due an increased R loops accumulation at this highly transcribed site, thus resulting in reduced ribosomal RNA synthesis and translation ²²².

Besides these roles in prevention of transcriptional stress-driven DNA damage, several evidence directly link SMN with different DNA damage response processes. First, recruited to centromeres via interaction with histone H3 (methylated histone H3K79 specifically) and participates in the induced Centromeric Damage Response (iCDR) ¹⁶⁸.

Second, Gemin2 (a well characterized interactor of SMN) is known to promote RAD51-mediated recombination homologous indicating that SMN may play a role in HR ²²³.

All these data show the importance of SMN in maintaining DNA integrity which is becoming more well-known. However, SMN role in other DNA lesions repair for example UV lesion or in restoration of cell activity after damage has not been addressed yet.

Chapter two

Background & Aim of the study

Background

DNA is constantly challenged by an array of endogenous and exogenous sources that damage it. Cells are equipped with various DNA repair pathways to counteract the damaging effects of DNA damage.

The nucleolus has emerged as a multifunctional organelle in the last 20 years, controlling cellular growth and stress response processes much beyond its traditional role in ribosome biogenesis. Deregulation of ribosomal synthesis at any stage, from transcription to processing to ribosomal subunit assembly, causes stress. Furthermore, because of the particular organization of rDNA in tandem arrays and its exceptionally high transcription rates, it is prone to RNA:DNA hybrids (R-loops) which cause DNA damage. If the rDNA damage is not repaired correctly can lead to disease and premature aging. Moreover, DNA damage causes dramatic changes in nucleolar architecture.

SMA is a neuromuscular disorder that affects the motoneurons, which control voluntary muscle movement. Motoneurons are gradually destroyed in SMA; therefore, muscles no longer receive signals from motor neurons in the spinal cord resulting in progressive muscle wasting and atrophy. Bi-allelic mutations in the SMN1 gene cause the SMA. SMN is a ubiquitous multifunctional protein involved in cellular functions, including ribonucleoprotein synthesis and mRNA trafficking. Indeed, recently more evidence about the involvement of SMN in the maintenance of DNA integrity and DNA repair.

Context

UV is among the cellular stressors known to alter nucleolar organization as well as CB. UV-irradiation has the advantage of being a rapid and chemically safe approach. Furthermore, cells can heal UV-induced damages, reversing their stress state. Our research team recently discovered that the rDNA/RNAP1 complexes are rearranged within the nucleolus during DNA

Repair and undergo relatively long-distance motions. UV lesions initiate the DNA repair response, which pushes the rDNA/RNAP1 complex to the nucleolus' periphery. This mobility is thought to be crucial for a suitable repair reaction because most repair proteins are found outside the nucleolus. The rDNA/RNAP1 complex returns to the nucleolus only when all repair processes have been finished in normal conditions.

Proteins could change their subcellular localization as part of their maturation process or in response to external or internal signaling events. SMN is found in CB in the nucleus, which has been demonstrated to connect with nucleoli. SMN protein shuttle between cytoplasm and nucleus as a chaperone for nuclear RNP also is implicated in the mRNA trafficking. Furthermore, the role of SMN has received increased attention across several disciplines in recent years due to its association with the first cause of fatal infant disease, the SMA.

Knowledge gap

Many aspects of the DNA Repair pathway have been revealed, and the majority of the key players have been identified. Although we have a good understanding of how cells repair DNA damage, we know relatively little about how they return to their usual activity once the repair process is completed. Therefore, a critical question is still unanswered how do the cells come back to their normal situation before the damage?

On the one hand, how the movement of the rDNA/RNAP1 complex happens during damage is still unknown. On the other hand, SMN has been reported to bind with hundreds of proteins (protein-protein interaction), among these proteins FBL which is a nucleolar and CB associated protein, suggesting that more major roles of SMN have not yet been discovered or proven!!

Aim and Purpose of the thesis

In my Ph.D. work, I tried to break down the scientific barrier to understanding and defining the cellular maintenance and molecular mechanisms that govern the nucleolar reorganization after stress induction with stress-dependent nucleolar rearrangement (UV). Using SMN as the best candidate may have a role in this process, which may allow us as well to enhance our understanding of SMN function and explain its association with SMA.

This thesis aims to fulfill the following purposes:

- i. Define possible localization and function of SMN in the nucleolus under UV damage.
- ii. Establish possible crosstalk among SMN, Coilin, and FBL in the context of UV damage.
- iii. Define the role of Coilin and FBL in maintaining the nucleolar organization and reorganizing the position of the RNAP1 after DNA damage.
- iv. Investigate the role of PRMTs in nucleolar reorganization, as it is required for several proteins to interact with SMN.
- v. Define the possible function of SMN in DNA repair.
- vi. Investigate the possible presence of SMN/SETX complex need for R-loops to resolve in the nucleolus.
- vii. Establish a list of candidate proteins that may be involved in this nucleolar reorganization based on the interactions of our primary candidates (ACTB, CETN2, FBL, MYO1C, and SMN) to create a siRNA library later.

Reference

1. Dizdaroglu, M. Oxidatively induced DNA damage: Mechanisms, repair and disease. *Cancer Lett.* **327**, 26–47 (2012).
2. De Bont, R. Endogenous DNA damage in humans: a review of quantitative data. *Mutagenesis* **19**, 169–185 (2004).
3. Hoeijmakers, J. H. J. Genome maintenance mechanisms for preventing cancer. *Nature* **411**, 366–374 (2001).
4. Chatterjee, N. & Walker, G. C. Mechanisms of DNA damage, repair, and mutagenesis: DNA Damage and Repair. *Environ. Mol. Mutagen.* **58**, 235–263 (2017).
5. Lindahl, T. Instability and decay of the primary structure of DNA. *Nature* **362**, 709–715 (1993).
6. Bartek, J. & Lukas, J. Mammalian G1- and S-phase checkpoints in response to DNA damage. *Curr. Opin. Cell Biol.* **13**, 738–747 (2001).
7. Heine, G. F., Horwitz, A. A. & Parvin, J. D. Multiple Mechanisms Contribute to Inhibit Transcription in Response to DNA Damage. *J. Biol. Chem.* **283**, 9555–9561 (2008).
8. Mei Kwei, J. S. *et al.* Blockage of RNA polymerase II at a cyclobutane pyrimidine dimer and 6–4 photoproduct. *Biochem. Biophys. Res. Commun.* **320**, 1133–1138 (2004).
9. De Zio, D., Cianfanelli, V. & Cecconi, F. New Insights into the Link Between DNA Damage and Apoptosis. *Antioxid. Redox Signal.* **19**, 559–571 (2013).
10. Roos, W. P. & Kaina, B. DNA damage-induced cell death by apoptosis. *Trends Mol. Med.* **12**, 440–450 (2006).
11. Asaithamby, A., Hu, B. & Chen, D. J. Unrepaired clustered DNA lesions induce chromosome breakage in human cells. *Proc. Natl. Acad. Sci.* **108**, 8293–8298 (2011).
12. Janssen, A., van der Burg, M., Szuhai, K., Kops, G. J. P. L. & Medema, R. H. Chromosome Segregation Errors as a Cause of DNA Damage and Structural Chromosome Aberrations. *Science* **333**, 1895–1898 (2011).
13. Klaunig, J. E., Wang, Z., Pu, X. & Zhou, S. Oxidative stress and oxidative damage in chemical carcinogenesis. *Toxicol. Appl. Pharmacol.* **254**, 86–99 (2011).
14. Abugable, A. A. *et al.* DNA repair and neurological disease: From molecular understanding to the development of diagnostics and model organisms. *DNA Repair* **81**, 102669 (2019).
15. Mladenov, E., Magin, S., Soni, A. & Iliakis, G. DNA double-strand-break repair in higher eukaryotes and its role in genomic instability and cancer: Cell cycle and proliferation-dependent regulation. *Semin. Cancer Biol.* **37–38**, 51–64 (2016).
16. Freudenthal, B. D. Base excision repair of oxidative DNA damage from mechanism to disease. *Front. Biosci.* **22**, 1493–1522 (2017).

17. Jiricny, J. The multifaceted mismatch-repair system. *Nat. Rev. Mol. Cell Biol.* **7**, 335–346 (2006).
18. Spivak, G. Nucleotide excision repair in humans. *DNA Repair* **36**, 13–18 (2015).
19. Reardon, J. T. & Sancar, A. Purification and Characterization of Escherichia coli and Human Nucleotide Excision Repair Enzyme Systems. in *Methods in Enzymology* vol. 408 189–213 (Elsevier, 2006).
20. Gillet, L. C. J. & Schärer, O. D. Molecular Mechanisms of Mammalian Global Genome Nucleotide Excision Repair. *Chem. Rev.* **106**, 253–276 (2006).
21. Hanawalt, P. C. & Spivak, G. Transcription-coupled DNA repair: two decades of progress and surprises. *Nat. Rev. Mol. Cell Biol.* **9**, 958–970 (2008).
22. Zhovmer, A., Oksenysh, V. & Coin, F. Two Sides of the Same Coin: TFIIH Complexes in Transcription and DNA Repair. *Sci. World J.* **10**, 633–643 (2010).
23. Graf, N., Ang, W. H., Zhu, G., Myint, M. & Lippard, S. J. Role of Endonucleases XPF and XPG in Nucleotide Excision Repair of Platinated DNA and Cisplatin/Oxaliplatin Cytotoxicity. *ChemBioChem* **12**, 1115–1123 (2011).
24. de Boer, J. & Hoeijmakers, J. H. J. Nucleotide excision repair and human syndromes. *Carcinogenesis* **21**, 453–460 (2000).
25. Kraemer, K. H. *et al.* Xeroderma pigmentosum, trichothiodystrophy and Cockayne syndrome: A complex genotype–phenotype relationship. *Neuroscience* **145**, 1388–1396 (2007).
26. Kajitani, G. S. *et al.* Transcription blockage by DNA damage in nucleotide excision repair-related neurological dysfunctions. *Semin. Cell Dev. Biol.* **114**, 20–35 (2021).
27. Andressoo, J.-O., Hoeijmakers, J. H. J. & Mitchell, J. R. Nucleotide Excision Repair Disorders and the Balance Between Cancer and Aging. *Cell Cycle* **5**, 2886–2888 (2006).
28. Jager, M. *et al.* Deficiency of nucleotide excision repair is associated with mutational signature observed in cancer. *Genome Res.* **29**, 1067–1077 (2019).
29. Black, J. O. Xeroderma Pigmentosum. *Head Neck Pathol.* **10**, 139–144 (2016).
30. Karikkineth, A. C., Scheibye-Knudsen, M., Fivenson, E., Croteau, D. L. & Bohr, V. A. Cockayne syndrome: Clinical features, model systems and pathways. *Ageing Res. Rev.* **33**, 3–17 (2017).
31. Spivak, G. UV-sensitive syndrome. *Mutat. Res. Mol. Mech. Mutagen.* **577**, 162–169 (2005).
32. Iyama, T. & Wilson, D. M. DNA repair mechanisms in dividing and non-dividing cells. *DNA Repair* **12**, 620–636 (2013).
33. Gupta, S., You, P., SenGupta, T., Nilsen, H. & Sharma, K. Crosstalk between Different DNA Repair Pathways Contributes to Neurodegenerative Diseases. *Biology* **10**, 163 (2021).
34. McMurray, C. T. To die or not to die: DNA repair in neurons. *Mutat. Res. Mol. Mech. Mutagen.* **577**, 260–274 (2005).
35. Marteijn, J. A., Lans, H., Vermeulen, W. & Hoeijmakers, J. H. J. Understanding nucleotide excision repair and its roles in cancer and ageing. *Nat. Rev. Mol. Cell Biol.* **15**, 465–481 (2014).

36. Daniel, L. *et al.* Mechanistic insights in transcription-coupled nucleotide excision repair of ribosomal DNA. *Proc. Natl. Acad. Sci.* **115**, (2018).
37. Sleeman, J. E. & Trinkle-Mulcahy, L. Nuclear bodies: new insights into assembly/dynamics and disease relevance. *Curr. Opin. Cell Biol.* **28**, 76–83 (2014).
38. Nuclear domains 2001.pdf.
39. Zhang, L. *et al.* Phase-Separated Subcellular Compartmentation and Related Human Diseases. *Int. J. Mol. Sci.* **23**, 5491 (2022).
40. Hou, C., Xie, H., Fu, Y., Ma, Y. & Li, T. MloDisDB: a manually curated database of the relations between membraneless organelles and diseases. *Brief. Bioinform.* **22**, bbaa271 (2021).
41. Pederson, T. The plurifunctional nucleolus. *Nucleic Acids Res.* **26**, 3871–3876 (1998).
42. Boisvert, F.-M., van Koningsbruggen, S., Navascués, J. & Lamond, A. I. The multifunctional nucleolus. *Nat. Rev. Mol. Cell Biol.* **8**, 574–585 (2007).
43. Boulon, S., Westman, B. J., Hutten, S., Boisvert, F.-M. & Lamond, A. I. The Nucleolus under Stress. *Mol. Cell* **40**, 216–227 (2010).
44. Sirri, V., Urcuqui-Inchima, S., Roussel, P. & Hernandez-Verdun, D. Nucleolus: the fascinating nuclear body. *Histochem. Cell Biol.* **129**, 13–31 (2008).
45. Tsekrekou, M., Stratigi, K. & Chatzinikolaou, G. The Nucleolus: In Genome Maintenance and Repair. *Int. J. Mol. Sci.* **18**, 1411 (2017).
46. Henderson, A. S., Warburton, D. & Atwood, K. C. Location of Ribosomal DNA in the Human Chromosome Complement. *Proc. Natl. Acad. Sci.* **69**, 3394–3398 (1972).
47. Roussel, P., André, C., Comai, L. & Hernandez-Verdun, D. The rDNA transcription machinery is assembled during mitosis in active NORs and absent in inactive NORs. *J. Cell Biol.* **133**, 235–246 (1996).
48. Hernandez-Verdun, D., Roussel, P., Thiry, M., Sirri, V. & Lafontaine, D. L. J. The nucleolus: structure/function relationship in RNA metabolism: Nucleolus. *Wiley Interdiscip. Rev. RNA* **1**, 415–431 (2010).
49. Savino, T. M., Gébrane-Younès, J., De Mey, J., Sibarita, J.-B. & Hernandez-Verdun, D. Nucleolar Assembly of the Rrna Processing Machinery in Living Cells. *J. Cell Biol.* **153**, 1097–1110 (2001).
50. Lam, Y. W. & Trinkle-Mulcahy, L. New insights into nucleolar structure and function. *F1000Prime Rep.* **7**, (2015).
51. Moss, T. & Stefanovsky, V. Y. At the Center of Eukaryotic Life. *Cell* **109**, 545–548 (2002).
52. Grummt, I. Life on a planet of its own: regulation of RNA polymerase I transcription in the nucleolus. *Genes Dev.* **17**, 1691–1702 (2003).
53. Azouzi, C. *et al.* Coupling Between Production of Ribosomal RNA and Maturation: Just at the Beginning. *Front. Mol. Biosci.* **8**, 778778 (2021).

54. Goodfellow, S. J. & Zomerdijk, J. C. B. M. Basic Mechanisms in RNA Polymerase I Transcription of the Ribosomal RNA Genes. in *Epigenetics: Development and Disease* (ed. Kundu, T. K.) vol. 61 211–236 (Springer Netherlands, 2013).
55. The TATA-Binding Protein and Associated Factors.pdf.
56. Friedrich, J. K., Panov, K. I., Cabart, P., Russell, J. & Zomerdijk, J. C. B. M. TBP-TAF Complex SL1 Directs RNA Polymerase I Pre-initiation Complex Formation and Stabilizes Upstream Binding Factor at the rDNA Promoter. *J. Biol. Chem.* **280**, 29551–29558 (2005).
57. Miller, G. *et al.* hRRN3 is essential in the SL1-mediated recruitment of RNA Polymerase I to rRNA gene promoters. *EMBO J.* **20**, 1373–1382 (2001).
58. Russell, J. & Zomerdijk, J. C. B. M. RNA-polymerase-I-directed rDNA transcription, life and works. *Trends Biochem. Sci.* **30**, 87–96 (2005).
59. Iben, S. *et al.* TFIIF Plays an Essential Role in RNA Polymerase I Transcription. *Cell* **109**, 297–306 (2002).
60. Panov, K. I., Friedrich, J. K. & Zomerdijk, J. C. B. M. A Step Subsequent to Preinitiation Complex Assembly at the Ribosomal RNA Gene Promoter Is Rate Limiting for Human RNA Polymerase I-Dependent Transcription. *Mol. Cell. Biol.* **21**, 2641–2649 (2001).
61. Jansa, P. The transcript release factor PTRF augments ribosomal gene transcription by facilitating reinitiation of RNA polymerase I. *Nucleic Acids Res.* **29**, 423–429 (2001).
62. Granneman, S. & Baserga, S. J. Crosstalk in gene expression: coupling and co-regulation of rDNA transcription, pre-ribosome assembly and pre-rRNA processing. *Curr. Opin. Cell Biol.* **17**, 281–286 (2005).
63. Farley-Barnes, K. I., Ogawa, L. M. & Baserga, S. J. Ribosomopathies: Old Concepts, New Controversies. *Trends Genet.* **35**, 754–767 (2019).
64. Fromont-Racine, M., Senger, B., Saveanu, C. & Fasiolo, F. Ribosome assembly in eukaryotes. *Gene* **313**, 17–42 (2003).
65. Klinge, S. & Woolford, J. L. Ribosome assembly coming into focus. *Nat. Rev. Mol. Cell Biol.* **20**, 116–131 (2019).
66. Schmeing, T. M. & Ramakrishnan, V. What recent ribosome structures have revealed about the mechanism of translation. *Nature* **461**, 1234–1242 (2009).
67. Machyna, M., Neugebauer, K. M. & Staněk, D. Coilin: The first 25 years. *RNA Biol.* **12**, 590–596 (2015).
68. Morris, G. E. The Cajal body. *Biochim. Biophys. Acta BBA - Mol. Cell Res.* **1783**, 2108–2115 (2008).
69. Wang, Q. *et al.* Cajal bodies are linked to genome conformation. *Nat. Commun.* **7**, 10966 (2016).
70. Andrade, L. E., Tan, E. M. & Chan, E. K. Immunocytochemical analysis of the coiled body in the cell cycle and during cell proliferation. *Proc. Natl. Acad. Sci.* **90**, 1947–1951 (1993).

71. Pellizzoni, L., Yong, J. & Dreyfuss, G. Essential Role for the SMN Complex in the Specificity of snRNP Assembly. *Science* **298**, 1775–1779 (2002).
72. Sleeman, J. E., Ajuh, P. & Lamond, A. I. snRNP protein expression enhances Cajal bodies. 13.
73. Cioce, M. & Lamond, A. I. CAJAL BODIES: A Long History of Discovery. *Annu. Rev. Cell Dev. Biol.* **21**, 105–131 (2005).
74. Dundr, M. *et al.* In vivo kinetics of Cajal body components. *J. Cell Biol.* **164**, 831–842 (2004).
75. Raška, I. *et al.* Association between the nucleolus and the coiled body. *J. Struct. Biol.* **104**, 120–127 (1990).
76. Lafarga, M., Tapia, O., Romero, A. M. & Berciano, M. T. Cajal bodies in neurons. *RNA Biol.* **14**, 712–725 (2017).
77. Trinkle-Mulcahy, L. & Sleeman, J. E. The Cajal body and the nucleolus: “In a relationship” or “It’s complicated”? *RNA Biol.* **14**, 739–751 (2017).
78. Berciano, M. T. *et al.* Cajal body number and nucleolar size correlate with the cell body mass in human sensory ganglia neurons. *J. Struct. Biol.* **158**, 410–420 (2007).
79. Girard, C. Depletion of SMN by RNA interference in HeLa cells induces defects in Cajal body formation. *Nucleic Acids Res.* **34**, 2925–2932 (2006).
80. Tapia, O. *et al.* Reorganization of Cajal bodies and nucleolar targeting of coilin in motor neurons of type I spinal muscular atrophy. *Histochem. Cell Biol.* **137**, 657–667 (2012).
81. Han, K.-J. *et al.* Monoubiquitination of survival motor neuron regulates its cellular localization and Cajal body integrity. *Hum. Mol. Genet.* **25**, 1392–1405 (2016).
82. Liu, Q. & Dreyfuss, G. A novel nuclear structure containing the survival of motor neurons protein. *EMBO J.* **15**, 3555–3565 (1996).
83. Navascues, J., Berciano, MariaT., Tucker, KarenE., Lafarga, M. & Matera, A. G. Targeting SMN to Cajal bodies and nuclear gems during neuritogenesis. *Chromosoma* **112**, (2004).
84. Boulon, S., Westman, B. J., Hutten, S., Boisvert, F.-M. & Lamond, A. I. The Nucleolus under Stress. *Mol. Cell* **40**, 216–227 (2010).
85. Al-Baker, E. A., Oshin, M., Hutchison, C. J. & Kill, I. R. Analysis of UV-induced damage and repair in young and senescent human dermal fibroblasts using the comet assay. *Mech. Ageing Dev.* **126**, 664–672 (2005).
86. Shav-Tal, Y. *et al.* Dynamic Sorting of Nuclear Components into Distinct Nucleolar Caps during Transcriptional Inhibition. *Mol. Biol. Cell* **16**, 2395–2413 (2005).
87. Greco, A. Involvement of the nucleolus in replication of human viruses: Nucleolus and human virus replication. *Rev. Med. Virol.* **19**, 201–214 (2009).
88. Gridasova, A. A. & Henry, R. W. The p53 Tumor Suppressor Protein Represses Human snRNA Gene Transcription by RNA Polymerases II and III Independently of Sequence-Specific DNA Binding. *Mol. Cell. Biol.* **25**, 3247–3260 (2005).

89. Cioce, M., Boulon, S., Matera, A. G. & Lamond, A. I. UV-induced fragmentation of Cajal bodies. *J. Cell Biol.* **175**, 401–413 (2006).
90. Andersen, J. S. *et al.* Nucleolar proteome dynamics. *Nature* **433**, 77–83 (2005).
91. Rodriguez-Corona, U., Sobol, M., Rodriguez-Zapata, L. C., Hozak, P. & Castano, E. Fibrillarin from Archaea to human: Review on fibrillarin. *Biol. Cell* **107**, 159–174 (2015).
92. Newton, K., Petfalski, E., Tollervey, D. & Cáceres, J. F. Fibrillarin Is Essential for Early Development and Required for Accumulation of an Intron-Encoded Small Nucleolar RNA in the Mouse. *Mol. Cell. Biol.* **23**, 8519–8527 (2003).
93. Feder, M., Pas, J., Wyrwicz, L. S. & Bujnicki, J. M. Molecular phylogenetics of the RrmJ/fibrillarin superfamily of ribose 2'-O-methyltransferases. *Gene* **302**, 129–138 (2003).
94. Jones, K. W. *et al.* Direct Interaction of the Spinal Muscular Atrophy Disease Protein SMN with the Small Nucleolar RNA-associated Protein Fibrillarin. *J. Biol. Chem.* **276**, 38645–38651 (2001).
95. Pellizzoni, L., Baccon, J., Charroux, B. & Dreyfuss, G. The survival of motor neurons (SMN) protein interacts with the snoRNP proteins fibrillarin and GAR1. *Curr. Biol.* **11**, 1079–1088 (2001).
96. Kolb, S. J. & Kissel, J. T. Spinal Muscular Atrophy. *Neurol. Clin.* **33**, 831–846 (2015).
97. Kolb, S. J. & Kissel, J. T. Spinal Muscular Atrophy. *Neurol. Clin.* **33**, 831–846 (2015).
98. D'Amico, A., Mercuri, E., Tiziano, F. D. & Bertini, E. Spinal muscular atrophy. *Orphanet J. Rare Dis.* **6**, 71 (2011).
99. Monani, U. R. Spinal Muscular Atrophy: A Deficiency in a Ubiquitous Protein; a Motor Neuron-Specific Disease. *Neuron* **48**, 885–895 (2005).
100. Verhaart, I. E. C. *et al.* Prevalence, incidence and carrier frequency of 5q-linked spinal muscular atrophy – a literature review. *Orphanet J. Rare Dis.* **12**, 124 (2017).
101. Melki, J. *et al.* Gene for chronic proximal spinal muscular atrophies maps to chromosome Sq. 2.
102. Gilliam, T. C. *et al.* Genetic homogeneity between acute and chronic forms of spinal muscular atrophy. *Nature* **345**, 823–825 (1990).
103. Lefebvre, S. *et al.* Identification and characterization of a spinal muscular atrophy-determining gene. *Cell* **80**, 155–165 (1995).
104. Wirth, B. An update of the mutation spectrum of the survival motor neuron gene (SMN1) in autosomal recessive spinal muscular atrophy (SMA). *Hum. Mutat.* **15**, 228–237 (2000).
105. Wirth, B. *et al.* De Novo Rearrangements Found in 2% of Index Patients with Spinal Muscular Atrophy: Mutational Mechanisms, Parental Origin, Mutation Rate, and Implications for Genetic Counseling. *Am. J. Hum. Genet.* **61**, 1102–1111 (1997).
106. Feng, Y. *et al.* The next generation of population-based spinal muscular atrophy carrier screening: comprehensive pan-ethnic SMN1 copy-number and sequence variant analysis by massively parallel sequencing. *Genet. Med.* **19**, 936–944 (2017).

107. Lorson, C. L., Hahnen, E., Androphy, E. J. & Wirth, B. A single nucleotide in the *SMN* gene regulates splicing and is responsible for spinal muscular atrophy. *Proc. Natl. Acad. Sci.* **96**, 6307–6311 (1999).
108. Monani, U. R. A single nucleotide difference that alters splicing patterns distinguishes the SMA gene SMN1 from the copy gene SMN2. *Hum. Mol. Genet.* **8**, 1177–1183 (1999).
109. Burnett, B. G. *et al.* Regulation of SMN Protein Stability. *Mol. Cell. Biol.* **29**, 1107–1115 (2009).
110. Taylor, J. E. *et al.* Correlation of SMNt and SMNc gene copy number with age of onset and survival in spinal muscular atrophy. *Eur. J. Hum. Genet.* **6**, 467–474 (1998).
111. Feldkötter, M., Schwarzer, V., Wirth, R., Wienker, T. F. & Wirth, B. Quantitative Analyses of SMN1 and SMN2 Based on Real-Time LightCycler PCR: Fast and Highly Reliable Carrier Testing and Prediction of Severity of Spinal Muscular Atrophy. *Am. J. Hum. Genet.* **70**, 358–368 (2002).
112. Keinath, M. C., Prior, D. E. & Prior, T. W. Spinal Muscular Atrophy: Mutations, Testing, and Clinical Relevance. *Appl. Clin. Genet.* **Volume 14**, 11–25 (2021).
113. Rudnik-Schoneborn, S. *et al.* Congenital heart disease is a feature of severe infantile spinal muscular atrophy. *J. Med. Genet.* **45**, 635–638 (2008).
114. Palladino, A. Cardiac involvement in patients with Spinal Muscular Atrophies. 4.
115. Pera, M. C. *et al.* Sleep disorders in spinal muscular atrophy. *Sleep Med.* **30**, 160–163 (2017).
116. Arnold, W. D., Kassar, D. & Kissel, J. T. Spinal muscular atrophy: Diagnosis and management in a new therapeutic era: Spinal Muscular Atrophy. *Muscle Nerve* **51**, 157–167 (2015).
117. Dubowitz, V. Very severe spinal muscular atrophy (SMA type 0): an expanding clinical phenotype. 3.
118. Farrar, M. A., Vucic, S., Johnston, H. M., du Sart, D. & Kiernan, M. C. Pathophysiological Insights Derived by Natural History and Motor Function of Spinal Muscular Atrophy. *J. Pediatr.* **162**, 155–159 (2013).
119. Wirth, B., Karakaya, M., Kye, M. J. & Mendoza-Ferreira, N. Twenty-Five Years of Spinal Muscular Atrophy Research: From Phenotype to Genotype to Therapy, and What Comes Next. *Annu. Rev. Genomics Hum. Genet.* **21**, 231–261 (2020).
120. Coovert, D. The survival motor neuron protein in spinal muscular atrophy. *Hum. Mol. Genet.* **6**, 1205–1214 (1997).
121. Martínez-Hernández, R. *et al.* The Developmental Pattern of Myotubes in Spinal Muscular Atrophy Indicates Prenatal Delay of Muscle Maturation. *J. Neuropathol. Exp. Neurol.* **68**, 474–481 (2009).
122. Rossoll, W. *et al.* Smn, the spinal muscular atrophy–determining gene product, modulates axon growth and localization of β -actin mRNA in growth cones of motoneurons. *J. Cell Biol.* **163**, 801–812 (2003).

123. Genabai, N. K. *et al.* Genetic inhibition of JNK3 ameliorates spinal muscular atrophy. *Hum. Mol. Genet.* ddv401 (2015) doi:10.1093/hmg/ddv401.
124. Signal transduction by the JNK group of MAP kinases.pdf.
125. Coffey, E. T. Nuclear and cytosolic JNK signalling in neurons. *Nat. Rev. Neurosci.* **15**, 285–299 (2014).
126. Giesemann, T. *et al.* A Role for Polyproline Motifs in the Spinal Muscular Atrophy Protein SMN. *J. Biol. Chem.* **274**, 37908–37914 (1999).
127. Bowerman, M., Shafey, D. & Kothary, R. Smn Depletion Alters Profilin II Expression and Leads to Upregulation of the RhoA/ROCK Pathway and Defects in Neuronal Integrity. *J. Mol. Neurosci.* **32**, 120–131 (2007).
128. Coque, E., Raoul, C. & Bowerman, M. ROCK inhibition as a therapy for spinal muscular atrophy: understanding the repercussions on multiple cellular targets. *Front. Neurosci.* **8**, (2014).
129. Chang, H.-C., Hung, W.-C., Chuang, Y.-J. & Jong, Y.-J. Degradation of survival motor neuron (SMN) protein is mediated via the ubiquitin/proteasome pathway. *Neurochem. Int.* **45**, 1107–1112 (2004).
130. Korhonen, L. & Lindholm, D. The ubiquitin proteasome system in synaptic and axonal degeneration. *J. Cell Biol.* **165**, 27–30 (2004).
131. Wishart, T. M. *et al.* Dysregulation of ubiquitin homeostasis and β -catenin signaling promote spinal muscular atrophy. *J. Clin. Invest.* **124**, 1821–1834 (2014).
132. Powis, R. A. *et al.* Systemic restoration of UBA1 ameliorates disease in spinal muscular atrophy. *JCI Insight* **1**, (2016).
133. Mercuri, E. *et al.* Diagnosis and management of spinal muscular atrophy: Part 1: Recommendations for diagnosis, rehabilitation, orthopedic and nutritional care. *Neuromuscul. Disord.* **28**, 103–115 (2018).
134. Schorling, D. C., Pechmann, A. & Kirschner, J. Advances in Treatment of Spinal Muscular Atrophy – New Phenotypes, New Challenges, New Implications for Care. *J. Neuromuscul. Dis.* **7**, 1–13 (2020).
135. De Vivo, D. C. *et al.* Nusinersen initiated in infants during the presymptomatic stage of spinal muscular atrophy: Interim efficacy and safety results from the Phase 2 NURTURE study. *Neuromuscul. Disord.* **29**, 842–856 (2019).
136. Mendell, J. R. *et al.* Single-Dose Gene-Replacement Therapy for Spinal Muscular Atrophy. *N. Engl. J. Med.* **377**, 1713–1722 (2017).
137. Ratni, H. *et al.* Discovery of Risdiplam, a Selective Survival of Motor Neuron-2 (SMN2) Gene Splicing Modifier for the Treatment of Spinal Muscular Atrophy (SMA). *J. Med. Chem.* **61**, 6501–6517 (2018).

138. Kannan, A., Bhatia, K., Branzei, D. & Gangwani, L. Combined deficiency of Senataxin and DNA-PKcs causes DNA damage accumulation and neurodegeneration in spinal muscular atrophy. *Nucleic Acids Res.* **46**, 8326–8346 (2018).
139. Yanling Zhao, D. *et al.* SMN and symmetric arginine dimethylation of RNA polymerase II C-terminal domain control termination. *Nature* **529**, 48–53 (2016).
140. Kashima, T., Rao, N. & Manley, J. L. An intronic element contributes to splicing repression in spinal muscular atrophy. *Proc. Natl. Acad. Sci.* **104**, 3426–3431 (2007).
141. Madocsai, C., Lim, S. R., Geib, T., Lam, B. J. & Hertel, K. J. Correction of SMN2 Pre-mRNA splicing by antisense U7 small nuclear RNAs. *Mol. Ther.* **12**, 1013–1022 (2005).
142. Ebert, A. D. *et al.* Induced pluripotent stem cells from a spinal muscular atrophy patient. *Nature* **457**, 277–280 (2009).
143. Rochette, C., Gilbert, N. & Simard, L. SMN gene duplication and the emergence of the SMN2 gene occurred in distinct hominids: SMN2 is unique to Homo sapiens. *Hum. Genet.* **108**, 255–266 (2001).
144. Schrank, B. *et al.* Inactivation of the survival motor neuron gene, a candidate gene for human spinal muscular atrophy, leads to massive cell death in early mouse embryos. *Proc. Natl. Acad. Sci.* **94**, 9920–9925 (1997).
145. Bowerman, M., Murray, L. M., Beauvais, A., Pinheiro, B. & Kothary, R. A critical smn threshold in mice dictates onset of an intermediate spinal muscular atrophy phenotype associated with a distinct neuromuscular junction pathology. *Neuromuscul. Disord.* **22**, 263–276 (2012).
146. Hsieh-Li, H. M. *et al.* A mouse model for spinal muscular atrophy. *Nat. Genet.* **24**, 66–70 (2000).
147. Monani, U. R. *et al.* The human centromeric survival motor neuron gene (SMN2) rescues embryonic lethality in *Smn*^{-/-} mice and results in a mouse with spinal muscular atrophy. **8**.
148. Le, T. T. *et al.* SMN Δ 7, the major product of the centromeric survival motor neuron (SMN2) gene, extends survival in mice with spinal muscular atrophy and associates with full-length SMN. *Hum. Mol. Genet.* **14**, 845–857 (2005).
149. Frugier, T. Nuclear targeting defect of SMN lacking the C-terminus in a mouse model of spinal muscular atrophy. *Hum. Mol. Genet.* **9**, 849–858 (2000).
150. Cifuentes-Diaz, C. *et al.* Deletion of Murine SMN Exon 7 Directed to Skeletal Muscle Leads to Severe Muscular Dystrophy. *J. Cell Biol.* **152**, 1107–1114 (2001).
151. McWhorter, M. L., Monani, U. R., Burghes, A. H. M. & Beattie, C. E. Knockdown of the survival motor neuron (*Smn*) protein in zebrafish causes defects in motor axon outgrowth and pathfinding. *J. Cell Biol.* **162**, 919–932 (2003).

152. Miguel-Aliaga, I., Chan, Y. B., Davies, K. E. & van den Heuvel, M. Disruption of SMN function by ectopic expression of the human *SMN* gene in *Drosophila*. *FEBS Lett.* **486**, 99–102 (2000).
153. Briese, M. *et al.* Deletion of *smn-1*, the *Caenorhabditis elegans* ortholog of the spinal muscular atrophy gene, results in locomotor dysfunction and reduced lifespan. *Hum. Mol. Genet.* **18**, 97–104 (2008).
154. Rajendra, T. K. *et al.* A *Drosophila melanogaster* model of spinal muscular atrophy reveals a function for SMN in striated muscle. *J. Cell Biol.* **176**, 831–841 (2007).
155. Praveen, K., Wen, Y. & Matera, A. G. A *Drosophila* Model of Spinal Muscular Atrophy Uncouples snRNP Biogenesis Functions of Survival Motor Neuron from Locomotion and Viability Defects. *Cell Rep.* **1**, 624–631 (2012).
156. Vitte, J. *et al.* Refined Characterization of the Expression and Stability of the SMN Gene Products. *Am. J. Pathol.* **171**, 1269–1280 (2007).
157. Setola, V. *et al.* Axonal-SMN (a-SMN), a protein isoform of the survival motor neuron gene, is specifically involved in axonogenesis. *Proc. Natl. Acad. Sci.* **104**, 1959–1964 (2007).
158. Seo, J., Singh, N. N., Ottesen, E. W., Lee, B. M. & Singh, R. N. A novel human-specific splice isoform alters the critical C-terminus of Survival Motor Neuron protein. *Sci. Rep.* **6**, 30778 (2016).
159. Survival motor neuron gene transcript analysis in muscles from spinal muscular atrophy patients.pdf.
160. Morse, R., Shaw, D. J., Todd, A. G. & Young, P. J. Targeting of SMN to Cajal bodies is mediated by self-association. *Hum. Mol. Genet.* **16**, 2349–2358 (2007).
161. Osman, E. Y. *et al.* Functional characterization of SMN evolution in mouse models of SMA. *Sci. Rep.* **9**, 9472 (2019).
162. Lorson, C. L. & Androphy, E. J. The domain encoded by exon 2 of the survival motor neuron protein mediates nucleic acid binding. *7*.
163. Young, P. J. *et al.* A Direct Interaction between the Survival Motor Neuron Protein and p53 and Its Relationship to Spinal Muscular Atrophy. *J. Biol. Chem.* **277**, 2852–2859 (2002).
164. Friesen, W. J., Massenet, S., Paushkin, S., Wyce, A. & Dreyfuss, G. SMN, the Product of the Spinal Muscular Atrophy Gene, Binds Preferentially to Dimethylarginine-Containing Protein Targets. *Mol. Cell* **7**, 1111–1117 (2001).
165. Hebert, M. D., Szymczyk, P. W., Shpargel, K. B. & Matera, A. G. Coilin forms the bridge between Cajal bodies and SMN, the Spinal Muscular Atrophy protein. *Genes Dev.* **15**, 2720–2729 (2001).
166. Yamazaki, T. *et al.* FUS-SMN Protein Interactions Link the Motor Neuron Diseases ALS and SMA. *Cell Rep.* **2**, 799–806 (2012).

167. Selenko, P. *et al.* SMN Tudor domain structure and its interaction with the Sm proteins. *Nat. Struct. Biol.* **8**, 7 (2001).
168. Sabra, M., Texier, P., El Maalouf, J. & Lomonte, P. The tudor protein survival motor neuron (SMN) is a chromatin-binding protein that interacts with methylated histone H3 lysine 79. *J. Cell Sci.* jcs.126003 (2013) doi:10.1242/jcs.126003.
169. Morse, R., Shaw, D. J., Todd, A. G. & Young, P. J. Targeting of SMN to Cajal bodies is mediated by self-association. *Hum. Mol. Genet.* **16**, 2349–2358 (2007).
170. Charroux, B. *et al.* Gemin3: A Novel DEAD Box Protein that Interacts with SMN, the Spinal Muscular Atrophy Gene Product, and Is a Component of Gems. *J. Cell Biol.* **147**, 13 (1999).
171. Zou, J. *et al.* Survival Motor Neuron (SMN) Protein Interacts with Transcription Corepressor mSin3A. *J. Biol. Chem.* **279**, 14922–14928 (2004).
172. Giavazzi, A., Setola, V., Simonati, A. & Battaglia, G. Neuronal-Specific Roles of the Survival Motor Neuron Protein: Evidence From Survival Motor Neuron Expression Patterns in the Developing Human Central Nervous System. *J Neuropathol Exp Neurol* **65**, 11 (2006).
173. Pellizzoni, L., Kataoka, N., Charroux, B. & Dreyfuss, G. A Novel Function for SMN, the Spinal Muscular Atrophy Disease Gene Product, in Pre-mRNA Splicing. *Cell* **95**, 615–624 (1998).
174. Zhang, R. *et al.* Structure of a Key Intermediate of the SMN Complex Reveals Gemin2's Crucial Function in snRNP Assembly. *Cell* **146**, 384–395 (2011).
175. Liu, Q., Fischer, U., Wang, F. & Dreyfuss, G. The Spinal Muscular Atrophy Disease Gene Product, SMN, and Its Associated Protein SIP1 Are in a Complex with Spliceosomal snRNP Proteins. *Cell* **90**, 1013–1021 (1997).
176. Fischer, U., Liu, Q. & Dreyfuss, G. The SMN–SIP1 Complex Has an Essential Role in Spliceosomal snRNP Biogenesis. *Cell* **90**, 1023–1029 (1997).
177. Tisdale, S. *et al.* SMN Is Essential for the Biogenesis of U7 Small Nuclear Ribonucleoprotein and 3'-End Formation of Histone mRNAs. *Cell Rep.* **5**, 1187–1195 (2013).
178. Sanchez, G. *et al.* A novel function for the survival motoneuron protein as a translational regulator. *Hum. Mol. Genet.* **22**, 668–684 (2013).
179. Hubers, L. *et al.* HuD interacts with survival motor neuron protein and can rescue spinal muscular atrophy-like neuronal defects. *Hum. Mol. Genet.* **20**, 553–579 (2011).
180. Fallini, C. *et al.* The Survival of Motor Neuron (SMN) Protein Interacts with the mRNA-Binding Protein HuD and Regulates Localization of Poly(A) mRNA in Primary Motor Neuron Axons. *J. Neurosci.* **31**, 3914–3925 (2011).
181. Fallini, C., Donlin-Asp, P. G., Rouanet, J. P., Bassell, G. J. & Rossoll, W. Deficiency of the Survival of Motor Neuron Protein Impairs mRNA Localization and Local Translation in the Growth Cone of Motor Neurons. *J. Neurosci.* **36**, 3811–3820 (2016).

182. Rage, F. *et al.* Genome-wide identification of mRNAs associated with the protein SMN whose depletion decreases their axonal localization. *RNA* **19**, 1755–1766 (2013).
183. Strasswimmer, J. Identification of survival motor neuron as a transcriptional activator-binding protein. *Hum. Mol. Genet.* **8**, 1219–1226 (1999).
184. Santos-Pereira, J. M. & Aguilera, A. R loops: new modulators of genome dynamics and function. *Nat. Rev. Genet.* **16**, 583–597 (2015).
185. Suraweera, A. *et al.* Functional role for senataxin, defective in ataxia oculomotor apraxia type 2, in transcriptional regulation. *Hum. Mol. Genet.* **18**, 3384–3396 (2009).
186. Gubitz, A. The SMN complex. *Exp. Cell Res.* **296**, 51–56 (2004).
187. Fischer, U., Englbrecht, C. & Chari, A. Biogenesis of spliceosomal small nuclear ribonucleoproteins. *WIREs RNA* **2**, 718–731 (2011).
188. Meier, I. D., Walker, M. P. & Matera, A. G. *Gemin4* is an essential gene in mice, and its overexpression in human cells causes relocalization of the SMN complex to the nucleoplasm. *Biol. Open* bio.032409 (2018) doi:10.1242/bio.032409.
189. Yong, J., Kasim, M., Bachorik, J. L., Wan, L. & Dreyfuss, G. Gemin5 Delivers snRNA Precursors to the SMN Complex for snRNP Biogenesis. *Mol. Cell* **38**, 551–562 (2010).
190. Ma, Y., Dostie, J., Dreyfuss, G. & Van Duyne, G. D. The Gemin6-Gemin7 Heterodimer from the Survival of Motor Neurons Complex Has an Sm Protein-like Structure. *Structure* **13**, 883–892 (2005).
191. Carissimi, C., Saieva, L., Gabanella, F. & Pellizzoni, L. Gemin8 Is Required for the Architecture and Function of the Survival Motor Neuron Complex. *J. Biol. Chem.* **281**, 37009–37016 (2006).
192. Singh, R. N., Howell, M. D., Ottesen, E. W. & Singh, N. N. Diverse role of survival motor neuron protein. *Biochim. Biophys. Acta BBA - Gene Regul. Mech.* **1860**, 299–315 (2017).
193. Matera, A. G. & Wang, Z. A day in the life of the spliceosome. *Nat. Rev. Mol. Cell Biol.* **15**, 108–121 (2014).
194. Marzluff, W. F., Wagner, E. J. & Duronio, R. J. Metabolism and regulation of canonical histone mRNAs: life without a poly(A) tail. *Nat. Rev. Genet.* **9**, 843–854 (2008).
195. Pillai, R. S. *et al.* Unique Sm core structure of U7 snRNPs: assembly by a specialized SMN complex and the role of a new component, Lsm11, in histone RNA processing. *Genes Dev.* **17**, 2321–2333 (2003).
196. Gardner, P. P., Bateman, A. & Poole, A. M. SnoPatrol: how many snoRNA genes are there? *J. Biol.* **9**, 4 (2010).
197. Jorjani, H. *et al.* An updated human snoRNAome. *Nucleic Acids Res.* **44**, 5068–5082 (2016).

198. Renvoise, B. *et al.* The loss of the snoRNP chaperone Nopp140 from Cajal bodies of patient fibroblasts correlates with the severity of spinal muscular atrophy. *Hum. Mol. Genet.* **18**, 1181–1189 (2009).
199. Kim, E., Goren, A. & Ast, G. Alternative splicing and disease. *RNA Biol.* **5**, 17–19 (2008).
200. Zhang, Z. *et al.* SMN Deficiency Causes Tissue-Specific Perturbations in the Repertoire of snRNAs and Widespread Defects in Splicing. *Cell* **133**, 585–600 (2008).
201. Shafey, D., Boyer, J. G., Bhanot, K. & Kothary, R. Identification of Novel Interacting Protein Partners of SMN Using Tandem Affinity Purification. *J. Proteome Res.* **9**, 1659–1669 (2010).
202. Sanchez, G. *et al.* A novel role for CARM1 in promoting nonsense-mediated mRNA decay: potential implications for spinal muscular atrophy. *Nucleic Acids Res.* **44**, 2661–2676 (2016).
203. Rossoll, W. *et al.* Smn, the spinal muscular atrophy–determining gene product, modulates axon growth and localization of β -actin mRNA in growth cones of motoneurons. *J. Cell Biol.* **163**, 801–812 (2003).
204. Piazzon, N. *et al.* In Vitro and in Cellulo Evidences for Association of the Survival of Motor Neuron Complex with the Fragile X Mental Retardation Protein. *J. Biol. Chem.* **283**, 5598–5610 (2008).
205. Fallini, C. *et al.* Dynamics of survival of motor neuron (SMN) protein interaction with the mRNA-binding protein IMP1 facilitates its trafficking into motor neuron axons: SMN Controls IMP1 Axonal Localization. *Dev. Neurobiol.* **74**, 319–332 (2014).
206. Andrade, L. E. *et al.* Human autoantibody to a novel protein of the nuclear coiled body: immunological characterization and cDNA cloning of p80-coilin. *J. Exp. Med.* **173**, 1407–1419 (1991).
207. Hebert, M. D., Shpargel, K. B., Ospina, J. K., Tucker, K. E. & Matera, A. G. Coilin Methylation Regulates Nuclear Body Formation. *Dev. Cell* **3**, 329–337 (2002).
208. Raimer, A. C., Gray, K. M. & Matera, A. G. SMN - A chaperone for nuclear RNP social occasions? *RNA Biol.* **14**, 701–711 (2017).
209. Friesen, W. J., Massenet, S., Paushkin, S., Wyce, A. & Dreyfuss, G. SMN, the Product of the Spinal Muscular Atrophy Gene, Binds Preferentially to Dimethylarginine-Containing Protein Targets. *Mol. Cell* **7**, 1111–1117 (2001).
210. Cuscó, I. & Barceló, M. J. CME Detection of novel mutations in the SMN Tudor domain in type I SMA patients. 4.
211. Hashimoto, M. *et al.* Severe Hypomyelination and Developmental Defects Are Caused in Mice Lacking Protein Arginine Methyltransferase 1 (PRMT1) in the Central Nervous System. *J. Biol. Chem.* **291**, 2237–2245 (2016).

212. Bezzi, M. *et al.* Regulation of constitutive and alternative splicing by PRMT5 reveals a role for *Mdm4* pre-mRNA in sensing defects in the spliceosomal machinery. *Genes Dev.* **27**, 1903–1916 (2013).
213. Paik, W. K. & Kim, S. Protein Methylase I. *J. Biol. Chem.* **243**, 2108–2114 (1968).
214. Bedford, M. T. & Clarke, S. G. Protein Arginine Methylation in Mammals: Who, What, and Why. *Mol. Cell* **33**, 1–13 (2009).
215. Tewary, S. K., Zheng, Y. G. & Ho, M.-C. Protein arginine methyltransferases: insights into the enzyme structure and mechanism at the atomic level. *Cell. Mol. Life Sci.* **76**, 2917–2932 (2019).
216. Yang, Y. & Bedford, M. T. Protein arginine methyltransferases and cancer. *Nat. Rev. Cancer* **13**, 37–50 (2013).
217. Lee, J., An, S., Lee, S.-J. & Kang, J.-S. Protein Arginine Methyltransferases in Neuromuscular Function and Diseases. *Cells* **11**, 364 (2022).
218. Wu, Q., Schapira, M., Arrowsmith, C. H. & Barsyte-Lovejoy, D. Protein arginine methylation: from enigmatic functions to therapeutic targeting. *Nat. Rev. Drug Discov.* **20**, 509–530 (2021).
219. Kannan, A., Jiang, X., He, L., Ahmad, S. & Gangwani, L. ZPR1 prevents R-loop accumulation, upregulates SMN2 expression and rescues spinal muscular atrophy. *Brain* **143**, 69–93 (2020).
220. Fayzullina, S. & Martin, L. J. Skeletal Muscle DNA Damage Precedes Spinal Motor Neuron DNA Damage in a Mouse Model of Spinal Muscular Atrophy (SMA). *PLoS ONE* **9**, e93329 (2014).
221. Jangi, M. *et al.* SMN deficiency in severe models of spinal muscular atrophy causes widespread intron retention and DNA damage. *Proc. Natl. Acad. Sci.* **114**, (2017).
222. Karyka, E. *et al.* SMN-deficient cells exhibit increased ribosomal DNA damage. *Life Sci. Alliance* **5**, e202101145 (2022).
223. Takizawa, Y. *et al.* GEMIN2 promotes accumulation of RAD51 at double-strand breaks in homologous recombination. *Nucleic Acids Res.* **38**, 5059–5074 (2010).

Chapter three

Materials & Methods

1. Cell culture and treatments

The cells used in this study were: (i) wild-type SV40-immortalized human fibroblasts (MRC5); (ii) XPC-deficient SV40-immortalized human fibroblast (XP4PA, GG-NER deficient); (iii) CSA-deficient SV40-immortalized human fibroblast (CS3BE, TC-NER-deficient); (iv) CSB-deficient SV40-immortalized human fibroblast (CS1AN, TC-NER-deficient); (v) CS3BE stably expressing CSA-GFP; (vi) CS1AN stably expressing CSB-GFP. Immortalized human fibroblasts were cultured in DMEM (Lonza) supplemented with 10% fetal bovine serum (FBS, Sigma) and 1% antibiotics (penicillin and streptomycin; Lonza) and incubated at 37°C in 20% O₂ and 5% CO₂.

CSA-GFP and CSB-GFP stably expressing cell line selection were performed with G418 at 2 mg/ml.

The SV40-immortalized human fibroblasts (MRC5 + Sh-scramble, MRC5 + Sh5-SMN, and MRC5 + Sh6-SMN) cells were obtained by transduction of lentiviral particles produced (as described <https://www.addgene.org/protocols/plko/#E>) from piSMART hEF1 α / turboGFP (Dharmacon) doxycycline-inducible lentiviral system containing a Short Hairpin (Sh) scramble (VSC6572). For (Sh) SMN: Sh5 SMN (V3IHSHEG_4923340), Sh6 SMN (V3IHSHEG_5297527), which target both telomeric SMN1 and centromeric SMN2 copies of the gene. The cells were cultured in DMEM (Lonza) supplemented with 10% fetal bovine serum (FBS, Sigma) and 1% antibiotics (penicillin and streptomycin; Lonza), maintained in 100 ng/ml puromycin then to induce the expression of the Sh products they were treated with 100 ng/ml doxycycline. The cells were incubated at 37°C in 20% O₂ and 5% CO₂.

The motor neuron culture protocol provided by our collaborator is confidential to them.

2. UV-C irradiation

Cells were irradiated under a UV-C lamp (254 nm, 6-Watt light) at 16 J/m², locally irradiated with a UV-C dose of 100 J/m² through a filter with holes of 5 µm of diameter (Millipore) or mock-irradiated (non-irradiated control). Following UV-irradiation, cells were incubated in the medium until the time of fixation.

3. Transfection of small interfering RNAs (siRNAs)

Two transient transfections of siRNAs were performed to increase the efficiency of protein downregulation. According to the manufacturers' protocols, the first and second transfections were performed on day 1 and day 2 after plating, using Lipofectamine® RNAiMAX reagent (Invitrogen; 13778150). Experiments were performed between 24h and 72h after the second transfection. siRNA efficiency was confirmed by western blot on whole-cell extracts. References or sequences for the siRNAs used are presented in Table 1.

Table 1

Target	Final Concentration	Reference/Sequence
siMock	10 nM	Dharmacon:D-001210-02
si coilin	10 nM	Dharmacon:M-019894-01-0005

4. Protein extraction

To verify siRNA efficiency, Western Blot analysis on whole cell extracts was performed using the PIERCE RIPA buffer (Thermo, #89900) complemented with PIC.

For immunoprecipitation, cells cultured in 10-cm dishes were harvested by scraping and the pellet was washed once with PBS supplemented with the Protease Inhibitor Cocktail (PIC, Roche). The extraction of nuclear proteins has been performed using the CellLytic™

NuCLEAR™ Extraction kit (Sigma-Aldrich) complemented with PIC. Protein concentration was determined using the Bradford method. The samples were diluted with Laemmli buffer (10% glycerol, 5% b-mercaptoethanol, 3% sodium dodecyl sulfate, 100mM Tris-HCL [pH -.8], bromophenol blue), and heated 95°C before loading on an SDS-PAGE gel.

5. Co-immunoprecipitation

For co-immunoprecipitation, 10 µl of protein G magnetic beads (Bio-ademead, Ademtech) were used per IP. 2µg of antibody (Table 2) were bound to the beads in PBS with BSA (3%) during 2h at 4°C with rotation. 100 µg of nuclear extracts were then incubated with beads antibodies complex for 2h at 4°C with rotation. After two washes at 100 mM salt, two washes at 150mM and one wash at 100mM, beads were boiled in 2x Laemmli buffer and eluted samples loaded on a SDS PAGE gel.

6. Western blot

Protein concentration was determined by using the Bradford method. Samples were diluted with 2x Laemmli buffer and heated at 95 °C 5 min spin down. Proteins were separated on 8% and 12% SDS/PAGE (37:5:1) and then transferred onto a polyvinylidene difluoride membrane (PVDF) (0.45 µm; Millipore). The membrane was blocked in 5% milk PBS 0.1% Tween (PBS-T) and incubated for 45 min or O/N with the primary antibodies (see Primary Antibodies, Table 2) in milk PBS-Tween. Subsequently, the membrane was washed with PBS-T (3x 10 min) and incubated with the secondary antibody in milk PBS-T. After the same washing procedure, protein bands were visualized via chemiluminescence (ECL Enhanced Chemo Luminescence; Pierce ECL Western Blotting Substrate) using the ChemiDoc MP system (BioRad).

7. Cytostripping

To improve the nuclear signal of SMN, cytoplasm of the cells was removed by Cytostripping prior fixation. Briefly, the coverslips were washed with cold PBS 2X then incubated 5 min with Cytoskeleton buffer (PIPES pH6,8 10mM; NaCl 100mM; Sucrose 300mM; MgCl₂ 3mM; EGTA 1mM; Triton X100 0,5%) followed by 5 min incubation with Cytostripping buffer (Tris-HCl pH7,4 10mM; NaCl 10mM; MgCl₂ 3mM; Tween 40 1%; Sodium deoxycholate 0,5%).

8. Proximity ligation assay

Duolink™ PLA (Merck, Darmstadt, Germany) kit was used following the manufacturer's instructions. In brief, cells were plated glass coverslips and fixed with 2% paraformaldehyde for 15 min at 37 °C and incubated in PLA blocking buffer for 60 min at 37 °C. After blocking, cells were incubated overnight at 4°C with appropriate primary antibodies. The following day, cells were incubated with PLUS and MINUS PLA probes for 60 min at 37 °C than incubated in the ligation mix for 30 min at 37 °C. Amplification reaction was performed for 100 min at 37 °C. Finally, washed coverslips were fixed microscope slides using VectaShield mounting medium H-1000 (Vector Laboratories, Burlingame, CA).

9. RNA Fluorescence in Situ Hybridization

Cells were grown on 18 mm coverslips, washed with PBS at RT, and fixed with 4% paraformaldehyde for 15 min at 37° C. Coverslips were washed twice with PBS. Cells were permeabilized by washing with PBS 0.4 % Triton X-100 for 7 min at 4° C. Cells were washed rapidly with PBS before incubating them with pre-hybridization buffer (2X SSPE and 15 % formamide) (20X SSPE, [pH 8.0]: 3 M NaCl, 157 mM NaH₂PO₄.H₂O and 25 mM EDTA) for at least 30 min. 3.5 µl of probe (10 ng/ml) was diluted in 70 µl of hybridization mix (2X SSPE, 15 % formamide, 10 % dextran sulphate, 0.5 mg/ml tRNA) and heated at 90° C for 1 min.

Hybridization of the probe was conducted overnight at 37° C in a humidified environment. Subsequently, cells were washed twice for 20 min with prehybridization buffer, then once for 20 min with 1X SSPE, and finally mounted with Vectashield (Vector Laboratories) and kept at -20° C. The probe sequence (5' to 3') is Cy5- AGACGAGAACGCCTGACACGCACGGCAC. At least 30 cells were imaged for each condition of each cell line

10. **Immunofluorescence**

Cells were grown on coverslips, washed with PBS at RT, and fixed with 2% paraformaldehyde for 15 min at 37° C. Cells were permeabilized with PBS 0.1 % Triton X-100 (3X short + 2X 10 min washes). Blocking of non-specific signals was performed with PBS+ (PBS, 0.5 % BSA, 0.15 % glycine) for at least 30 min. Then, coverslips were incubated with 70 µl of primary antibody mix for 18mm coverslips or 50 µl for 12mm coverslips. Incubation for 2h at RT in a moist chamber, washed with PBS (3X short + 2X 10 min), quickly washed with PBS+ before incubating with 70 µl of secondary antibody mix for 1h at RT in a moist chamber. After the same washing procedure, coverslips were finally mounted using Vectashield with DAPI (Vector Laboratories) and kept at - 20° C, or with Vectashield, vibrance with DAPI (Vector Laboratories) and kept at 4° C at least 30 cells were imaged for each condition.

Antibodies

Primary antibodies used for this study are listed in Table 2:

Antibody against	Source	Catalog Nr., Manufacture	Used conc /Application
CSB	Mouse	sc398022/SantaCruz Biotechnology	1/200 IF, 1/100 PLA
Coilin	Rabbit	10967-1-AP / <u>Proteintech</u>	1/500 IF, 1/250 PLA, 1/5000WB
Iselt-1	Goat	AF1837/r&d systems	1/500 IF
Olig-2	Rabbit	AB9610/Sigma-Aldrich	1/500 IF
R loops DNA-RNA hybrid	Rabbit	Ab01137-23.0/Absolute antibody	1/100 IF, 1/50 PLA
RNAP I	Mouse	sc48385/ santa cruz	1/500 IF, 1/250 PLA, 1/3 000 WB
RNAP II	Mouse	sc56767/santa cruz	1/200 IF
SETX	Rabbit	ab220827/Abcam	1/500 IF, 1/250 PLA,
SMN	Rabbit	11708-1-AP/Proteintech	1/100 IF, 1/50 PLA
SMN	Mouse	610646 /BD Biosciences	1/500 IF, GST, 1/250 PLA,1/5000 WB
Tubulin	Mouse	T6074/ Sigma	1/50 000 WB
γH2AX	Mouse	05-636/ Merck Millipore	1/750 IF

The following secondary antibodies were used:

Goat anti-mouse Alexa Fluor 488 A-11008 (Invitrogen) 1/400 and goat anti-Rabbit Alexa Fluor 594 A-11012 (Life technology) 1/400.

11. Fluorescent imaging and analysis

Imaging has been performed on a Zeiss 880 confocal laser-scanning microscope (Zeiss), using a 63x oil objective, and on a Zeiss Z1 imager right using a 100x oil objective or 40x. The acquisition software is Metavue. Images were analyzed with Image J software. For all images of this study, nuclei and nucleoli were delimited with dashed and dotted lines, respectively, using DAPI staining. The proportions of cells were quantified by observing at least 50 cells distributed in at least two different regions of the coverslip. (+, <50%; ++, 50–70%; +++, 70–90%; +++++, >90%).

12. Statistical analysis

Error bars represent the Standard Error of the Mean (SEM) of the biological replicates. GraphPad Prism version 8.1.0. was used for statistical analysis and plotting the numerical data, significatif ; * : $P < 0,05$; ** : $P < 0,01$; *** : $P < 0,001$; **** : $P < 0,0001$ Statistics of RNA FISH assay were performed using a test of Mann Whitney test two-tailed.

Chapter four

Results

I. Nucleolar reorganization after cellular stress is orchestrated by SMN shuttling between nuclear compartments

Shaqraa Musawi^{1,2}, Lise-Marie-Donnio¹, Charène Magnani¹, Olivier Binda^{1,3}, Jocelyn Côté³, Patrick Lomonte¹, Pierre-Olivier Mari¹ and Giuseppina GIGLIA-MARI^{1*}

1. Institut NeuroMyoGène, CNRS UMR 5310, INSERM U1217, Université de Lyon, Université Claude Bernard Lyon 1, Villeurbanne CEDEX, France
2. Department of Medical Laboratories Technology, College of Applied Medical Sciences, Jazan University, Jazan, Saudi Arabia.
3. University of Ottawa, Faculty of Medicine, Department of Cellular and Molecular Medicine, K1H 8M5, Ottawa, Ontario, CANADA

* Corresponding author

Keywords:

SMA, SMN, RNAP₁, DNA repair, UV lesions, Nucleolus, Coilin, Fibrillarin

Abstract

One of the most fascinating and understudied aspects of DNA repair is how cells resume their activities once the necessary reactions to eliminate DNA damage have been completed. We investigated the behavior of the nucleolus after UV damage recently. As a result of the repair reaction, rDNA/RNAP I is displaced at the nucleolus border, accompanied by a transcription block. rDNA/RNAP1 returns to the nucleolus after repair, and transcription resumes. To define the molecular mechanism that governs the nucleolar reorganization during rDNA repair. SMN was particularly interesting to analyze because its Tudor domain interacts with FBL. In the absence of SMN, RNAP1 and FBL remain at the periphery of the nucleolus, where RNAP1 transcription will resume. Restarting transcription from a non-canonical localization (the periphery of the nucleolus). Surprisingly, we demonstrated a shuttling of SMN inside the nucleolus 24 h after damage induction. SMN shuttles with proteins from his complex, such as Gemin5. Coilin and FBL are involved in different phases of SMN shuttling. When Coilin is absent, SMN cannot reach the nucleolus' periphery, and when FBL is absent, SMN cannot enter the nucleus. Furthermore, RNAP1 does not recover its proper nucleolus localization in either Coilin or FBL cells. Indeed, PRMT1 is essential to recruit SMN to the periphery of and within the nucleolus. Interestingly PRMT1 shuttles within the nucleolus in the same time frame as SMN; this shuttling is SMN-dependent. Here we discovered a new function for SMN in restoring the proper nucleolar structure after the completion of DNA Repair and the aberrant positioning of RNAP1 transcription. This defect may contribute to the neurodegenerative phenotype of SMA patients.

INTRODUCTION

The nucleolus is a nuclear membraneless organelle with a very structured internal organization, which associates with its different functions in ribosomal biogenesis: transcription of ribosomal DNA (rDNA) and early ribosomal RNA (rRNA) maturation ¹. Nucleoli are formed around the rDNAs which are composed by tandem head-to-tail repeats and their structure is thought to be strictly dependent on the transcriptional activity of the RNA polymerase I (RNAP1) ². Despite a very structured organization, nucleoli are very dynamic organelles, their shape and number can vary through the cell cycle and many proteins can enter or exit the nucleolus depending on physiological processes or cellular stress responses. This organized structure can be dynamically altered by both genotoxic agents and general cellular stress ³. For instance, drugs that alter RNAP1 transcription (i.e. cordycepin, actinomycin D, etc.) may cause nucleolar segregation at the periphery of the nucleolus into structures known as nucleolar caps. Furthermore, drugs that block rRNA processing or the topoisomerase II (i.e. doxorubicin) but do not interfere with RNAP1 transcription will induce a disruption of the compact nucleolar environment and nucleolar necklaces will appear ⁴.

Amongst different cellular stresses known to modify nucleolar organization, UV-irradiation has the benefit of being a quick and chemically clean method. Moreover, cells are able to repair UV-induced lesions and hence reverse their stress status. UV-induced DNA lesions are repaired by the Nucleotide Excision Repair system (NER) ⁵, which also repairs all bulky DNA lesions affecting the DNA structure, including environmental pollutants and the oxidative-damage derived cyclopurines ⁶.

During UV-irradiation, it has been showed that the nucleolus is not fully disrupted but nucleolar proteins (RNAP1, Fibrillarin) and nucleolar DNA are exported to the periphery (for simplicity this phase will be called “displacement”) of the nucleolus and when DNA repair is fully completed the proper nucleolar structure is restored (for simplicity this phase will be called “repositioning”) ^{7,8}. Using a best candidate approach, we recently found that structural proteins like Nuclear Myosin I (NMI) and -Actin (ActB) seem to play a prominent role in this process. In cells depleted from NMI and ActB, nucleolar structure is not restored and both nucleolar proteins and nucleolar DNA remain at the periphery of the nucleolus although DNA repair is completed and transcription is resumed ⁸. However, the exact mechanism of NMI and ActB actions on nucleolar reorganization has not yet been elucidated, probably because many

other molecular actors are still unknown. In order to find a complete molecular mechanism, several structural and nucleolar proteins have been scrutinized and a certain number of nucleolar proteins have been found to be crucial to restore a proper nucleolar structure after DNA repair completion. One of these proteins is Fibrillarlin (FBL). Consequently, we studied whether FBL interacting partners were also involved in this process. Amongst these different FBL partners, we investigated whether Survival of Motor Neuron (SMN) was implicated in the restoration of the nucleolar structure after DNA repair completion.

Spinal Muscular Atrophy (SMA) is an autosomal recessive neuromuscular disease, which affects neurons that control the voluntary movement of muscles (motoneurons) ⁹. In SMA, motoneurons are progressively lost leading to progressive muscle wasting and atrophy because muscles no longer receive signals from the motor neurons of the spinal cord. Children affected with SMA have symptoms that can vary greatly depending on the age of disease onset and its severity. Normal activities, such as crawling, walking, maintaining a seated position, controlling head movements, breathing and swallowing might be affected ⁹. With an incidence of 1 in 6,000-10,000 live births, SMA is the most prevalent hereditary cause of infant mortality ¹⁰.

SMA is caused by bi-allelic mutations in the *SMN1* gene (Survival of Motor Neuron: SMN) and the disease phenotype is modified by the number of copies of a second paralog gene, *SMN2*, which is always present in SMA patients ¹¹. *SMN1* produces a full-length functional version of the SMN protein whereas in *SMN2*, the absence of exon 7 in most of the transcripts produces an unstable version of the SMN protein (SMN Δ 7). *SMN2* can express about 10-15% of the full-length protein, which is insufficient to avoid the disease. SMN is a multifunctional ubiquitous protein involved in many cellular processes, such as biogenesis and trafficking of ribonucleoproteins, local translation of messenger RNAs, etc ¹². SMN protein is ubiquitously expressed and is localized to both cytoplasm and the nucleus. Within the nucleus, SMN localizes in Gems and Cajal bodies (CB), which have been shown to associate with nucleoli ¹³. Within CB, SMN interacts with the protein Coilin ¹⁴. Interestingly, in certain conditions, SMN is also detected in nucleoli of mammalian primary neurons and colocalized with FBL ¹⁵. In addition, a transient colocalization of SMN at the periphery of nucleoli with FBL after actinomycin D treatment in 10%–20% of HeLa cells ^{16,17} suggests that SMN could be present in the nucleolus under stress conditions. SMN Tudor domain is involved in the binding to FBL and Coilin.

We investigated the possible role of SMN in nucleolar reorganization during both displacement and repositioning of RNAP1 during and after DNA repair of UV-induced damage and generally after stress induction. We showed here that in the absence of a functional SMN, both RNAP1 and FBL did not return inside the nucleolus after DNA repair completion while transcription is fully restored. Interestingly, we could reveal a shuttling of SMN within the nucleolus after DNA repair and we determine that this shuttling is strictly dependent on physical interactions between SMN with FBL and Coilin and that methylation reactions from PRMTs governs this shuttling.

RESULTS

RNAP1 and FBL repositioning after DNA repair completion are SMN-dependent.

To investigate whether SMN plays a role in nucleolar reorganization in response to cellular stress, we investigated whether the previously reported ⁷ RNAP1 UV-induced displacement and the later repositioning was still happening in absence of SMN. As SMN deficient cells we used both primary fibroblasts from SMA patients (Figure S1A) and transformed fibroblasts in which SMN was down regulated by lentiviral transfection of 2 independent inducible shRNAs against SMN 3'UTR (Figure S1B). Using these cell lines, we performed an immunofluorescent assay to detect both RNAP1 and FBL positioning in the absence of damage (non UV), 3 hours post UV-irradiation (PUVI) (this time point corresponds to the minimum of RNAP1 transcriptional activity as found in ⁷) and at 40 hours PUVI (this time point corresponds to the RNAP1 full recovery of transcriptional activity and full DNA repair as described in ⁷). Wild-type transformed MRC5-SV40 fibroblasts and C5RO primary fibroblasts were used as a positive control, while Cockayne Syndrome type B (CSB) TC-NER deficient fibroblasts (both transformed and primary; termed CSB-deficient thereafter) were used as negative control as used in ⁷.

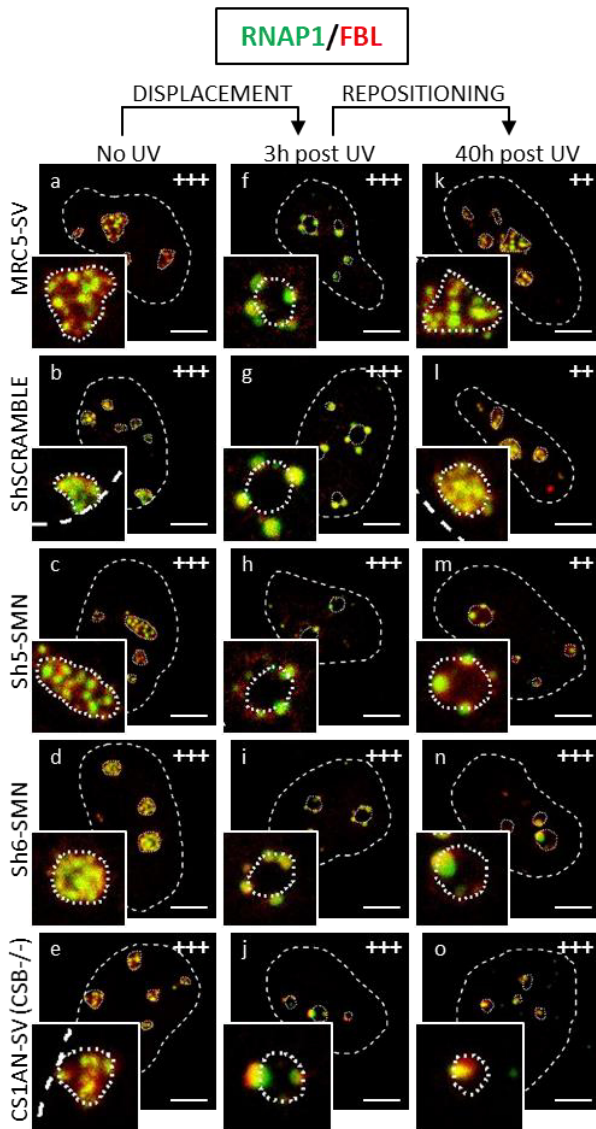
As described in ⁷, UV irradiation induced a displacement of both RNAP1 and FBL to the periphery of nucleoli in all cell lines tested (Figure 1A, panels f to j and 1B panels d to f). As expected, in wild-type cells (MRC5, shscramble and C5RO) both RNAP1 and FBL recovered their position within the nucleoli at 40 hours after UV-irradiation (Figure 1A, panels k and l, and 1B panel g). In contrast, in cells depleted of SMN (Figure 1A, panels m and n) or mutated in *SMN1* (Figure 1B panel h) neither RNAP1 nor FBL recovered the proper position within the nucleoli after DNA repair completion. As previously demonstrated ⁷, in CSB-deficient cells no return of the RNAP1 and FBL was observed (Figure 1A panel o and 1B panel i).

In CSB-deficient cells the repositioning of RNAP1 and FBL is impeded because DNA lesions on the transcribed strand of rDNA genes are not properly repaired and RNAP1 transcription is not restored ⁷. To investigate whether this was the case or not in SMN-deficient cells, we performed an RNA-fish assay detecting the pre-rRNA transcript using a specific probe against the 47S product (Figure S1C) and could determine (Figure S1D and S1E) and

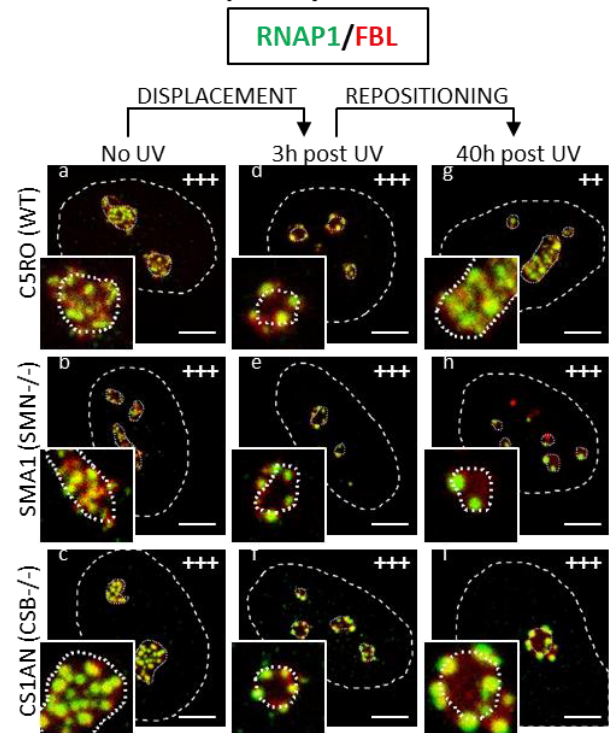
quantify (Figure 1C and D) that RNAP1 transcription is restored in SMN-deficient cells at 40 hours PUVI as in wild-type cells. In parallel, the involvement of SMN in Nucleotide Excision Repair (NER) was studied by performing UDS (Figure S2A), RRS (Figure S2B) and TCR-UDS (Figure S2C) experiments in cells depleted of SMN. Our results clearly show that SMN has no role in NER (Figure S2).

These results indicated that in the absence of SMN, RNAP1 and FBL are displaced at the periphery of the nucleolus in response to DNA damage but are not repositioned within the nucleolus once DNA repair reactions are completed and RNAP1 transcription is restored.

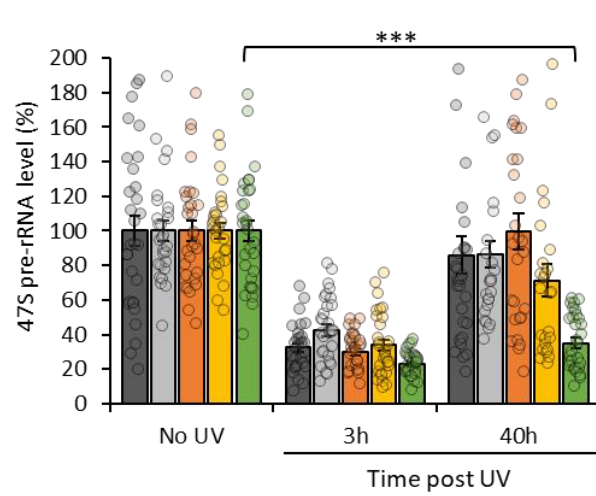
A IF in transformed fibroblasts



B IF in primary fibroblasts



C RNA-FISH 47S in transformed fibroblasts



D RNA-FISH 47S in primary fibroblasts

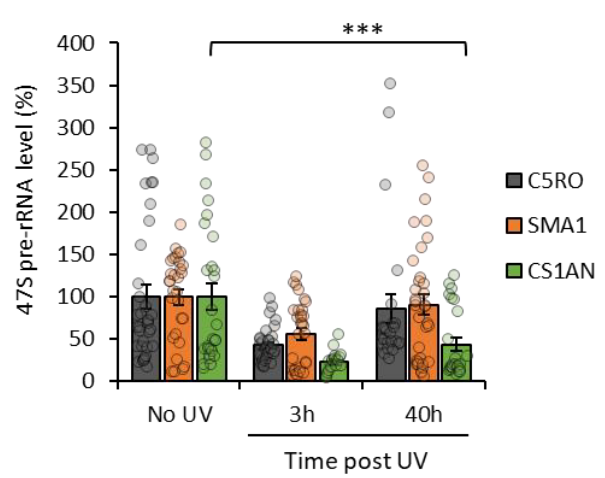
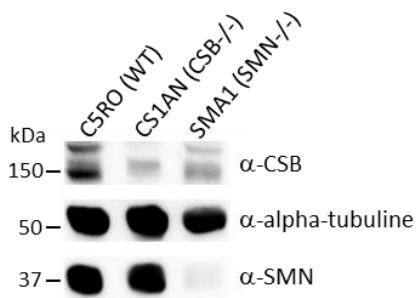


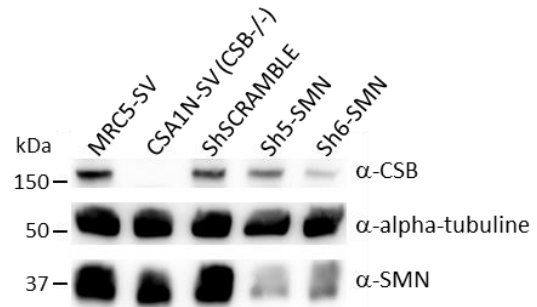
Figure 1: RNAP1 and FBL movement during DNA repair in SMN deficient cells

A and B) Confocal images of immunofluorescence assay against RNAP1 (green) and FBL (red) in transformed **(A)** and primary **(B)** fibroblasts. Nuclei and nucleoli are indicated by dashed lines and dotted lines respectively. The number of the representative cells are indicated as followed + : 50–70%; ++ : 70–90%; +++ : >90%. Scale bar: 5 μm . **(C and D)** Quantification of RNA-FISH assay showing the 47S pre-rRNA level after UV-C exposure in transformed **(C)** and primary **(D)** fibroblasts. Error bars represent the SEM obtained from at least 27 cells. P-value of student's test compared to No UV condition: ***<0.001

A WB in primary fibroblasts

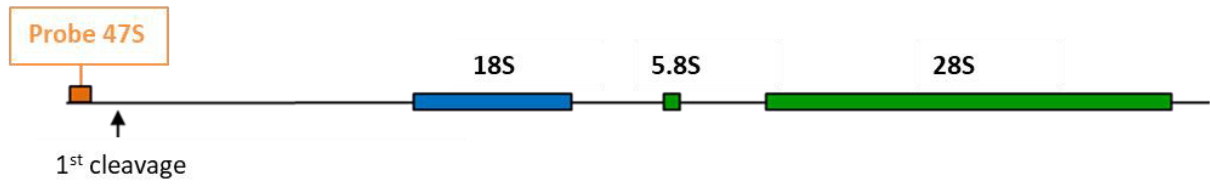


B WB in transformed fibroblasts

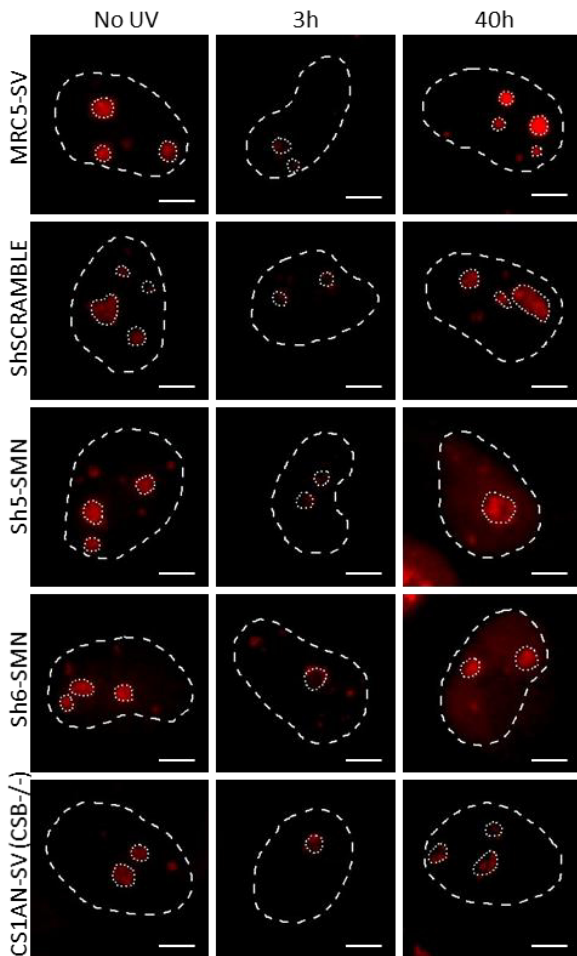


C

47S representation and localisation of the probe



D RNA-FISH 47S in transformed fibroblasts



E RNA-FISH 47S in primary fibroblasts

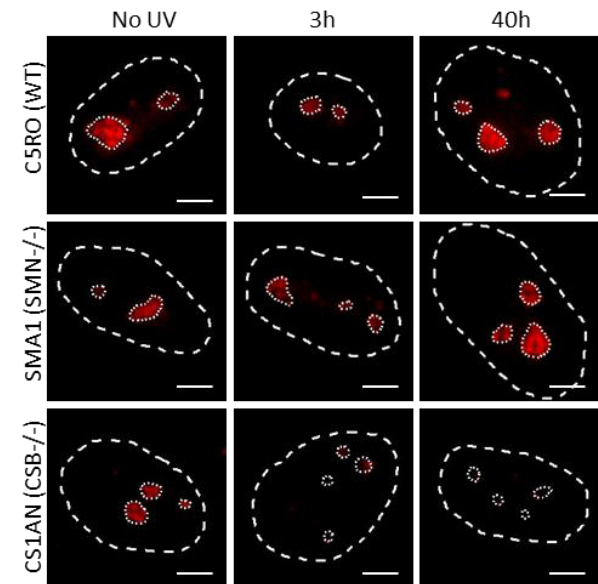


Figure S1 : Western blot showing the reduction of SMN and representative images of RNA-FISH 47S in primary and transformed fibroblasts.

A and B) Western Blot of SMN and CSB on whole cell extracts of MRC5, ShScramble, sh5-SMN, sh6-SMN and CSB-/- transformed cells **(A)**, and of C5RO, CS1AN and SMA1 primary cells **(B)**. **(C)** Schematic representation of rRNA unit and localisation of the 47S pre-rRNA probe. **(D and E)** Representative images of RNA-FISH from figure 1C and 1D respectively. Scale bar 5µm

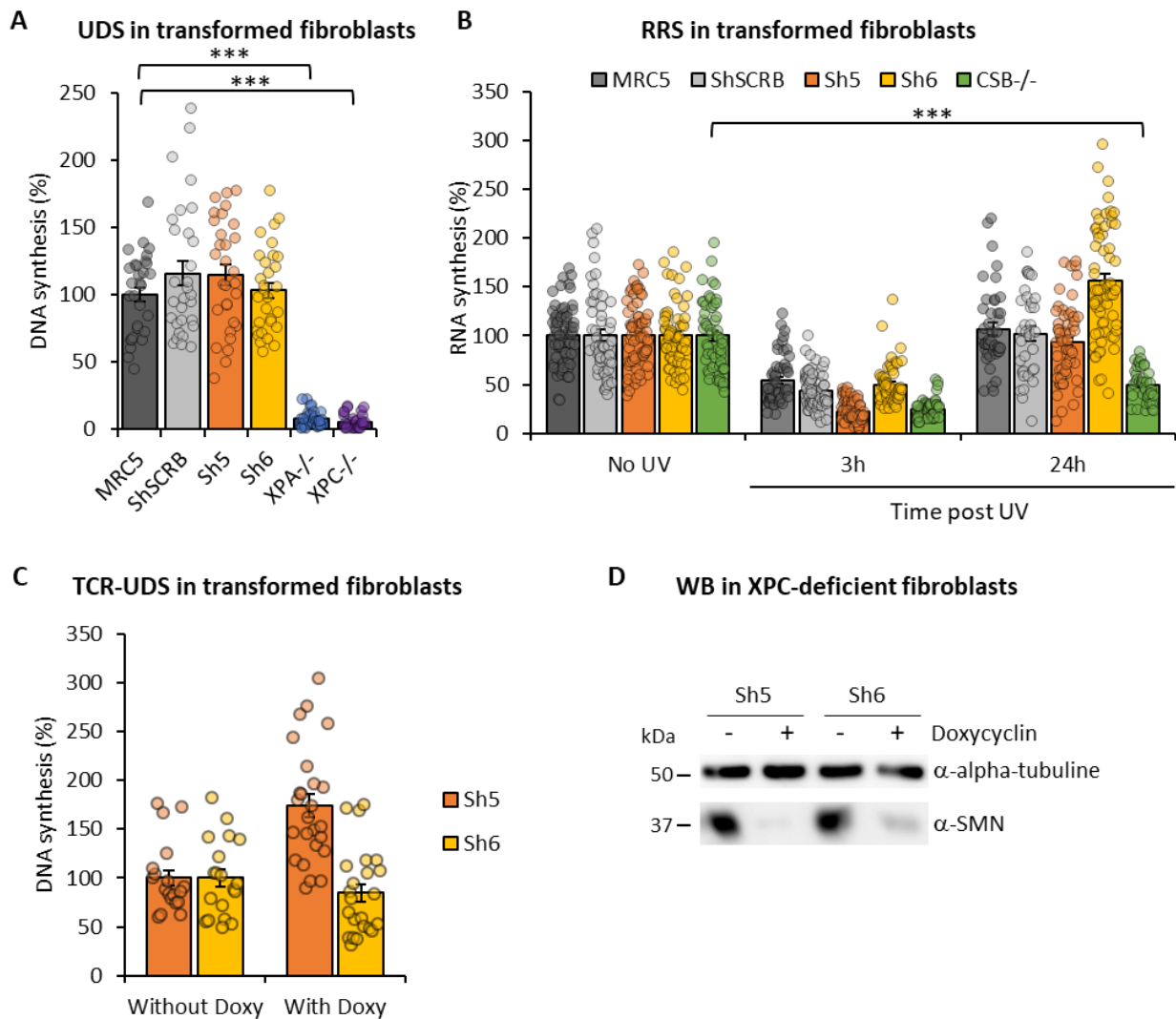


Figure S2 : No role of SMN in NER

A) Quantification of Unscheduled DNA Synthesis assay (UDS) determined by EdU incorporation after local damage (LD) induction with UV-C (100J/m²) in transformed fibroblasts. Error bars represent the SEM obtained from at least 30 LDs. **B)** Quantification of RNA Recovery Synthesis (RRS) assay determined by EU incorporation after UV-C (10J/m²) exposure in transformed fibroblasts. Error bars represent the SEM obtained from at least 50 cells. **C)** Quantification of TCR-UDS assay determined by

EdU incorporation after LD induction with UV-C (100J/m²) in GG-NER deficient cells (XPC-/- cells) with Sh5-SMN or Sh6-SMN induced or not by doxycyclin. Error bars represent the SEM obtained from at least 15 LDs. **D)** Western Blot of SMN whole cell extracts of XPC-deficient cells with sh5-SMN or sh6-SMN. The expression of the ShSMN is induced by doxycycline treatment.

SMN-complex shuttles in the nucleolus and colocalizes with nucleolar proteins after UV irradiation.

We showed that SMN is required for the proper repositioning of RNAP1 and FBL at late time points PUVI. We questioned how SMN could be involved in this mechanism if generally it is not present in the nucleoli. In fact, SMN protein is usually located in the cytoplasm and within the nucleus where SMN is found in CB together with Coilin and in Gems without Coilin. To study the localization of SMN and RNAP1 during the DNA repair process, we performed immunofluorescence assays at 3 hours and 40 hours PUVI in wild-type cells. Remarkably, at 40h PUVI, two co-existing populations of cells could be detected: (i) a majority of cells in which RNAP1 is repositioned within the nucleolus and SMN is localized in the CB and (ii) a minority of cells in which RNAP1 is still localized at the periphery of the nucleolus and SMN is unusually localized within the nucleolus and cannot be detected in CB anymore (Figure 2A panel d and e). Because of this result, we decided to extend our analysis adding a time point intermediate between 3h and 40h PUVI (24 h PUVI) and a time point beyond the 40h PUVI (48h PUVI) and performed the IF assays against SMN and different nucleolar proteins or SMN protein partners (Figure 2). Importantly, we verified the RNAP1 transcriptional activity by RNA-Fish of 47S at 24h and 48h and show that RNAP1 transcription is not yet restored at 24h but it's fully recovered at 48h PUVI (Figure S3A). Surprisingly, at 24h PUVI, our results revealed the presence of SMN at the periphery of and/or within the nucleolus in the vast majority of cells. Concomitantly, at 24h PUVI, RNAP1 was found to be localized at the periphery of the nucleolus (Figure 2A). On the other hand, we observed a complete return to the undamaged condition (RNAP1 within the nucleolus and SMN in the CB) at 48 h PUVI in the vast majority of cells. Despite the presence of SMN and RNAP1 at the nucleolar periphery together at 24 h post-UV, no colocalization between these two proteins was observed (Figure 2A).

We showed that the loss of SMN alters the FBL localization at 40 h PUVI (Figure 1A and 1B). FBL interacts with SMN via SMN Tudor domain^{18,19}, we therefore examined the

localization of SMN and FBL during the DNA repair process (Figure 2B). Interestingly, we observed a substantial colocalization between SMN and FBL at 24 h PUVI within the nucleolus. The colocalization can also be observed at 40 h PUVI in the population of cells that at this time point have not yet restored FBL position within the nucleolus (Figure 2B).

In the absence of damage, SMN colocalizes and interacts with Coilin in CBs ¹⁴, however after DNA damage induction, it has been shown that CBs are disrupted²⁰. Because of these evidences, we examined the localization of Coilin and its interactions with SMN during the DNA repair process. Interestingly, Coilin is localized to the periphery of the nucleolus already at 3h PUVI and remains in this location at 24h PUVI and at 40h PUVI in the subset of cells that did not yet repositioned RNAP1 (Figure 2C). Remarkably, when Coilin is at the periphery of the nucleolus it does not colocalize with SMN (Figure 3B) but show a peri-nucleolar colocalization with RNAP1 instead (Figure S3B).

Interestingly and differently from Coilin, at 3h PUVI SMN is still visible in a focal pattern within the nucleus, reminiscent of Gems. Because of this Coilin-independent localization and to investigate whether SMN shuttles within the nucleolus as an individual protein or as a complex, we investigated whether Gemin5 (one of the subunits of the SMN complex) changes location after UV-irradiation. Remarkably, we could show that Gemin5 interacts with SMN all along this process of displacement and repositioning (Figure 2D), indicating that it is not just SMN that shuttles in and out of the nucleolus, but that the whole SMN complex is likely involved in this process, or at least some components of the complex.

Moreover, to investigate whether the shuttling of SMN within the nucleolus is specific to UV damage or a general role in stress response, we treated the MRC5-SV cells with Cordycepin, a RNAP1 transcription blocking drug (FigureS4A) and checked the localization of SMN (Figure S4B). We observed the same phenomenon concerning the shuttling of SMN into the nucleolus but with a kinetic that is faster than with UV (Figure S4B).

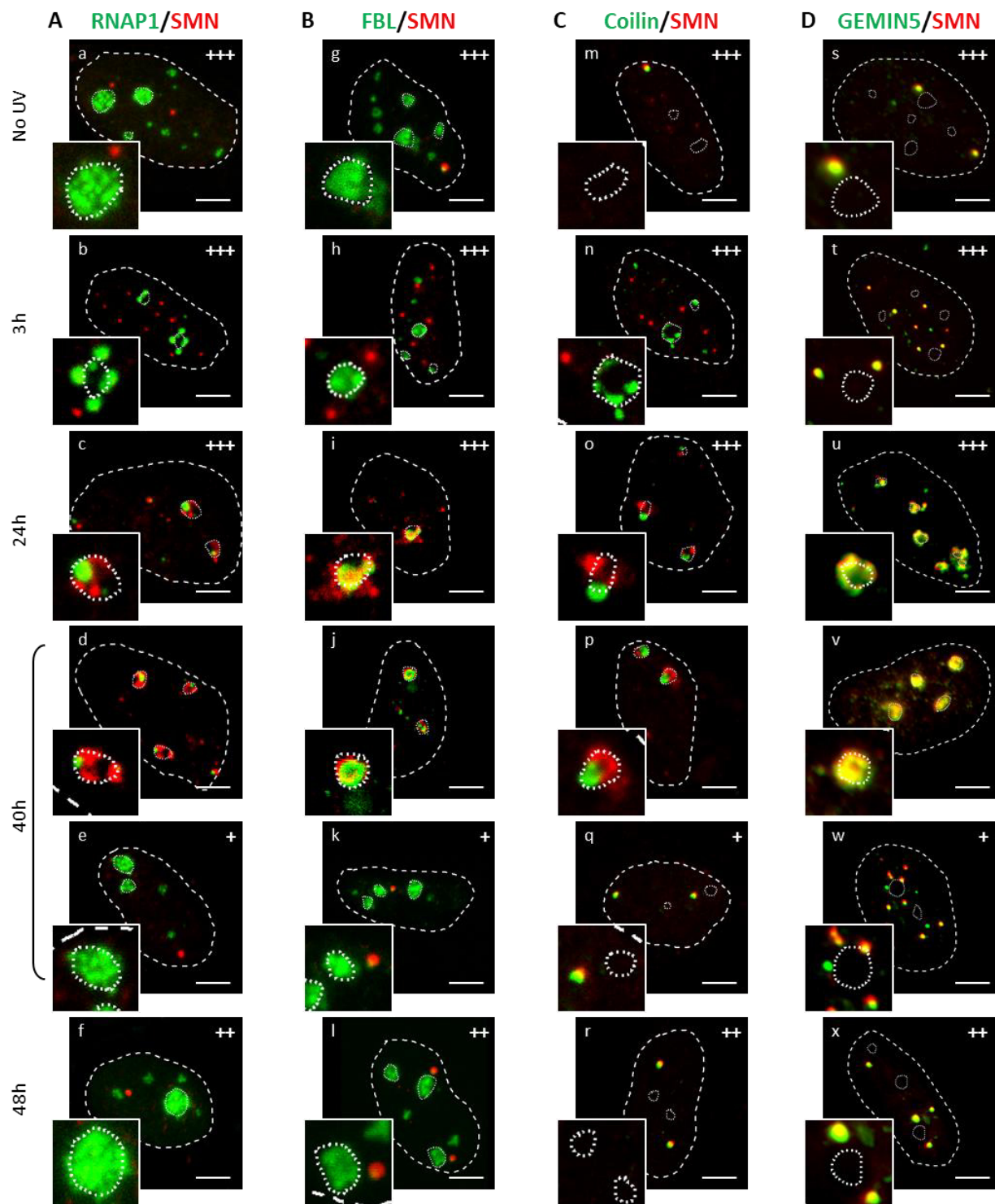


Figure 2: SMN and nucleolar proteins movement during DNA repair

Confocal microscopy images of immunofluorescence assay in MRC5 cells showing, after 16J/m² UV-C irradiation, the localization of SMN in red and in green A. RNAP1, B. FBL, C. Coilin, D. GEMIN5. Nuclei and nucleoli are indicated by dashed lines and dotted lines respectively. The number of the representative cells are indicated as followed + : 50–70%; ++ : 70–90%; +++ : >90%. Scale bar represents 5 μm.

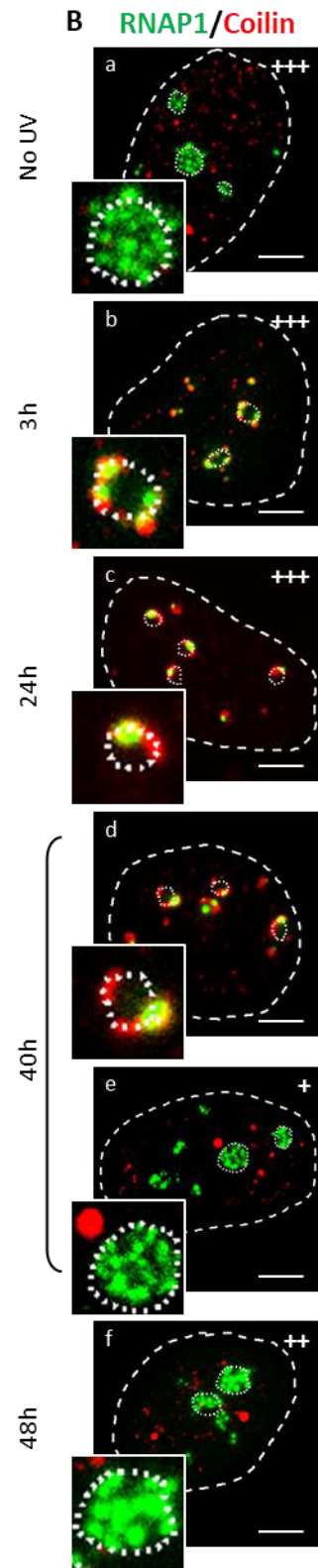
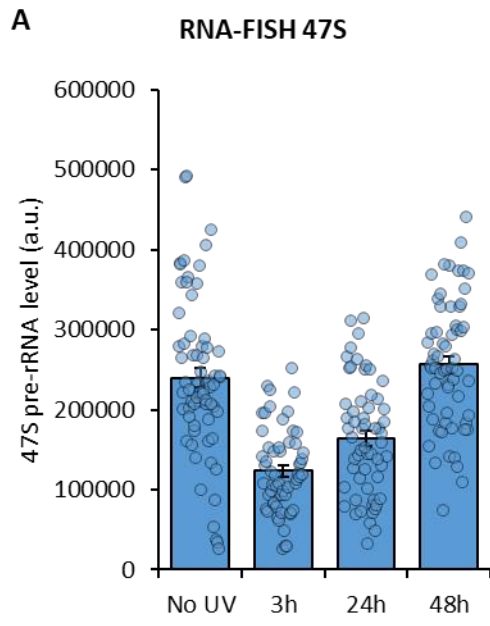
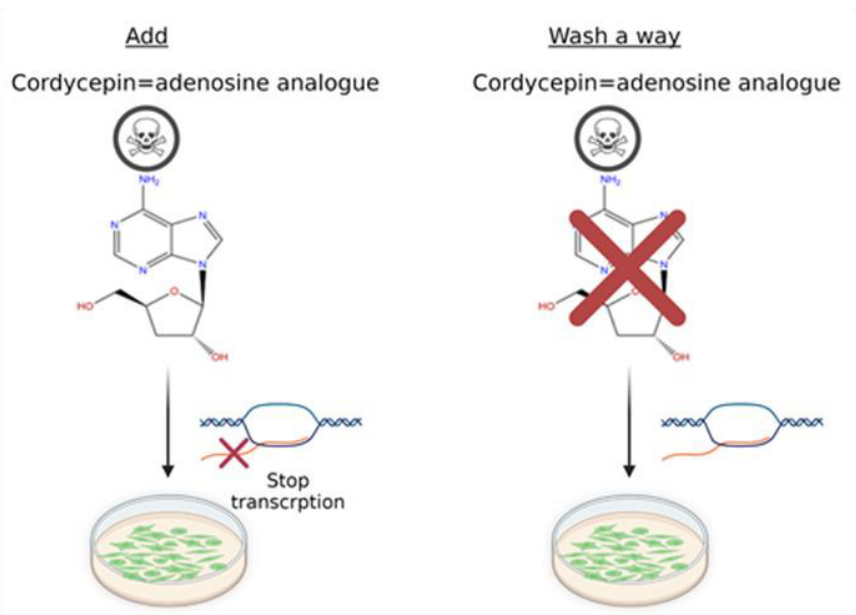


Figure S3 : RNA-FISH 47S and shuttling of Coilin and RNAP1 at different time after UV irradiation

A) Quantification of RNA-FISH assay showing the 47S pre-rRNA level after 16J/m² of UV-C exposure in MRC5-SV cells. Error bars represent the SEM obtained from at least 50 cells. **B)** Confocal images of immunofluorescence assay against RNAP1 (green) and Coilin (red) in MRC5 cells. Nuclei and nucleoli are indicated by dashed lines and dotted lines respectively. The number of the representative cells are indicated as followed + : 50–70%; ++ : 70–90%; +++ : >90%. Scale bar represents 5 μm.

A Cordycepin experiment



B Immunofluorescence after Cordycepin treatment

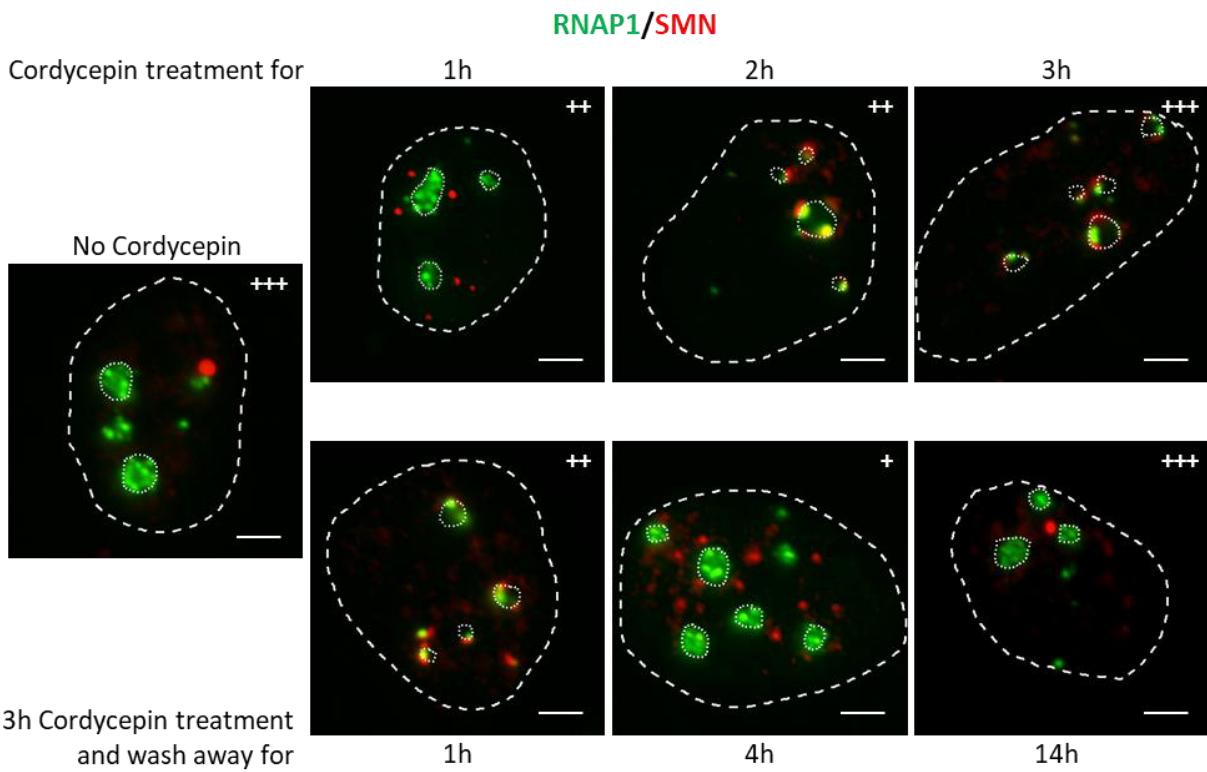


Figure S4 : SMN Shuttle to the nucleolus after transcription blockage

A) Schematic representation of experiment with Cordycepin drug. **B)** Confocal images of immunofluorescence assay against RNAP1 (green) and SMN (red). Nuclei and nucleoli are indicated by dashed lines and dotted lines respectively. The number of the representative cells are indicated as followed + : 50–70%; ++ : 70–90%; +++ : >90%. Scale bar represents 3µm.

SMN interacts with FBL and Coilin inside nucleolus after UV Irradiation *in vivo* and *in vitro*.

We showed that SMN colocalizes with FBL within the nucleolus at 24h PUVI. To assess the interaction between SMN and FBL, we performed a PLA (proximity ligation assay) on wild-type cells at different time PUVI (Figure 3A). The majority of the cells at 24h PUVI presented a strong PLA signal specifically in the nucleolus between SMN and FBL, this signal persisted at 40h and 48h post UV although the fraction of cells presenting this signal almost 40% (Figure 3A). We then test SMN-FBL interaction *in vitro* by GST pull-down assays (GST) (Figure 3B and 3C). Using GST pulldown assays we confirmed that FBL from cell extracts interacts with recombinant GST-tagged SMN (Figure 3B). Furthermore, using a panel of SMA-linked TUDOR domain mutants, we establish that FBL-SMN interactions require an intact TUDOR domain. Using a similar approach, we assessed FBL-SMN interactions from control or UV-treated cells at different time points and observed that UV treatment seemed to enhance FBL-SMN interactions (Figure 3C), while GST alone failed to associate with FBL even if more GST alone than GST-SMN was used in pulldown assays.

UV-irradiation induces a disruption of CBs²⁰, this disruption allows the release of both SMN and Coilin and both these proteins shuttle at the periphery of nucleolus after DNA damage although at different times : Coilin is present at the periphery of the nucleolus already at 3h PUVI (Figure 2C) while SMN localizes at the periphery of the nucleolus and within the nucleolus at 24h PUVI. Because of these results we wondered whether we could observe a difference in the interactions between SMN and Coilin before and after DNA damage, knowing that these proteins are tightly interacting within the CBs. We performed PLA assay between SMN and Coilin before DNA damage induction and at different time PUVI. As expected, before damage induction the CBs are intact, and the only PLA positive signal was observed in dots within the nucleus and outside the nucleolus (likely representing the CBs). While at 3h PUVI no PLA signal was detected in the cells, a strong PLA signal in the nucleolus was

detected at 24h PUVI, indicating that at this time point, the interaction between SMN and Coilin is restored (or partially restored) in a non-canonical compartment: the nucleolus (Figure 3D). We confirmed these findings by GST-pull down assays and showed that *in vitro* the interaction between Coilin and SMN is stronger already after 3h PUVI (Figure 3E). This apparent discrepancy between PLA and GST-pull down might be explained by the fact that PLA is an in-situ technique and detect interactions within cellular compartments and it is strictly dependent of the localization of proteins within the nucleus, while GST-pull down detects interactions that can happen independently of their localization.

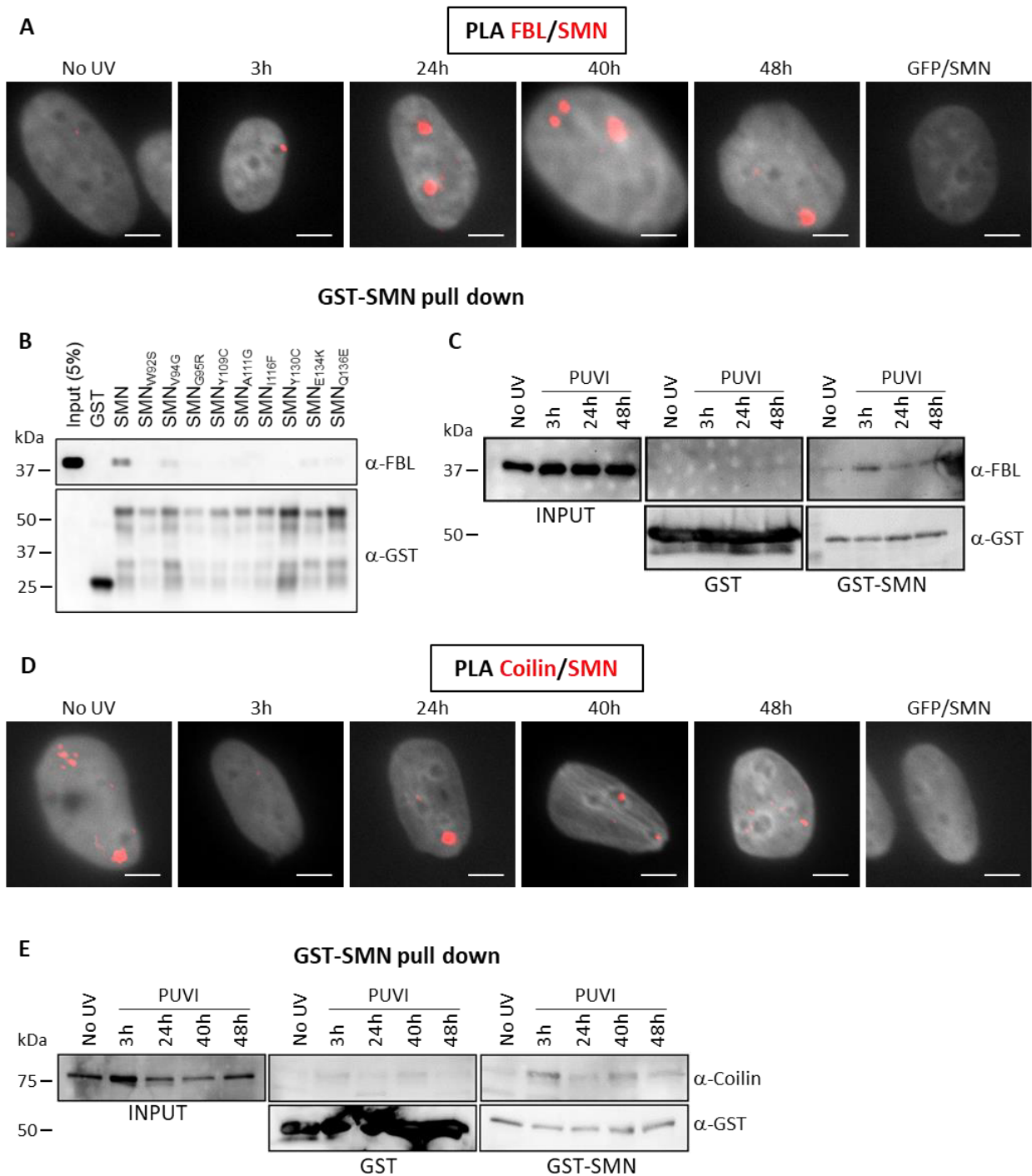


Figure 3 : SMN interact with FBL and Coilin after UV irradiation.

A and D) Microscopy images of proximity ligation assay showing the interaction between FBL and SMN (**A**) and between Coilin and SMN (**D**) in WT cells after UV-C irradiation. Scale bar: 5μm **B, C and E)** GST pull-down assay using purified recombinant SMN protein and cellular extracts. **B)** GST-SMN WT or with different mutation in the Tudor domain. **C and E)** cellular extracts after UV-C irradiation.

Coilin is required for SMN import into the nucleolus and the nucleolar rearrangement following UV exposure.

We showed that Coilin and SMN interact in cell extracts by GST (Figure 3E) and *in vivo* by PLA (Figure 3D). We also observed that Coilin localized to the nucleolus during UV damage (3h post UV) before SMN (Figure 2C). These results led us to hypothesize that Coilin is the factor that recruits the SMN to the nucleolus. To test this idea, we depleted cells of Coilin by using a specific siRNA (FigureS5A) and performed IF of SMN and RNAP1 on wild-type cells before damage and at different time PUVI (Figure 4A) in presence or absence of Coilin. Our results show that without Coilin, the shuttling of SMN within the nucleolus is impaired and SMN remains in the nucleus at any time points (Figure 4A, panel f to j). Consequently, in cells deficient for Coilin, the nucleolar reorganization after DNA damage and repair is not reestablished and RNAP1 remains at the periphery of the nucleolus at 48h PUVI, indicating that the shuttling of SMN and the presence of Coilin are both important to insure the reestablishment of the nucleolar reorganization.

To investigate whether the absence of Coilin would impact the interaction between SMN and FBL, we performed IF of SMN and FBL on wild-type cells before damage and at different time PUVI (Figure 4B) in presence or absence of Coilin. Our results show that without Coilin, SMN remaining outside of the nucleolus, no colocalization with FBL was observed and a decreased interaction between SMN and FBL was observed in Coilin depleted cells (Figure 4C).

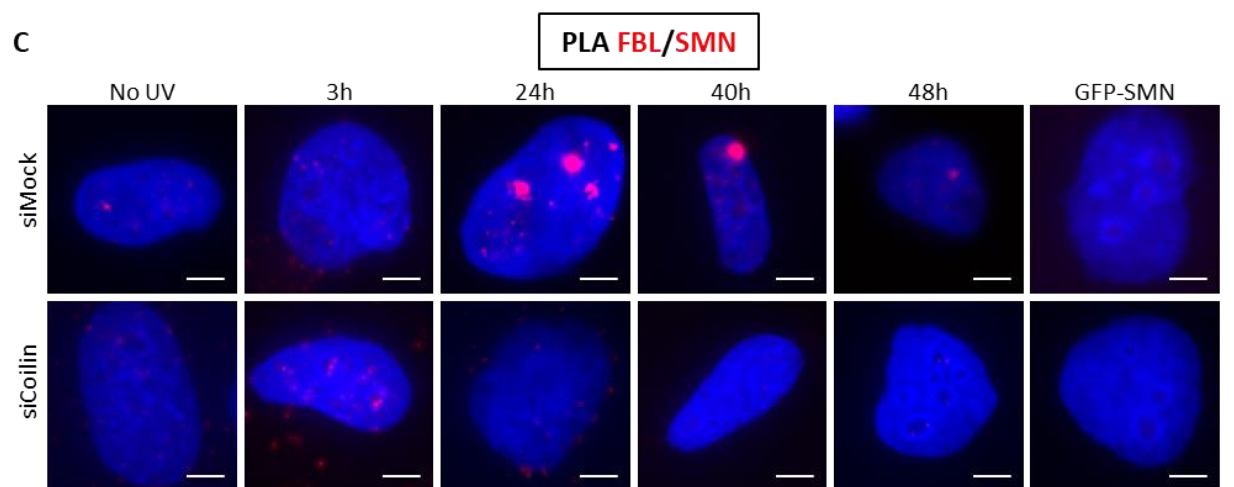
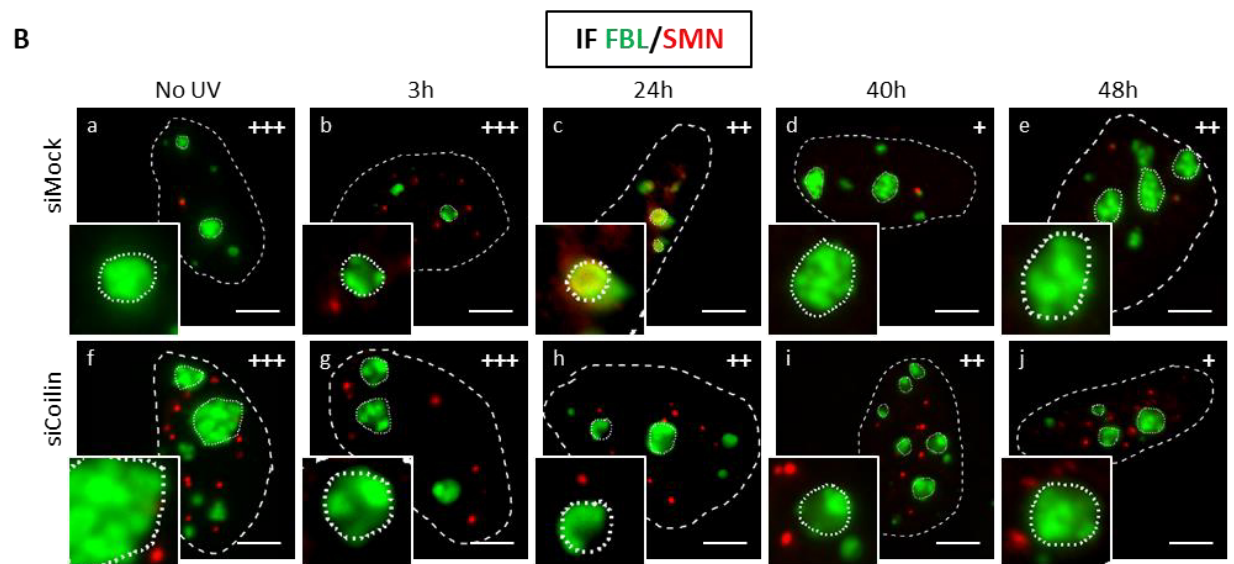
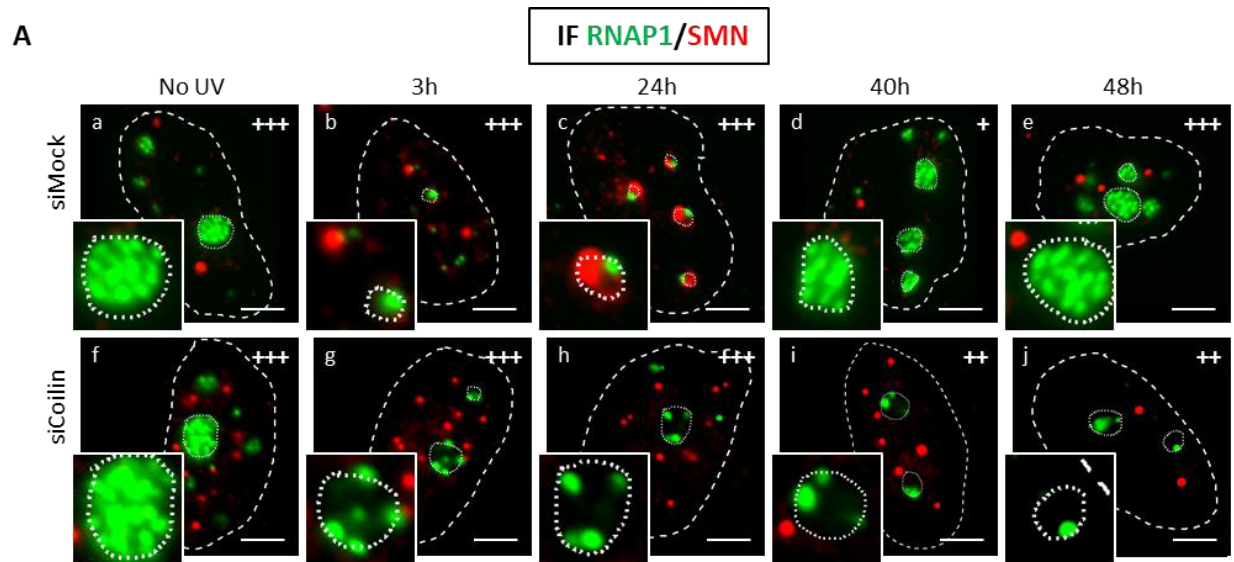


Figure 4 : SMN shuttling is Coilin-dependent

A and B) Confocal microscopy images of immunofluorescence assay in MRC5 cells transfected with siMock or siCoilin after 16J/m² UV-C irradiation showing the localization of SMN in red and in green **A.** RNAP1 or **B.** FBL. Nuclei and nucleoli are indicated by dashed lines and dotted lines respectively. The number of the representative cells are indicated as followed + : 50–70%; ++ : 70–90%; +++ : >90%. **C)** Microscopy images of proximity ligation assay showing the interaction between FBL and SMN in MRC5 cells transfected with siMock or siCoilin after UV-C irradiation. Scale bar for all images: 5µm

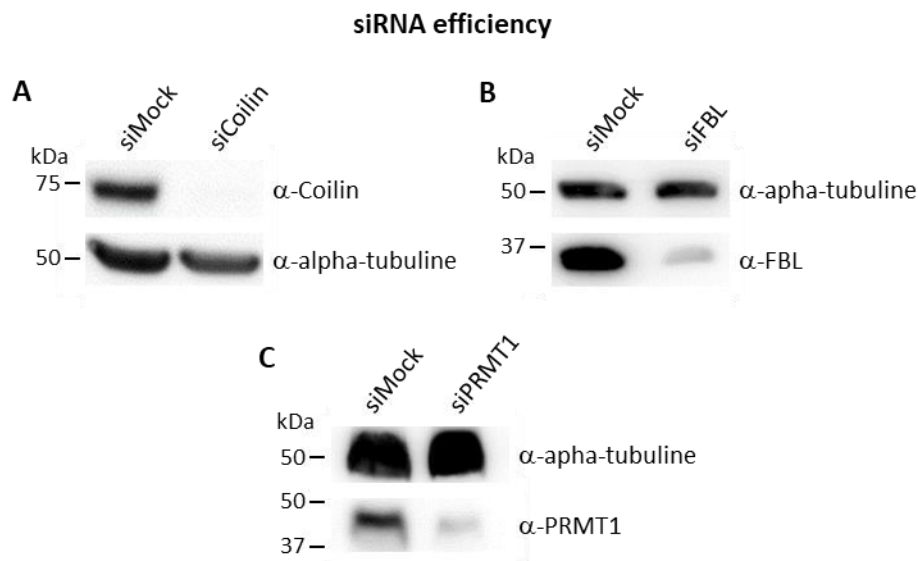


Figure S5 : WB to check siRNA efficiency

Western Blot on whole cell extracts of MRC5 cells treated with siRNA against indicated factors. **A)** siCoilin used in Figure 4, **B)** siFBL used in Figure 5, **C)** siPRMT1 used in Figure 6.

FBL is required for SMN export from the nucleolus and the nucleolar rearrangement following UV exposure.

As Coilin, FBL is an essential partner of SMN and a nucleolar protein that can methylate rDNAs and Histones within the nucleolus^{19,21}. We showed that FBL and SMN interact in cell extracts by GST (Figure 3B and 3C) and *in vivo* by PLA (Figure 3A), notably stronger after SMN shuttling into the nucleolus (Figure 3A). As the SMN shuttling is dependent on Coilin (Figure 4), we wondered whether FBL depletion would play a role in the same shuttling process. To test this hypothesis, we depleted cells of FBL by using a specific siRNA (FigureS5B) and performed IF of SMN and RNAP1 on wild-type cells before damage and at different time PUVI (Figure 5A) in presence or absence of FBL. Our results show that without FBL, the shuttling of SMN within the nucleolus is altered and SMN, namely SMN is localized at the periphery of the nucleolus already at 3h PUVI and stays at the periphery of the nucleolus at all time points, without entering the nucleolus (Figure 5A). Importantly, in cells deficient for FBL, the nucleolar reorganization after DNA damage and repair is not reestablished and RNAP1 remains at the periphery of the nucleolus at 48h PUVI, indicating that the shuttling of SMN within the nucleolus and the presence of FBL are both important to insure the reestablishment of the nucleolar reorganization. Interestingly, in the absence of FBL, some colocalization between RNAP1 and SMN can be observed (Figure 5A).

To verify if and how the absence of FBL affects the interaction between SMN and Coilin, we performed IF of SMN and Coilin on wild-type cells before damage and at different time PUVI (Figure 5B) in presence or absence of FBL. Our results show that without FBL, the interaction between SMN and Coilin is present at all times PUVI (Figure 5C and Figure 5D) and both SMN and Coilin are localized at the periphery of the nucleolus already at 3h PUVI, this localization does not change at 24h or 40h PUVI (Figure 5B). These findings show that FBL is also a critical player in SMN shuttling and appropriate nucleolar reorganization following UV Irradiation and DNA repair.

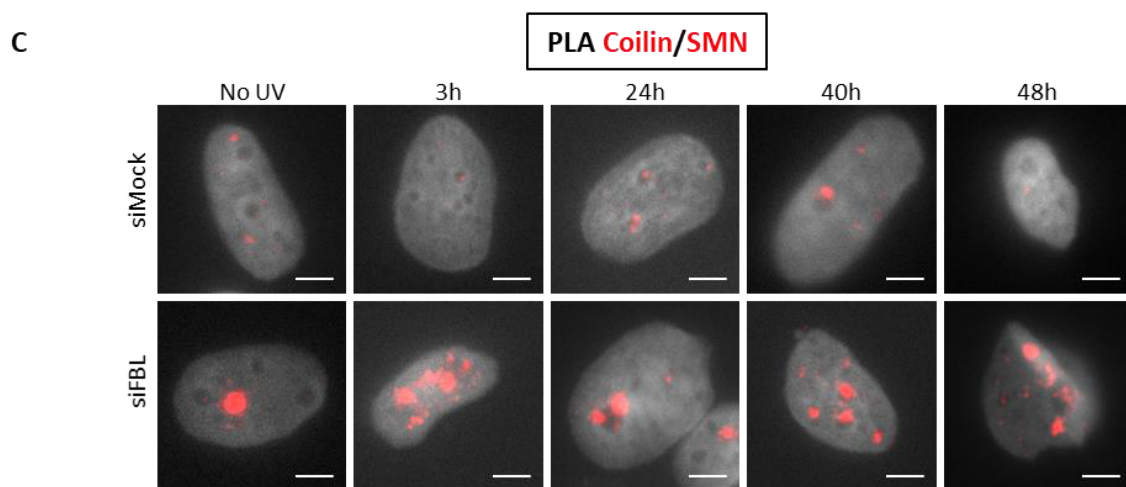
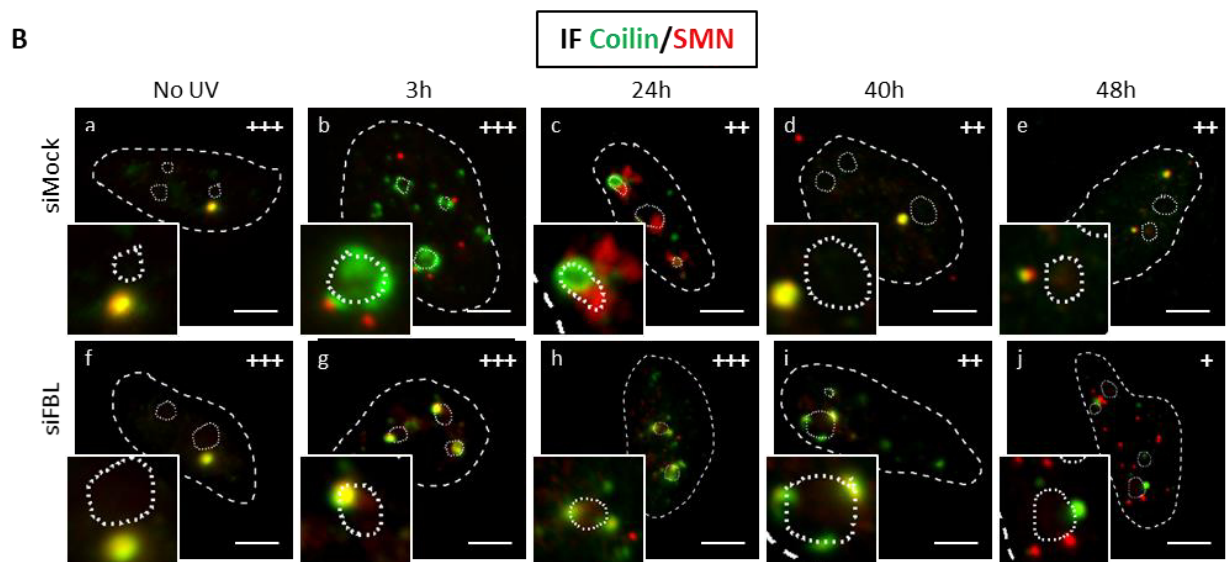
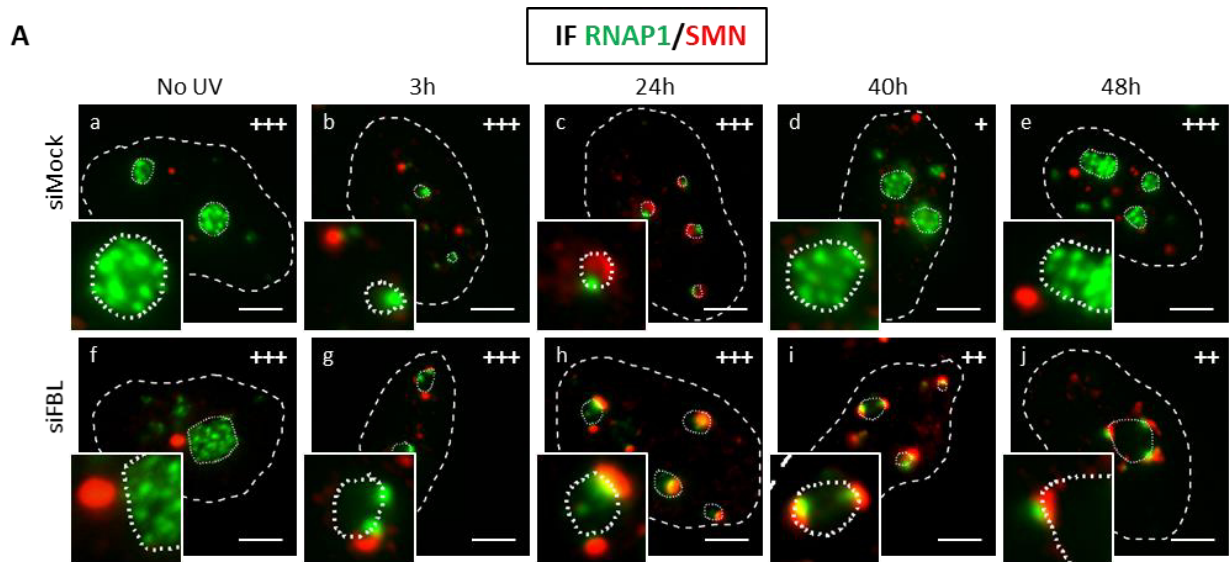


Figure 5 : The release of SMN into the nucleolus is FBL-dependent

A and B) Confocal microscopy images of immunofluorescence assay in MRC5 cells transfected with siMock or siFBL after 16J/m² UV-C irradiation showing the localization of SMN in red and in green **A.** RNAP1 or **B.** Coilin. Nuclei and nucleoli are indicated by dashed lines and dotted lines respectively. The number of the representative cells are indicated as followed + : 50–70%; ++ : 70–90%; +++ : >90%. **C)** Microscopy images of proximity ligation assay showing the interaction between Coilin and SMN in MRC5 cells transfected with siMock or siFBL after UV-C irradiation. Scale bar for all images: 5µm

PRMT1 activity mediates the nucleolar shuttling of SMN

One of the activities of SMN is to bind, via the Tudor domain, Arginine methylated proteins²². Arginine methylation is a widespread post-translational modification that can occur in histones and non-histone proteins. The enzymes catalyzing the transfer of a methyl group to Arginines are part of a family called the PRMTs (Protein Arginine Methyl Transferases). PRMTs can mono-methylate Arginines (MMA) or di-methylate Arginines either symmetrically (SDMA) or asymmetrically (ADMA). Because these proteins affect SMN activity but also the interaction of SMN with Coilin²³, we wondered whether one of the PRMTs could affect, disturb or enhance SMN shuttling after DNA damage. We depleted cells from PRMT1 by siRNA silencing (Figure S5C) and performed immunofluorescence against SMN and FBL and find that PRMT1 inhibited the entry of SMN within the nucleolus at 24h PUVI (Figure 6A). In fact, in PRMT1 depleted cells, SMN reaches the periphery of the nucleolus already at 3h PUVI but remains at the periphery and cannot enter the nucleolus at later time points. This SMN localization after DNA damage is reminiscent of the one observed in FBL depleted cells (Figure 5A). To investigate if the depletion of PRMT1 affects the interactions between SMN and its partners (Coilin and FBL), we performed PLA assays and measured a stronger interaction of SMN and FBL specifically at 3h PUVI which correlates with the localization of SMN at the periphery of the nucleolus at this precise time point (Figure 6B). We also quantified a stronger interaction of SMN with Coilin in absence of PRMT1 (Figure 6C) before damage induction and up to 40h PUVI. PRMT1 is part of the class I PRMTs which perform ADMA and MMA, in this class other PRMTs are found (PRMT-3 -4 -6 and -8). To verify whether the perturbation of SMN shuttling observed in Figure 6A is due to the physical depletion of PRMT1 or the inhibition of the ADMA methylase activity, we treated the cells with the PRMT-class I specific inhibitor MS023²⁴ (Figure 7A) prior to DNA damage and IF

assays. We could verify that the inhibition of the methylase activity of PRMTs from class I is perturbing SMN shuttling (Figure 7A) and that SMN is unable to enter the nucleolus at 24h PUVI and is localized at the periphery of the nucleolus already at 3h PUVI, a situation that is reminiscent of both FBL depletion (Figure 5A) and PRMT1 depletion (Figure 6A). Interestingly, by using the more specific and potent PRMT1 inhibitor, Furamidine ^{25,26}, we could observe a complete abolishment of SMN shuttling at all time points (Figure 7B). Remarkably, we showed by IF that PRMT1 is also shuttling during nucleolar reorganization in wild type cells and could detect PRMT1 at 24h PUVI and 40h PUVI (in a subset of cells) within the nucleolus (Figure 7C upper panel). Importantly, this shuttling is dependent of the SMN protein as in SMN depleted cells (sh6-SMN) PRMT1 is not detect inside the nucleoli at this time point (Figure 7C lower panel). Moreover, at late time points, when SMN localization within the CBs is restored, PRMT1 is no more localized in the nucleolus and surprisingly PRMT1 levels increase in the nucleoplasm (Figure 7C lower panel), this increase in nuclear PRMT1 levels is independent of the presence of a functional SMN.

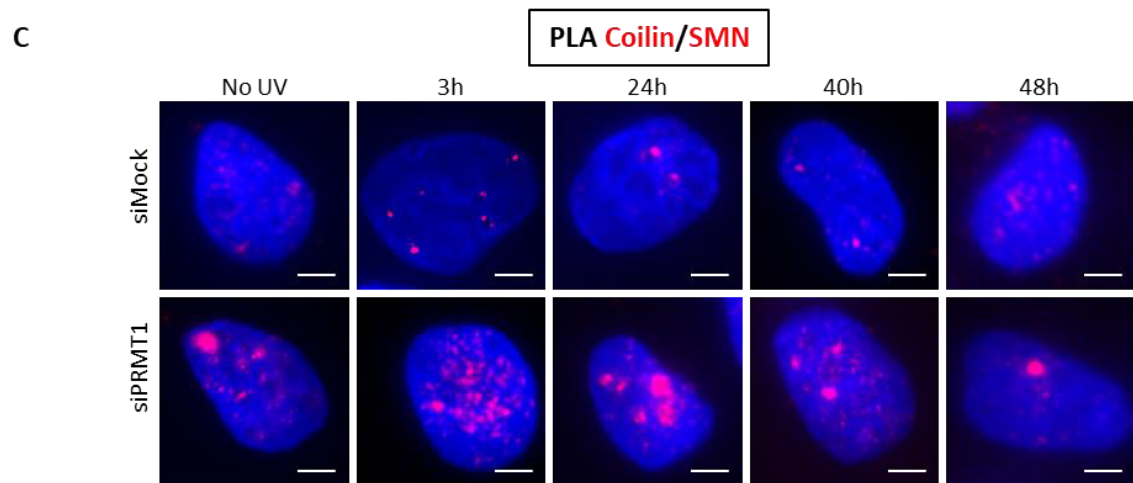
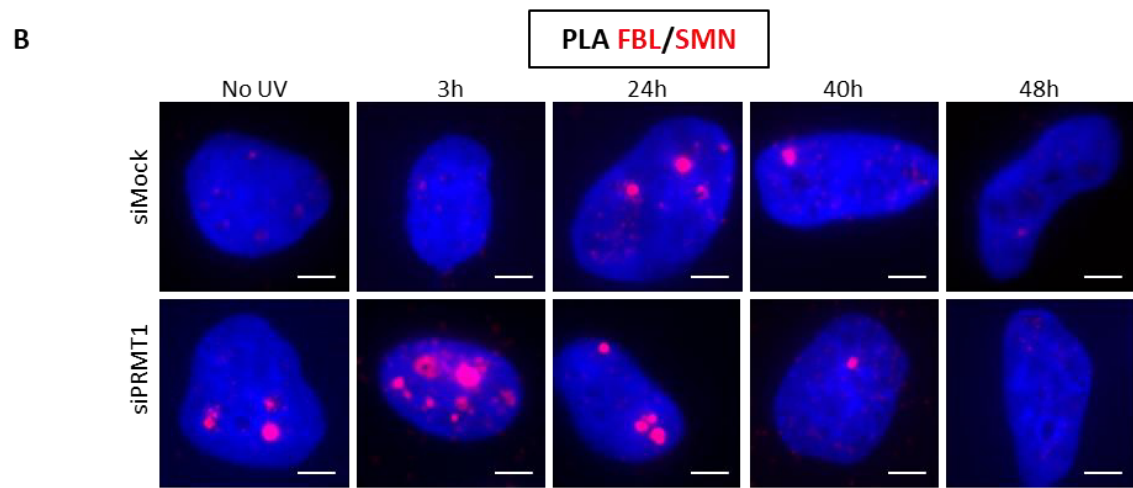
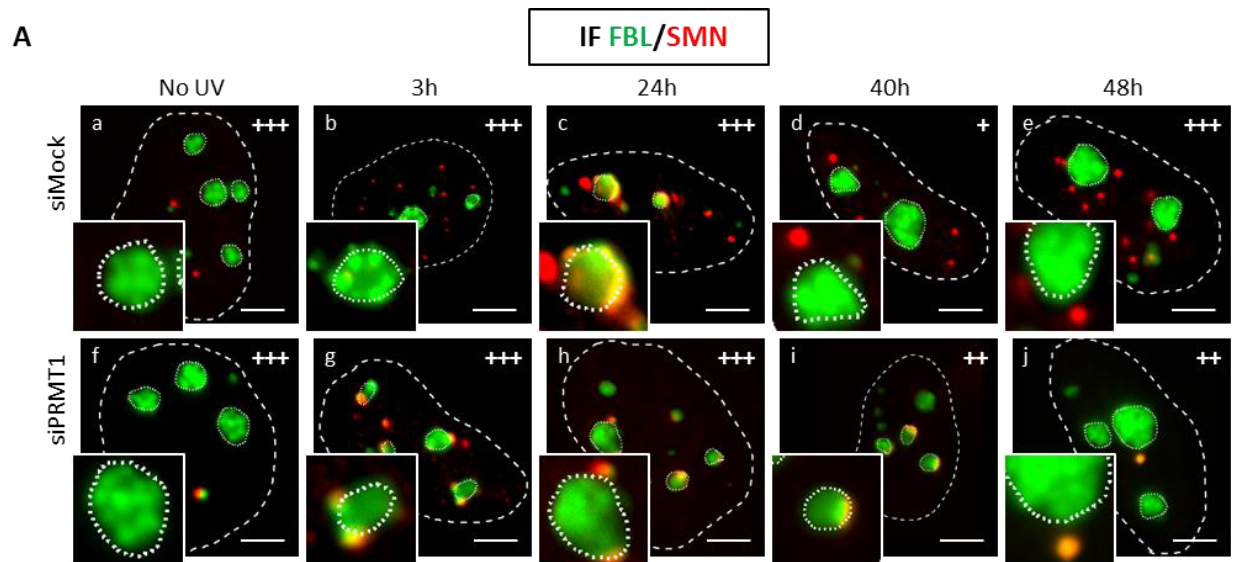


Figure 6 : PRMT1 remodel the interaction of SMN with FBL and Coilin

A) Confocal microscopy images of immunofluorescence assay in MRC5 cells transfected with siMock or siPRMT1 after 16J/m² UV-C irradiation showing the localization of SMN in red and FBL in green. Nuclei and nucleoli are indicated by dashed lines and dotted lines respectively. **B and C)** Microscopy images of proximity ligation assay showing the interaction between SMN and FBL (**A**) and between Coilin and SMN (**B**) in MRC5 cells transfected with siMock or siPRMT1 after UV-C irradiation. Scale bar for all images: 5µm

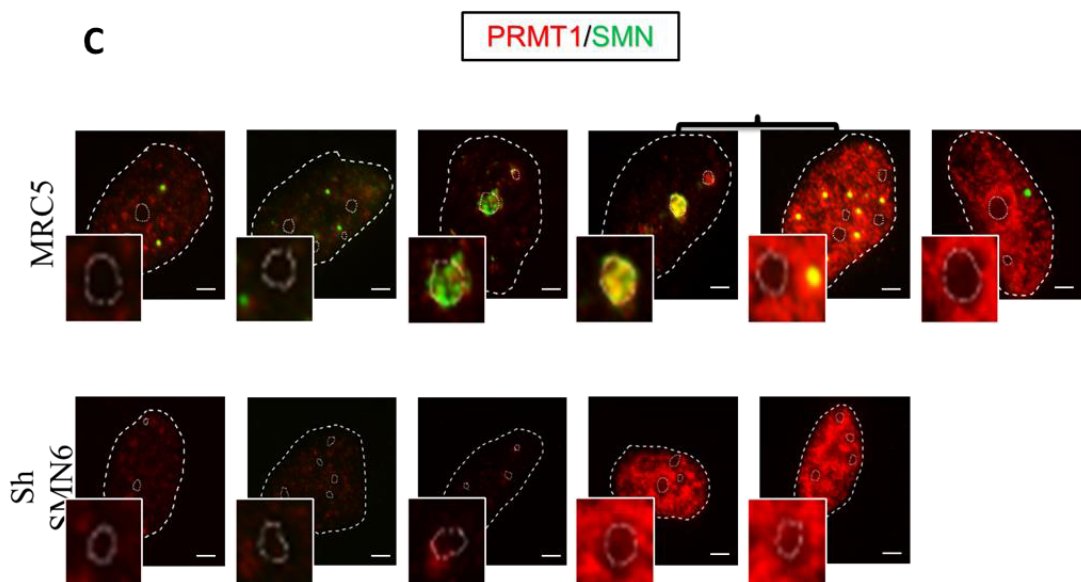
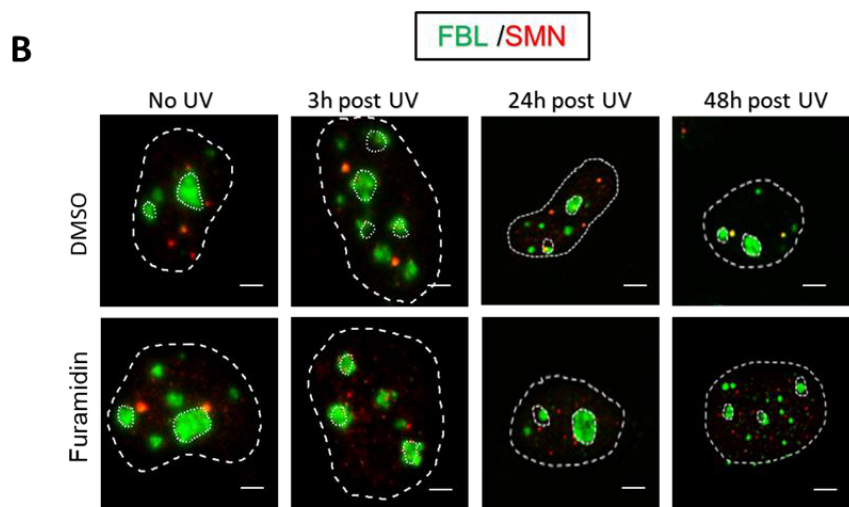
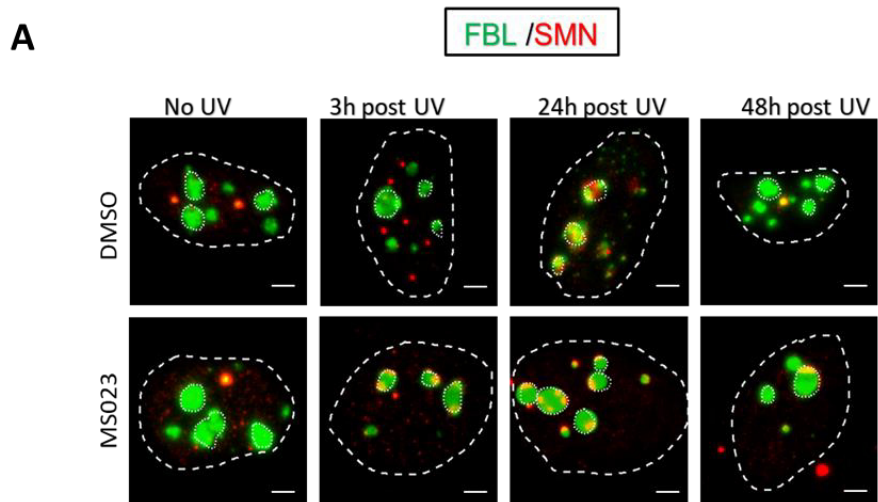


Figure 7: PRMT1 activity mediates the nucleolar shuttling of SMN

(A-C) Confocal microscopy images of immunofluorescence assay **A)** in MRC5 cells treated with DMSO or MS023 followed by 16J/m² UV-C irradiation showing the localization of SMN in red and FBL in green.

B) in MRC5 cells treated with DMSO or Furamidine followed by 16J/m² UV-C irradiation showing the localization of SMN in red and FBL in green. **C)** MRC5 and Sh6 SMN followed by 16J/m² UV-C irradiation showing the localization of SMN in green and FBL in red. Nuclei and nucleoli are indicated by dashed lines and dotted lines respectively. Scale bar for all images: 5µm

DISCUSSION

One of the most fascinating and nearly unexplored area in the DNA repair field is how cells reprimarize their cellular activities after the completion of all the reactions that allow cells to eliminate DNA lesions. Most DNA lesions block transcription and replication and although we have an extensive knowledge on how cells recognize and repair these lesions, very little is known on how cells restart these cellular processes. In post-mitotic cells, restoration of the DNA-lesions induced block of transcription is essential for cell survival. We have shown that RNAP1 transcription is blocked after UV lesions and that TC-NER pathway is responsible for the repair of UV-lesions on ribosomal DNA ⁷. Importantly, UV-damage impact the organization of the nucleolus and during DNA repair both nucleolar DNA and RNAP1 are displaced at the periphery of the nucleolus ⁸. Interestingly, although RNAP1 transcription restarts when UV-lesions on the transcribed strand are repaired, the positioning of the RNAP1 within the nucleolus is dependent on the presence of DNA lesions on the untranscribed nucleolar DNA ⁷, in this particular case RNAP1 transcription restarts in a non-canonical compartment and might influence the proper ribosome biogenesis. Hence, the restoration of the proper nucleolar structure and organization might be important for the cellular viability or for the efficiency of cellular processes. The recovery of a normal nucleolar structure is not a passive process and require the presence of some key proteins ⁸, although their exact mechanistic role have not been established yet. In a quest of finding the exact molecular mechanism for the reestablishment of the nucleolar organization after DNA repair completion, we set up a best candidate approach that guided us to inspect the effect of depletion of different

nucleolar proteins' interactors. One of these candidates was the protein SMN, which was a particularly interesting protein to scrutinize because of the known interaction with the FBL via its Tudor domain. We demonstrated in this study that depletion or mutation of the SMN protein impedes RNAP1 and FBL to recover the proper position within the nucleolus after DNA repair, despite the restart of RNAP1 transcription. To note this mis-localization is not induced by the presence of DNA lesions on untranscribed ribosomal DNA because SMN deficient cells are proficient in the GGR pathway, repairing UV-lesions on untranscribed regions of the genome.

Interestingly, we have observed that SMN, together with proteins of his complex like Gemin5, shuttles within the nucleolus, prior the reestablishment of the proper nucleolar landscape. Briefly, in normal wild type cells, after UV irradiation (or RNAP1 transcription inhibition), the CBs are disrupted ²⁷ and Coilin is displaced to the periphery of the nucleolus. At later time points, likely when DNA repair is mostly completed, SMN reaches the periphery of the nucleolus and is localized within the nucleolus. Finally, when cells that have reestablished the proper RNAP1/FBL localization within the nucleolus, SMN and Coilin are found in their physiological localization within the CBs. The different phases of SMN shuttling are dependent on both Coilin and FBL. In Coilin depleted cells, SMN does not reach the periphery of the nucleolus and in FBL depleted cells, SMN does not enter the nucleolus. In both Coilin and FBL cells, RNAP1 does not recover the proper localization within the nucleolus but remains at the periphery of the nucleolus. Because FBL interacts with SMN via its Tudor domain and SMN interacts mainly with methylated Arginines residues, we explored the possibility that one of the PRMTs would be responsible for SMN shuttling within the nucleolus. Indeed, the activity of PRMT1, responsible for ADMA, is essential to recruit SMN to the periphery of and within the nucleolus and interestingly PRMT1 shuttles within the nucleolus in the same time frame as SMN. Remarkably, this shuttling is SMN dependent. Although we do not know if the substrate of PRMT1 is a protein that directly interact with SMN, we showed that methylation is essential for SMN shuttling. It is plausible to assume that because FBL is methylated by PRMT1 ²⁸, FBL might be the substrate methylated during the process of RNAP1repositioning within the nucleolus after completion of DNA repair.

Still to determine the exact role of the protein SMN in the process of repositioning of nucleolar proteins and DNA within the nucleolus and the impact of a defect in re-establishing a proper nucleolar structure in SMA patients' cells and motoneurons.

MATERIALS AND METHODS

Cell culture and treatments

Wild type SV40-immortalized human fibroblasts (MRC5) and (CS1AN) were cultured DMEM (Lonza) supplemented with 10% fetal bovine serum (FBS, Sigma) and 1% antibiotics (penicillin and streptomycin; Lonza) and incubated at 37°C with 20% O₂ and 5% CO₂.

The SV40-immortalized human fibroblasts (MRC5 + Sh scramble, MRC5 + Sh SMN5, and MRC5 + Sh SMN6) cells were obtained from Dr. Olivier BINDA from Patrick LOMONTE team from Institut NeuroMyogène. The cells were transduced with lentiviral particules produced (as described <https://www.addgene.org/protocols/plko/#E>) from piSMART hEF1α / turboGFP (Dharmacon) doxycycline-inducible lentiviral system containing a Short Hairpin (Sh) scramble (VSC6572). For (Sh) SMN: Sh5 SMN (V3IHSHEG_4923340), Sh6 SMN (V3IHSHEG_5297527), which target both telomeric *SMN1* and centromeric *SMN2* copies of the gene. The cells were cultured in DMEM (Lonza) supplemented with 10% fetal bovine serum (FBS, Sigma) and 1% antibiotics (penicillin and streptomycin; Lonza), maintained in 100 ng/ml puromycin then the (Sh) induction with 100 ng/ml doxycycline. The cells were incubated at 37°C with 20% O₂ and 5% CO₂.

Primary fibroblast cells from unaffected (C5RO) and the CSB-/- patients (CS1AN) used as negative control were cultured in DMEM (GIBCO) supplemented with 10% fetal bovine serum and 1% antibiotics (penicillin and streptomycin; Lonza). For SMA type I patients (GM00232), fibroblast cell lines were obtained from Coriell Cell Repositories and cultured in (MEM) (Sigma) supplemented with 15% non-inactivated fetal bovine serum (FBS; Gibco), 1% non-essential amino acids (MEM)(Gibco) and 1% antibiotics (penicillin and streptomycin; Lonza) and incubated at 37°C with 3% O₂ and 5% CO₂.

UV-C irradiation

Cells were irradiated under the a UV-C lamp (254 nm, 6-Watt light). For the required time globally, the cells were irradiated at 16 J/m² doses or not irradiated as control and left in the medium for 40h or 3h before fixation.

Transfection of small interfering RNAs (siRNAs)

transient transfection, Lipofectamine and Plus Reagents from Invitrogen were used. Cells were harvested on day 0, 100 000 cells were seeded in a 6-wells plate on 18 or 12 mm coverslips. According to the manufacturers ' protocols, the first and second transfections were performed on day 1 and day 2, using Lipofectamine® RNAiMAX reagent (Invitrogen; 13778150). Experiments were performed

between 24h and 72h after the second transfection. SiRNA efficiency was confirmed by western blot on whole-cell extracts. The siRNAs of PRMTs 1-8 were obtained from Dr. Olivier BINDA from Patrick LOMONTE team from Institut neuromyogène. siRNAs Reference/Sequence are described in Table 1.

Target	Final Concentration	Reference/Sequence
siMock	10 nM	Dharmacon:D-001210-02
Si coilin	10 nM	Dharmacon:M-019894-01-0005
Si PRMT 1	10 nM	Thermo Scientific: L-010102

Table 1

Whole-cell extracts

The whole-cell extracts were collected using trypsin, adding the medium and Centrifuge at 2000-3000 rpm for 3-5 minutes. Remove the supernatant, then add PBS+ (PIC) Protease Inhibitor Cocktail, Centrifuge at 2000-3000 rpm for 3-5 minutes. Then remove the supernatant. Extraction of complete proteins with a commercial lysis buffer RIPA buffer ThermoFisher (#89900). Estimate the cells volume, add 10 volumes of RIPA buffer + PIC to 1 volume of cells. Resuspend the pellet incubate 15min on ice. Centrifuge at a speed of 14000rpm for 10min. Recover the supernatant and put it in a low binding tube. Determine the amount of protein by the Bradford method.

Western blot

Protein concentration was determined by using the Bradford method. Samples were diluted with 2x Laemmli buffer, heated at 95 °C 5 min spin down, and loaded on a SDS/PAGE gel. Proteins were separated on 8% and 12% SDS/PAGE, and then transferred onto a polyvinylidene difluoride membrane (PVDF) (0.45 µm; Millipore) 2h. The membrane was blocked in 5% milk PBS 0.1% Tween (PBS-T) and incubated for 45 min or O/N with the primary antibodies (see Primary Antibodies, Table 4) in milk PBS-T. The loading was controlled with the Tubulin antibody. Subsequently, the membrane was washed with PBS-T (3x 10 min) and incubated with the secondary antibody in milk PBS-T. After the same washing procedure, protein bands were visualized via chemiluminescence (ECL Enhanced Chemo Luminescence; Pierce ECL Western Blotting Substrate) using the ChemiDoc MP system (BioRad).

GST-SMN purification and GST pulldowns

Briefly, SMN was cloned in pGEX6P1 between *Bam*HI and *Xho*I sites, sequenced verified, and transformed in BL21 cells. Single colonies were grown overnight in 2.5 mL LB broth, scaled up to 250 mL, grown at 37 °C until density at OD₆₀₀ reached 0.6, then GST or GST-SMN were induced with 0.2 mM IPTG overnight. The next day, cells were collected by centrifugation and resuspended in 10 mL lysis buffer (50 mM Tris pH 8.0, 150 mM NaCl, 0.05% NP₄₀, supplemented with EDTA-free complete protease inhibitor cocktail [Roche]). While working on ice, cells were briefly sonicated and extracts clarified by centrifugation. Recombinant proteins were then purified using Glutathione-sepharose beads (thumbling at 4 °C overnight), washed extensively, and released from the beads using elution buffer (100 mM Tris pH 8.0, 10% Glycerol, 15 mg/mL reduced glutathione).

GST pulldowns were performed in 600 µL TAP buffer (50 mM Tris pH 7.5, 200 mM NaCl, 0.1% Triton-X, and 10% glycerol supplemented with EDTA-free Complete protease inhibitor cocktail) with 5 µg GST and 85 µL HEK293T whole cell lysate (1 x 100 mm plate lysed in 1 mL TAP buffer). A 10% input (8.5 µL in 20 µL Laemmli sample buffer) was set aside. Samples were incubated 2-3 at 4°C with rotation, then 25 µL Glutathione-sepharose beads were added for 1 hour. Then, the beads were washed 4 times with 1 mL TAP buffer and finally resuspended in 20 µL Laemmli sample buffer before immunoblotting analyses.

For time course experiments following UV-induced DNA damage, HeLa cells (?) were lysed in 1 mL lysis buffer (what is the buffer you used?) and 17 µg of proteins (amount available per pulldown) were used as above.

Cyostripping

It was used to remove the cytoplasm of the cells used for SMN experiment. Briefly, the coverslips were washed on the ice with cold PBS 2X then 5min with Cytoskeleton buffer, 5min with Cyto stripping buffer. Finally, wash it with cold PBS 3X. after that, the cells were fixed to start the designated experiment. See Table 2. 3

Cytoskeleton buffer:

	Concentration	Stock concentration	For 100ml
PIPES pH6,8	10mM	1M	1ml
NaCl	100mM	5M	2ml

Sucros	300mM	1M	30ml
MgCl ₂	3mM	1M	300µl
EGTA	1mM	0,5M	200µl
Triton X100	0.5%	100%	500µl
H ₂ O			66ml

Table 2

Cyto stripping buffer:

	Concentration	Concentration stock	Pour 100ml
Tris-HCl pH7,4	10mM	1M	1ml
NaCl	10mM	5M	200µl
MgCl ₂	3mM	1M	300µl
Tween 40	1%	100%	1ml
Sodium deoxycholate	0,5%	10%	5ml
H ₂ O			92,5ml

Table 3

Proximity ligation assay

Duolink™ PLA (Merck, Darmstadt, Germany) kit was used following the manufacturer's instructions. In brief, MRC-5 cells were plated on round 12 mm glass coverslips. On day 1, cells were washed in PBS, fixed with 2% paraformaldehyde for 15 min at 37 °C, washed again, and incubated in PLA blocking buffer for 60 min at 37 °C. After blocking, cells were incubated overnight at 4°C with appropriate primary antibodies. On day 2, the incubation with PLUS and MINUS PLA probes for 60 min at 37 °C, ligation mix for 30 min at 37 °C, and amplification mix for 100 min at 37 °C. Finally, washed coverslips were fixed on 26 × 76 mm microscope slides using VectaShield mounting medium H-1000 (Vector Laboratories, Burlingame, CA).

Immunofluorescence

Cells were grown on 18 or 12 mm coverslips, washed with PBS at RT, and fixed with 2% paraformaldehyde for 15 min at 37° C. Cells were permeabilized with PBS 0.1 % Triton X-100 (3X short + 2X 10 min washes). Blocking of non-specific signals was performed with PBS+ (PBS, 0.5 % BSA, 0.15 % glycine) for at least 30 min. Then, coverslips were incubated with 70 µl of primary antibody mix for 18mm coverslips or 50 µl for 12mm coverslips. Incubation for 2h at RT in a moist chamber, washed with PBS (3X short + 2X 10 min), quickly washed with PBS+ before incubating with 70 µl of secondary antibody mix for 1h at RT in a moist chamber. After the same washing procedure, coverslips were finally mounted using Vectashield with DAPI (Vector Laboratories) and kept at - 20° C, or with Vectashield, vibrance with DAPI (Vector Laboratories) and kept at 4° C at least 30 cells were imaged for each condition.

Antibodies

The following primary antibodies were used; see Table 4.

Antibody against	Source	Manufacturer	Catalog Nr	IF/PLA	WB
Alpha-Tubulin	Mouse	Sigma	T6074		1/50 000
Coilin	Rabbit	Proteintech	10967-1-AP	1/500	1/5000
CSB	Mouse	Santa Cruz Biotechnology	sc398022		1/100
FBL	Rabbit	abcam	ab5821	1/500	1/500
GST	Rabbit	abcam	ab3416		1/3000
PRMT1	Rabbit	Abcam	ab190892	1/5000	1/1000
RNAP1	Mouse	Santa-cruz	sc48385	1/500	
SMN	Rabbit	Proteintech	11708-1-AP	1/100	
SMN	Mouse	BD Biosciences	610646	1/500	1/5000

Table 4

The following secondary antibodies were used:

goat anti-mouse Alexa Fluor 488 A-11008 (Invitrogen) 1/400 and goat anti-Rabbit Alexa Fluor 594 A-11012 (Life technology) 1/400.

RNA Fluorescence In Situ Hybridization

Cells were grown on 18 mm coverslips, washed with PBS at RT, and fixed with 4% paraformaldehyde for 15 min at 37° C. Coverslips were washed twice with PBS. Cells were permeabilized by washing with PBS 0.4 % Triton X-100 for 7 min at 4° C. Cells were washed rapidly with PBS before incubating them with pre-hybridization buffer (2X SSPE and 15 % formamide) (20X SSPE, [pH 8.0]: 3 M NaCl, 157 mM NaH₂PO₄.H₂O and 25 mM EDTA) for at least 30 min. 3.5 µl of probe (10 ng/ml) was diluted in 70 µl of hybridization mix (2X SSPE, 15 % formamide, 10 % dextran sulphate, 0.5 mg/ml tRNA) and heated at 90° C for 1 min. Hybridization of the probe was conducted overnight at 37° C in a humidified environment. Subsequently, cells were washed twice for 20 min with prehybridization buffer, then once for 20 min with 1X SSPE, and finally mounted with Vectashield (Vector Laboratories) and kept at -20° C. The probe sequence (5' to 3') is Cy5- AGACGAGAACGCCTGACACGCACGGCAC. At least 30 cells were imaged for each condition of each cell line.

Recovery of RNA synthesis (RRS) assay

MRC5, MRC5+ Sh Scramble, MRC5+ Sh5-SMN, MRC5+ Sh6-SMN and CSB-/- cells were grown on 18 mm coverslips. RNA detection was done using a Click-iT RNA Alexa Fluor Imaging kit (Invitrogen), according to the manufacturer's instructions. Briefly, cells were UV-C irradiated (10 J/m²) and incubated for 0, 3 and 24 h at 37°C. Then, cells were incubated for 2 hours with 5-ethynyl uridine. After fixation and permeabilization, cells were incubated for 30 min with the Click-iT reaction cocktail containing Alexa Fluor Azide 594. After washing, the coverslips were mounted with Vectashield (Vector). The average fluorescence intensity per nucleus was estimated after background subtraction using ImageJ and normalized to not treated cells.

Fluorescent imaging and analysis

Imaging has been performed on a Zeiss 880 confocal laser-scanning microscope (Zeiss), using a 63x oil objective. Images were analyzed with Image J software. For all images of this study, nuclei and nucleoli were delimited with dashed and dotted lines, respectively, using DAPI staining or transmitted light.

Unscheduled DNA synthesis (UDS or TCR-UDS).

MRC5, MRC5+ Sh Scramble (WT cells), MRC5+ Sh5-SMN, MRC5+ Sh6-SMN (SMN deficiency cells), XPA deficient (XP12RO, NER deficient cells), and XPC deficient (XP4PA, GG-NER deficient cells), were grown on 18 mm coverslips. After local irradiation at 100 J/m² with UV-C through a 5 µm pore polycarbonate

membrane filter, cells were incubated for 3 or 8 hours (UDS and TCR-UDS respectively) with 5-ethynyl-2'-deoxyuridine (EdU), fixed and permeabilized with PBS and 0.5% triton X-100. Then, cells were blocked with PBS+ solution (PBS containing 0.15% glycine and 0.5% bovine serum albumin) for 30 min and subsequently incubated for 1h at room temperature with mouse monoclonal anti- γ H2AX antibody (Ser139 [Upstate, clone JBW301]) 1:500 diluted in PBS+. After extensive washes with PBS containing 0.5% Triton X100, cells were incubated for 45min at room temperature with secondary antibodies conjugated with Alexa Fluor 594 fluorescent dyes (Molecular Probes, 1:400 dilution 504 in PBS+). Next, cells were washed several times and then incubated for 30 min with the Click-iT reaction cocktail containing Alexa Fluor Azide 488. After washing, the coverslips were mounted with Vectashield containing DAPI (Vector). Images of the cells were obtained with the same microscopy system and constant acquisition parameters. Images were analyzed as follows using ImageJ and a circle of constant size for all images: (i) the background signal was estimated in the nucleus (avoiding the damage, nucleoli and other non-specific signal) and subtracted, (ii) the locally damaged area was defined by using the γ H2AX staining, (iii) the average fluorescence correlated to the EdU incorporation was then measured and thus an estimate of DNA synthesis after repair was obtained.

Statistical analysis

All I experiments were performed at least three independent times. Values were expressed as mean \pm estimated standard error of the mean (SEM) of the biological replicates.

Conflicts of interest

The authors disclose no potential conflict of interest.

Acknowledgments

We would like to thank Dr Leonardo Beccari for fruitful discussions and Dr Laurent Schaeffer for supporting and encouraging this research. We are grateful to the imaging platform CYOLE and Dr Christophe Vanbel together with the CRCL imaging facility.

Reference

1. Dubois, M.-L. & Boisvert, F.-M. The Nucleolus: Structure and Function. in *The Functional Nucleus* (eds. Bazett-Jones, D. P. & Dellaire, G.) 29–49 (Springer International Publishing, 2016). doi:10.1007/978-3-319-38882-3_2.
2. Hernandez-Verdun, D. Assembly and disassembly of the nucleolus during the cell cycle. *Nucl. Austin Tex* **2**, 189–194 (2011).
3. Boulon, S., Westman, B. J., Hutten, S., Boisvert, F.-M. & Lamond, A. I. The Nucleolus under Stress. *Mol. Cell* **40**, 216–227 (2010).
4. Louvet, E., Junéra, H. R., Le Panse, S. & Hernandez-Verdun, D. Dynamics and compartmentation of the nucleolar processing machinery. *Exp. Cell Res.* **304**, 457–470 (2005).
5. Giglia-Mari, G., Zotter, A. & Vermeulen, W. DNA Damage Response. *Cold Spring Harb. Perspect. Biol.* **3**, a000745 (2011).
6. Brooks, P. J. The case for 8,5'-cyclopurine-2'-deoxynucleosides as endogenous DNA lesions that cause neurodegeneration in xeroderma pigmentosum. *Neuroscience* **145**, 1407–1417 (2007).
7. Daniel, L. *et al.* Mechanistic insights in transcription-coupled nucleotide excision repair of ribosomal DNA. *Proc. Natl. Acad. Sci. U. S. A.* **115**, E6770–E6779 (2018).
8. Cerutti, E. *et al.* β -Actin and Nuclear Myosin I are responsible for nucleolar reorganization during DNA Repair. <http://biorxiv.org/lookup/doi/10.1101/646471> (2019) doi:10.1101/646471.
9. Talbot, K. & Tizzano, E. F. The clinical landscape for SMA in a new therapeutic era. *Gene Ther.* **24**, 529–533 (2017).
10. Monani, U. R. Spinal muscular atrophy: a deficiency in a ubiquitous protein; a motor neuron-specific disease. *Neuron* **48**, 885–896 (2005).
11. Calucho, M. *et al.* Correlation between SMA type and SMN2 copy number revisited: An analysis of 625 unrelated Spanish patients and a compilation of 2834 reported cases. *Neuromuscul. Disord. NMD* **28**, 208–215 (2018).
12. Singh, R. N., Howell, M. D., Ottesen, E. W. & Singh, N. N. Diverse role of survival motor neuron protein. *Biochim. Biophys. Acta BBA - Gene Regul. Mech.* **1860**, 299–315 (2017).
13. Trinkle-Mulcahy, L. & Sleeman, J. E. The Cajal body and the nucleolus: 'In a relationship' or 'It's complicated'? *RNA Biol.* **14**, 739–751 (2017).
14. Hebert, M. D., Szymczyk, P. W., Shpargel, K. B. & Matera, A. G. Coilin forms the bridge between Cajal bodies and SMN, the spinal muscular atrophy protein. *Genes Dev.* **15**, 2720–2729 (2001).

15. Wehner, K. A. *et al.* Survival motor neuron protein in the nucleolus of mammalian neurons. *Brain Res.* **945**, 160–173 (2002).
16. Jones, K. W. *et al.* Direct interaction of the spinal muscular atrophy disease protein SMN with the small nucleolar RNA-associated protein fibrillarin. *J. Biol. Chem.* **276**, 38645–38651 (2001).
17. Renvoisé, B. *et al.* Distinct domains of the spinal muscular atrophy protein SMN are required for targeting to Cajal bodies in mammalian cells. *J. Cell Sci.* **119**, 680–692 (2006).
18. Whitehead, S. E. *et al.* Determinants of the interaction of the spinal muscular atrophy disease protein SMN with the dimethylarginine-modified box H/ACA small nucleolar ribonucleoprotein GAR1. *J. Biol. Chem.* **277**, 48087–48093 (2002).
19. Pellizzoni, L., Baccon, J., Charroux, B. & Dreyfuss, G. The survival of motor neurons (SMN) protein interacts with the snoRNP proteins fibrillarin and GAR1. *Curr. Biol. CB* **11**, 1079–1088 (2001).
20. Cioce, M., Boulon, S., Matera, A. G. & Lamond, A. I. UV-induced fragmentation of Cajal bodies. *J. Cell Biol.* **175**, 401–413 (2006).
21. Tessarz, P. *et al.* Glutamine methylation in histone H2A is an RNA-polymerase-I-dedicated modification. *Nature* **505**, 564–568 (2014).
22. Côté, J. & Richard, S. Tudor Domains Bind Symmetrical Dimethylated Arginines. *J. Biol. Chem.* **280**, 28476–28483 (2005).
23. Hebert, M. D., Shpargel, K. B., Ospina, J. K., Tucker, K. E. & Matera, A. G. Coilin methylation regulates nuclear body formation. *Dev. Cell* **3**, 329–337 (2002).
24. Eram, M. S. *et al.* A Potent, Selective, and Cell-Active Inhibitor of Human Type I Protein Arginine Methyltransferases. *ACS Chem. Biol.* **11**, 772–781 (2016).
25. Fulton, M. D., Brown, T. & Zheng, Y. G. Mechanisms and Inhibitors of Histone Arginine Methylation. *Chem. Rec. N. Y. N* **18**, 1792–1807 (2018).
26. Yan, L. *et al.* Diamidine compounds for selective inhibition of protein arginine methyltransferase 1. *J. Med. Chem.* **57**, 2611–2622 (2014).
27. Cioce, M., Boulon, S., Matera, A. G. & Lamond, A. I. UV-induced fragmentation of Cajal bodies. *J. Cell Biol.* **175**, 401–413 (2006).
28. Lin, C.-H., Huang, H.-M., Hsieh, M., Pollard, K. M. & Li, C. Arginine methylation of recombinant murine fibrillarin by protein arginine methyltransferase. *J. Protein Chem.* **21**, 447–453 (2002).

II. Coilin governs the displacement of RNAP1 in response to UV-C damage.

Introduction

Ramon Y. Cajal originally described the Cajal bodies (CB) as spherical bodies in all vertebrates in 1903. CB is a dynamic nuclear structure serving as a storehouse and maturation site for small RNA. Molecular analysis revealed that CB is enriched with its signature protein p80 Coilin and survival motor neuron protein (SMN). A twin structure of CB, called a Gemini of Cajal bodies (Gems), contains high concentrations of SMN complex (SMN and Gemins 2-8). It is typical for CB and Gems to colocalize^{1 2}.

The nucleolus, the most visible nuclear structure, is the ribosome factory of the cells. As a result of the frequent proximity of CB to the nucleolus, Cajal described CB as 'nucleolar accessory bodies. Electron microscopy analyses confirmed the relationship between the two structures¹. It has also been observed that the two structures are intimately associated in many plant cells as well³. Detailed analyses also suggest a close functional relationship. In which certain proteins in the nucleolus are shared with CB, such as Fibrillarin (FBL)⁴.

Coilin's name derives from the term "coiled body," which was common for CB due to their "coiled thread" morphology in electron microscopy images. Coilin plays a structural role in CB formation, and it has Nucleic Acid Binding and RNase Activities^{5 6}. The UV-C-induced DNA damage induces CB fragmentation and redistributes Coilin to interact with the proteasome protein PA28 γ ⁷. In addition, a subset of UV-C-irradiated cells forms nucleolar caps containing Coilin similar to those observed upon inhibition of RNAP1 by actinomycin D^{7 8}. Coilin also is rapidly recruited to UVA-induced DNA lesions that occurred immediately after local micro-

irradiation⁹. Furthermore, Coilin contributes to the cellular response to DNA damage induced by cisplatin treatment and γ -irradiation, where it is located within the nucleolus and regulates RNAP1 activity¹⁰. Indeed, mutant Coilin variants disrupted CB and nucleolar compartments¹¹, suggesting that, Coilin may play an important role for the nucleolus's functional properties. We consider these findings to be noteworthy since they suggest new functions for Coilin regarding DNA damage.

UV-C lesions cause DNA damage, which induces the re-localization of the rDNA/RNAP1 complex to the periphery of the nucleolus (for simplicity, this phase will be called “displacement”). After the repair process completion, the rDNA/RNAP1 complex returns to the nucleus (hereafter referred to as “repositioning”, for simplicity)¹². The proteins governing this reorganization remain poorly understood.

We recently demonstrated an unexpected function of SMN in the nucleolar reorganization induced by UV-C (manuscript in preparation chapter four Results I). SMN depleted cells, the nucleolar structure is not restored, and the nucleolar proteins (RNAP1 and FBL) remain at the periphery of the nucleolus. We observed a shuttling of SMN within the nucleolus after DNA repair, which depends on the physical interactions between SMN and Coilin. As a result, RNAP1 repositioning upon DNA damage and repair does not occur in Coilin-deficient cells, and RNAP1 persists at the nucleolus' periphery. This demonstrates that SMN shuttling, and the presence of Coilin are both required for nucleolar restructuring to resume. Here are more details about the involvement of Coilin itself in the nucleolar reorganization process induced by UV-C.

Results, Discussion & Perspectives

SMN and Coilin interact with RNA polymerase 1.

In CB, Coilin interacts with SMN, thus maintaining CB integrity in homeostatic conditions⁵. Moreover, after DNA damage induction by UV-C, CB is disrupted⁷. In our study to investigate the role of SMN in nucleolar reorganization during and after DNA repair of UV-induced damage, we already examined the localization of Coilin by immunofluorescence assay at different time points post-UV irradiation (PUVI) in wild-type (wt) cells, transformed MRC5-SV40 fibroblast with both SMN and RNAP1. We showed that Coilin colocalized with RNAP1 within nucleolus after damage induced by UV (manuscript in preparation chapter four Results I).

Furthermore, to complete the result obtained by immunofluorescence of Coilin, and to check the interaction between SMN and RNAP1, we studied SMN- Coilin-RNAP1 direct interaction by performing co-immunoprecipitation experiments with RNAP1 antibody at the (No UV, 3h PUVI, and 40h PUVI) time points. We demonstrated an interaction between these proteins at all the time points tested (Figure 1A).

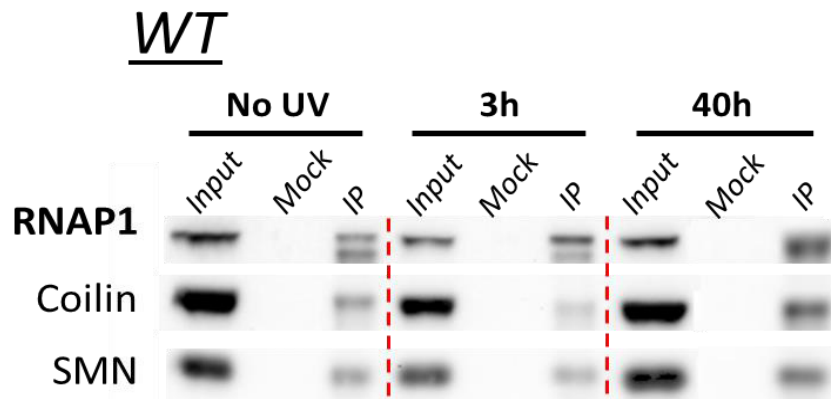


Figure 1: SMN and Coilin interact with RNA polymerase 1.

(A) Western blot of immunoprecipitation (IP) against RNAP1 in MRC5- SV40, Coilin and SMN are revealed. INPUT, 10% of the lysate used for immunoprecipitation (IP) reaction, (no UV, 3h PUVI & 40h PUVI).

SMN-depleted cells and UV-C damage show nucleolar Coilin accumulation with loss of CB.

The severe motor neuron failure of type I SMA has been correlated with a nucleolar localization of Coilin¹³. We then questioned how SMN depletion could impact Coiled nuclear distribution both in homeostatic conditions and upon UV-C. For that, we down-regulated SMN expression by lentiviral transfection of inducible shRNA directed against the SMN 3'UTR (Sh5 *SMN*), and we analyzed Coilin and RNAP1 localization by an immunofluorescent (no UV, 3h and 40h PUVI). Contrary to wt fibroblasts, we observed a nucleolar Coilin accumulation in non-UV treated Sh5 *SMN* cells, with a strong colocalization with RNAP1 (Figure 2A&B). At 3h PUVI the RNAP1 Coilin colocalization to the periphery of the nucleolus was similarly observed in wt and Sh5 *SMN* cells. However, at 40h PUVI the proportion of cells displaying Coilin localization at CB was significantly lower in Sh5 *SMN* cells compared to wt fibroblasts and was paralleled by failure reposition of RNAP1 inside of the nucleolus. Thus, the majority

of cells showed the same RNAP1 and Coilin localization observed at 3h PUVI in the pre-nucleolar position (Figure 2B).

We also examined the localization of Coilin and FBL by an immunofluorescent assay in wt, Sh Scramble, and Sh5 *SMN* fibroblasts cells. In No UV, 3h and 40h PUVI conditions. We observed the same pattern shown with RNAP1. (Figure S1).

To further assess how SMN depletion impacts the Coilin/ RNAP1 dynamics that accompanying the UV-induced DNA repair process, we performed PLA assays in wt fibroblasts and in Sh5 *SMN* cells before and after UV treatment. In agreement with the dynamics of Coilin/RNAP1 localization, we observed that SMN depletion strongly increased the nucleolar Coilin/RNAP1 PLA signal in Sh5 *SMN* cells compared to the wt controls in the No UV condition when Coilin does not normally localize in the nucleolus of wt cells (Figure 2C). At 3h PUVI, both wt and Sh5 *SMN* cells showed a strong Coilin/RNAP1 PLA signal in the periphery of the nucleolus, in agreement with the idea that the rDNA displacement process induces the displacement of Coilin to the periphery of the nucleolus in SMN independent manner (Figure 2C). However, while in wt cells, most Coilin/RNAP1 PLA staining had disappeared from the nucleolus, a strong Coilin/RNAP1 PLA signal is detected at the periphery of the nucleolus in Sh5 *SMN* cells, reflecting the lack of RNAP1 repositioning caused by SMN depletion (Figure 2C).

These results were backed up by an analysis of the interaction between Coilin and RNAP1 in the absence of SMN in vitro by co-immunoprecipitation assay (Figure 2D). No changes were observed in Coilin distribution between wt and Scramble ShRNA transfected cells (Figure S2).

These results indicate that in the absence of SMN, Coilin strongly increases its colocalization with RNAP1 both in homeostatic conditions and upon UV light exposure at the expense of CB disassembly.

Interestingly, our immunoprecipitation results showed in the absence of SMN there always seems to be an interaction between Coilin and RNAP1(Figure 2D). Nevertheless, the interaction between RNAP1 and Coilin appear to increase at 40h PUVI in wt cells (Figure 1A); in Sh5 *SMN*, we can observe a decrease in this interaction (Figure 2D). These results may show a correlation between the increase in interaction between Coilin and RNAP1 at 40h PUVI and the repositioning. This experiment was done once and must be repeated to confirm the results.

Moreover, it has been shown that the SMN and the Coilin can carry many posttranscriptional modifications that can change their location and facilitate specific interactions¹⁴. Coilin hypomethylation can target Coilin to the nucleolus, according to Tapia paper¹³. As a result, DNA damage may influence Coilin's methylation status and hence its cellular distribution. We need more studies to explore this part of DNA damage and posttranscriptional modifications of our factors.

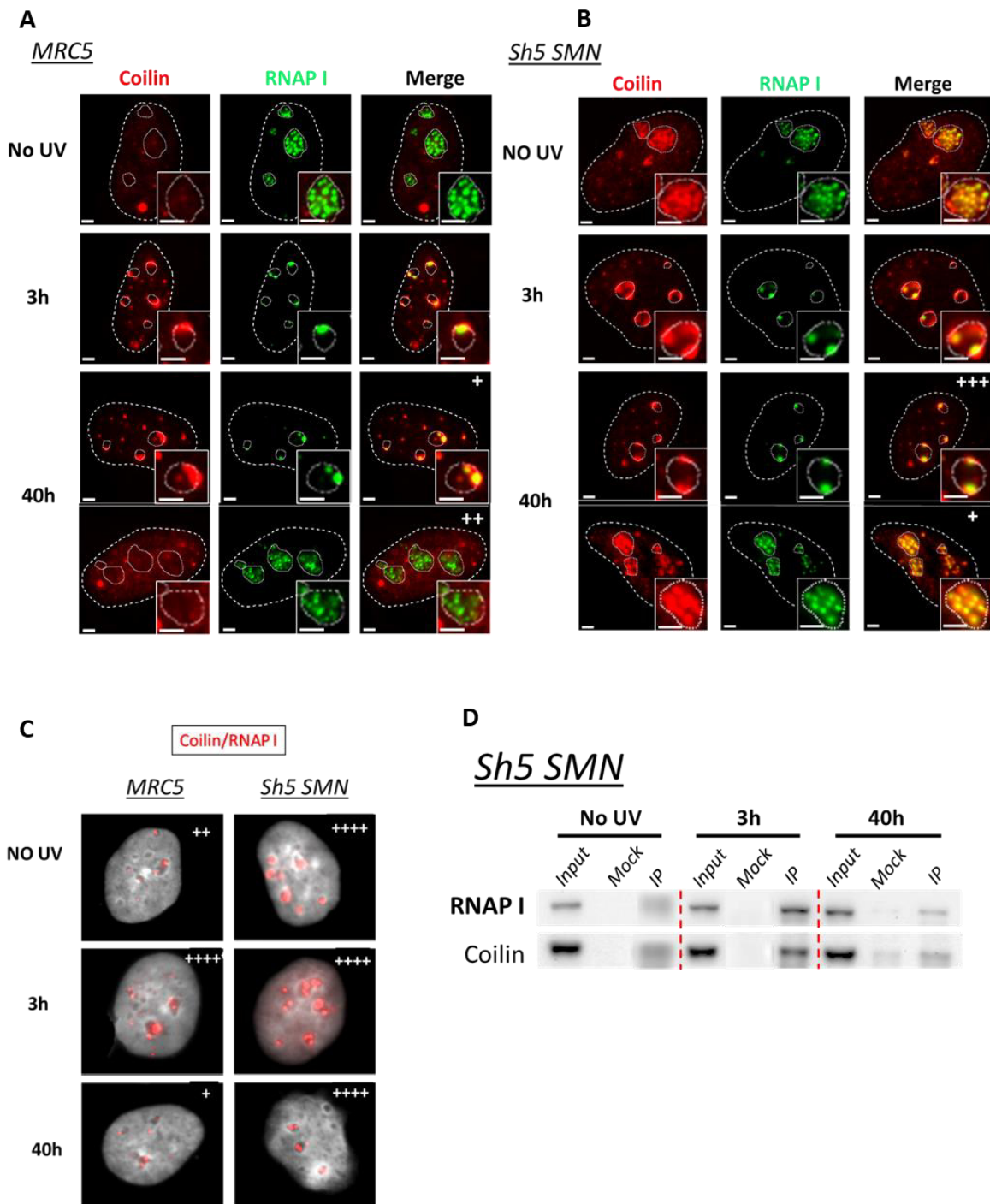


Figure 2: SMN-depleted cells and UV-C damage show nucleolar coilin accumulation with loss of CB.

(A&B) Microscopy images of immunofluorescence assay against Coilin (red) and RNAP I (green) in MRC5 cells **(A)** and in MRC5+Sh5 SMN in **(B)**. **(C)** Microscopy images of proximity ligation assay show the interaction between Coilin/RNAP I for MRC5 and MRC5+Sh5 SMN. **(D)** Western blot of immunoprecipitation (IP) against RNAP I in MRC5+Sh5 SMN, RNAP I and Coilin are revealed. INPUT, 10% of the lysate used for immunoprecipitation (IP) reaction. Nuclei and nucleoli in **(A&B)** are indicated by dashed lines and dotted lines respectively. The quantity of cells indicated for the condition 40h, post UV shown (+, <50%; ++, 50–70%; +++, 70–90%; +++, >90%). Scale bar represents 5 μ m.

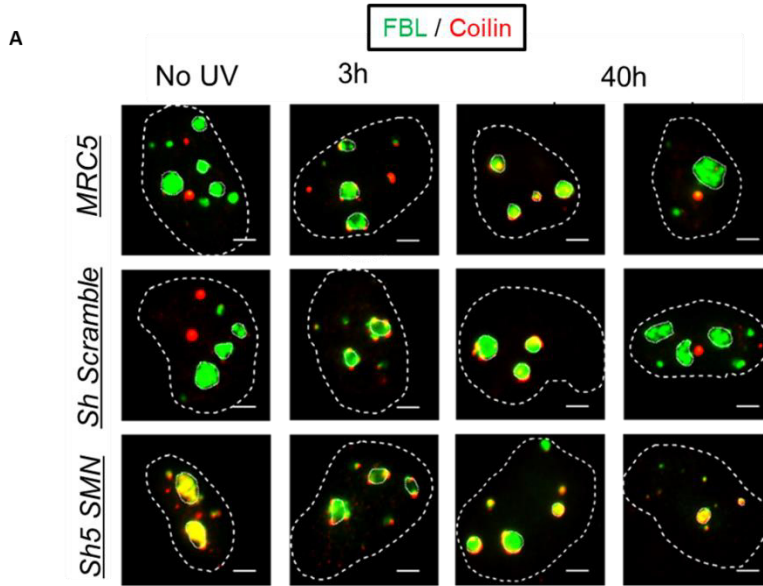
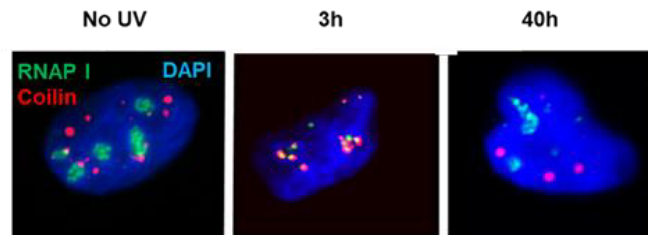


Figure S1: Coilin redistributes with Fibrillaritin in the nucleoles in the absence of SMN as well as in UV-C damage.

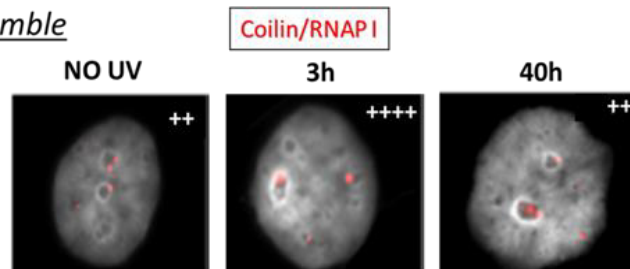
(A) Microscopy images of immunofluorescence assay against Coilin (red) and Fibrillaritin (green) in *MRC5*, *MRC5+Sh Scramble* and *MRC5+Sh5 SMN*. Nuclei and nucleoli are indicated by dashed lines and dotted lines respectively. Scale bar represents 5 μ m.

A
Sh Scramble



B

Sh Scramble



C

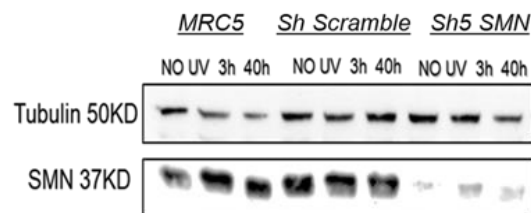


Figure S2: (A) Microscopy images of immunofluorescence assay against Coilin (red) and RNAP I (green) in MRC5+Sh Scramble. (B) Microscopy images of proximity ligation assay show the interaction between Coilin/RNAP I for MRC5+Sh Scramble. Nuclei and nucleoli are indicated by dashed lines and dotted lines respectively. The quantity of cells indicated for the condition 40h, post UV shown (+, <50%; ++, 50–70%; +++, 70–90%; +++, >90%). Scale bar represents 5 μ m. (C) Western Blot on whole cell extracts of SMN for in MRC5, MRC5+Sh Scramble and MRC5+Sh5 SMN (no uv, 3h and 40h).

Gemin5 is induced by UV in the lack of SMN but within the nucleolus.

In fact, SMN can be detected in the cytoplasm and the nucleus. Within the nucleus, SMN is found in CB together with Coilin and in Gems without Coilin. Gems are known to be enriched with SMN complex (SMN with Gemin proteins 2-8). It acts as a chaperone to promote the assembly of spliceosomal snRNP particles and hence plays a crucial role in pre-mRNA splicing¹⁵. We showed previously in (SMN results in chapter four Results I) that Gemin5 together with SMN shuttle into the nucleolus upon the UV induced damage.

Furthermore, it was described before that the low amounts of SMN protein reduce the stability of the other SMN complex components. Accordingly, when SMN levels are reduced, snRNP assembly is impaired, Gems disappear, and various Gemin proteins are depleted¹³. We then decided to compare Gems dynamics during the UV-induced DNA damage repair process in wt vs SMN depleted cells. For that, we performed an immunofluorescent assay to detect both SMN and Gemin5 in wt and Sh5 *SMN* cells in the absence of damage (No UV), 3h PUVI, and 40h PUVI. We confirmed that Gemin5 colocalizes with SMN and follows SMN dynamics after UV-irradiation and in wt cells (Figure 3A).

Instead, in SMN depleted cells no Gemin5 signal was detected in no UV condition, but, surprisingly, we revealed the presence of Gemin5 at the periphery of the nucleolus of Sh5*SMN* cells at 3h PUVI. Finally, we observed a strong accumulation of Gemin5 within the nucleolus at 40h PUVI, accompanied by the disappearance of the Gems bodies like Gemin5 staining from

the nucleus (Figure 3A). Other Gemins proteins could also have the same behavior as Gemin5 upon UV damage.

These results clearly demonstrate that Gems component (Gemin5) was induced by UV in the lack of SMN and accumulated in the nucleolus resulting in the disappearance of Gems, suggesting that the presence of Gemins proteins within the nucleolus could be a hallmark of SMA cells.

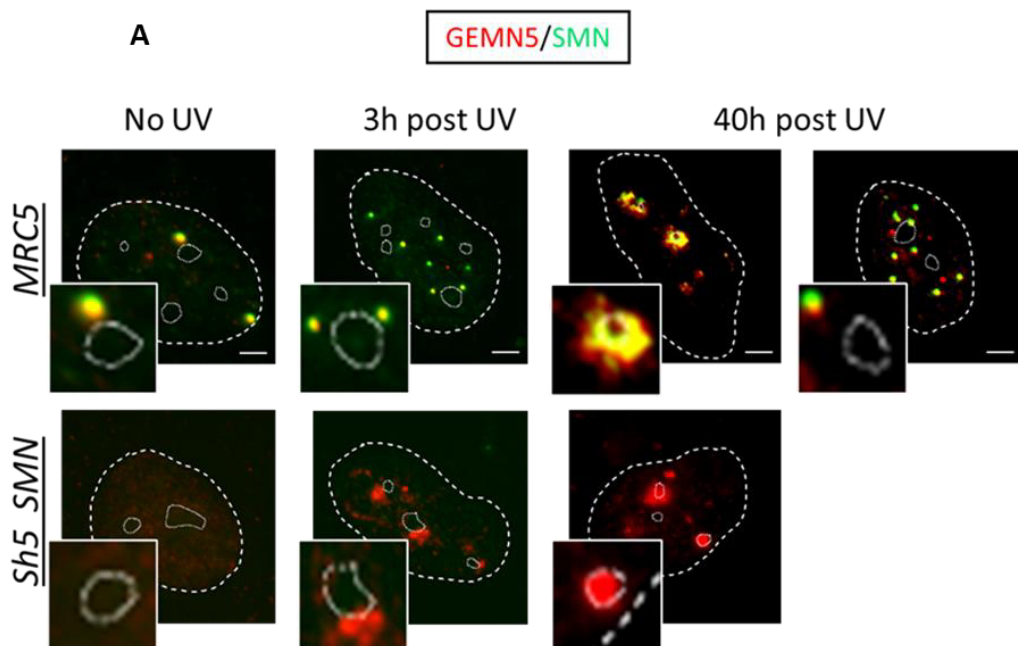


Figure 3 : Gemin5 is induced by UV in the lack of SMN but within the nucleolus.

(A) Microscopy images of immunofluorescence assay against GEMN5 (red) and SMN (green) in MRC5 cells and in MRC5+Sh5 SMN. Nuclei and nucleoli in are indicated by dashed lines and dotted lines respectively. The quantity of cells indicated for the condition 40h, post UV shown (+, <50%; ++, 50–70%; +++, 70–90%; +++++, >90%). Scale bar represents 5 μ m.

Coilin knockdown affects the displacement step by rescuing the RNAP1 transcription in the presence of UV damage.

Since it has been shown that double-strand break damage rapidly attracts Coilin to the damaged area⁹, we asked whether the UV-C induced lesions could also recruit Coilin. To address this question, we induced local UV-C damage and analyzed the colocalization of Coilin and the DNA damage marker γ H2AX at 3h PUVI by fluorescent co-immunostaining. In parallel, we also checked SMN, whether it is recruited to the damaged area caused by UV-C or its shuttling within the nucleolus is a specific response to nucleolus damage. During the local damage irradiation, we used a higher irradiation power to keep the same quantity of lesions as in the absence of a filter. Remarkably, we did not observe any accumulation of Coilin or SMN at the UV-C lesion areas delimited by γ H2AX staining (Figure 4A).

Despite the same amount of lesion used in the previous experiments, we do not observe CB dissolution or Coilin or SMN accumulation at the periphery of the nucleolus (Figure 4A). These results suggest that Coilin and SMN shuttling to the nucleolus is triggered specifically by DNA lesion accumulation in the nucleolar rDNA, while these proteins are not generally recruited to DNA lesions in other nuclear chromatin regions (Figure 4A).

Our previous data demonstrate that Coilin is recruited at the nucleolus during early phases of the rDNA UV-induced displacement while SMN shuttling allows nucleolar reconfiguration upon completion of the repair process (manuscript in preparation chapter four Results D). Besides, it has been demonstrated that Coilin participates in the suppression of RNAP1 in response to cisplatin-induced DNA lesions¹⁰ (which are also repaired by the NER system). Therefore, we asked whether Coilin depletion would impact RNAP1 localization and transcriptional dynamics during the UV-induced DNA repair process.

Remarkably, in the lack of Coilin at 3h PUVI we observed a partial impairment of RNAP1 displacement into the periphery of the nucleolus in 50% of the cells; moreover, at 40h PUVI we confirmed that RNAP1 remains more frequently at the periphery of the nucleolus (Figure.4B), compared to wt or sh scramble transfected cells.

Next, we quantified RNAP1 transcriptional activity by performing an RNA-FISH assay using a specific probe against the 47S pre-rRNA product quantifying (Figure.4C) to investigate whether the role of Coilin in the displacement step could be explained by its role in RNAP1 activity if we have the same case in the damage induced by UV. Remarkably, the loss of Coilin showed an increase in the RNAP1 transcription in all conditions (Figure.4C).

In Coilin deficient cells, we observed an increase in 47s rRNA precursor in No UV condition compared to si mock cells, suggesting an increase in the RNAP1 transcriptional activity. Remarkably, while in control cells, 47sRNA levels decreased at 3hPUVI, reflecting the RNAP1 transcriptional blockage, si Coilin cells did not display such behavior, suggesting that Coilin depletion prevents both the displacement of rDNA/ RNAP1 complexes and the RNAP1 transcription. Even more strikingly, Si Coilin cells displayed a strong increase of 47s RNA levels at 40h PUVI, contrary to the normal dynamic observed in si mock cells. While the causes of this response are not clear, these data suggest that it may be related to the longer permanence of RNAP1/rDNA complexes at the periphery of the nucleolus and the repair of the UV-induced DNA lesions.

Collectively, our findings demonstrate a novel function of Coilin in the nucleolar reorganization displacement step induced by UV-C damage. Thus, our data identify Coilin as the first protein to influence the displacement steps of RNAP1.

We report that the lack of Coilin partially affects the displacement step to the periphery of the nucleolus (Figure 4B). The effect of Coilin on the displacement step seems to be temporary by delaying the movement of rDNA/RNAP1 upon the damage, as we observed in 40h PUVI (Figure 4B) that the majority of cells showed RNAP1 at the periphery of the nucleolus.

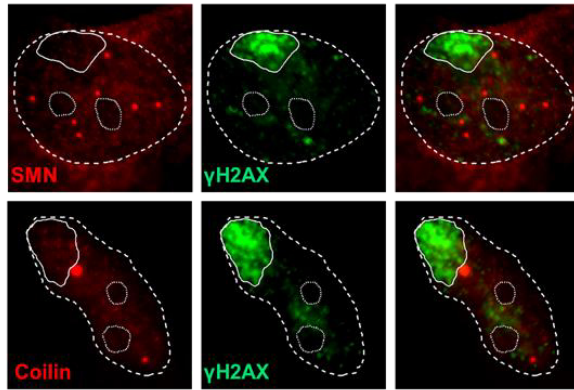
This displacement of RNAP1 is probably essential for inhibiting the RNAP1 activity during damage¹². We illustrated the defect observed in the displacement step of RNAP1 in the low level of Coilin by the significant increase in the RNAP1 transcription shown by the RNA-FISH assay (Figure 4C).

Interestingly, other proteins sharing between nucleolus and CB could have a function in this process, such as Nopp140. Coilin can interact with Nopp140¹⁶, which has been demonstrated to be associated with RNAP1. Moreover, the activity of RNAP1 was reduced by full-length and transfected Nopp140¹⁷. Therefore, it could be interesting to study the Nopp140 behavior with UV-C damage in our conditions that may act together with Coilin to repress the RNAP1 activity during damage.

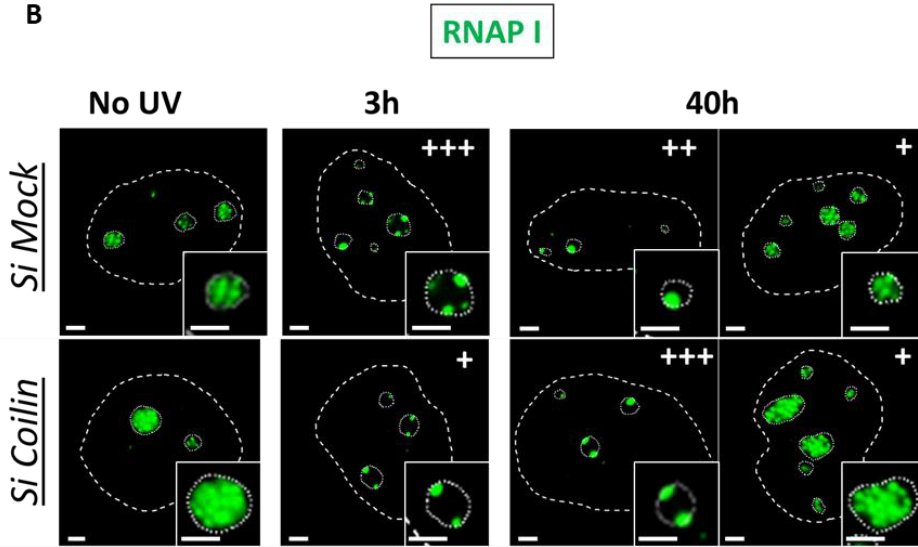
Furthermore, another nucleolar factor has been shown to interact with Coilin upon damage (e.g; UBF)¹⁰, which modulates the association of RNAP1 with rDNA. To assess whether Coilin affects RNAP1 occupancy of rDNA, chromatin immunoprecipitation (ChIP) with an RNAP1 also with UBF can be done on rDNA loci in the low level of Coilin (Si Coilin).

MRC5

A

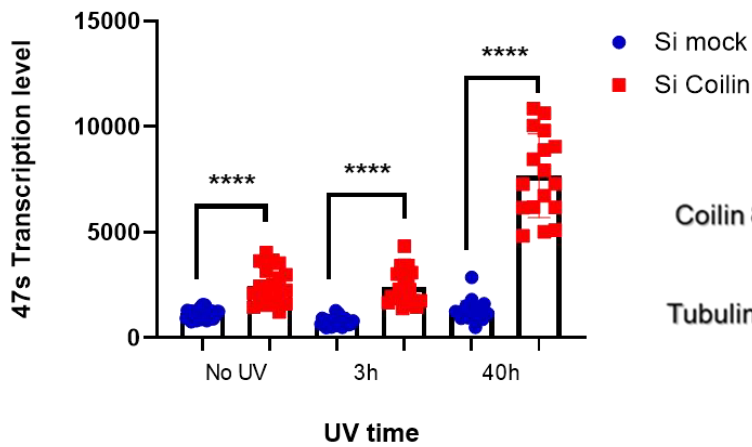


B



C

RNA FISH



D

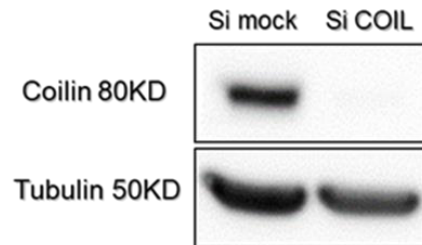


Figure 4: Coilin knockdown affects the displacement step by rescuing the RNAP1 transcription in the presence UV damage.

(A) Microscopy images of immunofluorescence assay against Coilin (red) and γ H2AX (green) in MRC5.
(B) Microscopy images of immunofluorescence assay against RNAP I (green) in MRC5 treated with either Si mock or Si Coilin. The quantity of cells indicated for the condition 3h and 40h, post UV shown (+, <50%; ++, 50–70%; +++, 70–90%; +++, >90%). Nuclei and nucleoli in **(A&B)** are indicated by dashed lines and dotted lines respectively. Scale bar represents 5 μ m. **(C)** Quantification of RNA-FISH assay showing the 47S pre-rRNA level after UV-C (16J/m²) exposure in WT MRC5 cells treated with siRNAs against indicated factors(Si mock and Si Coilin). Error bars represent the SEM obtained from the cells and the p-value of Mann Whitney test two-tailed compared to No UV SiMock and No UV Si Coilin : ****<0,0001, 3h SiMock and 3h Si Coilin : ****<0,0001, 40h SiMock and 40h Si Coilin : ****<0,0001.
(D) Western Blot on whole cell extracts of Coilin for in MRC5 either with Si mock or Si Coilin.

III. Design human siRNA libraries targeted the mechanistic of RNAP1 (displacement & repositioning) induced by UV-C for future screening project

In the field of DNA repair, one of the most intriguing and understudied aspects is how cells resume their activities once all the reactions required to eliminate DNA damage have been completed. Recently, our research team described a specific behavior of the nucleolus in response to UV damage¹⁸. During the repair reaction, rDNA transcription is blocked, and the rDNA/RNAP1 complex is displaced at the nucleolus border. When repair is completed, rDNA/RNAP1 returns within the nucleolus, and transcription restarts¹⁸.

It is conceivable to think that a complex network of proteins will govern long-distance rDNA movements within the nucleolus during DNA repair. The two phases of this nucleolar reorganization (Displacement and Repositioning) might implicate different proteins.

Previous works in the lab demonstrated that Nuclear Actin β (ACT β) and Nuclear Myosin (NMI), two motor proteins involved in different cellular processes, including chromatin organization^{19 20} and transcription of RNAP1^{21 22}, are required for the correct repositioning of rDNA/RNAP1 inside the nucleolus after the repair of the UV damage is completed (Figure 1). However, the mechanism of action for these protein have not been found for the moment. This work is still in progress²³.

Besides, as described in (chapter four, Results I), I demonstrated that SMN and FBL play a critical role in the UV- triggered nucleolar rDNA dynamics.

Finally, in a set of preliminary experiments, we observed that in cells deficient for Centrin2 (CEN-2), a calcium-binding protein that acts as a partner of the GG-NER repair factor

Xeroderma Pigmentosum Group C (XPC)²⁴, RNAP1 can be displaced at the nucleolus' periphery after DNA damage, but it cannot re-enter the nucleolus once DNA repair is complete (Figure 2).

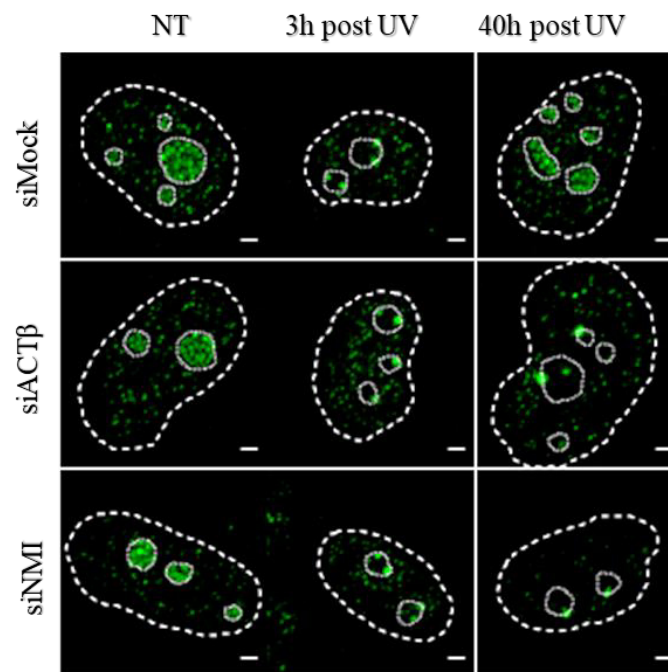


Figure 1 : ACT β & NMI role on RNAP1 repositioning after UV damage.

Confocal images of immunofluorescence staining against RNAP1 (green) performed on WT cells. Cells were transfected with small interfering RNAs (siRNA) against Nuclear Actin β (siACT β) and Nuclear Myosin (siNMI) or with a non-targeting siRNA (siMock), exposed to 16J/m² of UV-C (3h post UV) or not (NT) 24h after the second transfection, and fixed 3h or 40h later. Nuclei and nucleoli are indicated by dashed and dotted lines respectively. Scale bar: 2 μ m. Adapted from Laurianne Daniel thesis.

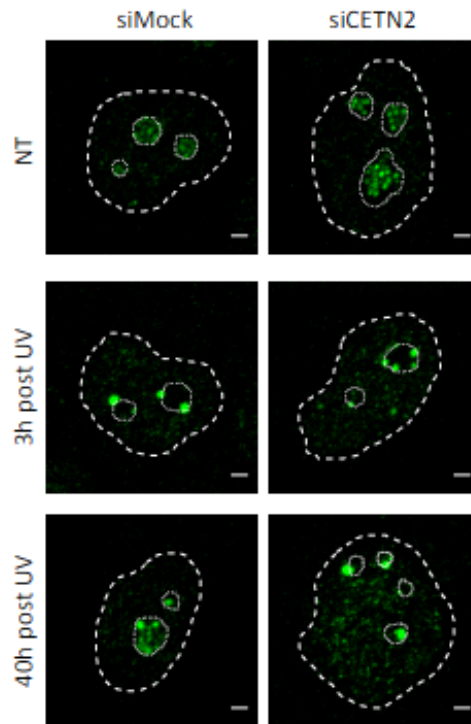


Figure 2 : Centrin2 role on RNAP1 repositioning after UV damage.

Confocal images of immunofluorescence staining against RNAP1 (green) performed on WT cells. Cells were transfected with small interfering RNAs (siRNA) against Centrin2 (siCETN2) or with a non-targeting siRNA (siMock), exposed to 16J/m² of UV-C (3h post UV) or not (NT) 24h after the second transfection, and fixed 3h or 40h later. Nuclei and nucleoli are indicated by dashed and dotted lines respectively. Scale bar: 2µm . Adapted from Laurianne Daniel thesis.

siRNA SCREENING

RNA interference (siRNA) screens are a helpful tool for studying gene function, earlier illness detection, diagnosis, and identifying prospective therapeutic targets, as well as for identifying novel signaling network components. This method is a rapid and cost-effective tool. Moreover, the recent development of new instrumentation and image analysis has made microscopy useful for high-throughput screening (HTS). The 'High-Content Screening' is accomplished using modern automated microscopy systems in which multiple colors of fluorescently stained cells are imaged simultaneously during the screening process using high throughput²⁵.

The companies can now provide human siRNA libraries ready to use targeting specific signaling pathways or a group of proteins related together by their functions (DNA Damage Response library, Epigenetics library, Protein Kinases library, Membrane Trafficking library, Tyrosine Kinases library, etc).

Therefore, we decided to create our siRNA libraries based on the interaction with our 5 identified proteins ACT β , CEN-2, FBL, NMI, and SMN. The position of RNAP1 within the nucleolus at different timepoint upon UV light exposure will be used as a read-out. Interestingly, the siRNA libraries will probably contain siRNAs against structural proteins, chromatin remodelers, kinases, transcription factors, and DNA Damage Response factors.

We extracted the information from BioGRID/ Database of Protein, Genetic, and Chemical Interactions (<https://thebiogrid.org/>). A biomedical interaction repository with data compiled through comprehensive curation efforts.

Below is a detailed description of the candidate selection process and the screening procedure.

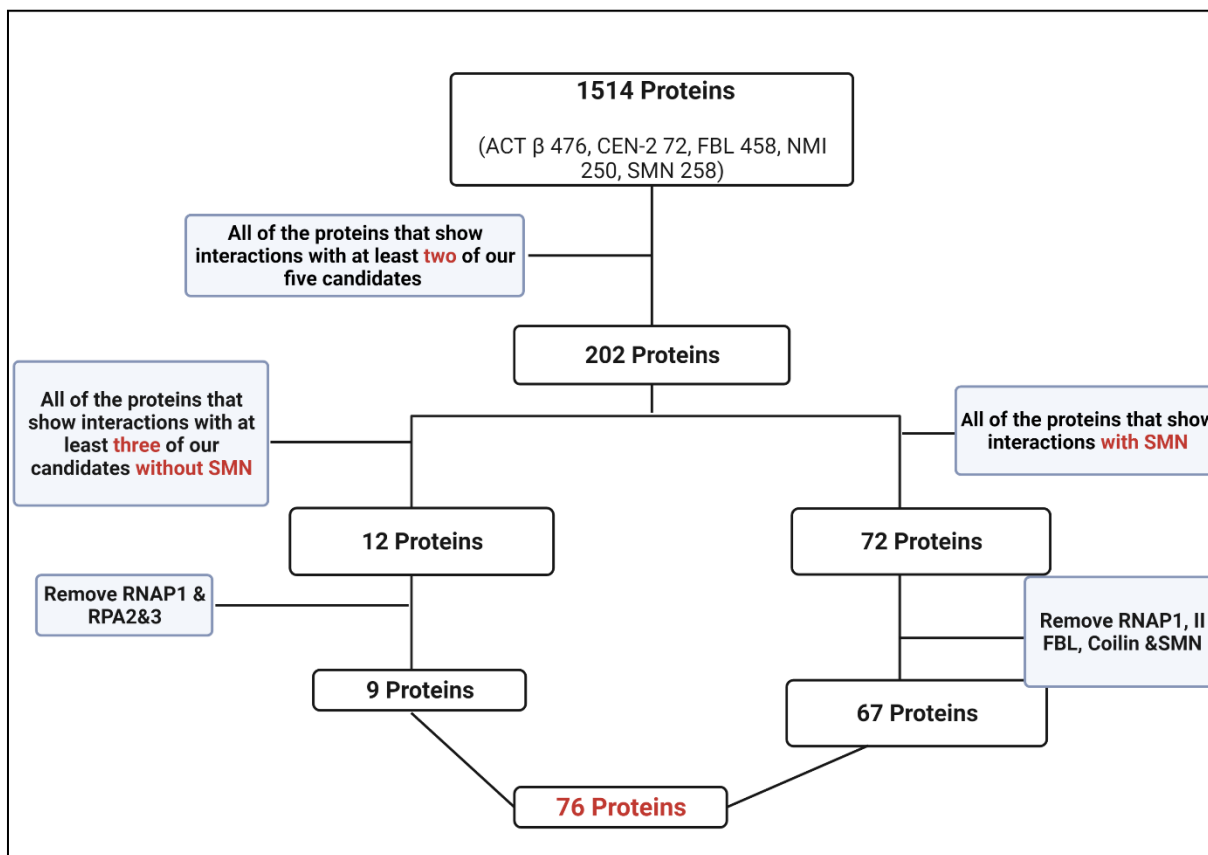


Figure 3 : Flowchart of the selection steps used to design our siRNA libraries.

A flowchart of the selection steps is shown in (Figure 3). We cross 1514 interactors together; (ACT β has 476 Proteins interactors in human demonstrated in 268 publications, CEN-2 has 72 Proteins interactors in human shown in 33 publications, FBL has 458 Proteins interactors in human established in 122 publications, NMI has 250 Protein interactors in human demonstrated in 84 publications, and SMN has 258 Proteins interactors in human shown in 93 publications).

For the first filter we decided to find all the proteins that show interactions with at least two of our five candidates. The result gives us 202 proteins. Then, two filters were done simultaneously in parallel. (i) As my work focuses on the SMN protein, we selected all the proteins that show interactions with SMN, which mean 72 proteins. Then, we excluded our

control RNAP1 and RNAP II, but also our candidates FBL and SMN. Finally, we also removed Coilin from our selection as we already demonstrated the role of this protein in RNAP1 movement as described in (chapter four, Results I).

By the end of this filter, 67 proteins were selected. These proteins show enormous diversity in their categories (Figure 4).

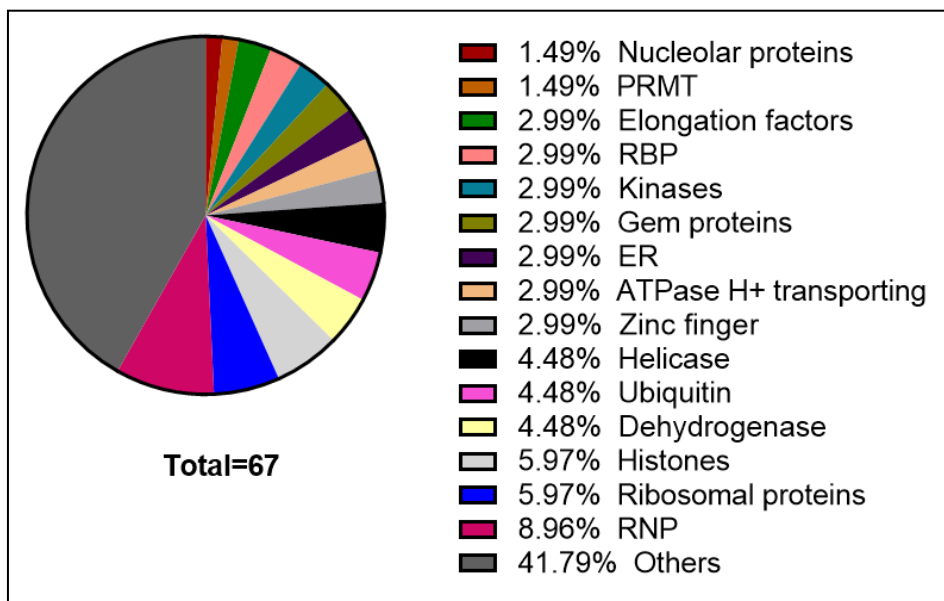


Figure 4 : pie chart shows the categories of the selected proteins that interact with SMN. PRMT; Protein Arginine Methyltransferase, RBP; RNA binding proteins, ER; estrogen receptor, RNP; ribonucleoprotein.

(ii) As a second filter, we also decided to select all the proteins that show interactions with at least three of our candidates (ACT β , CEN-2, FBL & NMI) without SMN. Interestingly we found 12 proteins all show an interaction with (ACT β , FBL & NMI). Then we excluded our read-out the RNAP1 and RPA2&3 as they were working as a complex with RPA1 and keep only the RPA1 in our selection. The 9 proteins that we have at the end of this filter are summarized with their related Gene Ontology in (Table 1).

proteins	Gene Ontology (GO) - Molecular Function
ARRB2 : Arrestin, beta 2	G protein-coupled receptor binding, signaling receptor binding, protein binding, enzyme binding, protein domain specific binding
CDK2 : Cyclin-dependent kinase 2	Nucleotide-binding, magnesium ion binding, protein kinase activity, protein serine/threonine kinase activity, cyclin-dependent protein serine/threonine kinase activity
CDKN2A : Cyclin-dependent kinase inhibitor 2A	p53 binding, DNA binding, RNA binding, cyclin-dependent protein serine/threonine kinase inhibitor activity, protein binding
EGFR : Epidermal growth factor receptor	Glycoprotein binding, chromatin binding, double-stranded DNA binding, protein kinase activity, MAP Kinase kinase activity
LMNA : Lamin A/C	Structural molecule activity, protein binding, identical protein binding
MYC : V-myc avian myelocytomatosis viral oncogene homolog	RNA polymerase II proximal promoter sequence-specific DNA binding, DNA-binding transcription factor activity, RNA polymerase II-specific, core promoter sequence-specific DNA binding, DNA-binding transcription repressor activity, RNA polymerase II-specific, DNA-binding transcription activator activity, RNA polymerase II-specific
NUPR1 : Nuclear protein, transcriptional regulator, 1	DNA binding, chromatin binding, transcription coactivator activity, protein binding, acetyltransferase activator activity
RPA : Replication Factor A Protein	Nucleic acid-binding, DNA binding, enables damaged DNA binding, enables single-stranded DNA binding, enables protein binding
STAUI : Staufen Double-Stranded RNA Binding Protein 1	Enables RNA binding, enables double-stranded RNA binding, enables protein binding, enables protein phosphatase 1 binding

Table 1 : Nine proteins with their related Gene Ontology interact with (ACT β , FBL & NMI) without SMN.

Finally, we have 76 proteins to screen with siRNA and investigate its possible implication in the displacement or repositioning steps of RNAP I in response to UV damage.

Design of the screening procedure

Some tests have already been done to find the good condition to perform the siRNA screening. The experiments will be done in 96 well plates with HeLa cells. Indeed, contrary to MRC5 cells, which need two transfections to reach a good reduction of siRNA targets, only one transfection with a double dose of siRNAs is enough for HeLa cells. Then, the transfected cells will be irradiated at $16\text{J}/\text{m}^2$ with a UV-C lamp. After immunofluorescence of RNAP1, images will be taken using automated microscopy systems. This last step still needs to be set up before starting the screening (Figure 5).

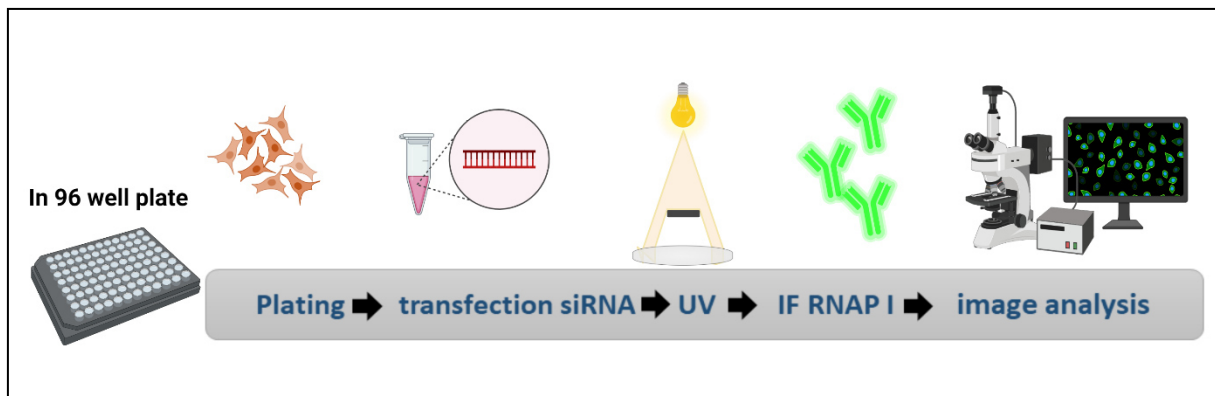


Figure 5 : The experimental design workflow.

IV. Accumulation of damage in SMN deficiency cells & R loops resolving complex (SMN&SETX) in the nucleolus together with RNAP2

Introduction

A major energy-intensive activity of cells is the biogenesis of ribosomes, particularly in cells with high metabolic rates, such as neurons and muscles²⁶. Nucleoli are dynamic nuclear membrane-free organelles in which ribosomal DNA (rDNA) transcription and ribosomal assembly take place. rDNA transcription is carried out by RNA polymerase1²⁷. In response to the high transcription rates of rDNA, R-loops may arise. It is a transient three-stranded nucleic acid structure that form physiologically during transcription when a nascent RNA transcript hybridizes with the DNA template strand, leaving a single strand of displaced nontemplate DNA. The cells have developed various mechanisms to degrade or unwind R-loops²⁸.

Survival Motor Neuron (SMN) and Senataxin (SETX) are components of an R-loop resolution pathway in transcription termination regions of RNAP2²⁹. In addition, SMN plays an important role in DNA repair. Indeed, SMN-deficient cells exhibit an increase in rDNA damage as well as reorganization of nucleoli³⁰. Low levels of SMN are shown to result in (SETX)-deficiency, increasing R-loops and DNA double-strand breaks (DSBs), which impair DNA double-strand break repair. In consequence, DNA damage accumulates in SMA cells and, more particularly, in SMA spinal cord tissues³¹. SETX is a DNA–RNA helicase encoded by the SETX gene that is important for termination by RNAP2³². Interestingly, a study in yeast has demonstrated that the Sen1 protein, the yeast homolog of human SETX, participates in the termination of transcription of the 35S pre-rRNA³³.

Of note, the nucleolus is also a stress sensor whose activity is modulated by the severity of the stress³⁴. Our research team demonstrated that, during the repair reaction of UV damage, a transcription block occurs concurrently with the displacement of the rDNA/RNAP1 complex at the nucleolus's border. After the repair is complete, rDNA/RNAP1 returns to the nucleolus, where transcription is reactivated¹². Recently we revealed a novel and essential role of SMN in this process. Indeed, SMN was detected within the nucleolus in response to UV damage, and without SMN, the return of rDNA/RNAP1 inside the nucleolus after the repair is impaired (chapter four, Results I).

Results, Discussion & Perspectives

An increase in the DNA damage markers γ H2AX has been shown in SMN depleted cells, indicating that higher levels of endogenous DNA lesions accumulate upon SMN loss function, even in the absence of additional sources of DNA damage³¹.

To investigate the SMN deficiency cell's behavior under stress, we irradiated cells with 16 J/m² of UV-C at the time points described previously (No UV, 3h post-UV-irradiation (PUVI), and 40h PUVI)³⁵. For that, we artificially decreased SMN protein levels by lentiviral transfection of 2 independent inducible shRNAs against SMN 3'UTR in the wt MRC5-SV40 fibroblast cell line. Cells with Scramble ShRNA were used as controls. We used these cell lines to perform an immunofluorescent assay at different time points before and after UV exposure (Figure 1A). We observed an increase in γ H2AX levels at 3h PUVI compared to the non-UV condition in all cell lines. However, while at 40h PUVI γ H2AX levels decreased in Sh Scramble- transfected cells at 40h PUVI, the SMN deficient cells displayed an accumulation of γ H2AX almost two-fold compared to the normal cells (Figure 1B). As described in (chapter four, Results I), at 40h PUVI, there are two co-existing populations of cells that could be detected: (i) a majority of

cells in which SMN is localized in the CB and (ii) a minority of cells in which SMN is unusually localized within the nucleolus and cannot be detected in CB anymore.

Interestingly, at 40h PUVI, WT cells that still have SMN within the nucleolus showed high γ H2AX staining compared to the cells where SMN was already back to the CB localization (Figure 1C). Altogether, these data suggested that SMN contributes to modulating the DNA damage level. However, we demonstrated in SMN results by UDS, RRS, and TCR-UDS experiments that SMN is not involved in NER repair (chapter four, Results I). Therefore, SMN could have a role in DNA damage responses (DDR) pathways.

It has been reported that the lack of SMN causes DNA double-strand breaks (DSBs) and its consequent DNA damage response (DDR) pathways activation³¹. The persistence of damage shown here in the low level of SMN by UV damage could be evaluated into DSBs. Investigating the DSB factors or bloc its signal could clarify the exact action of SMN.

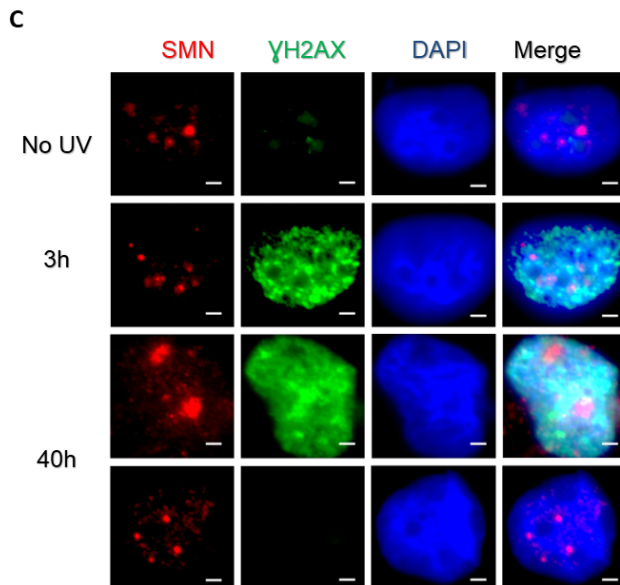
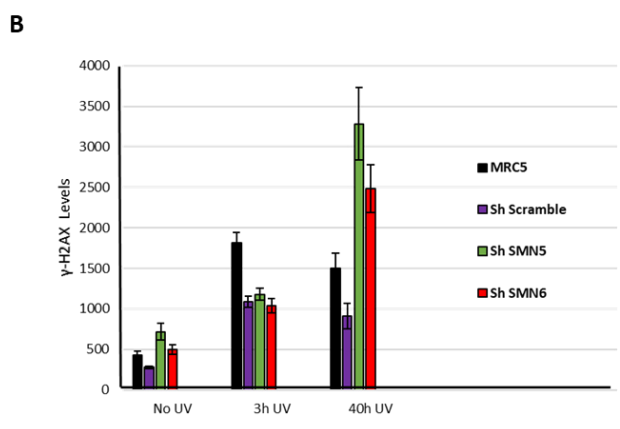
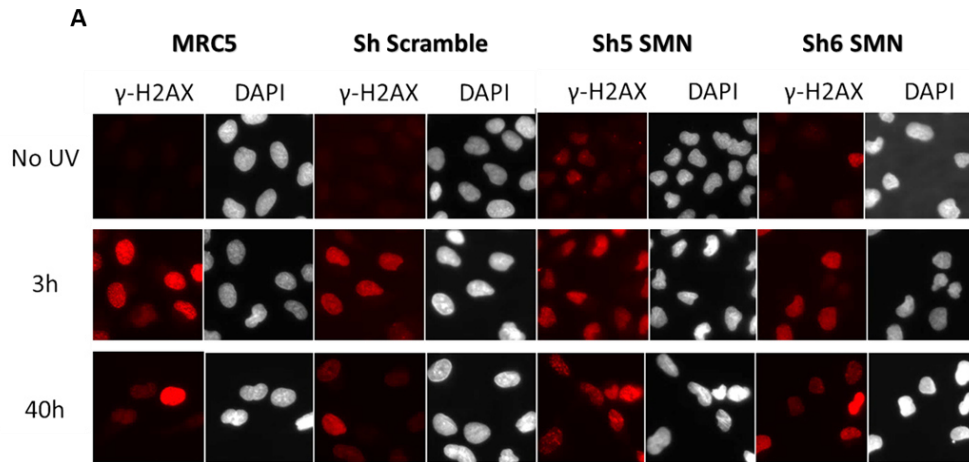


Figure 1 : UV-C DNA damage with SMN deficiency cause increase the γ H2AX.

(A) Microscopy images of immunofluorescence assay against γ H2AX (red) and DAPI (grey) in MRC5, Sh scramble, Sh5 SMN and Sh6 SMN, cells in condition (No UV, 3h and 40 PUVI). (B) Quantification of immunofluorescence assay against γ H2AX in (A), error bars represent the SEM obtained from at least 20 cells. (C) Microscopy images of immunofluorescence assay against SMN (red), γ H2AX (green) and DAPI (blue) in MRC5 cells in condition (No UV, 3h and 40 PUVI).

In addition, to increase the signal of γ H2AX in SMN-deficient cells, Kannan et al. observed downregulation of SETX and accumulation of R-loops in the absence of any source of damage³¹.

R-loops occur in highly transcribed areas, and rDNA arrays are particularly prone to R-loop accumulation³⁶. Here, we assessed R-loop levels in SMN deficient cells before and after UV light exposure (Figure 2A). We observed a higher level of R-loop signal in the nucleolus of SMN depleted cells compared to control and Sh scramble transfected MRC5 cells. Besides, in all conditions, we observed a similar increase in R-loops levels at 3h PUUVI, R-loops increase in response to UV damage at 3h PUUVI in all conditions, and the SMN deficient fibroblast displayed a stronger R-loops signal compared to their control counterparts (Figure 2A). These findings need to be quantified and confirmed.

In addition, pretreatment with Ribonuclease H (RNase H) should establish signal specificity. RNase H is known to work by destroying the RNA molecule of RNA/DNA hybrids³⁷.

These preliminary results, together (Figures 1&2), demonstrated that the SMN knockdown cells seem more sensitive to the damage; therefore, the SMA patients should avoid such sources of damage.

Furthermore, different damage sources, such as oxidative damage, must be studied to understand the SMN role in DNA repair.

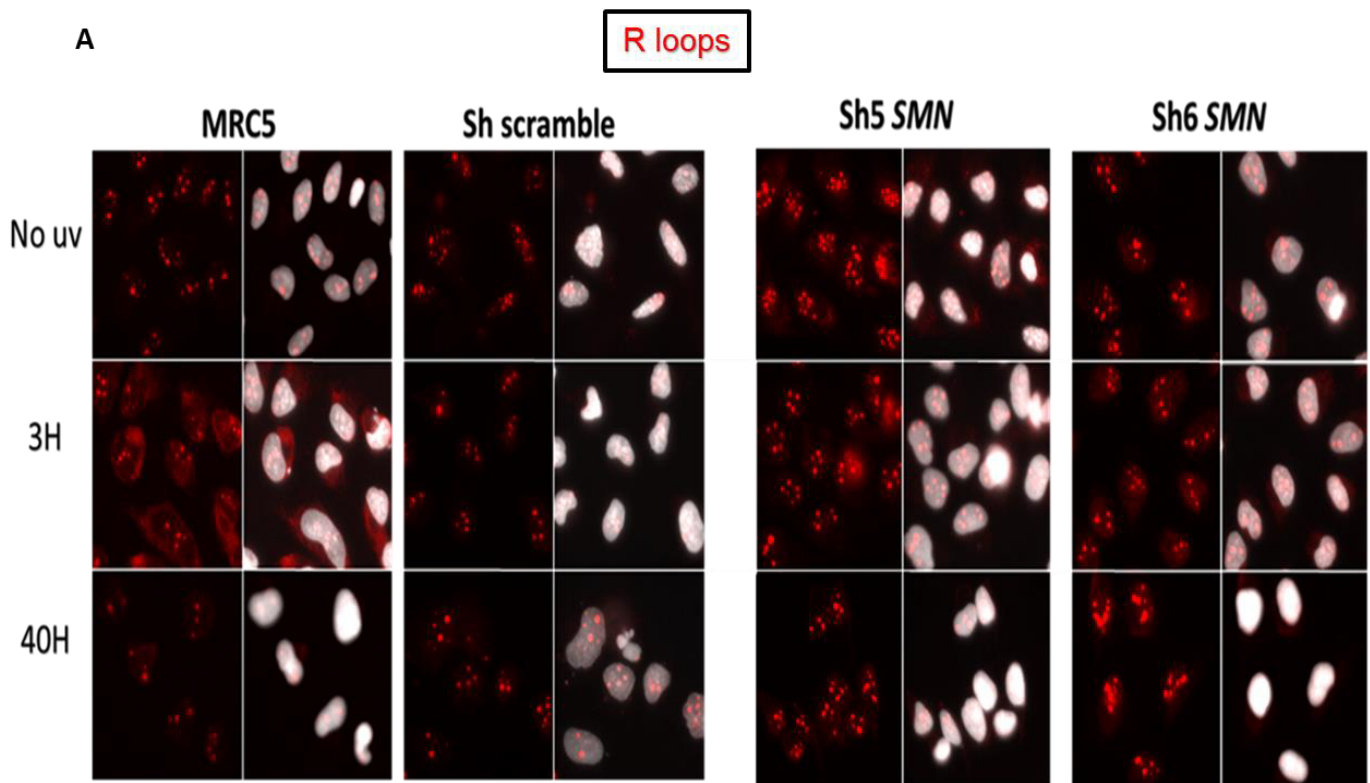


Figure 2 : UV-C DNA damage with SMN deficiency cause increase the R-loops.

(A) Microscopy images of immunofluorescence assay against R loops (red) in MRC5, Sh scramble, Sh5 SMN and Sh6 SMN, cells in condition (No UV, 3h and 40 PUVI).

To investigate the possible interaction between SMN and R-loops, we performed a proximity ligation assay (PLA) between SMN and DNA: RNA hybrids in wt cells and Sh5 SMN cells as a negative control for PLA specificity (Figure 3A). Interestingly, the proximity between CB and nucleolus could explain the interaction of SMN and R-loops in No UV condition (Figure 3A), but not at 3h PUVI. Remarkably, a significant increase of PLA signal at 40h PUVI is observed, as shown in the quantification. This time point corresponds to the time point when SMN is present inside the nucleolus (Figure 3B).

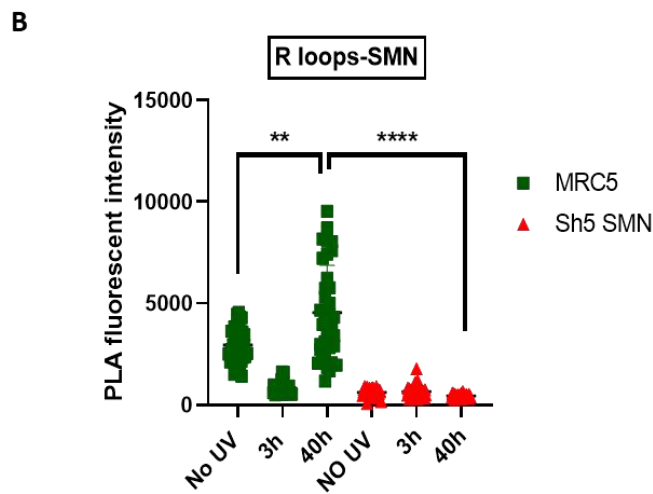
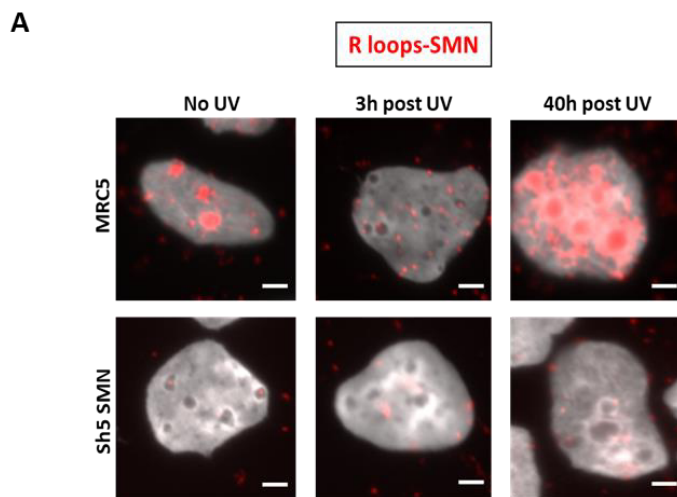


Figure 3 : SMN interacts with R-loop in the nucleolus.

(A) Microscopy images of proximity ligation assay showing the interaction between R loops and SMN in MRC5 and Sh5 SMN after UV-C irradiation. **(B)** Quantification of proximity ligation assay in (A), error bars represent the SEM obtained and the p-value of Mann Whitney test two-tailed compared to No UV MRC5 and 40h MRC5: ** 0,0038, 40h MRC5 and 40h Sh5 SMN: ****<0,0001.

By co-IP and GST pull-down SMN has been reported to interact with SETX³⁸. Moreover, in SMN deficient cells, SEXT is down-regulated. We thus investigated the interaction of SETX with SMN under our conditions of UV using the PLA (Figure 4A). The advantage of PLA is that we can detect and visualize the interaction localization inside the cells. We detected the PLA signal in the nucleus at No UV. This result was expected as SMN: SETX interaction is required to resolve R-loops at the termination site of RNAP2²⁹. Also, at 3h PUUVI, a PLA signal was observed in the nucleus. Interestingly, at 40h PUUVI, we showed PLA signals at the periphery of the nucleolus, as indicated with the white arrow in (Figure 4A). Moreover, the interaction seems to increase at 40h PUUVI (Figure 4A), which could be related to the transcription restart after UV damage and, therefore, more R-loops.

To confirm our hypotheses about the involvement of SMN and SETX in R-loops elimination formed on rDNA genes, PLA of RNAP1 and SETX performed as well. An interaction was also observed at the periphery of the nucleolus.

In conclusion, the SETX seems to be found at the periphery of the nucleolus. However, we would like to confirm these results by repeating the experiment with a negative control for PLA specificity. We also need to check whether this interaction between SETX and RNAP1 is affected by the low level of SMN.

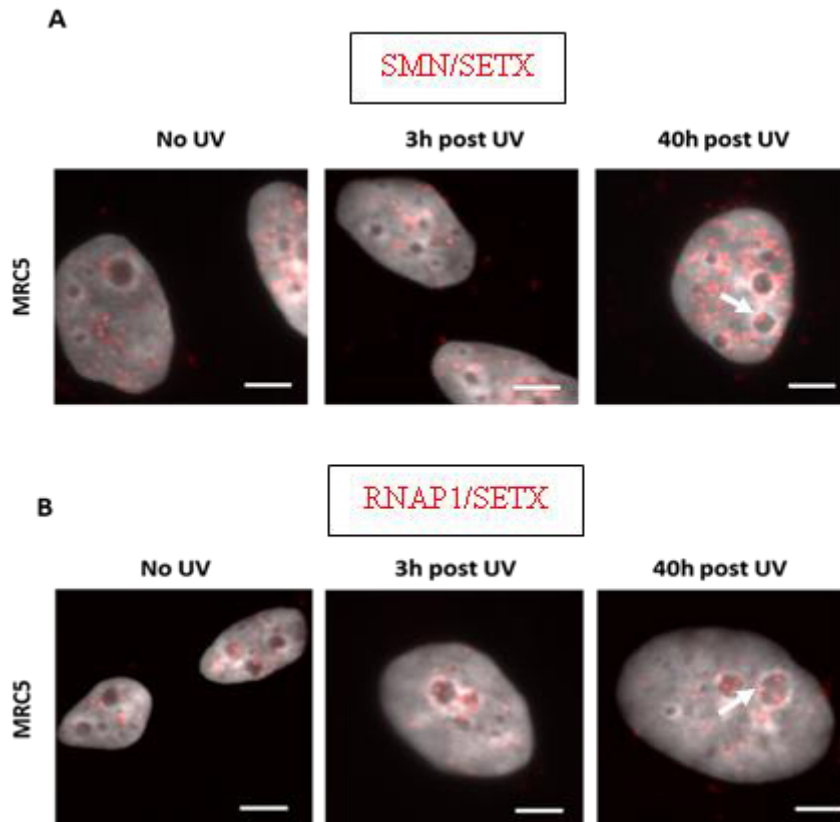


Figure 4 : SETX interacts with SMN and RNAP1.
(A&B) Microscopy images of proximity ligation assay in MRC5 after UV-C irradiation between SMN and SETX (A), between RNAP I and SETX (B) The white arrows showed the interaction at 40h PUVI at the periphery of the nucleolus.

For the last finding of this part, we questioned whether this complex was detected at 40h PUVI with RNAP2.

Indeed, repair of RNAP2 gene has never been studied at this time point. We thus performed an immunofluorescence assay against RNAP2 with SMN in wt MRC5 cells. Surprisingly, at 40h PUVI, we observed for the first time the presence of RNAP2 at the periphery of the nucleolus together with SMN (Figure 5A). Interestingly, our results indicate that SMN accumulation in the nucleolus proceeded that of RNAP2. In agreement with these observations, in Sh6 *SMN*, the

RNAP2 does not accumulate at the periphery of the nucleolus at 40h PUVI (Figure 5A), further confirming that RNAP2 accumulation requires SMN activity.

The observation of RNAP2 at 40h PUVI was also confirmed with SETX in wt MRC5 cells, where the two proteins colocalized at the periphery of the nucleolus (Figure 5B). More experiments are needed to study the interaction between these factors.

In a recent work, Abraham, et al detected foci of RNAP2 within nucleoli by immunofluorescence coupled to super-resolution microscopy. Moreover, an R-loop shield is generated by RNAP2, together with SETX, at intergenic spacers (IGS) flanking nucleolar rRNA genes. The R-loop protection prevented RNAP1 from producing sense intergenic noncoding RNAs (sincRNAs), which could disrupt the nucleolar organization and rRNA expression.³⁹ Furthermore, the RNAP2 inhibition and SETX loss result in disruptive of sincRNAs produced³⁹.

This mechanism could explain our data on the enrichment of RNAP2 around the nucleolus at 40h PUVI. RNAP2 is thus probably needed to restore sincRNAs after DNA damage.

Interestingly, an increase in sincRNA levels was related to the aberrant nucleolar morphologies commonly observed in cancer³⁹; however, there is no evidence yet about the sincRNA levels in neurodegenerative diseases such as SMA. To that end, it could be interesting to measure the sincRNA levels in the knockdown of SMN and SMA patient's cells, which could reveal a novel physiopathological pathway related to the SMA.

In conclusion, only RNAP1, in agreement with the current paradigms, exists within the nucleolus. This could change under stress conditions; according to our preliminary results, the RNAP 2 was detected at the nucleolus's periphery in response to UV damage.

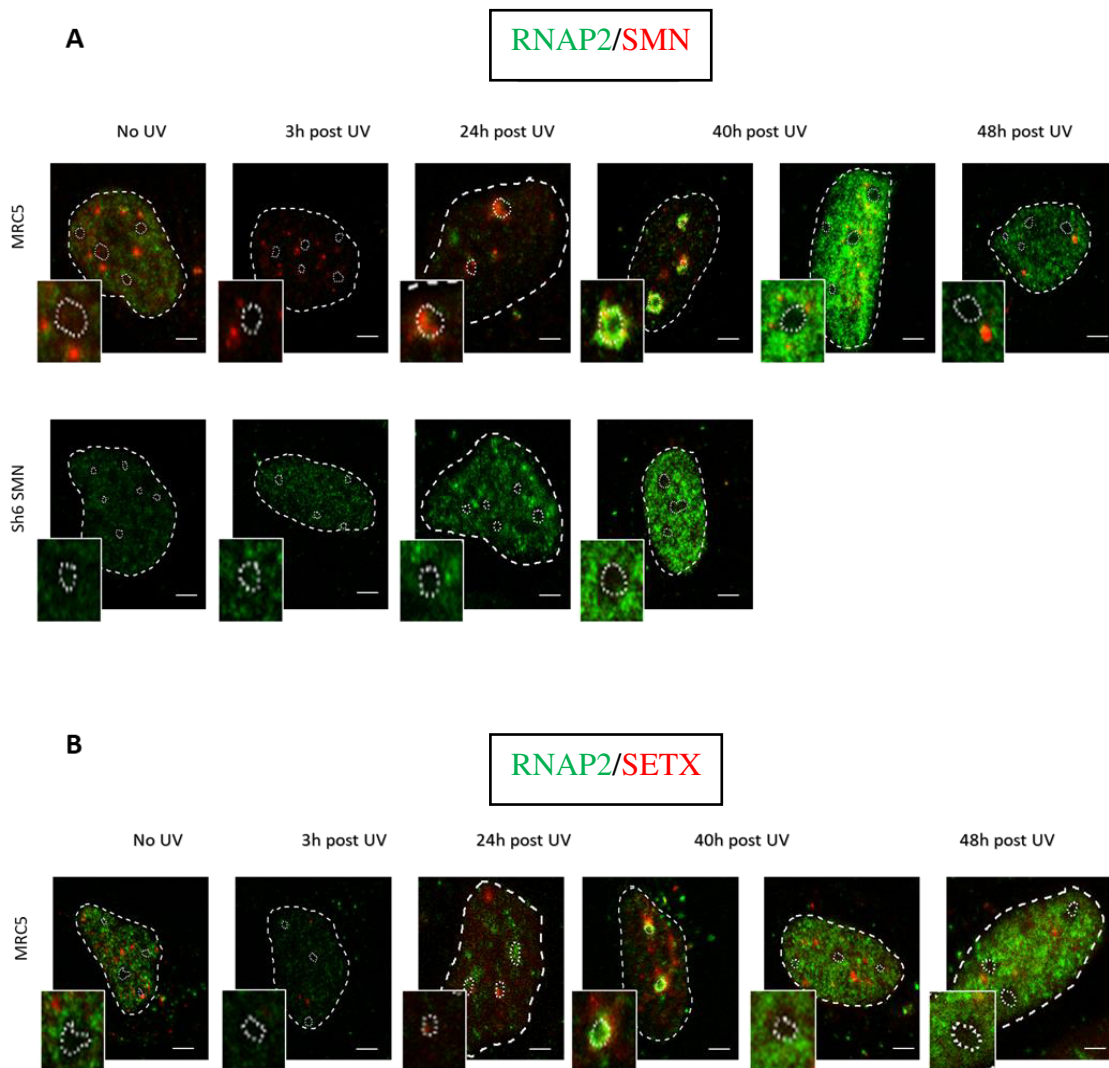


Figure 5 : RNAP2 in the nucleolus after UV damage with SMN and SETX.

(A&B) Microscopy images of immunofluorescence assay against RNAP2 (green) in **(A)** with SMN (red) in MRC5 cells in conditions (No UV, 3h, 24h, 40h and 48h) and in Sh6 SMN (No UV, 3h, 24h and 40h). **(B)** with SETX (red) in MRC5 cells in conditions (No UV, 3h, 24h, 40h and 48h).

V. SMN and Cockayne syndrome

Introduction

UV irradiations induce DNA helix distorting lesions and DNA photoproducts, damages repaired by nucleotide excision repair (NER) pathway. In the sub-pathway of transcription-coupled repair (TC-NER), CSA and CSB play key roles in removing lesions DNA that block the progress of transcription machinery⁴⁰. Cockayne Syndrome (CS) is a rare, autosomal recessive neurodegenerative disorder, which is associated primarily with mutations in the genes ERCC8/CSA and ERCC6/CSB. In general, CSA patients present with less severe phenotypes than CSB patients. CS's complex pathological clinical presentation is likely due to the multiple functions of CS proteins, which have not yet been completely clarified⁴¹.

Results, Discussion & Perspectives

UV-C-induced lesions are repaired by the NER system. This process begins with the identification of the DNA lesion by one of its two sub pathways: in the global genomic repair (GGR), the lesion is recognized by the XPC protein, while in the transcription-coupled repair (TCR), the lesion is identified by the CSA and CSB proteins⁴⁰.

In TC-NER and GG-NER deficient cells (mutant for CSA/ and CSB or for XPC, respectively), the RNAP1/ rDNA complexes are displaced at the nucleolar periphery at 3 h PUVI as in WT cells., but they fail to return into the nucleolus at 40h PUVI, likely because the failure of the repair process, impacting the normal restart of rDNA transcription. However, the transcription of RNAP1 resumed over time in XPC cells, whereas in TC-NER-deficient cells CSA and CSB, no resumption of RNAP1 activity has been observed³⁵.

To address whether SMN shuttling within the nucleolus in response to UV damage is transcription-dependent, we performed immunofluorescence experiments to investigate the localization of SMN in WT MRC5 vs CSA, CSB, or XPC deficient cells.

While in WT cells, SMN shuttling was highlighted by the identification of two cells population differing in their SMN localization at 40h PUVI (a population was displaying SMN within the nucleolus and RNAP1 at the periphery vs a population in which SMN localized back to Cajal bodies and RNAP1 inside the nucleolus) (Figure 1A). Instead, both in CSA and XPC deficient cells, SMN was mostly found within the nucleolus, with RNAP1 distributed at the periphery, indicating that SMN shuttling is not directly related to the rDNA transcription but is associated with the position of RNAP1 (Figure 1A).

However, in CSB deficient cells, SMN levels were strongly decreased (Figure 1A). As I found no studies in the literature about the relation between SMN and CSB, I decided to explore these strange results in more detail.

By performing PLA of SMN and CSB, we observed a strong interaction within the nucleolus at 40h PUVI in WT cells where it was not detected in the CSB deficient cells confirming the specificity of the PLA signal (Figure 1B).

Moreover, we observed by immunofluorescence CSB did not alter in the absence of SMN (Figure 1C). Thus, it seems that CSB controls the level of SMN and not the opposite.

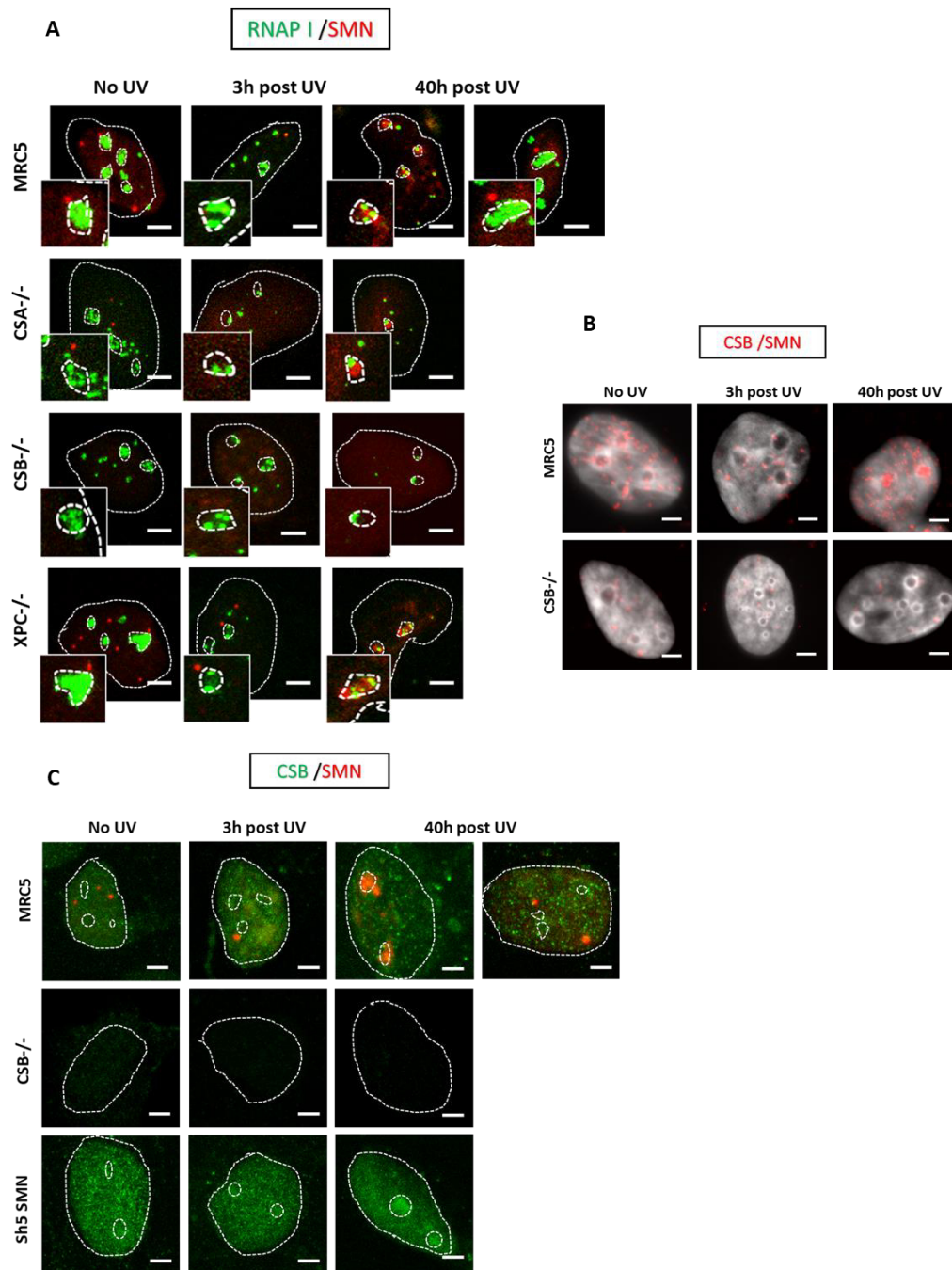


Figure 1 : CSB controls the SMN expression.

(A) Microscopy images of immunofluorescence assay against RNAP1 (green) and SMN (red) in CSA, CSB and XPC deficiency cells (No UV, 3h and 40h). **(B)** Microscopy images of proximity ligation assay show the interaction between CSB and SMN in MRC5 and CSB deficiency cells (No UV, 3h and 40h). **(C)** Microscopy images of immunofluorescence assay against CSB (green) and SMN (red) in MRC5, CSB deficiency cells and Sh5 SMN (No UV, 3h and 40h), Nuclei and nucleoli in **(A&C)** are indicated by dashed lines and dotted lines respectively.

The previous immunofluorescent results of SMN (Figure 1A) were obtained with cytostripping method in which we removed the cytoplasm to have a clearest view of the nuclear SMN. Thus, we repeated the experiment, immunofluorescence against SMN and RNAP1 in WT and CSB deficient cells, with or without cytostripping to test whether CSB affected the total level of SMN or only the nuclear level. SMN level in CSB deficient cells was very low with cytostripping compared to WT cells. Without cytostripping, the cytoplasmic SMN in CSB deficient cells was also lower than in WT cells but still detected (Figure 2A). In conclusion, CSB seems to affect the total level of SMN. However, these results need to be confirmed. Therefore, we planned to perform western blots (WB) with whole, cytoplasmic, and nuclear extract of WT and CSB deficient cells after UV-C irradiation.

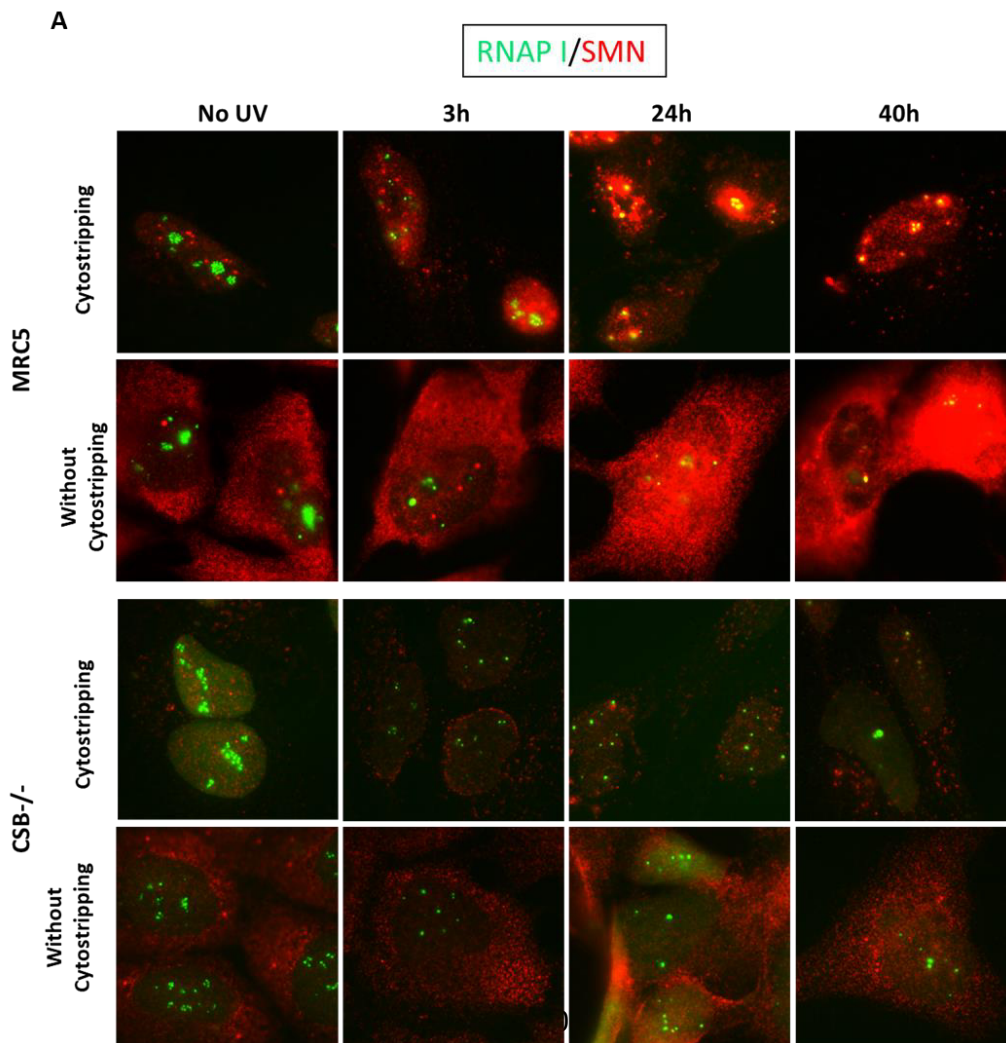


Figure 2 : Loss of the nuclear and cytoplasmic SMN in CSB cells.

(A) Microscopy images of immunofluorescence assay against RNAP1 (green) and SMN (red) in MRC5 and CSB deficiency cells (No UV, 3h, 24h and 40h) with or without cytostripping method to remove the cytoplasm.

In parallel of WB experiment, we decided to quantify the signal of SMN obtained by immunofluorescence in CSB deficient cells mixed with CSB deficient cells stably expressing CSB-GFP. To confirm that SMN difference was only observed in CSB deficient cells, the experiment was performed in parallel on CSA deficient cells mixed with CSA deficient cells stably expressing GFP and in the wt MRC5 cells.

Without cytostripping there was no observed difference of SMN staining in CSA deficient cells with or without CSA-GFP. However, in CSB deficient cells, we observed a difference of SMN in the nuclear level, but not the cytoplasmic level, between the cells with GFP and cells without GFP (Figure 3A). By removing the cytoplasmic SMN, the difference of SMN nuclear level between cells proficient (in green) or deficient (white arrow) for CSB became more apparent (Figure 3B). However, this experiment should be reproduced to approve these findings.

Our findings could provide an explanation for why CSB patients have severe symptoms compared to CSA patients, CSB patient combines two diseases at the same time. However, before we jump to this curious conclusion, three hypotheses must be tested to explain why in CSB-deficient cells we have a reduction of SMN proteins.

1. **Less expression of SMN gene.** We will investigate this hypothesis by quantifying by qPCR the expression of SMN in wt and CSB cells. The SMN primers was already ordered.

2. **Less stability of SMN protein.** It was reported that SMN is degraded by the proteasome, and the turnover of SMN is reduced by complex formation^{42 43}. We will examine this possibility by treating the CSB cells with MG-132, a proteasome inhibitor, and checking the SMN level.
3. **Less nuclear transport.** The phosphorylation of the SMN complex regulates its localization. SMN complex is dephosphorylated by nuclear phosphatase PPM1G/PP2C γ .

SMN and Gemin3 are altered in their phosphorylation patterns when PPM1G is lost and CB disappears; thus, no nuclear SMN is detected. Upon overexpression of PPM1G, nuclear SMN within CB accumulation is restored⁴⁴.

Moreover, PP1 γ , a protein phosphatase, has been shown to interact with the SMN complex. Depletion of PP1 γ enhances the localization of the SMN complex to CB⁴⁵.

Therefore, the SMN phosphorylation mediators could explain the CSB influence on the SMN level.

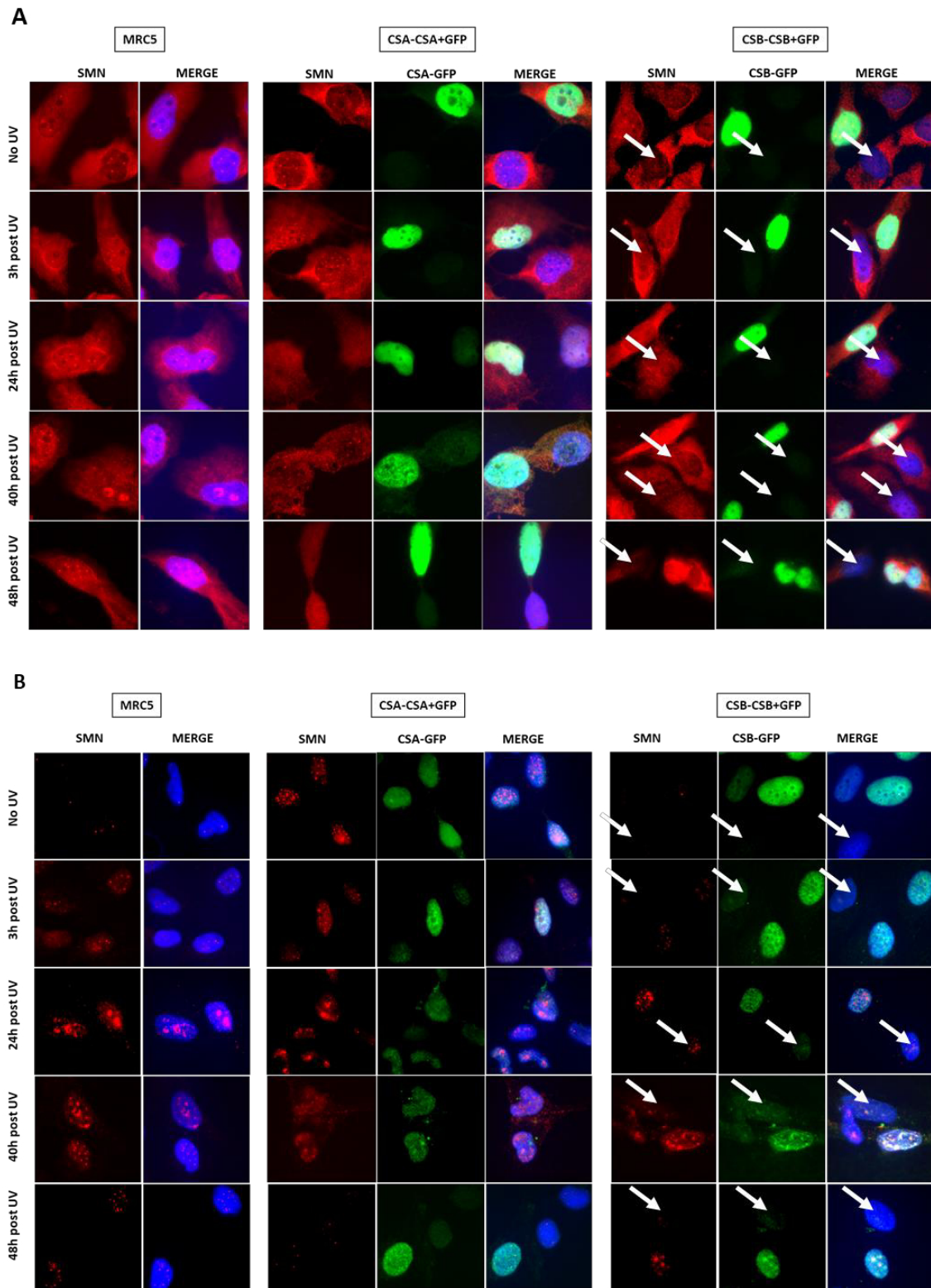


Figure 3 : Quantitative Immunofluorescence of SMN in CSA and CSB cells

(A&B) Microscopy images against GFP (green) and SMN (red) and DAPI (blue) in MRC5, CSA deficiency cells + CSA-GFP and CSB deficiency cells + CSB-GFP (No UV, 3h, 24h, 40h and 48h) **(A)** without cytostripping **(B)** cytostripping. The arrows in CSB deficiency cells + CSB-GFP show the cells without CSB= No GFP.

VI. SMN and motor neurons

Discussion & Perspectives

To gain insight into the mechanisms underlying the neurodegenerative phenotype of SMA patients, we further investigated the role of SMN in DNA repair.

In collaboration with the team of Motor neuron diseases from I-Stem Institute, as a first step, they provide us with the motor neuron wt cells as a progenitor of motor neurons at J11. We cultured them in our laboratory to obtain the general motor neurons at J14 as indicated in the red box (Figure 1A). The quality control was validated with antibody OLIG2 for stage J11 with ISL1 for stage J14 (Figure 1A). Then I decided to do an immunofluorescence assay against RNAP1 and SMN on the motor neurons at J14 after UV-C irradiation at the following time: No UV; 3h, 24h, and 48h PUVI.

A high rate of cell death was observed after UV irradiation and almost no more vital cells 48h PUVI, which is expected for post-mitotic neurons cells (Figure 1B).

The localization of RNAP1 was difficult to conclude whether it was within or at the periphery of the nucleolus except for 3h PUVI where RNAP1 was found at the periphery of the nucleolus (Figure 1C). For SMN labeling, we usually remove the cytoplasm before fixation to improve the signal inside the nucleus. As the numbers of cells were very low after being cultured and we do not know the effect of cytoplasm removal on cells that need coating treatment for adhesion, we decided to continue without doing the cytostripping step for the first experiment. Unfortunately, the SMN was strongly found everywhere in motor neurons (Figure 1C). Thus, the experiment must be repeated with the cytostripping, to gain a clear view of SMN in the nucleus.

One of the unsolved mysteries of SMA is why motor neurons are selectively degenerated and vulnerable to cell death. Recently, a reduction in rRNA levels was observed only in SMA motor neurons but did not detect any significant differences in rRNA levels between control and SMA cells when analyzing embryonic cortical neurons⁴⁶. Thus, it would be interesting to study the behavior of RNAP1 in these cells. This line of our project could participate directly in the explanation of the mechanism of neurodegeneration in SMA patients.

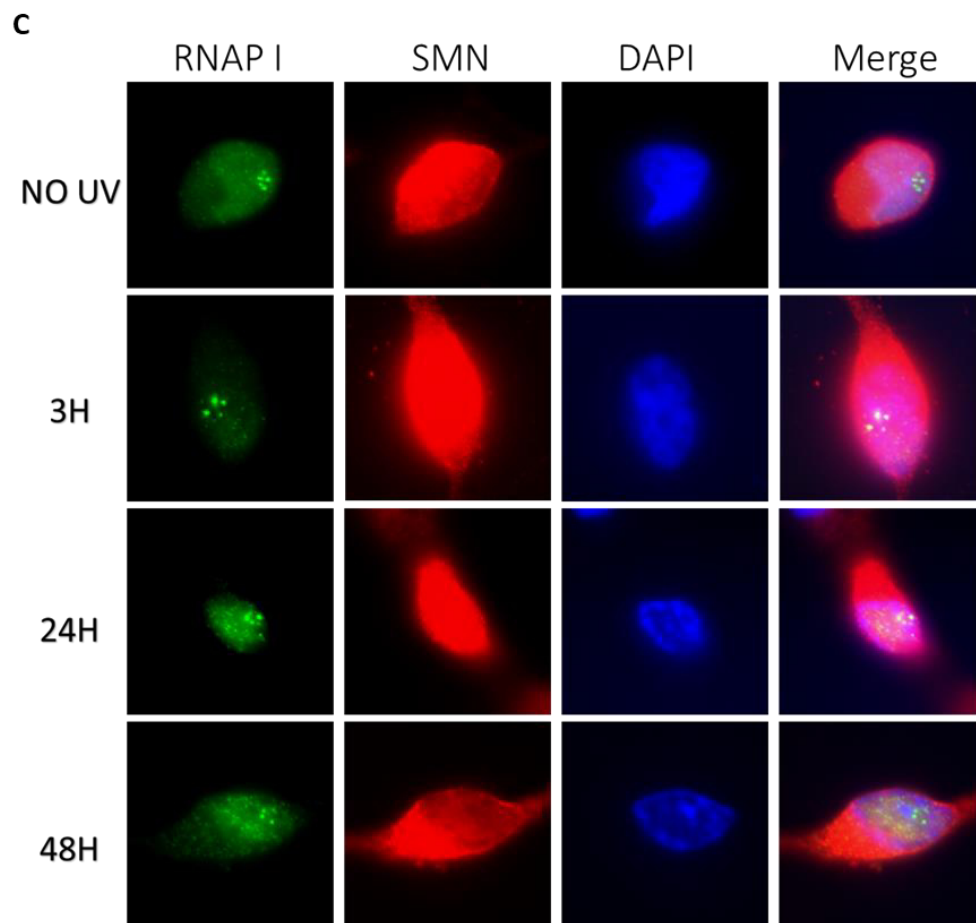
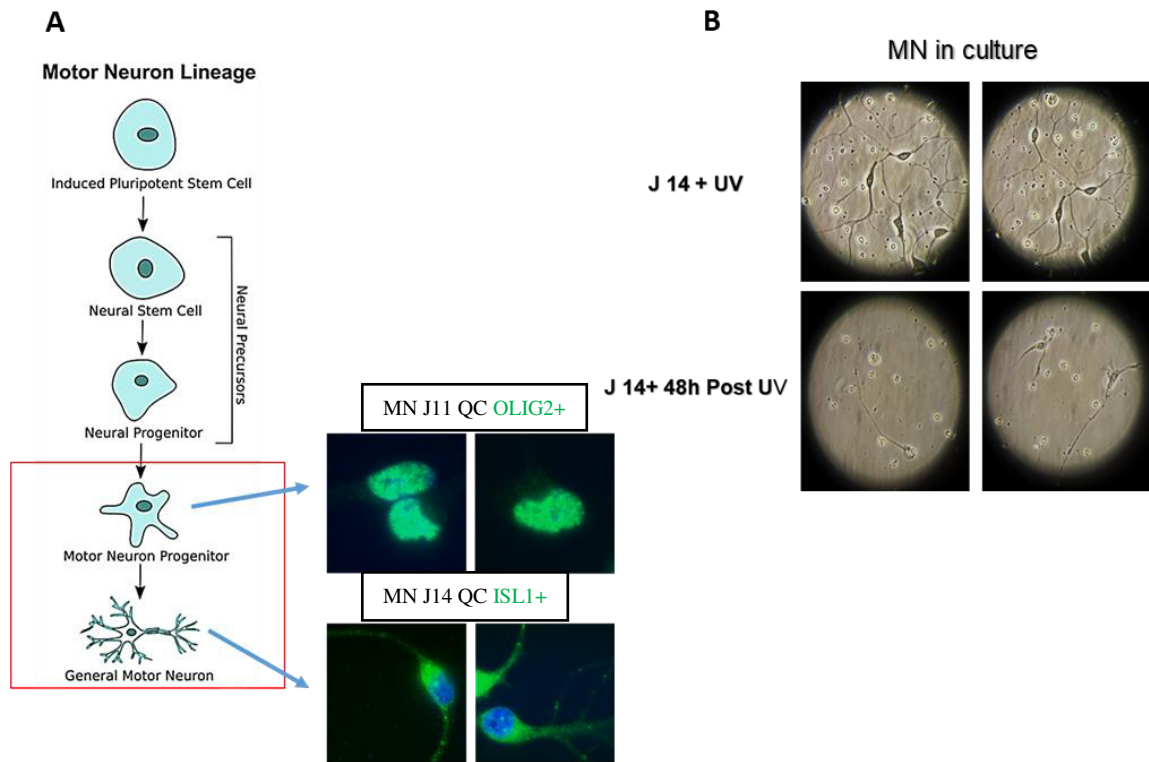


Figure 1 : SMN & RNAP1 in Motor Neuron

(A) Motor neurons (MN) lineage. The red box indicated the stage of cells we have: the progenitor of motor neurons at J11 is validated by the quality control (QC) of OLIG2, and the general motor neurons at J14 is validated by the (QC) of ISL1. **(B)** Motor neurons in culture at J14 after UV irradiation and 48h post UV. **(C)** Microscopy images of immunofluorescence assay against RNAP1 (green) SMN (red) and DAPI (blue) in MN cells after UV-C irradiation (No UV, 3h, 24h and 48h).

Reference

1. Morris, G. E. The Cajal body. *Biochim. Biophys. Acta BBA - Mol. Cell Res.* **1783**, 2108–2115 (2008).
2. Machyna, M., Neugebauer, K. M. & Staněk, D. Coilin: The first 25 years. *RNA Biol.* **12**, 590–596 (2015).
3. Brown, J. W. S. Arabidopsis nucleolar protein database (AtNoPDB). *Nucleic Acids Res.* **33**, D633–D636 (2004).
4. Raška, I. *et al.* Immunological and ultrastructural studies of the nuclear coiled body with autoimmune antibodies. *Exp. Cell Res.* **195**, 27–37 (1991).
5. Hebert, M. D., Szymczyk, P. W., Shpargel, K. B. & Matera, A. G. Coilin forms the bridge between Cajal bodies and SMN, the Spinal Muscular Atrophy protein. *Genes Dev.* **15**, 2720–2729 (2001).
6. Broome, H. J. & Hebert, M. D. In Vitro RNase and Nucleic Acid Binding Activities Implicate Coilin in U snRNA Processing. *PLoS ONE* **7**, e36300 (2012).
7. Cioce, M., Boulon, S., Matera, A. G. & Lamond, A. I. UV-induced fragmentation of Cajal bodies. *J. Cell Biol.* **175**, 401–413 (2006).
8. Shav-Tal, Y. *et al.* Dynamic Sorting of Nuclear Components into Distinct Nucleolar Caps during Transcriptional Inhibition. *Mol. Biol. Cell* **16**, 2395–2413 (2005).
9. Bártoová, E. *et al.* Coilin is rapidly recruited to UVA-induced DNA lesions and γ -radiation affects localized movement of Cajal bodies. *Nucleus* **5**, 269–277 (2014).
10. Gilder, A. S. *et al.* Coilin participates in the suppression of RNA polymerase I in response to cisplatin-induced DNA damage. *Mol. Biol. Cell* **22**, 1070–1079 (2011).
11. Trinkle-Mulcahy, L. & Sleeman, J. E. The Cajal body and the nucleolus: “In a relationship” or “It’s complicated”? *RNA Biol.* **14**, 739–751 (2017).
12. Daniel, L. *et al.* Mechanistic insights in transcription-coupled nucleotide excision repair of ribosomal DNA. *Proc. Natl. Acad. Sci.* **115**, (2018).
13. Tapia, O. *et al.* Reorganization of Cajal bodies and nucleolar targeting of coilin in motor neurons of type I spinal muscular atrophy. *Histochem. Cell Biol.* **137**, 657–667 (2012).
14. Hebert, M. D. & Poole, A. R. Towards an understanding of regulating Cajal body activity by protein modification. *RNA Biol.* **14**, 761–778 (2017).
15. Gubitz, A. The SMN complex. *Exp. Cell Res.* **296**, 51–56 (2004).
16. Isaac, C., Yang, Y. & Thomas Meier, U. Nopp140 Functions as a Molecular Link Between the Nucleolus and the Coiled Bodies. *J. Cell Biol.* **142**, 319–329 (1998).

17. Chen, H.-K., Pai, C.-Y., Huang, J.-Y. & Yeh, N.-H. Human Nopp140, Which Interacts with RNA Polymerase I: Implications for rRNA Gene Transcription and Nucleolar Structural Organization. *Mol. Cell. Biol.* **19**, 8536–8546 (1999).
18. Daniel, L. *et al.* Mechanistic insights in transcription-coupled nucleotide excision repair of ribosomal DNA. *Proc. Natl. Acad. Sci.* **115**, (2018).
19. Chuang, C.-H. *et al.* Long-Range Directional Movement of an Interphase Chromosome Site. *Curr. Biol.* **16**, 825–831 (2006).
20. Dundr, M. *et al.* Actin-dependent intranuclear repositioning of an active gene locus in vivo. *J. Cell Biol.* **179**, 1095–1103 (2007).
21. Philimonenko, V. V. *et al.* Nuclear actin and myosin I are required for RNA polymerase I transcription. *Nat. Cell Biol.* **6**, 1165–1172 (2004).
22. Sarshad, A. *et al.* Nuclear Myosin 1c Facilitates the Chromatin Modifications Required to Activate rRNA Gene Transcription and Cell Cycle Progression. *PLoS Genet.* **9**, e1003397 (2013).
23. β -Actin and Nuclear Myosin I are responsible for nucleolar reorganization.pdf.
24. Araki, M. *et al.* Centrosome Protein Centrin 2/Caltractin 1 Is Part of the Xeroderma Pigmentosum Group C Complex That Initiates Global Genome Nucleotide Excision Repair. *J. Biol. Chem.* **276**, 18665–18672 (2001).
25. Krausz, E. High-content siRNA screening. *Mol. Biosyst.* **3**, 232 (2007).
26. Grummt, I. Life on a planet of its own: regulation of RNA polymerase I transcription in the nucleolus. *Genes Dev.* **17**, 1691–1702 (2003).
27. Thiry, M. & Lafontaine, D. L. J. Birth of a nucleolus: the evolution of nucleolar compartments. *Trends Cell Biol.* **15**, 194–199 (2005).
28. Crossley, M. P., Bocek, M. & Cimprich, K. A. R-Loops as Cellular Regulators and Genomic Threats. *Mol. Cell* **73**, 398–411 (2019).
29. Yanling Zhao, D. *et al.* SMN and symmetric arginine dimethylation of RNA polymerase II C-terminal domain control termination. *Nature* **529**, 48–53 (2016).
30. Karyka, E. *et al.* SMN-deficient cells exhibit increased ribosomal DNA damage. *Life Sci. Alliance* **5**, e202101145 (2022).
31. Kannan, A., Bhatia, K., Branzei, D. & Gangwani, L. Combined deficiency of Senataxin and DNA-PKcs causes DNA damage accumulation and neurodegeneration in spinal muscular atrophy. *Nucleic Acids Res.* **46**, 8326–8346 (2018).

32. Skourti-Stathaki, K., Proudfoot, N. J. & Gromak, N. Human Senataxin Resolves RNA/DNA Hybrids Formed at Transcriptional Pause Sites to Promote Xrn2-Dependent Termination. *Mol. Cell* **42**, 794–805 (2011).
33. Kawauchi, J., Mischo, H., Braglia, P., Rondon, A. & Proudfoot, N. J. Budding yeast RNA polymerases I and II employ parallel mechanisms of transcriptional termination. *Genes Dev.* **22**, 1082–1092 (2008).
34. Boulon, S., Westman, B. J., Hutten, S., Boisvert, F.-M. & Lamond, A. I. The Nucleolus under Stress. *Mol. Cell* **40**, 216–227 (2010).
35. Daniel, L. *et al.* Mechanistic insights in transcription-coupled nucleotide excision repair of ribosomal DNA. *Proc. Natl. Acad. Sci.* **115**, (2018).
36. El Hage, A., French, S. L., Beyer, A. L. & Tollervey, D. Loss of Topoisomerase I leads to R-loop-mediated transcriptional blocks during ribosomal RNA synthesis. *Genes Dev.* **24**, 1546–1558 (2010).
37. Hausen, P. & Stein, H. Ribonuclease H. An Enzyme Degrading the RNA Moiety of DNA-RNA Hybrids. *Eur. J. Biochem.* **14**, 278–283 (1970).
38. Suraweera, A. *et al.* Functional role for senataxin, defective in ataxia oculomotor apraxia type 2, in transcriptional regulation. *Hum. Mol. Genet.* **18**, 3384–3396 (2009).
39. Abraham, K. J. *et al.* Nucleolar RNA polymerase II drives ribosome biogenesis. *Nature* **585**, 298–302 (2020).
40. Spivak, G. Nucleotide excision repair in humans. *DNA Repair* **36**, 13–18 (2015).
41. Karikkineth, A. C., Scheibye-Knudsen, M., Fivenson, E., Croteau, D. L. & Bohr, V. A. Cockayne syndrome: Clinical features, model systems and pathways. *Ageing Res. Rev.* **33**, 3–17 (2017).
42. Chang, H.-C., Hung, W.-C., Chuang, Y.-J. & Jong, Y.-J. Degradation of survival motor neuron (SMN) protein is mediated via the ubiquitin/proteasome pathway. *Neurochem. Int.* **45**, 1107–1112 (2004).
43. Burnett, B. G. *et al.* Regulation of SMN Protein Stability. *Mol. Cell. Biol.* **29**, 1107–1115 (2009).
44. Petri, S., Grimmler, M., Over, S., Fischer, U. & Gruss, O. J. Dephosphorylation of survival motor neurons (SMN) by PPM1G/PP2C γ governs Cajal body localization and stability of the SMN complex. *J. Cell Biol.* **179**, 451–465 (2007).
45. A role for protein phosphatase PP1 γ in SMN complex formation and subnuclear localization to Cajal bodies 2012.pdf.

46. Karyka, E. *et al.* SMN-deficient cells exhibit increased ribosomal DNA damage. *Life Sci. Alliance* **5**, e202101145 (2022).

Chapter five

Concluding remarks and future perspectives

My thesis will contribute to understanding the reorganization of the nucleolar structure during DNA damage induction and after the completion of DNA repair reactions and fill a part of the huge blank we still have. The main results were discovering SMN and Coilin as the key players intervening in this process and how they synergistically affect the reorganization of the nucleolus (manuscript in preparation).

SMN and Coilin are involved in the restoration of the nucleolar structure. In the absence of these two proteins, RNAP1 and FBL remain at the periphery of the nucleolus, where RNAP1 transcription will nonetheless resume. Implies that both SMN and coilin are necessary to reestablish nucleolar structure after DNA repair. Surprisingly, SMN was moving around or inside the nucleolus at 24h after the damage induction. Different stages of SMN shuttling involve Coilin and FBL. PRMT1 is required to recruit SMN to the periphery of and within the nucleolus. PRMT1 shuttles within the nucleolus concurrently with SMN; this shuttling is SMN-dependant.

There are also a lot of open questions that need to be addressed:

The exact role of the SMN in repositioning the nucleolar proteins within the nucleolus and the impact of a defect in re-establishing a proper nucleolar structure in SMA patients' cells after repair completion are still unclear. In addition, the outcome of canonical RNAP1 transcription position (at the periphery of the nucleolus) is unrecognized. All of these might lead to an improper maturation of ribosomal RNAs with consequences for ribosome biogenesis and, consequently for, protein translation. Notably, the nucleolus's periphery is a region with a high content of heterochromatin, while the inner parts of the nucleolus are rich in euchromatin. It is important to verify whether RNAP1 transcription at the periphery of the nucleolus is as efficient as within the nucleolus and whether this positioning influences the proper rRNAs

maturation. Conversely, it is also very interesting to verify whether the presence of an active transcriptional unit within a heterochromatin region affects the heterochromatin at the nucleolar periphery. Therefore, we need to determine the biological consequences of a perturbed nucleolar organization on ribosome biogenesis). We could address this question at different levels using the following ways. Determine the amount of the pre-matured rRNAs 47S by RNA Fish which is already shown in my results. Determine the proper binding of RNAP1 and UBF on rDNAs by ChIP-qPCR. Measure the excess of R-loops on rDNA, known to hinder transcription, using DNA-RNA immunoprecipitation (DRIP). Examine the rRNA maturation profile of rRNAs by Northern Blot assays. Determine the polysome profile.

In view of this new SMN function, it can be anticipated that in cells and motor neurons of SMA patients. According to our hypotheses, daily exogenous and endogenous DNA damage might progressively disrupt the nucleolar structure and disturb ribosome biogenesis, leading to perturbed protein translation. This defect may contribute to the neurodegenerative phenotype of SMA motor neurons. Therefore, a direct impact on the lives and well-being of SMA patients is expected, who may be advised to prevent deleterious DNA damage to avoid a reorganization of the nucleolus. Furthermore, following a diet high in antioxidants may help reduce its burden and delay the neurodegeneration of motor neurons, thereby slowing the progression of SMA.

The number and size of nucleoli in a cell strictly depend on the metabolic activity and size of the cell. Neurons are highly metabolic cells and present a unique prominent and large nucleolus. On the other hand, the Spinal motor neurons are affected in SMA patients. Therefore, they are the most appropriate cell type to investigate the consequences of SMN and DNA damage-related defects in nucleolar reorganization.

We are the first to report an unexpectedly dynamic shuttling of SMN within the nucleolus after DNA repair. It would be of great interest to generate new cell lines expressing GFP-tagged (SMN, Coilin, and FBL) to measure the dynamics in live-cell imaging to understand how SMN moves into and out of the nucleolus in response to damage. Also, how the nucleolar (re)organization takes place, using Time-lapse microscopy, or fluorescence recovery after photobleaching (FRAP). Under both physiological and pathophysiological conditions.

We suppose that the nucleolar structure may take different amounts of time to recover depending on the type of stress. It is also anticipated that variations in the stress response timeline will depend on the cell type. Therefore, by imaging, we need to select the recovery time of a nucleolar structure following different kinds of cellular treatments (e.g. RNAP1 transcription inhibition using different rinseable drugs), oxidative damage, or UV exposure, as well as for each cell line.

Disclosing new partners of nucleolar proteins and SMN interactions during cellular stress opens new avenues for future discoveries in this field. The importance of these interactions appears in some SMN mutants derived from SMA patients, which were shown to be deficient in many interactions. Moreover, our results suggest that protein-protein interactions with SMN could alter the dynamics distribution between the Gems/CB and the nucleolus. Interestingly, these distributions between the Gems/CB are involved in the pathogenesis severe of SMA.

Different proteins are implicated in the two phases of nucleolar reorganization (Displacement and Repositioning). To date, we have six candidates (ACT β , CEN-2, Coilin, FBL, NMI, and SMN), which have a role in the reorganization of the nucleolus. Accordingly, there could also be different proteins involved in different stress conditions, as well as different concomitant mechanisms. Therefore, further studies of other stress reactions (Apply various stresses to the

cells: (i) drug-induced RNAP1 transcription inhibition; (ii) oxidative damage stress, and (iii) UV-irradiation could reveal new findings and improve our understanding of this process. Furthermore, we expect to get more proteins involved in this process by using the human siRNA libraries which were created based on our identified candidates. After that, functional studies could be conducted by knocking down the new proteins.

The fine details of the organization of the cell nucleus are becoming increasingly evident in specific pathologies. These effects, whether direct or indirect, likely reflect the disruption of cellular function contributing to the disease state and may serve as useful clinical markers or provide insights into the underlying pathogenic mechanisms. Our findings establish a new link between CB and nucleolus regarding the DNA damage response. And now, our team is working on more than one line based on the promising results shown in this thesis, which make me proud and happy. As we learn more about the SMN mechanisms behind diverse cellular activities, our understanding of SMN functions will increase. We will reveal novel disease processes with a better understanding of SMN functions, bringing us closer to effective and focused therapeutics for SMA and other associated diseases.

Finally, the great possibility of future implications of this relationship for human disease is a perfect example of an observation that Cajal himself made in *Advice for a Young Investigator*, saying that,

“each problem solved stimulates an infinite number of new questions, and that today’s discovery contains the seed of tomorrow’s.”

Chapter six

Annex

A list of 289 known interactors of SMN, showing the gene name interacting with SMN, the related publication (PubMed ID (PMID)), the formation adapted from The National Center for Biotechnology Information (NCBI).

(<https://www.ncbi.nlm.nih.gov/gene/6606>).

Gene name	PubMed ID	Description
POP7	PMID: 14715275	Rpp20 interacts with SMN
SMN1	PMID: 14715275	hSMN interacts with a second hSMN molecule
SNRPB	PMID: 15494309	SMN interacts with SmB'
A1BG	PMID: 21900206	Two-hybrid
A2M	PMID: 21900206	Two-hybrid
ACRBP	PMID: 33961781	Affinity Capture-MS
ACTB	PMID: 21900206 PMID: 19928837	Affinity Capture-MS; Two-hybrid
ACTL6B	PMID: 21900206	Two-hybrid
ADAMTS10	PMID: 21900206	Two-hybrid
AGAP1	PMID: 21900206	Two-hybrid
ANXA2	PMID: 30165668	Protein-RNA
APLP1	PMID: 21900206	Two-hybrid
ARFGAP1	PMID: 21900206	Two-hybrid
ARHGAP9	PMID: 32203420	Affinity Capture-MS
ATP5F1B	PMID: 21900206	Two-hybrid
ATP6V1A	PMID: 21900206	Two-hybrid
ATRX	PMID: 31551363	Synthetic Lethality
Apc2	PMID: 32129710	Affinity Capture-MS
BAD	PMID: 31980649	Affinity Capture-MS
BAG6	PMID: 21900206 PMID: 16169070	Two-hybrid
BCL2	PMID: 9389483	Affinity Capture-Western; Reconstituted Complex; Two-hybrid
BLOC1S6	PMID: 32296183	Two-hybrid
BMI1	PMID: 24457600	Affinity Capture-MS
BYSL	PMID: 32296183	Two-hybrid
C9orf72	PMID: 30165668	Protein-RNA
CARHSP1	PMID: 21900206	Two-hybrid
CCDC90B	PMID: 21900206	Two-hybrid
CDC5L	PMID: 20467437	Affinity Capture-MS
CENPB	PMID: 21900206	Two-hybrid
CHMP4B	PMID: 31586073	Affinity Capture-MS
CHMP4C	PMID: 31586073	Affinity Capture-MS
CHTOP	PMID: 32296183	Two-hybrid
CHUK	PMID: 28214532	Affinity Capture-Western
CLNS1A	PMID: 35271311	Affinity Capture-MS
COIL	PMID: 34079125 PMID: 22939629 PMID: 12361597 PMID: 11641277	Affinity Capture-Western; Co-fractionation; Proximity Label-MS; Reconstituted Complex

COL4A2	PMID: 21900206	Two-hybrid
COL4A5	PMID: 21900206	Two-hybrid
COPA	PMID: 23727837 PMID: 21300694	Affinity Capture-Western
COPS6	PMID: 21900206 PMID: 16169070	Two-hybrid
CPNE6	PMID: 21900206	Two-hybrid
CPSF6	PMID: 35271311	Affinity Capture-MS
CRIP2	PMID: 21900206	Two-hybrid
CSAD	PMID: 21900206	Two-hybrid
CTBP2	PMID: 30585266	Affinity Capture-MS
CUL3	PMID: 21145461	Affinity Capture-MS
DDAH2	PMID: 21900206	Two-hybrid
DDRKG1	PMID: 32807901	Affinity Capture-MS
DDX17	PMID: 19928837	Affinity Capture-MS
DDX20	PMID: 35271311 PMID: 29395067 PMID: 26908624 PMID: 24981860 PMID: 23752268 PMID: 22939629 PMID: 21300694 PMID: 19928837 PMID: 12668731 PMID: 11914277	Affinity Capture-MS; Affinity Capture-Western; Co-fractionation; Co-purification; Proximity Label-MS; Reconstituted Complex
DDX5	PMID: 19928837	Affinity Capture-MS
DHX9	PMID: 11149922	Affinity Capture-Western; Reconstituted Complex
DICER1	PMID: 23752268	Affinity Capture-Western
DLD	PMID: 29128334	Affinity Capture-MS
DMPK	PMID: 21900206	Two-hybrid
DOCK7	PMID: 21900206	Two-hybrid
DUS2	PMID: 21900206	Two-hybrid
DYNC111	PMID: 21900206	Two-hybrid
ECT2	PMID: 31586073	Affinity Capture-MS
EEF1A1	PMID: 21900206	Two-hybrid
EEF1A2	PMID: 30165668	Protein-RNA
EGFR	PMID: 34373451	Negative Genetic
EGLN3	PMID: 26972000	Affinity Capture-MS
EHHADH	PMID: 32296183	Two-hybrid
EIF3G	PMID: 21900206	Two-hybrid
ERH	PMID: 19928837	Affinity Capture-MS
ESR1	PMID: 31527615	Affinity Capture-MS
ESR2	PMID: 29509190	Affinity Capture-MS
EWSR1	PMID: 29884807 PMID: 19928837	Affinity Capture-MS
EXT2	PMID: 21900206	Two-hybrid
EZH2	PMID: 21900206	Two-hybrid
FAM120C	PMID: 29395067	Proximity Label-MS

FAM20C	PMID: 21900206	Two-hybrid
FAM9B	PMID: 32296183	Two-hybrid
FBL	PMID: 19928837 PMID: 11509230	Affinity Capture-MS; Affinity Capture-Western; Co-localization; Reconstituted Complex
FGB	PMID: 21900206	Two-hybrid
FLAD1	PMID: 21900206	Two-hybrid
FNDC11	PMID: 32296183	Two-hybrid
FUBP1	PMID: 19928837 PMID: 10734235	Affinity Capture-MS; Affinity Capture-Western; Reconstituted Complex; Two-hybrid
FUS	PMID: 35271311 PMID: 29884807	Affinity Capture-MS
GAPDH	PMID: 21900206	Two-hybrid
GAR1	PMID: 12244096 PMID: 11509230	Affinity Capture-Western; Co-localization; Reconstituted Complex
GDF9	PMID: 21900206 PMID: 16169070	Two-hybrid
GEMIN2	PMID: 35271311 PMID: 33961781 PMID: 32296183 PMID: 26908624 PMID: 26092730 PMID: 24981860 PMID: 23221635 PMID: 21900206 PMID: 21300694 PMID: 19928837	Affinity Capture-MS; Affinity Capture-Western; Co-fractionation; Co-purification; Reconstituted Complex; Two-hybrid
GEMIN4	PMID: 35271311 PMID: 26908624 PMID: 24981860 PMID: 23752268 PMID: 23221635 PMID: 19928837 PMID: 12668731 PMID: 10942426	Affinity Capture-MS; Affinity Capture-Western; Co-fractionation; Co-purification
GEMIN5	PMID: 35271311 PMID: 26908624 PMID: 26496610 PMID: 24923560 PMID: 23221635 PMID: 11714716	Affinity Capture-MS; Affinity Capture-Western; Reconstituted Complex
GEMIN6	PMID: 35271311 PMID: 33961781 PMID: 26186194 PMID: 24981860 PMID: 19928837	Affinity Capture-MS; Affinity Capture-Western

	PMID: 11748230	
GEMIN7	PMID: 26496610 PMID: 24981860 PMID: 19928837 PMID: 12065586 PMID: 11748230	Affinity Capture-MS; Affinity Capture-Western; Reconstituted Complex
GEMIN8	PMID: 35271311 PMID: 26908624 PMID: 24981860 PMID: 19928837	Affinity Capture-MS; Affinity Capture-Western
GIGYF2	PMID: 20696395	Affinity Capture-MS
H2AC20	PMID: 19928837	Affinity Capture-MS
H3-4	PMID: 21172665	Protein-peptide
H4C1	PMID: 19928837	Affinity Capture-MS
HADHB	PMID: 21900206	Two-hybrid
HBP1	PMID: 29911972	Affinity Capture-MS
HDAC1	PMID: 26949739	Affinity Capture-MS
HDAC11	PMID: 23752268	Affinity Capture-MS; Affinity Capture-Western
HDAC2	PMID: 14749338	Affinity Capture-Western
HMGXB3	PMID: 21900206	Two-hybrid
HNRNPA1	PMID: 19928837	Affinity Capture-MS
HNRNPA2B1	PMID: 19928837	Affinity Capture-MS
HNRNPH1	PMID: 19928837	Affinity Capture-MS
HNRNPH3	PMID: 19928837	Affinity Capture-MS
HNRNPR	PMID: 19928837 PMID: 11773003 PMID: 11574476	Affinity Capture-MS; Affinity Capture-Western; Reconstituted Complex
HNRNPUL1	PMID: 22365833	Two-hybrid
HSPB1	PMID: 17916631	Affinity Capture-Western
IGHM	PMID: 21900206	Two-hybrid
IKBKB	PMID: 28214532	Affinity Capture-Western
IKBKG	PMID: 28214532	Affinity Capture-Western
IMMT	PMID: 21900206	Two-hybrid
INPP5K	PMID: 21900206	Two-hybrid
IQCB1	PMID: 21565611	Affinity Capture-MS
IQUB	PMID: 32296183	Two-hybrid
ITCH	PMID: 26908624	Affinity Capture-Western; Reconstituted Complex
JADE1	PMID: 21900206	Two-hybrid
KDM1A	PMID: 23455924	Two-hybrid
KIF14	PMID: 31586073	Affinity Capture-MS
KIF23	PMID: 31586073	Affinity Capture-MS
KIF5A	PMID: 21900206	Two-hybrid
KLF16	PMID: 35140242	Affinity Capture-MS
KLHL5	PMID: 21900206	Two-hybrid
KMT2B	PMID: 21900206	Two-hybrid
KPNB1	PMID: 12095920	Affinity Capture-Western; Reconstituted Complex

KRAS	PMID: 34373451	Negative Genetic
KRTAP19-6	PMID: 32296183	Two-hybrid
KRTAP19-7	PMID: 32296183	Two-hybrid
KRTAP21-2	PMID: 32296183	Two-hybrid
KRTAP6-1	PMID: 32296183	Two-hybrid
KRTAP6-2	PMID: 32296183	Two-hybrid
LENG8	PMID: 16189514	Two-hybrid
LGALS1	PMID: 11522829	Affinity Capture-Western
LRIF1	PMID: 21900206 PMID: 16169070	Two-hybrid
LSM1	PMID: 29395067	Proximity Label-MS
LSM10	PMID: 19928837 PMID: 16087681	Affinity Capture-MS; Reconstituted Complex
LSM11	PMID: 35271311 PMID: 19928837 PMID: 16087681	Affinity Capture-MS; Reconstituted Complex
LSM2	PMID: 29395067 PMID: 10851237	Affinity Capture-MS; Reconstituted Complex
LSM4	PMID: 29395067 PMID: 10851237	Affinity Capture-MS; Reconstituted Complex
LSM6	N/A	Reconstituted Complex
LSM7	PMID: 10851237	Reconstituted Complex
MAGED1	PMID: 32296183	Two-hybrid
MAP3K5	PMID: 21496457	Affinity Capture-Western
MAST2	PMID: 21900206	Two-hybrid
MDC1	PMID: 22990118	Affinity Capture-MS
MED31	PMID: 24981860 PMID: 21900206	Affinity Capture-MS; Two- hybrid
MIB1	PMID: 23615451	Affinity Capture-Western
MKI67	PMID: 21900206	Two-hybrid
MPP1	PMID: 21900206	Two-hybrid
MRPL37	PMID: 21900206	Two-hybrid
MSH2	PMID: 21900206	Two-hybrid
MYBBP1A	PMID: 19928837	Affinity Capture-MS
MYO6	PMID: 24981860	Affinity Capture-MS
N	PMID: 34029587	Affinity Capture-Western
NEURL2	PMID: 33979606	Affinity Capture-Western; Biochemical Activity
NGFR	PMID: 21900206	Two-hybrid
NKIRAS2	PMID: 21900206	Two-hybrid
NMRAL1	PMID: 31796584	Affinity Capture-MS
NMT2	PMID: 21900206	Two-hybrid
NONO	PMID: 19928837	Affinity Capture-MS
NOP56	PMID: 19928837	Affinity Capture-MS
NOP58	PMID: 19928837	Affinity Capture-MS
NOS2	PMID: 23438482	Affinity Capture-MS
NPM1	PMID: 19928837	Affinity Capture-MS
NRN1	PMID: 30165668	Protein-RNA
NSD2	PMID: 24923560	Affinity Capture-MS; Affinity

		Capture-Western
NTAQ1	PMID: 16189514	Two-hybrid
NUFIP1	PMID: 26275778	Affinity Capture-Western
OTUD4	PMID: 31138677	Affinity Capture-Western
P4HA1	PMID: 19928837	Affinity Capture-MS
PAN2	PMID: 23398456	Affinity Capture-MS
PDE4DIP	PMID: 21900206	Two-hybrid
PDHA1	PMID: 29128334	Affinity Capture-MS
PFN2	PMID: 24981860	Affinity Capture-MS
PKM	PMID: 21900206	Two-hybrid
PLXNA3	PMID: 21900206	Two-hybrid
POLR1C	PMID: 32296183	Two-hybrid
POLR2A	PMID: 26700805	Affinity Capture-Western; Reconstituted Complex
PPIG	PMID: 21516116	Two-hybrid
PPP4C	PMID: 12668731	Affinity Capture-Western
PRKAA2	PMID: 31900314	Affinity Capture-MS
PRMT5	PMID: 35271311 PMID: 26700805	Affinity Capture-MS; Affinity Capture-Western
PRPF31	PMID: 26275778	Affinity Capture-Western
PSME1	PMID: 21900206	Two-hybrid
PSPC1	PMID: 35271311	Affinity Capture-MS
PTPN9	PMID: 27432908	Affinity Capture-MS
PTPRA	PMID: 32062451	Affinity Capture-MS; Proximity Label-MS
QARS1	PMID: 21900206	Two-hybrid
RAB5A	PMID: 31980649	Affinity Capture-MS
RBBP4	PMID: 21900206	Two-hybrid
RBBP6	PMID: 18624398	Two-hybrid
RBFOX2	PMID: 22365833	Two-hybrid
RBM25	PMID: 22939629	Co-fractionation
RBM39	PMID: 28546157	Affinity Capture-MS
RBM48	PMID: 21900206	Two-hybrid
RET	PMID: 32062451	Affinity Capture-MS
REX1BD	PMID: 21900206	Two-hybrid
RIT1	PMID: 34373451	Negative Genetic
RN7SL1	PMID: 30165668 PMID: 23221635	Affinity Capture-RNA; Protein- RNA
RNF2	PMID: 24457600	Affinity Capture-MS
RNU1-1	PMID: 23221635	Protein-RNA
RNU11	PMID: 30165668	Protein-RNA
RNU2-1	PMID: 23221635	Protein-RNA
RNU4-1	PMID: 30165668	Protein-RNA
RPL10	PMID: 19928837	Affinity Capture-MS
RPL13	PMID: 21900206 PMID: 19928837	Affinity Capture-MS; Two- hybrid
RPL6	PMID: 19928837	Affinity Capture-MS
RPL7	PMID: 19928837	Affinity Capture-MS
RPS2	PMID: 21900206	Two-hybrid

RXRA	PMID: 21900206	Two-hybrid
SCARNA1	PMID: 30165668	Protein-RNA
SDF4	PMID: 21900206	Two-hybrid
SELENOW	PMID: 30165668	Protein-RNA
SEMA5B	PMID: 21900206	Two-hybrid
SETDB1	PMID: 21900206	Two-hybrid
SETX	PMID: 26700805	Affinity Capture-Western
SFMBT2	PMID: 24981860	Affinity Capture-MS
SFPQ	PMID: 19928837	Affinity Capture-MS
SIN3A	PMID: 14749338	Affinity Capture-Western
SIN3B	PMID: 14749338	Affinity Capture-Western
SIRT6	PMID: 34244565	Affinity Capture-MS
SLX1B	PMID: 19596235	Affinity Capture-MS
SMC5	PMID: 21900206	Two-hybrid
SMN1	PMID: 35271311 PMID: 32296183 PMID: 22365833 PMID: 21516116 PMID: 21300694 PMID: 19447967 PMID: 16189514	Affinity Capture-MS; Two-hybrid
SMN2	PMID: 32296183 PMID: 29997244 PMID: 28514442 PMID: 26264872 PMID: 26186194 PMID: 19447967 PMID: 10942426	Affinity Capture-Luminescence; Affinity Capture-MS; Co-fractionation; Co-purification; FRET; Two-hybrid
SNORA81	PMID: 30165668	Protein-RNA
SNRNP70	PMID: 35271311 PMID: 33961781 PMID: 28514442 PMID: 24981860 PMID: 19928837	Affinity Capture-MS
SNRPA	PMID: 35271311	Affinity Capture-MS
SNRPA1	PMID: 19928837	Affinity Capture-MS
SNRPB	PMID: 35271311 PMID: 19928837 PMID: 16087681 PMID: 11720283	Affinity Capture-MS; Reconstituted Complex
SNRPB2	PMID: 35271311	Affinity Capture-MS
SNRPC	PMID: 35271311	Affinity Capture-MS
SNRPD1	PMID: 35271311 PMID: 24981860 PMID: 19928837 PMID: 10942426 PMID: 16087681 PMID: 10851237 PMID: 9323129	Affinity Capture-MS; Co-fractionation; Co-purification; Reconstituted Complex

SNRPD2	PMID: 35271311 PMID: 24981860 PMID: 19928837 PMID: 16087681 PMID: 10942426	Affinity Capture-MS; Co-fractionation; Co-purification; Reconstituted Complex
SNRPD3	PMID: 10851237	Reconstituted Complex
SNRPE	PMID: 24981860 PMID: 9323129	Affinity Capture-MS; Reconstituted Complex
SNRPF	PMID: 35271311 PMID: 24981860 PMID: 19928837	Affinity Capture-MS
SNRPG	PMID: 19928837	Affinity Capture-MS
SNU13	PMID: 32296183	Two-hybrid
SNUPN	PMID: 12095920	Reconstituted Complex
SNW1	PMID: 20467437	Affinity Capture-MS
SP110	PMID: 21900206	Two-hybrid
SPANXN2	PMID: 32296183	Two-hybrid
SQSTM1	PMID: 29672276	Affinity Capture-Western
SRP19	PMID: 23221635	Affinity Capture-Western
SRP54	PMID: 23221635	Affinity Capture-Western
SRP68	PMID: 23221635	Affinity Capture-Western
SRP9	PMID: 23221635	Affinity Capture-Western
SRSF3	PMID: 19928837	Affinity Capture-MS
SRSF5	PMID: 22939629	Co-fractionation
STRAP	PMID: 35271311 PMID: 29395067 PMID: 26496610 PMID: 24981860 PMID: 24923560 PMID: 19928837	Affinity Capture-MS; Affinity Capture-Western; Proximity Label-MS
SULT1A3	PMID: 21900206	Two-hybrid
SUMO3	PMID: 21900206	Two-hybrid
SYNCRIP	PMID: 29395067	Proximity Label-MS
Smn1	PMID: 21300694	Two-hybrid
Snrnp70	PMID: 26496610	Affinity Capture-MS
TAF1C	PMID: 21900206	Two-hybrid
TCERG1	PMID: 17218272	Affinity Capture-Western
TERC	PMID: 30165668	Protein-RNA
THRAP3	PMID: 19928837	Affinity Capture-MS
TIA1	PMID: 29395067	Proximity Label-MS
TLE1	PMID: 21900206	Two-hybrid
TMPO	PMID: 19928837	Affinity Capture-MS
TMSB4X	PMID: 21900206	Two-hybrid
TP53	PMID: 21900206 PMID: 11704667	Affinity Capture-Western; Reconstituted Complex; Two-hybrid
TP53BP1	PMID: 29656893	Proximity Label-MS
TPTE	PMID: 28330616	Affinity Capture-MS
TRAF6	PMID: 28214532	Affinity Capture-Western

TRMT2A	PMID: 21900206	Two-hybrid
TUBA1A	PMID: 21900206	Two-hybrid
TUBB3	PMID: 21900206	Two-hybrid
TULP3	PMID: 33187986	Affinity Capture-MS
TUSC1	PMID: 24981860	Affinity Capture-MS
UBL4A	PMID: 23246001	Affinity Capture-MS
UCHL1	PMID: 20713032	Affinity Capture-Western; Biochemical Activity
UNC119	PMID: 21900206 PMID: 16169070	Two-hybrid
USP15	PMID: 33378683	Affinity Capture-MS
USP4	PMID: 21900206	Two-hybrid
USP9X	PMID: 35271311	Affinity Capture-MS
VPS28	PMID: 21516116	Two-hybrid
WDR18	PMID: 21900206	Two-hybrid
WDR73	PMID: 21900206	Two-hybrid
WDR77	PMID: 35271311 PMID: 28977470	Affinity Capture-MS
WIZ	PMID: 21900206	Two-hybrid
XPO1	PMID: 26673895	Affinity Capture-MS
XRN2	PMID: 26700805	Affinity Capture-Western
ZBTB16	PMID: 21900206	Two-hybrid
ZNF431	PMID: 21900206	Two-hybrid
ZNF746	PMID: 25315684	Affinity Capture-MS
ZRANB1	PMID: 33853758	Affinity Capture-MS
ZXDC	PMID: 21900206	Two-hybrid
vpr	PMID: 22190034	Affinity Capture-MS

Table 8 : A list of 289 known interactors of SMN. The formation adapted from The National Center for Biotechnology Information (NCBI).

A big list of PRMT inhibitors, some are in preclinical, and some are already in Phase I clinical trials; these formations are adapted from (Jarrold J, 2019).

Compound	PRMTs inhibited (i) Type I preclinical compounds	Mode of action
Allantodapsone	PRMT1 (IC50 1.7 mM in vitro)	Competitive (substrate)
AMI-1	PRMT1 (IC50 8.8 μM in vitro) PRMT3 (ND) CARM1 (IC50 169.8 μM in vitro) PRMT6 (ND)	Competitive (substrate)
AMI-408	PRMT1 (ND)	N/A
MS023	PRMT1 (IC50 9 nM cell assay) PRMT3 (IC50 119 nM cell assay) PRMT6 (IC50 56 nM cell assay)	Noncompetitive (SAM and substrate)
MS049	CARM1 (IC50 34 nM in vitro, 1.4 μM cell assay) PRMT6 (IC50 43 nM in vitro, 0.97 μM cell assay)	Noncompetitive
E84	PRMT1 (IC50 3.38 μM in vitro) CARM1 (IC50 21.5 μM in vitro) PRMT5 (IC50 35.4 μM in vitro) PRMT8 (IC50 84.9 μM in vitro)	N/A
Furamidine (DB75)	PRMT1 (IC50 9.4 μM in vitro) CARM1 (IC50 >400 μM in vitro) PRMT5 (IC50 166 μM in vitro) PRMT6 (IC50 283 μM in vitro)	Competitive (substrate)
GMS	PRMT1 (IC50 500 nM in vitro) PRMT3 (IC50 700 nM in vitro) CARM1 (IC50 <15 nM in vitro) PRMT5 (IC50 300 nM in vitro) PRMT6 (IC50 90 nM in vitro) PRMT8 (IC50 11 nM in vitro)	Competitive (SAM and substrate)

PT1001B (DCPR049_12)	PRMT1 (IC50 1.1 nM in vitro) PRMT3 (IC50 22 nM in vitro) CARM1 (IC50 63 nM in vitro) PRMT5 (IC50 >100 μM in vitro) PRMT6 (IC50 1.2 nM in vitro) PRMT8 (IC50 1.1 nM in vitro)	Noncompetitive
SGC707	PRMT3 (IC50 31 nM in vitro, 91–225 nM cell assay)	Noncompetitive
SGC2085	CARM1 (IC50 50 nM in vitro) PRMT6 (IC50 5.2 μM in vitro) PRMT8 (IC50 >50 μM in vitro)	Noncompetitive
EPZ020411	PRMT1 (IC50 0.119 μM in vitro) PRMT6 (IC50 0.010 μM in vitro, 0.637 μM cell assay) PRMT8 (IC50 0.223 μM in vitro)	Competitive (substrate)
EPZ0025654 (GSK3536023)	CARM1 (IC50 3 nM in vitro)	Competitive (substrate)
EZM2302 (GSK3359088)	CARM1 (IC50 6 nM in vitro, 0.015– >10 μM cell assay)	Competitive (substrate), synergistic with SAH
TP-064	PRMT1 (IC50 >10 μM in vitro) PRMT3 (IC50 >10 μM in vitro) CARM1 (IC50 <10 nM in vitro, 400–716 nM cell assay) PRMT5 (IC50 >10 μM in vitro) PRMT6 (IC50 1.6 μM in vitro) PRMT7 (IC50 >10 μM in vitro) PRMT8 (IC50 8.1 μM in vitro)	Competitive (substrate)

	PRMT9 (IC50 >10 µM in vitro)	
--	------------------------------	--

Compound	PRMTs inhibited (ii) II and III preclinical compounds	Mode of action
EPZ015666 (GSK3235025)	PRMT5 (IC50 22 nM in vitro, 64–904 nM cell assay)	Competitive (substrate)
EPZ015866 (GSK591)	PRMT5 (IC50 4 nM in vitro)	Competitive (substrate)
EPZ004777	PRMT5 (IC50 30 µM in vitro) PRMT7 (IC50 7.5 µM in vitro)	Competitive (SAM)
LLY-283	PRMT5 (IC50 22 nM in vitro, 25 nM cell assay)	Competitive (SAM)
HLCL-61	PRMT5 (ND)	N/A
DS-437	PRMT5 (IC50 5.9 µM in vitro) PRMT7 (IC50 6 µM in vitro)	Competitive (SAM)
SGC3027	PRMT7 (IC50 2.4 µM cell assay)	Cell-permeable prodrug; converted to the active form (SGC8158) in the cell
SGC8158	PRMT7 (IC50 <2.5 nM in vitro)	Competitive (SAM)

Compound	PRMTs inhibited (iii) Inhibitors in Phase I clinical trials	Mode of action
GSK3368715	PRMT1	N/A

EPZ015938 (GSK3326595)	PRMT5 (IC50 3–9.9 nM in vitro) PRMT9 (IC50 >40 μM in vitro)	Competitive (substrate)
JNJ-64619178	PRMT5	N/A
PF-06939999	PRMT5	N/A

Table 9 : PRMTs inhibited (i) Type I preclinical compounds, PRMTs inhibited (ii) II and III preclinical compounds, and PRMTs inhibited (iii) Inhibitors in Phase I clinical trials.

IC50, The half-maximal inhibitory concentration. N/A, not available; ND, not determined; SAH, S-adenosylhomocysteine; SAM, S-adenosyl methionine. The table modified from (Jarrold J, 2019).

Curriculum vitae

Name: Shaqraa MUSAWI

From: Saudi Arabia

Date of birth: 16/11/1990

Current Position (2022): Ph.D. Student Claude Bernard University
& Lecturer at Jazan University

Email: shaqraa_musawi@univ-lyon1.fr
smusawi@jazanu.edu.sa

Interuniversity diploma: 14-26 Mar 2022, (56H)
The European Diploma in Classical
and Molecular Cytogenetics
Montpellier, France

European Human Genetics Conference: (Participated by scientific poster)
28-31 Aug 2021, (20H)

Master of Research (MRes): 2017 – 2019
Biology health (Genetics, Physiology,
pathologies) Clermont Ferrand, France

**University degree of French language
and civilization :** 2015-2016
DELF:(Diplôme d’Etude en Langue
Française) B2 level, Saint-Etienne, France

Lecturer at Jazan University: 2013-2014
Faculty of Applied Medical Sciences,
Jazan, Kingdome of Saudi Arabia

University diploma: May - June 2013
Cytogenetic& Molecular Genetics
Montreal, Canada

Bachelor of Science Course (BSc):
Faculty of Applied Medical Sciences
2009 – 2013
Medical Laboratory Technology
Jazan, Kingdome of Saudi Arabia